Electronic Thesis and Dissertation Repository

7-26-2019 2:30 PM

Energy Reduction in Fluidized Bed Bioreactors for Municipal and Ammonia-rich Wastewater Treatment

Haolong Wang, *The University of Western Ontario*

Supervisor: Zhu, Jesse, *The University of Western Ontario*
Joint Supervisor: Nakhla, George, *The University of Western Ontario*
A thesis submitted in partial fulfillment of the requirements for the Doctor of Philosophy degree
in Chemical and Biochemical Engineering
© Haolong Wang 2019

Follow this and additional works at: https://ir.lib.uwo.ca/etd

Part of the Chemical Engineering Commons

Recommended Citation

Abstract

The combination of biological nutrient removal (BNR) with fluidization technology has demonstrated advantages over suspended growth systems. Previous studies about fluidized bed bioreactor (FBBR) mainly focused on the BNR performance, rarely paid attention to the operation and energy consumption, while high energy consumption is the main hurdle for the industrial application of FBBR systems.

In this work, the BNR performance of a novel inverse fluidized bed bioreactor (IFBBR) treating synthetic wastewater was studied. TCOD removal efficiencies of >84% were achieved, concomitantly with complete nitrification. Compared with other FBBR systems, the energy consumption for this IFBBR system was an average 59% less. Bacterial community structures of attached and detached biomass revealed that the dominant phyla were *Proteobacteria, Bacteroidetes,* and *Epsilonbacteraeota*, etc. The relative abundance of AOB and NOB in aerobic attached biomass were 0.451% and 0.110%, respectively. The IFBBR system was further studied of BNR performance with synthetic high particulate COD wastewater. 87% COD, 73% TN, and 48% TP removal was achieved at OLR of 2.8 kg COD/(m^3 d) and nitrogen loading rate (NLR) of 0.26 kg N/(m^3 d). Organic shock test was conducted to examine the system sustainability with short term response to the variance of influent COD. A calibrated IFBBR model built in Biowin was efficient to simulate COD and nitrogen concentrations.

Although the energy consumption of IFBBR system was reduced, the maximum OLR of 2.8 kg/(m^3 d) achieved in the IFBBR system was approximately half of the maximum OLR of 5.3 kg/(m^3 d) in the CFBBR system due to high shear force in the aerobic zone and small specific surface area for biomass attachment. The selection of carriers is a crucial issue for FBBRs. Minimum fluidization velocity (U_{lmf}) affects system design and operation. Four carrier particles (L-HDPE, S-HDPE, pottery, and zeolite) were chosen to study the U_{lmf} under gas velocities of 0-12.4 mm/s. Partial nitrification (PN) was an alternative way to eliminate ammonia. An FBBR with S-HDPE as carriers was operated to study PN performance at NLRs of 1.2-4.8 kg N/(m^3 d). Stable PN was successfully achieved with

low effluent NO_3-N concentration of <15 mg/L. At NLR of 3.6 kg N/(m^3 d), the system effluent NO_2-N/NH_4-N ratio was 1.27.

Keywords

Summary for Lay Audience

Based on the idea of growing bacteria on small particle surface, the circulating fluidized bed bioreactor (CFBBR) was developed to combine the advantages of biological nutrient removal (BNR) process and fluidized bed technology. Previous studies showed that CFBBR system could achieve efficient nutrient removal at short hydraulic retention time of 2-3h with low biomass yield. However, high energy consumption was the main hurdle for the industrial application of CFBBR system. Two approaches were proposed to address this problem - changing carrier particles and employing new BNR processes.

A novel inverse fluidized bed bioreactor (IFBBR) with polypropylene beads (true density of 904 kg/m^3) as carrier media for biomass attachment was built to study the BNR performance of treating synthetic wastewater. TCOD removal efficiencies of >84% were achieved, concomitantly with complete nitrification. The energy consumption of this IFBBR system was 59% less than that of CFBBR system. Bacterial community structures of anoxic, aerobic and effluent biomass were tested by 16S rRNA sequencing. The dominant phyla were *Proteobacteria, Bacteroidetes, and Epsilonbacteraeota*, etc. Biomass were classified into different functional groups based on the functions of genera and a new method to calculate sludge retention time was proposed. An organic shock test was conducted to examine the system short-term resilience to influent variations. A calibrated IFBBR model was built in Biowin and this model was efficient of simulating COD and nitrogen removal performance.

Minimum fluidization velocity (U_{lmf}) affects system design, operation, and energy consumption. U_{lmf} of four carrier particles (L-HDPE, S-HDPE, pottery, and zeolite) were studied under different gas velocities of 0-12.4 mm/s for carrier selection. S-HDPE has the lowest U_{lmf} at all gas velocities. The experimental results were examined by semiempirical equations. Partial nitrification (PN) was an emerging BNR process to eliminate ammonia. An FBBR system with S-HDPE as carriers was operated to study PN performance. Stable PN was successfully achieved with effluent nitrate of <15 mg/L. At a nitrogen loading rate of 3.6 kg $N/(m^3$ d), the system effluent with NO_2-N/NH_4-N of 1.27 could be directly used as the influent to anaerobic ammonia oxidation process, hence significantly reducing aeration energy demand.

Co-Authorship Statement

This PhD thesis contains material that is published, 'under review' or in preparation for submission in peer-reviewed journals as listed below.

Chapter 3: Performance and Bacterial Community Structure of a Novel Inverse Fluidized Bed Bioreactor (IFBBR) Treating Synthetic Wastewater

Haolong Wang, Xiaoqin He, George Nakhla, Jesse Zhu, Yi-Kai Su, Yuanyuan Shao

Submitted to *Chemical Engineering Journal*

The primary author of this chapter was Haolong Wang under the supervision of Dr. Zhu and Dr. Nakhla. The experimental plan was developed by Haolong Wang with the guidance of Dr. Zhu and Dr. Nakhla, as well as the execution of experiments, data collection and analysis, and drafting the manuscript. Feedback on the manuscript was received from other co-authors. Bacterial community structure was tested with the help of Xiaoqin He and YI-Kai Su.

Chapter 4: Inverse Fluidized Bed Bioreactor (IFBBR) for Municipal Wastewater Treatment – Performance and Modeling

Haolong Wang, George Nakhla, Jesse Zhu, Yuanyuan Shao

In preparation for submission to *Biochemical Engineering Journal*

The primary author of this chapter was Haolong Wang under the supervision of Dr. Zhu and Dr. Nakhla. The execution of experiments, data collection and analysis, and drafting the manuscript was conducted by Haolong Wang. Feedback on the manuscript was received from other co-authors.

Chapter 5: Minimum Fluidization Velocity of Carrier Particles in (Gas-)Liquid-Solid Fluidized Bed

Haolong Wang, Jesse Zhu, George Nakhla, Yuanyuan Shao

In preparation for submission to *Powder technology*

The primary author of this chapter was Haolong Wang under the supervision of Dr. Zhu and Dr. Nakhla. The experimental plan was developed by Haolong Wang with the guidance of Dr. Zhu and Dr. Nakhla, as well as the execution of experiments, data collection and analysis, and drafting the manuscript. Feedback on the manuscript was received from other co-authors.

Chapter 6: Effective Partial Nitrification of Ammonia in a Fluidized Bed Bioreactor

Haolong Wang, Mingu Kim, Kai Li, Yuanyuan Shao, Jesse Zhu, George Nakhla

Published in *Environmental Technology*

The primary author of this chapter was Haolong Wang under the supervision of Dr. Zhu and Dr. Nakhla. The experimental plan was developed by Haolong Wang with the guidance of Dr. Zhu and Dr. Nakhla, as well as the execution of experiments, data collection and analysis, and drafting the manuscript. Feedback on the manuscript was received from other co-authors.

Acknowledgement

I would like to express my sincere gratitude to my supervisors, Professor Jesse Zhu and Professor George Nakhla. This thesis would not have been possible without their help and continuous support. I greatly appreciate Dr. Zhu for his wisdom, patience, and guidance for my PhD work. Deep thanks to Dr. Nakhla for his knowledge, passion, and motivation. I am fortunate to have had the opportunity to learn from two brilliant professors.

I would like to extend my appreciation to my colleagues at the University of Western Ontario for their friendship and support - Zhijie Fu, Tian Nan, Lin Wang, Xiaoyang Wei, Xiaoqin He, Michael Nelson, Dr. Mingu Kim, Xiaoguang Liu, Chenyang Zhou, Zhehao Jing, Zeneng Sun, and Shuai Yang. You all contributed to create a very friendly working environment and a highly efficient team. Thanks for being such great colleagues. Many thanks to Mr. Jianzhang Wen, Geroge Zhang, Danni Bao and Tang Li for their guidance and assistance to this work. The devices for my experiment could not be setup without the time and efforts spent by Mr. Wen. I am also grateful to the visiting professors and students who did the projects with me.

Special thanks to Professor Yuanyuan Shao from Tianjin University, China. I could not have the opportunity to study in Canada without your generous help. I also want to appreciate my colleagues from Tianjin University for your support and friendship. The time of staying at Tianjin University for my master degree is a precious memory and experience.

I acknowledge China Scholarship Council (CSC) and Natural Sciences and Engineering Research Council of Canada (NSERC) for providing me the finical support.

Lastly, I want to express my deepest appreciation to my parents, Guofu Wang and Fenling Qi, as well as my sister, Haoying Wang. Your tremendous love, support, and encouragement always motivate me to progress and become a better person.

Table of Contents

List of tables

List of figures

List of abbreviations and symbols

Abbreviations

Anammox	anaerobic ammonium oxidation
AOB	ammonia-oxidizing bacteria
BNR	biological nutrient removal
CFBBR	circulating fluidized bed bioreactor
COD	chemical oxygen demand
CSTR	continuous stirred tank reactor
DO	dissolved oxygen
EBCT	empty bed contact time
FBBR	fluidized bed bioreactor
HRT	hydraulic retention time
IFBBR	inverse fluidized bed bioreactor
MBBR	moving bed bioreactor
NLR	nitrogen loading rate
NOB	nitrite-oxidizing bacteria
OLR	organic loading rate
PN	partial nitrification
PNFBR	partial nitrification fluidized bed bioreactor
SDNR	biomass specific denitrification rate
SWW	synthetic wastewater
SNR	biomass specific nitrification rate
SRT	sludge retention time
TN	total nitrogen
TP	total phosphorus
TSS	total suspended solids
VSS	volatile suspended solids
WWTPs	wastewater treatment plants

Nomenclature (Chapters 3, 4 and 6)

b	specific decay rate (d^{-1})
g	gravitational acceleration (N/kg)
h	liquid circulation height (m)
K_{NO_2}	nitrite half saturation coefficient for NOB (mg/L)
$K_{O,NOB}$	oxygen half saturation coefficient for NOB (mg/L)
M_{ae}	amount of particles in the aerobic zone (g)
M_{an}	amount of particles in the anoxic zone (g)
P_g	blower power requirement (kWh/d)
P_l	pump power requirement (kWh/d)
P_1	blower inlet absolute pressure (atm)
P_2	blower outlet absolute pressure (atm)
Q_{eff}	effluent flow rate (L/d)
Q_g	air flow rate at standard condition (m^3/d)
Q_l	liquid flow rate (m^3/d)
RA_{ae}	relative abundance in anerobic attached biomass
RA_{an}	relative abundance in anoxic attached biomass
RA_{eff}	relative abundance in effluent biomass
S_{NO_2}	bulk nitrite concentration (mg/L)
S_O	bulk oxygen concentration (mg/L)
$SRT_{aerobic}$	sludge retention time based on aerobic biomass (d)
SRT_{min}	minimum sludge retention time for biomass growth (d)
SRT_{total}	sludge retention time based on total biomass (d)
T	temperature (K)
VSS_{eff}	effluent VSS concentration (g/L)
X_{ae}	g VSS/g particle in the aerobic zone
X_{an}	g VSS/g particle in the anoxic zone
X_{waste}	sludge discharge (g/d)
Y_{obs}	biomass observed yield (g VSS/g SCOD)
ρ_l	liquid density (kg/m^3)
ρ_m	mixed density in fluidized bed (kg/m^3)

η_b	blower efficiency
η_P	pump efficiency
μ	specific growth rate (d^{-1})
μ_{max}	maximum specific growth rate (d^{-1})

Nomenclature (Chapter 5)

A	cross-sectional area of the fluidized bed (m^2)
A_f	cross-sectional area occupied by the continuous phase (m^2)
Ar	Archimedes number (kg/m)
D_e	equivalent diameter of channel for liquid flow (m)
D_H	hydraulic diameter (m)
D_m	mean diameter of solid particles (m)
f_c	friction factor
F_f	form drag (N)
F_s	skin friction (N)
g	gravitational acceleration (m/s^2)
H	bed height (m)
k_1	constant
k_2	constant
$k_1^{'}$	empirical constant
$k_2^{'}$	empirical constant
Re	Reynolds number
U_f	fluid velocity (m/s)
U_g	gas velocity (m/s)
U_l	liquid velocity (m/s)
U_{lmf}	liquid velocity at minimum fluidization (m/s)
U_{mf}	fluid velocity at minimum fluidization (m/s)
V	bed volume before incipient fluidization (m^3)
W_{bed}	bed weight (kg)
ΔP	total pressure drop of the fluidized bed (kPa)

ΔS	wetted surface (m^2)
$(-\Delta P_F)$	frictional pressure drop
α	fractional gas holdup over total fluid volume fraction
α_{mf}	fractional gas holdup over total fluid volume fraction at minimum fluidization
ε	bed voidage
ε_g	gas fraction
ε_l	liquid fraction
ε_{mf}	bed voidage at minimum fluidization
ε_s	solid fraction
ρ_f	fluid density (kg/m^3)
ρ_g	gas density (kg/m^3)
ρ_l	liquid density (kg/m^3)
ρ_s	solid density (kg/m^3)
μ	fluid viscosity (Pa·S)
Φ	sphericity of solid particle

Chapter 1

Introduction

1.1 Rationale

The need for clean water resources has soared due to the rapid growth of population and economy. As reported, the municipal wastewater produced every year was over 330 billion m^3 across the world (Hernández-Sancho et al., 2015). Before discharging to the rivers and oceans, there are several contaminants need to be removed from the wastewater, such as organic matters, nitrogen, phosphorus, suspended solids, and bacteria. In response to the increasing demand to clean water and stringent effluent nutrient criteria for wastewater treatment plants, biological nutrient removal (BNR) processes have been widely applied to treat the wastewater (Eddy et al., 2014).

BNR processes incorporate aerobic zone with anoxic and/or anaerobic zone to achieve nutrient removal, which provides advantages over the conventional activated sludge processes, i.e. high effluent water quality, utilization of nitrates as electron acceptors for organic removal, saving aeration energy, and reducing sludge production. Consequently, BNR processes offer significant reduction of both capital and operation costs (Oleszkiewicz and Barnard, 2006; Villaverde, 2004). In the cases of treating the low carbon-to-nitrogen ratio wastewater with low concentrations of readily biodegradable organics, external sources of carbon may be required to add to the anoxic zone for denitrification for achieving nitrogen and phosphorus removal (Eddy et al., 2014). In addition, large amount of nitrous oxide (N_2O) emission was reported for the BNR wastewater treatment plants, whose carbon footprint on climate was over 300 times greater than CO_2 in a 100-year period (Massara et al., 2017). Alternatively, new processes have been proposed to treat the high-ammonia wastewater, including partial nitrification-denitrification and partial nitrification-anammox processes. By controlling of several operational parameters, large portion of ammonia was converted to nitrite instead of nitrate. With nitrite further denitrified by carbon sources or react with ammonia, the nitrogen

removal can be achieved by these short-cut ways, which provide advantages of low aeration energy consumption, reduced carbon source requirement, and less sludge production (Chen et al., 2009; Ge et al., 2015; Massara et al., 2017; Okabe et al., 2011; Wang et al., 2010). Both of the BNR and partial nitrification-denitrification (anammox) are effective processes for wastewater treatment.

The combination of the BNR process with fixed-bed technology has been studied over the last four decades. Various fixed-bed wastewater treatment bioreactors have been developed, such as fluidized bed bioreactors (FBBRs), moving bed bioreactors (MBBRs), biological aerated filter reactors, and upflow anaerobic sludge blanket (UASB) (Andalib et al., 2010). Among them, one kind of FBBR systems, circulating fluidized bed bioreactor (CFBBR) has been extensively studied in lab-scale and pilot-scale for wastewater treatment. The results highlighted the advantages of CFBBR system, including simultaneous carbon/nitrogen/phosphorus removal, long sludge retention time, short hydraulic retention time, and small footprint (Cui et al., 2004; Eldyasti et al., 2010; Nelson et al., 2017). However, although the efficient nutrient removal had been demonstrated by the CFBBR system, high energy consumption was the hurdle for industrial applications due to the required liquid circulation to fluidize carrier particles. Two strategies are considered to reduce the energy consumption – applying new carrier particles and alternating wastewater treatment process. From the hydrodynamic perspectives, carrier particles affect the design and operational conditions of the fluidized beds, which further have impacts on energy consumption. Particles with density slightly lower than water density required less/no liquid velocity to be fluidized in the (gas-)liquid-solid fluidized bed, and this system was defined as inverse fluidized bed. (Fan et al., 1982; Nikolov and Karamanev, 1987). The hydrodynamic properties of several lighter particles have been extensively studied by Sun (2017), which provided basic fluidization knowledge and guidance for the selection of carrier particles in this study. For alternative wastewater treatment pathway, partial nitrification together with denitrification/anammox process was an efficient approach to reduce the overall energy consumption.

1.2 Objectives

The combination of BNR with integrated anoxic/aerobic IFBBR system and application of partial nitrification in the fluidized bed bioreactor are novel and practical ways to realize the reduction of energy consumption for FBBR systems. Several long-term experiments were undertaken to test system performance. The specific objectives of this thesis are as follows:

1) To assess the carbon and nitrogen removal performance of integrated anoxic/aerobic IFBBR system with treating synthetic wastewater, analyze the energy consumption, and identify the bacterial community structure of the biomass.

2) To investigate the carbon, nitrogen, and phosphorus removal performance of this IFBBR system, and develop the IFBBR model in Biowin software.

3) To determine the minimum fluidization velocity of four carrier particles in the liquid-solid fluidized bed and in the gas-liquid-solid fluidized bed.

4) To assess the feasibility of achieving partial nitrification in the fluidized bed bioreactor with S-HDPE particles as carriers for biomass attachment, and explore the maximum loading rate.

1.3 Thesis organization

Chapter 1 presents an overview of the thesis and the rationale behind utilizing inverse fluidized bed as bioreactor as well as an alternative way of partial nitrification-denitrification/anammox for wastewater treatment. The specific research objectives are also provided in Chapter 1.

Chapter 2 provides a comprehensive literature review including the background about (gas-)liquid-solid fluidized bed, biological nutrient removal (BNR) processes, and the particulate biofilm technologies, as well as the modeling for BNR processes.

Chapter 3 is a research article entitled "*Performance and Bacterial Community Structure of a Novel Inverse Fluidized Bed Bioreactor (IFBBR) Treating Synthetic Wastewater*". In this study, six phases were run to treat high-strength and low-strength wastewater by increasing the particle loading and flow rate gradually. The carbon and nitrogen removal efficiencies and the fate of nutrients in the anoxic and aerobic zones were explored. Energy consumption was calculated for this IFBBR system and compared with the CFBBR system. The bacterial community structure of anoxic attached biomass, aerobic attached biomass, and effluent biomass were identified and analyzed. The main drive for this work was to explore the feasibility of achieving biological nutrient removal in the integrated anoxic and aerobic IFBBR system.

Chapter 4 is a research article entitled "*Inverse Fluidized Bed Bioreactor (IFBBR) for Municipal Wastewater Treatment - Performance and Modeling*". The objective of this work was to explore the BNR performance of IFBBR system with high particulate COD wastewater. In this study, the carbon, nitrogen, and phosphorous removal efficiencies were studied at a hydraulic retention time of 3.7 hrs. Organic shock test was conducted to examine the stability of this IFBBR system with the response to the short-term variation of influent COD. A calibrated model was built in Biowin software. The maximum flow rate under the operational conditions was determined by setting the limitations for the system effluent.

Chapter 5 is a research article entitled "*Minimum Fluidization Velocity of Carrier Particles in the (Gas-)Liquid-Solid Fluidized Bed*". In this study, four carrier particles were selected to study the impact of particle diameter and density on minimum fluidization velocity under gas velocities of 0-12.4 mm/s. twenty-four data points were obtained and compared with the predicted data from semiempirical models of Ergun equation for liquid-solid fluidized bed, along with Song et al. and Zhang et al. equations for gas-liquid-solid fluidized bed.

Chapter 6 is a research article entitled "*Effective Partial Nitrification of Ammonia in a Fluidized Bed Bioreactor*", that discussed the feasibility of achieving partial nitrification in the fluidized bed bioreactor with HDPE carrier particles. Five phases with two empty bed contact time and four different influent ammonia concentrations were run to examine

the maximum loading rate. Stable effluent with nitrite-to-ammonia ratio of 1.27 and nitrate concentration of <15 mg/L was maintained at the nitrogen loading rate of 3.6 kg N/(m^3 d) due to the successful suppression of nitrite-oxidizing bacteria activity.

Chapter 7 summarizes the main conclusions of this thesis and the recommendations for future work.

1.4 Thesis format

This thesis is written in the article-integrated format according to the specifications provided by the School of Graduate and Postdoctoral Studies at the University of Western Ontario. Chapter 3 of this thesis is submitted to *Chemical Engineering Journal*. Chapter 4 is prepared to be submitted to *Biochemical Engineering Journal*. Chapter 5 is prepared to be submitted to *Powder Technology* journal. Chapter 6 has been published in *Environmental Technology* journal.

1.5 Scientific contribution

Although CFBBR system was very efficient for carbon, nitrogen, and phosphorus removal from wastewater, high fluidization energy consumption was the main obstacle for the industrial application of CFBBR system. Two approaches were examined to reduce the overall energy consumption – employing new carrier particles that are lighter than water in an inverse fluidized bed and applying new BNR process using partial nitrification/denitrification instead of full nitrogen process.

Chapters 3 and 4 are about using new carrier particles for biomass attachment. A novel IFBBR system with polypropylene beads (average diameter of 3.2 mm and density of 904 kg/m^3) as carriers was initially developed to examine BNR performance for synthetic wastewater treatment. The results showed that this IFBBR system was very efficient for nutrient removal, and saved 59% of the fluidization energy compared to then CFBBR system when treating same amount of THCOD. Bacterial community structures of attached and detached biomass were initially revealed by 16S rRNA sequencing test for integrated nitrification/denitrification IFBBR system. Organic shock test showed that IFBBR system

has good recovery ability in term of influent COD disturbance. A calibrated model was built in Biowin for IFBBR system.

Chapters 5 and 6 are about applying new BNR process. In Chapter 5, for particle selection, the U_{mf} of four carrier particles (L-HDPE, S-HDPE, pottery, and zeolite) were experimentally determined in (gas-)liquid-solid fluidized bed and examined with semiempirical equations. The results showed S-HDPE has the lowest U_{mf} at all gas velocities, which means the fluidization energy required for S-HDPE is lowest among these four particles. With S-HDPE as carriers, stable partial nitrification was achieved by controlling several operational parameters in Chapter 6. At NLR of 3.6 kg N/(m^3 d), stable effluent with NO_2-N/NH_4-N ratio of 1.27 was achieved, which can be directly used as the influent of ANAMMOX process.

References

Andalib, M., Nakhla, G., Zhu, J., 2010. Dynamic testing of the twin circulating fluidized bed bioreactor (TCFBBR) for nutrient removal from municipal wastewater. Chem. Eng. J. 162, 616–625.

Chen, H., Liu, S., Yang, F., Xue, Y., Wang, T., 2009. The development of simultaneous partial nitrification, ANAMMOX and denitrification (SNAD) process in a single reactor for nitrogen removal. Bioresour. Technol. 100, 1548–1554.

Cui, Y., Nakhla, G., Zhu, J., Patel, A., 2004. Simultaneous carbon and nitrogen removal in anoxic-aerobic circulating fluidized bed biological reactor (CFBBR). Environ. Technol. 25, 699–712.

Eddy, M., Burton, F., Tchobanoglous, G., Tsuchihashi, R., 2014. Wastewater engineering : treatment and resource recovery. McGraw-Hill Education

Eldyasti, A., Chowdhury, N., Nakhla, G., Zhu, J., 2010. Biological nutrient removal from leachate using a pilot liquid – solid circulating fluidized bed bioreactor (LSCFB). J. Hazard. Mater. 181, 289–297.

Fan, L.-S., Muroyama, K., Chern, S.-H., 1982. Hydrodynamic characteristics of inverse fluidization in liquid—solid and gas—liquid—solid systems. Chem. Eng. J. 24, 143–150.

Ge, S., Wang, S., Yang, X., Qiu, S., Li, B., Peng, Y., 2015. Detection of nitrifiers and evaluation of partial nitrification for wastewater treatment: A review. Chemosphere 140, 85–98.

Hernández-Sancho, F., Lamizana-Diallo, B., Mateo-Sagasta, J., Qadir, M., 2015. Economic valuation of wastewater: the cost of action and the cost of no action., United Nations Environment Programme (UNEP).

Massara, T.M., Malamis, S., Guisasola, A., Baeza, J.A., Noutsopoulos, C., Katsou, E., 2017. A review on nitrous oxide (N2O) emissions during biological nutrient removal from municipal wastewater and sludge reject water. Sci. Total Environ. 596–597, 106–123.

Nelson, M.J., Nakhla, G., Zhu, J., 2017. Fluidized-bed bioreactor applications for biological wastewater treatment: a review of research and developments. Engineering 3, 330–342.

Nikolov, L., Karamanev, D., 1987. Experimental study of the inverse fluidized bed biofilm reactor. Can. J. Chem. Eng. 65, 214–217.

Okabe, S., Oshiki, M., Takahashi, Y., Satoh, H., 2011. Development of long-term stable partial nitrification and subsequent anammox process. Bioresour. Technol. 102, 6801–6807.

Oleszkiewicz, J.A., Barnard, J.L., 2006. Nutrient Removal Technology in North America and the European Union: A Review. Water Qual. Res. J. 41, 449–462.

Sun, X., 2017. Bubble-Induced Inverse Gas-Liquid-Solid Fluidized Bed. Electron. Thesis Diss. Repos. Western University.

Villaverde, S., 2004. Recent developments on biological nutrient removal processes for wastewater treatment. Rev. Environ. Sci. Bio/Technology 3, 171–183.

Wang, C.-C., Lee, P.-H., Kumar, M., Huang, Y.-T., Sung, S., Lin, J.-G., 2010. Simultaneous partial nitrification, anaerobic ammonium oxidation and denitrification (SNAD) in a full-scale landfill-leachate treatment plant. J. Hazard. Mater. 175, 622–628.

Chapter 2

Literature Review

2.1 Fluidization

2.1.1 Flow regimes

The fluidization technology has been widely applied to chemical processes (Zhu et al., 2000). Depending on the superficial liquid velocity, the flow regimes in the liquid-solid fluidization system can be divided into four parts, including fixed bed regime, conventional fluidization regime, circulating fluidization regime, and transport regime in Figure 2-1 (Liang et al., 1997). There are two critical velocities for particle fluidization – minimum fluidization velocity (U_{lf}) and terminal settling velocity (U_{lt}). In the fixed bed regime, the superficial liquid velocity is lower than the minimum fluidization velocity. With increasing of the superficial liquid velocity, the bed begins to be expended and the liquid-solid system gets into the conventional fluidization regime. In the conventional fluidization regime, two distinguished sections can be observed – dense phase at the bottom and dilute phase at the top. The bed expansion becomes higher and the boundary of dense and dilute phases becomes more unclear with further increasing of the superficial liquid velocity. When the liquid velocity is higher than the terminal settling velocity of particles, some particles will be entrained out of the system and the phenomena of particle entrainment will be more severe with the increase of liquid velocity. If the entrained particles are collected and transported back to the liquid-solid system, radial non-uniform flow structure will be observed, and the fluidized bed is in the circulating fluidization regime. The other condition is to achieve particle replacement and transportation, the liquid-solid fluidization system is in the transport fluidization regime (Grace, 1986; Zheng et al., 1999).

It is important to identify the flow regimes for the industrial application of liquid-solid fluidized bed due to different systems have different operational conditions. For the ion-exchange process of extracting protein from cheese whey, the liquid-solid fluidization system is operated at the circulating fluidization regime (Lan et al., 2002). For the

biological wastewater treatment process, the (gas-)liquid-solid fluidization system is usually operated at the conventional fluidization regime, while circulating fluidized bed bioreactor is operated at the circulating fluidization regime in order to achieve particles exposed to anoxic and aerobic conditions for phosphorus removal (Andalib et al., 2010; Patel et al., 2006).
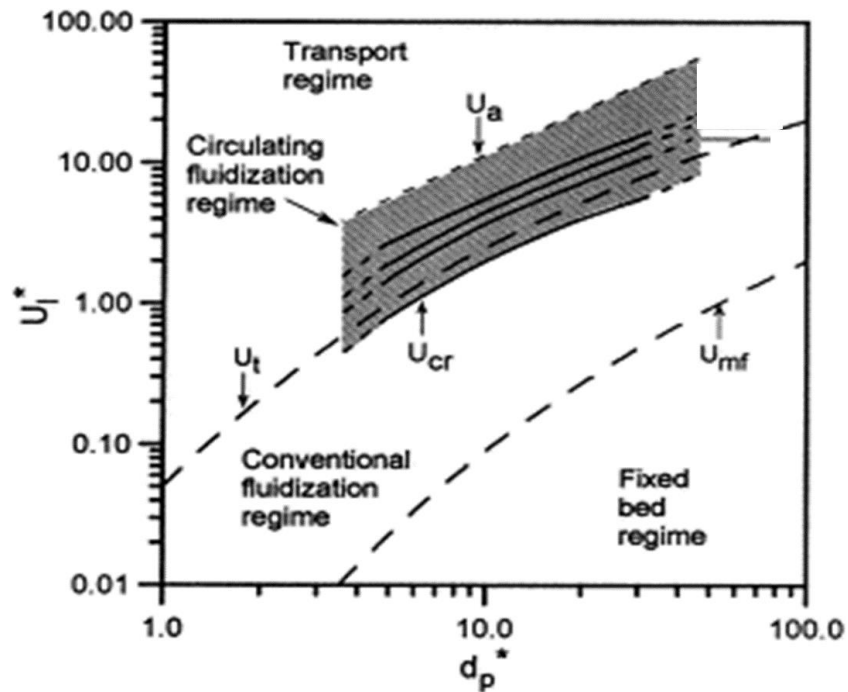
Figure 2-1. The flow regimes of liquid-solid fluidized bed (Liang et al., 1997)

2.1.2 Liquid-solid fluidized bed

In the liquid-solid fluidized bed, liquid phase is the continuous phase and solid phase is the dispersed phase. Bed expansion and the distance among particles increase with the increase of superficial liquid velocity (Fan et al., 1993). Unlike the gas-solid fluidized bed, axial particle distribution is more uniform in the liquid-solid fluidized bed due to the density difference between the liquid and solid phases are much lower than the density difference between the gas and solid phases. Besides, much less turbulence occurs in the liquid-solid fluidized bed. Solid holdup near the wall is usually higher than the solid holdup at the center (Kunii and Levenspiel, 2013). The advantages of liquid-solid fluidized bed include effective liquid-solid contact, uniform particle distribution, and high rates of heat and mass

transfer (Cheng and Zhu, 2008). Liquid-solid fluidized bed has been applied for catalytic liquid reactions, recovery of materials from liquid phase, sedimentation, separation, and wastewater treatment (Epstein, 2002).

Minimum fluidization velocity (U_{lmf}) is an important parameter for particles. It represents the superficial liquid velocity of the transition between fixed bed and fluidized bed. Minimum fluidization velocity is related to particle properties (sphericity, size, and density). The minimum fluidization velocity is usually acquired from the plot of pressure drop versus superficial liquid velocity (Kunii and Levenspiel, 2013). Numerous studies have investigated the minimum fluidization velocity in the liquid-solid fluidized bed, and correlations have been developed to calculate the values of minimum fluidization velocity. The most famous correlations are Ergun equation (Ergun, 1952) along with Wen and Yu equation (Wen and Yu, 1966). Ergun equation is derived from the pressure balance through packed bed in the gas-solid fluidized bed, while is still applicable in the liquid-solid fluidized bed, which is written as:

$$Ar = 150 Re_{mf}(1 - \varepsilon)/(\emptyset^2 \varepsilon^3) + 1.75\ Re_{mf}^2/(\emptyset \varepsilon^3) \tag{2.1}$$

Where

$$Ar = \rho_g(\rho_p - \rho_g)g d_p^3/\mu^2 \tag{2.2}$$

$$Re_{mf} = \rho_g d_p U_{mf}/\mu \tag{2.3}$$

Wen and Yu (Wen and Yu, 1966) developed another equation without knowing of bed voidage by utilizing the data cover particle diameter range from 0.002 to 1.97 in, bed voidage at minimum fluidization from 0.385 to 0.935, and sphericity of 0.136 to 1.0.

$$Re_{mf} = \sqrt{33.7^2 + 0.0408 Ar} - 33.7 \tag{2.4}$$

Richardson-Zaki equation is applied to predict the bed expansion in the liquid-solid fluidized bed based on superficial liquid velocity (Richardson and Zaki, 1997).

$$\frac{Re}{Re_t} = k\varepsilon^n \tag{2.5}$$

This correlation has been demonstrated to be valid for a wide range of operating conditions by many researchers. There are different correlations for calculation of the bed expansion index n, such as:

The Garside and Al-Dibouni correlation (Garside and Al-Dibouni, 1977),

$$n = 4.65 + 20\frac{d_p}{d_c} \qquad Re < 0.2 \qquad (2.6)$$

$$n = \left(4.4 + 18\frac{d_p}{d_c}\right)Re_t^{-0.03} \qquad 0.2 < Re < 1 \qquad (2.7)$$

$$n = \left(4.4 + 18\frac{d_p}{d_c}\right)Re_t^{-0.1} \qquad 1 < Re < 200 \qquad (2.8)$$

$$n = 4.4Re_t^{-0.1} \qquad 200 < Re < 500 \qquad (2.9)$$

$$n = 2.4 \qquad Re > 500 \qquad (2.10)$$

And the Richardson and Zaki correlation (Richardson and Zaki, 1997),

$$\frac{5.1-n}{n-2.7} = 0.1Re_t^{0.9} \qquad (2.11)$$

2.1.3 Gas-liquid-solid fluidized bed

Gas-liquid-solid fluidized bed has been widely applied for chemical, petrochemical, and biochemical engineering. The industrial application includes methanol synthesis, fermentation, aerobic wastewater, Fischer-Tropsch synthesis, and particle collection (Muroyama and Fan, 1985). The hydrodynamic conditions in the gas-liquid-solid fluidized bed are much more complex than that in the liquid-solid fluidized bed. Review papers and books about the hydrodynamic conditions, mass transfer, and heat transfer of gas-liquid-solid fluidized bed have been published since 1968 (Kim and Kang, 1997).

According to the flow directions of the two fluids, the gas-liquid-solid fluidized bed can be classified into three operational models, namely cocurrent (same direction), countercurrent

(opposite direction), and stationary liquid (zero liquid flow rate). The models of expended bed regime in the gas-liquid-solid fluidization are shown in Figure 2-2 (Epstein, 1981). With low gas velocity conditions, the continuous phase is the liquid phase and the system is liquid supported fluidization. For the high gas velocity conditions, the gas phase is the continuous phase and the system is bubble supported fluidization. The system is bubble flow when the superficial liquid velocity is higher than the minimum fluidization velocity, while the system is trickle flow when the superficial liquid velocity is lower than the minimum fluidization velocity.
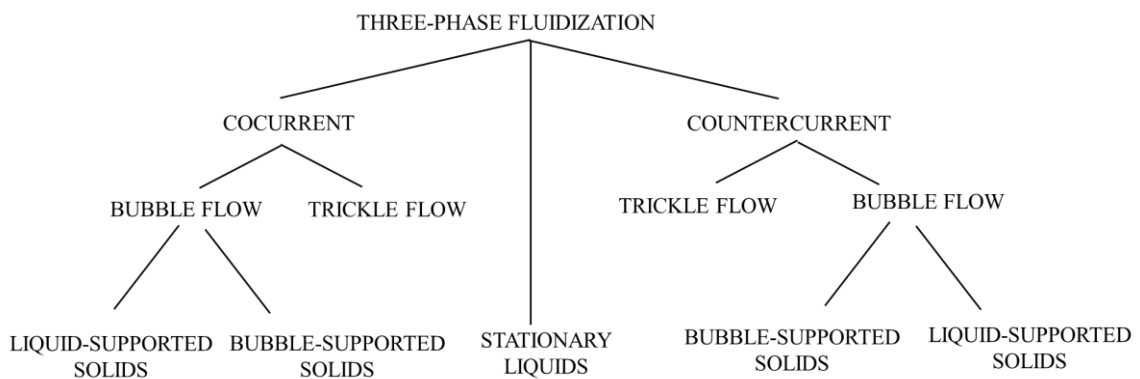
Figure 2-2. Taxonomy of three-phase fluidized beds (Epstein, 1981)

The gas or bubble behavior in the gas-liquid-solid fluidized bed has gained numerous attention due to the turbulence caused by bubbles affects the system performance. The size of bubbles coming out from the gas distributor initially is small. Bubble breakup and coalescence occur with the raising of bubbles into the liquid phase. There are many factors affect bubble behavior, such as gas velocity, liquid velocity, liquid viscosity, and bed dimensions (Darton and Harrison, 1975). Bubble wake is an important phenomenon observed in the gas-liquid-solid fluidized bed (Darton and Harrison, 1976). With the raising of bubbles, there are wakes generated due to the relatively low pressure left behind the bubbles. Small bubble, liquid and solid phase will be sucked into this field, which causes the renew and exchange of phases between this field and the bulk flow, further affects the overall mass and heat transfer. The bubble wake is also the direct reason for the bed contraction before incipient fluidization. Besides, particle entrainment to the top liquid surface is also caused by bubble wakes (Muroyama and Fan, 1985).
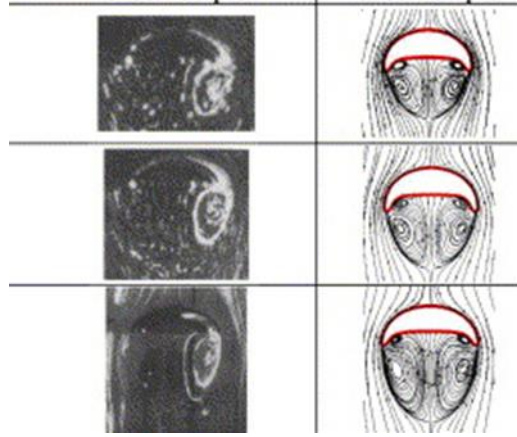
Figure 2-3. Acquired and simulated bubble wakes (Hua and Lou, 2007)

At the incipient fluidization, the effect of gas velocity on solid phase can not be ignored, several semiempirical correlations were proposed for calculating the minimum liquid fluidization velocity in the cocurrent upward gas-liquid-solid fluidized bed.

(Begovich and Watson, 1978),

$$Re_{lmf} = 5.1213 \times 10^{-3} (Ar_l)^{0.6629} (Fr_g)^{-0.118} \tag{2.12}$$

(Song et al., 1989),

$$\frac{U_{lmf}}{U'_{lmf}} = 1 - 376\, U_g^{0.327} \mu_l^{0.227} d_m^{0.213} (\rho_s - \rho_l)^{-0.423} \tag{2.12}$$

(Zhang et al., 1998),

$$Re_{lmf} = \sqrt{[150(1 - \varepsilon_{mf})/3.5\emptyset]^2 + \varepsilon_{mf}^3 (1 - \alpha_{mf})^3 Ar_l/1.75} - 150(1 - \varepsilon_{mf})/3.5\emptyset$$

$$\tag{2.13}$$

Where

$$\alpha_{mf} = \frac{0.16 U_g}{\varepsilon_{mf}(U_g + U_{lmf})} \tag{2.14}$$

(Ramesh and Murugesan, 2002),

$$Re_{lmf} = 0.6(1 + Fr_g)^{-1.85}(Ar_l)^{0.3}(Mo_l)^{-0.09}(\emptyset)^{0.04} \tag{2.15}$$

The correlations were examined with the experimental data, and the error was within 30%.

2.2 Biological nutrient removal process

Eutrophication is a serious issue recently with more nutrients discharged to the rivers and oceans. The accelerated growth of algae and plankton can lead to the depletion of dissolved oxygen in the aquatic system, deterioration of water quality, and threaten the life of aquatic organisms (Smith et al., 1999). The organic organism, ammonia nitrogen, and phosphorus in the wastewater generated by human beings need to be removed to meet the stringent discharge standards (Eddy et al., 2014).

Activated sludge system is widely adopted by many countries as an efficient technology for wastewater treatment since initially invented in 1914 (Barnard, 1975). With the more growth of requirement of advanced technology, various nutrient removal processes have been developed and optimized. The biological nutrient removal (BNR) process has been demonstrated to be a successful modification of the activated sludge process to accomplish nitrogen and phosphorus removal (Ahn, 2006). Nitrification and denitrification are important steps in the BNR process. In the anoxic zone, nitrites or nitrates are the electron acceptors and organic matters are the electron donors for denitrification. In the aerobic zone with supplying of oxygen as the electron acceptors, the ammonia and organic matters are oxidized. Sludge removal is necessary for phosphorus removal. The division of bioreactor into two separate biochemical environments is the successful feature of BNR systems (Ekama and Wentzel, 1999).

2.2.1 Nitrification

Nitrification represents autotrophic oxidation of ammonia to nitrate under aerobic condition. The process is accomplished by two sequential steps: nitritation and nitratation (Sharma and Ahlert, 1977). The first stage nitritation is to convert ammonia to nitrite by ammonia-oxidizing bacteria (AOB) and the second stage is to convert nitrite to nitrate by nitrite-oxidizing bacteria (NOB). In the nitrification process, the reactants ammonia or

nitrite are served as the electron donors and energy sources, with molecular oxygen is used as electron acceptors. Inorganic carbon sources are required in the nitrification process due to both the AOB and NOB are autotrophs (Ge et al., 2015). The stoichiometry of biological nitrification is shown as Equation (2.16), (2.17), and (2.18).

Nitritation: $\quad NH_4^+ + 1.5\ O_2 \rightarrow NO_2^- + 2H^+ + H_2O$ $\hfill$ (2.16)

Nitratation: $\quad NO_2^- + 0.5O_2 \rightarrow NO_3^-$ $\hfill$ (2.17)

Nitrification: $\quad NH_4^+ + 2O_2 \rightarrow NO_3^- + 2H^+ + H_2O$ $\hfill$ (2.18)
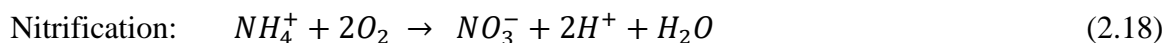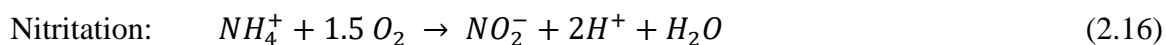
As shown in the equations of nitrification process, theoretically 3.43 g O_2 are utilized for nitritation and 1.14 g O_2 are utilized for nitratation with each g of ammonia nitrogen (as N) consumed. Acid is generated during the reaction, which requires the addition of alkalinity to neutralize the solution. The bicarbonate alkalinity requirement can be estimated base on Equation (2.19).

$$NH_4^+ + 2HCO_3^- + 2O_2 \rightarrow NO_3^- + 2CO_2 + H_2O \qquad (2.19)$$
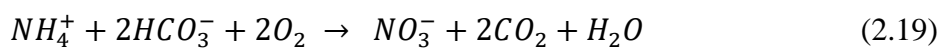
According to the equation above, 7.14 g alkalinity as $CaCO_3$ for oxidizing each g of ammonia is required for the nitrification process.

With consideration of new cells synthesis and unitarization of carbon deoxidate as the carbo1n source during the nitrification process, the overall reaction for complete oxidation of ammonia to nitrate is written as:

$$NH_4^+ + 0.098CO_2 + 1.863O_2 \rightarrow 0.0196\ C_5H_7NO_2 + 0.98NO_3^- + 0.094H_2O +$$
$$1.98\ H^+ \qquad (2.20)$$
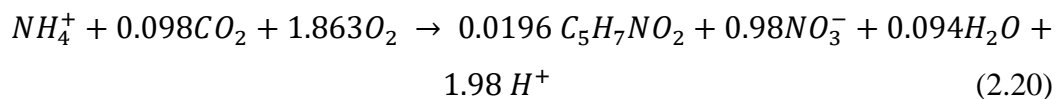
Based on the equation above, for each g of ammonia converted, 4.25 g O_2 is utilized, 0.16 g of new cells are formed, 7.07 g of alkalinity are removed, and 0.08 g of inorganic carbon is utilized for biomass synthesis (Eddy et al., 2014).

Various studies have investigated the genera related to the bacteria of AOB and NOB. The most common genus of AOB is reported as *Nitrosomonas* (Siripong and Rittmann, 2007),

while other genera found in the wastewater treatment bioreactors have the function of oxidizing bacteria, such as *Nitrosopira, Nitrosococcus, Nitrosolobus, Nitrosocystis*, and *Nitrosorobrio* (Prosser, 1990). Meanwhile, the dominant genera for NOB are found as *Nitrobacter*, *Nitrococcus,* and *Nitrospira* (Wagner et al., 1996). Although the function bacteria for nitrification process are AOB and NOB, the bacterial population in the activated sludge process is dominated by heterotrophs, due to the lower growth rate of nitrifying bacteria. The relative abundance and types of these genera present in the biomass are different in various wastewater treatment plants. There are several parameters affected the bacterial community structure, such as influent wastewater ingredients, temperature, location, and inflow loading rates (Wang et al., 2012).

The growth of nitrifying bacteria requires longer solid retention time (SRT) than the heterotrophs, and the SRT is reported as 10-20 d at 10°C and 4-7 d at 20°C. The kinetic parameters are different for AOB and NOB. The maximum specific growth rate of AOB and NOB are 0.4-1.9 d^{-1} and 0.5-1.0 d^{-1}, and the biomass yield of AOB and NOB are 0.15 mg cell/g NH_4-N and 0.02 mg cell/g NH_4-N, with the decay rates of AOB and NOB are 0.05-0.4 d^{-1} and 0.09-0.4 d^{-1}, respectively. The growth of nitrifying bacteria follow the Monod model, there are several parameters affect the growth, such as temperature, pH, and dissolved oxygen. The effect of temperature can be described by the equation of van't Hoff-Arrhenius (Cervantes, 2009),

$$\mu = \mu_{20} \times \theta^{T-20} \tag{2.21}$$

Where μ and μ_{20} represent the growth rates at the current temperature and 20°C, θ is the coefficient of temperature and the common value of θ is 1.123. The effect of temperature on the growth of AOB and NOB is different, so the control of temperature is an effective strategy to suppression the growth of NOB and achieve partial nitrification.

The effect of pH on the nitrification reactions can be divided in two ways- directly impact the enzyme reaction mechanism and indirectly change the equilibrium of ammonium/ammonia (NH_4^+/NH_3) and nitrite/nitrous acid (NO_2^-/HNO_2). There is a suitable range of free ammonia and free nitrous acid for nitrification and usually the optimal conditions for nitrification are at the neutral to moderate alkaline with pH of 7.5-8.0.

Ammonia oxidation rates decline significantly at pH lower than 7.0 (Park et al., 2010). In addition, Nitrification is sensitive to dissolved oxygen concentration. In the activated sludge tank, the DO concentration in bulk liquid is suggested to be above 2 mg/L. However, there are reports that the DO concentration in the aerobic tank was maintained lower than 2 mg/L and good nitrification occurs (Stenstrom and Poduska, 1980). Metals like nickel, chromium, and copper also affect the nitrification rates, and high values of metals are toxic to the nitrifying bacteria (Hu et al., 2003). The values for the biomass specific nitrification rates (SNRs) are in a wide range due to different operating conditions, but usually as 0.10-0.77 g NH_4-N/g (VSS d) for biological nutrient removal systems (Eddy et al., 2014).

2.2.2 Denitrification

Denitrification represents the biological process of reducing nitrates or nitrites to nitric oxide, nitrous oxide, and nitrogen gas (mainly) by heterotrophs with the degradation of organic matter under anoxic conditions. The nitrogen removal is achieved dissimilarly due to the reduction of nitrate/nitrite ions to molecular nitrogen, and small part of nitrate/nitrite being assimilated into the cells (Gerardi, 2002). In the denitrification process, organic matter is utilized as the electron donor and nitrate/nitrite is utilized as the electron acceptor instead of oxygen. The organic matter comes from different forms, such as the readily biodegradable organics (rbCOD), slowly biodegradable organic (sbCOD), and the sbCOD generated through endogenous respiration (Beauchamp et al., 1989). In the wastewater treatment, $C_{10}H_{19}O_3N$ is used to represent the carbon source (Andalib, 2011), and the stoichiometric relationship for denitrification process is shown below:

$$C_{10}H_{19}O_3N + 10NO_3^- \rightarrow 5N_2 + 10CO_2 + 3H_2O + NH_3 + 10OH^- \qquad (2.22)$$
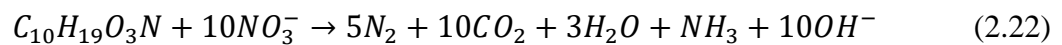
Different organic forms have different stoichiometric reactions, the readily biodegradable organics commonly used as the external carbon sources are acetate and methanol,

$$5CH_3COOH + 8NO_3^- \rightarrow 4N_2 + 10CO_2 + 6H_2O + 8OH^- \qquad (2.23)$$

$$5CH_3OH + 6NO_3^- \rightarrow 3N_2 + 5CO_2 + 7H_2O + 6OH^- \qquad (2.24)$$
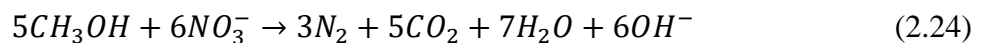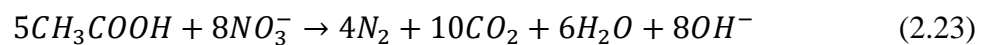
Based on the Equation (2.23), theoretically it consumes 3.51 g of acetate carbon to reduce 1 g of nitrate (as N), and 3.57 g alkalinity is generated, which is half of the alkalinity consumed for each g ammonia (as N) consumed in the nitrification process (Eddy et al., 2014). The actual COD consumption for denitrification can be calculated according to Equation (2.24).

$$\frac{g\ bsCOD}{g\ NO_3-N} = \frac{2.86}{1-1.42Y_n} \tag{2.24}$$

Where Y_n is the biomass yield (g VSS/g COD).

The denitrifying organisms identified in the literature are mostly facultative heterotrophic bacteria, including the genera of *Archromobacter*, *Acinetobacter*, *Flavobacterium, Pseudomonas, Bacillus*, *Chromobacterium*, and *Agrobacterium*. Some of the genera have the alternative function to utilize oxygen for COD removal at aerobic conditions, while some of the genera can perform fermentation at anaerobic conditions in the absence of nitrate and nitrite (McIlroy et al., 2016). For some denitrifiers, they are reported as autotrophs with sulfur compounds as the electron donor instead of carbon source. In this case, the desulfurization and denitrification can be achieved simultaneously. The reported autotrophic denitrifiers include *Thioalkalivibrio denitrificans, Thiohalomonas denitrificans, Thiohalorhabdus denitrificans, Thioalkalivibrio thiocyanodenitrificans,* and *Thiohalophilus thiocyanoxidans* (Shao et al., 2010).

The biomass specific denitrification rates (SDNRs) of bacteria depend on the influent COD components, temperature, the biomass concentrations, and other parameters. One empirical relationship has been proposed to estimate the SDR in the pre-denitrification systems, which relates the SNDR with the food-to-microorganisms ratio (F/M) (Albertson and Stensel, 1994).

$$SDNR = 0.03(F/M) + 0.029 \tag{2.25}$$

The reported SDNRs are within a wide range of 0.04-0.50 g NO$_3$-N/(g VSS d) (Peng et al., 2007). The combination of anoxic and aerobic zones has been commonly used for wastewater plants, including pre-denitrification and post-denitrification processes. In the

pre-denitrification process, liquid recirculation of nitrate is required. The nitrate removal rate is related to the recirculation-to-influent (R/I) ratio, it can be up to 80% with the R/I ratio of 400%.
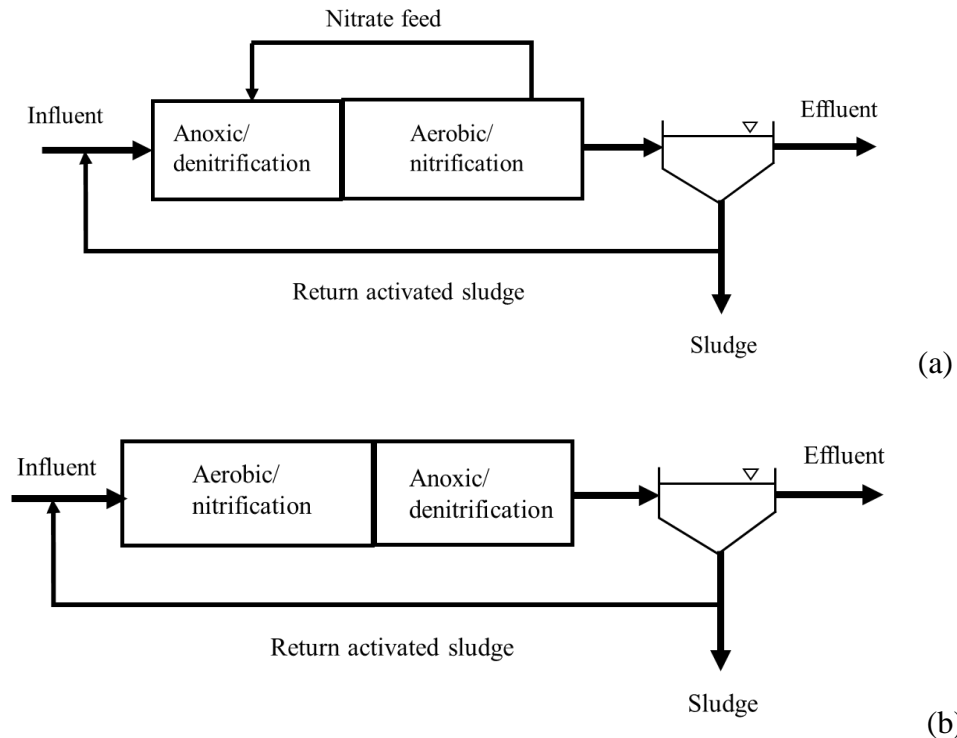
Figure 2-4. Typical denitrification processes and the reactors arrangement: (a) pre-denitrification and (b) post-denitrification (Eddy et al., 2014)

2.2.3 Biological phosphorus removal

Phosphorus is a key nutrient that stimulates the growth of aquatic microorganisms and must be removed from wastewater. The risk of adverse effects on the plant and animal communities in aquatic system declines as phosphorus concentrations approach to the background levels (Mainstone and Parr, 2002). Biological phosphorus removal (BPR) has been adopted by the wastewater treatment plants due to the saving of chemical precipitants. BPR process is accomplished by creating conditions of recirculating the biomass through anaerobic and aerobic zones, which favors the growth of phosphorus accumulating organisms (PAOs). The PAOs has the ability to store phosphate as intracellular polyphosphate and phosphorus removal from the bulk wastewater through enriched PAOs

activated sludge wastage (Ekama et al., 1983). In the anaerobic conditions with the absence of oxygen and nitrate/nitrite as the electron acceptor, microorganisms can not oxidize the organic matter, which provides selective advantages for the growth of PAOs over other heterotrophic bacteria. PAOs can utilize the fermentative products like the volatile fatty acids (VFAs) and store them intracellularly as carbon polymers (poly-b-hydroxyalkanoates (PHAs)). The energy for these bio-transformations is mainly generated by the cleavage of intracellular polyphosphate and releasing of inorganic phosphate. After biomass get in the aerobic zone with the mixed liquor flows, PAOs can use their stored PHAs as the energy source for biomass growth, glycogen replenishment, phosphorus uptake and polyphosphate storage. As a consequence, the proportion of PAOs in the biomass community has increased significantly due to only slowly biodegradable substrate available to the other heterotrophs. Net phosphorus removal from the wastewater is achieved by the removal of activated sludge containing a high content of PAOs (Comeau et al., 1986; Oehmen et al., 2007; Seviour et al., 2003). The phosphorus content of activated sludge is usually in the range of 1.5-2% based on the volatile suspended solids (VSS), while with the enrichment of PAOs, the P/VSS ratio typically increase to 5-7% (Eddy et al., 2014).

The identification of PAOs started from the 1970s, and the genus *Acinetobacter* was first proposed to be the primary organism as PAOs and long believed as the sole PAO present in the wastewater treatment plants (Fuhs and Chen, 1975). With the development of detection technologies such as fluorescence in *situ* hybridization (FISH), 16S rRNA sequencing and denaturing gradient gel electrophoresis (DGGE), other genera are found to have the function of phosphorus removal, i.e. *Accumulibacter* and *Tetrasphaera* (Marques et al., 2017).
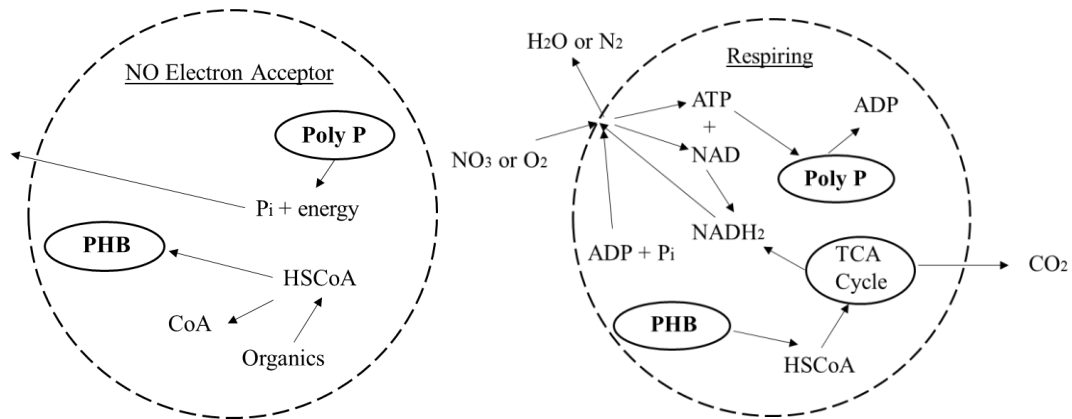
Figure 2-5. Biochemical mechanisms of enhanced biological phosphorus removal
(Rittmann and McCarty, 2012)

2.2.4 Partial nitrification

The nitrification process is the typical solution for ammonia removal, including two steps of converting ammonia to nitrite by AOB and nitrite to nitrate by NOB. Under normal conditions, the oxidation of ammonia to nitrite is a rate-limiting step and nitrite can be rapidly oxidized to nitrate, which results in the seldom accumulation of nitrite in the nitrifying reactors. With realizing of nitrite as the intermediary compound in both nitrification and denitrification steps, partial nitrification emerged as an alternative technology of BNR process for various strong nitrogenous wastewater treatment, such as landfill leachate, animal wastes, and low carbon-to-ammonia wastewater (Ciudad et al., 2005; Peng and Zhu, 2006). The feasibility of achieving the short-cut nitrification and denitrification process has been studied widely in the past decades. Compared with the conventional BNR process via nitrate, the main advantages of the short-cut BNR process are listed below (Ge et al., 2015; van Kempen et al., 2001):

1) 25% lower oxygen consumption in the aerobic zone,
2) The electron donor (mainly carbon) requirement in the anoxic zone can be saved up to 40%
3) Denitrification rate is 1.5-2 times higher
4) About 35% reduction of sludge in nitrification process and 55% in denitrification process.

The pathway of partial nitrification-denitrification is shown in Figure 2-6.
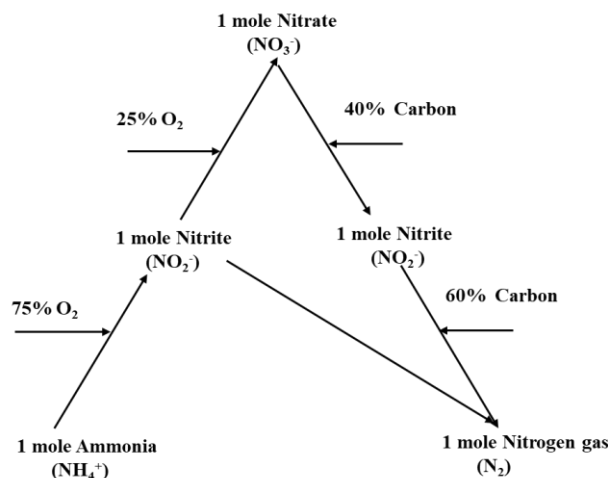
Figure 2-6. The pathway of (short-cut) nitrification and denitrification process

The enrichment of AOB and the suppression of NOB are required to accumulate nitrite. There are numerous control strategies have been developed to achieve and maintain partial nitrification. The controlled parameters include dissolved oxygen concentration, temperature, pH, SRT, and inhibitors (X. Liu et al., 2017). These parameters affect the kinetics of AOB and NOB.

DO is the substrate for both AOB and NOB, and the competition between AOB and NOB for DO affect their growth. The oxygen half saturation concentrations for AOB and NOB are 0.2-0.4 mg/L and 12-1.5 mg/L, respectively (Picioreanu et al., 1997). The relatively low oxygen half-saturation concentration for AOB means low ambient oxygen concentration is more restrictive for the growth of NOB than AOB. As reported, when the nitrifying reactor is operated at DO concentration of lower than 1.0 mg/L, the growth rate of AOB is 2.56 times higher than the growth of NOB (Tokutomi, 2004). Ruiz et al. (2003) observed ammonium accumulation with DO below 0.5 mg/L and complete nitrification to nitrate with DO over 1.7 mg/L. The suggested DO concentration for achieving partial nitrification is 1.0-1.5 mg/L with consideration of both ammonia oxidation rate and nitrite accumulation.

Both the growths of AOB and NOB are sensitive to temperature. When the temperature is higher than 15°C, the growth of AOB is faster than the growth of NOB and the difference of specific growth rate became larger with the increase of temperature. The recommended temperature for distinguishing AOB and NOB was higher than 25°C (Balmelle et al., 1992). The temperature highest activity is 35°C for pure AOB-*Nitrosomonas* and 38°C for NOB-*Nitrobacter* (Grunditz and Dalhammar, 2001). The temperature in one successful partial nitrification-denitrification process of SHARON was maintained at 35°C to accumulate nitrite, which achieved stable partial nitrification for two years in the lab-scale batch reactor and then applied to the full-scale of 1800 m^3 for rejection wastewater treatment (Mulder et al., 2001; van Dongen et al., 2001).

pH affects the growth of AOB and NOB directly by changing the mechanism of enzymatic reaction or indirectly by free ammonia (FA) and free nitrous acid (FNA). due to different inhibition on AOB and NOB, pH control is the commonly used method to achieve partial nitrification. Usually, pH ranging from 7.5 to 8.5 is recommended for nitrite accumulation (Pambrun et al., 2008; Park and Bae, 2009). FA and FNA are related to pH, temperature, ammonia or nitrite concentration. The correlations for FA and FNA calculation are listed below (Anthonisen et al., 1976):

$$FA = \frac{17}{14} \times \frac{TAN}{[\exp\left(\frac{6344}{273+T}\right)+10^{pH}]} \tag{2.26}$$

$$FNA = \frac{47}{14} \times \frac{TNN}{\left[\exp\left(\frac{-2300}{273+T}\right)\times10^{pH}\right]+1} \tag{2.27}$$

Where TAN is the total ammonium nitrogen, mg N/L; TNN is the total nitrite nitrogen mg N/L.

FA affects the activities of both AOB and NOB, while the reported inhibition values varied from studies. The first reported FA to inhibit AOB and NOB were 10-150 mg N/L and 0.1-1.0 mg N/L, respectively (Anthonisen et al., 1976). Bae et al. (2001) reported that influent FA concentrations at 0.1-4.0 mg/L were inhibitory to NOB. Blackburne et al. (2008) found that no inhibition to AOB at FA of up to 33 mg N/L. In addition, FNA is a crucial factor for NOB inhibition at low pH condition of (<7.5) (Sinha and Annachhatre, 2007). 50%

reduction of AOB activity occurred with FNA in the range of 0.42-1.72 mg/L, while NOB activity was inhibited at FNA of 0.011-0.07 mg N/L and complete inhibition of NOB activity at FNA of 0.026-0.22 mg N/L (Zhou et al., 2011).

The difference between the maximum specific growth rates of AOB and NOB makes it important to control SRT for achieving partial nitrification. At 35°C, the minimum doubling times for AOB and NOB were 7-8 h and 10-13 h, respectively (Peng and Zhu, 2006). Short SRT benefits the growth of AOB over NOB. In the full-scale SHARON process, SRT was maintained as 1-2.5 days for partial nitrification (van Kempen et al., 2001), while in a CSTR system, the SRT was 3 days for washing out of NOB (Ahn et al., 2008). All the controlled parameters should be synthetically considered, and real-time control system with automatic feed-forward capability is a more reliable strategy for achieving stable partial nitrification (Zanetti et al., 2012).

2.2.5 Anammox

Anammox represents of anaerobic ammonium oxidation, which is an alternative approach for nitrogen removal. In the anammox process, ammonium is oxidized by the electron acceptor nitrite other than organic carbon source. The anammox process occurs in nature and is responsible for more than 50% of the nitrogen turnover in marine environments (He et al., 2015). The bacteria involved in the anammox process belong to the group *Planctomycetes*, which has a slow growth rate and is strict anaerobic autotrophs (Jetten et al., 2001). CO_2 is the sole carbon source for anammox bacteria. The stoichiometry of the overall anammox metabolic reaction with cell synthesis is shown in Equation (2.28).

$$NH_4^+ + 1.32NO_2^- + 0.066HCO_3^- + 0.13H^+ \rightarrow 1.02N_2 + 0.256NO_3^- +$$
$$0.066CH_2O_{0.5}N_{0.15} + 2.03H_2O \tag{2.28}$$
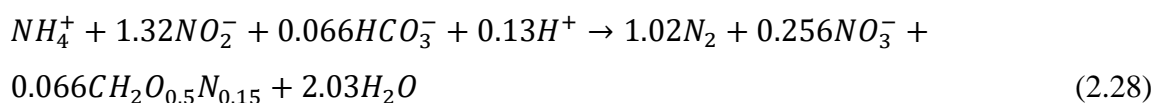
As indicated by the equation above, the optimum influent for the anammox process is with the nitrite to ammonium ratio of 1.32. Compared with the denitrification with nitrate, the anammox process requires less energy and carbon source, and produce less sludge (Mulder et al., 1995). Nitrifying sludge, denitrifying sludge, and anaerobic granular sludge from the wastewater treatment plants have been used as the inocula of anammox bacteria (Hu et al.,

2013; Jin et al., 2008; H. Li et al., 2012). Due to the slow growth rate of anammox bacteria, many efforts have been implemented to increase the reaction rate and maintain the steady performance of the anammox process. The anammox bacteria have been successfully cultivated in the sequencing batch reactor (SBR), upflow anaerobic sludge blanket (UASB), airlift reactor, membrane bioreactors (MBR), and upflow biofilters (UBF) (Ibrahim et al., 2016). The fixe-bed bioreactors are applicable to enrich the slow growth microorganisms. There are several parameters affect the growth of anammox bacteria, such as the substrate concentrations, dissolved oxygen, temperature, pH, and organic matter (Jin et al., 2012). For most successful running of the anammox process, temperature was controlled at around 35°C (Dosta et al., 2008). The representative lab-scale studies including UASB granular sludge system by Tang et al. (2011), MBR biofilm system by Ni et al. (2010), and SBR flocculent sludge system by Dapena-Mora et al. (2004). For the full-scale anammox process, a 900 m^3 reactor for distillery wastewater treatment and a 1760 m^3 reactor for reject wastewater treatment were reported (Ni and Zhang, 2013).

Anammox organisms belong to the same monophyletic order *Brocadiales*, and are related to the order *Planctomycetales*. The species found in wastewater are *Kuenenia stuttgartiensis, Anammoxoblobus propionicus, Jettenia asiatica, Brocadia anammoxidans, Brocadia fulgida, Scalindua wagneri*, and *Scalindua brodae* (Jetten et al., 2001; Kuenen, 2008).

2.3 Particulate biofilm technologies

2.3.1 Carrier particles for biomass attachment

Particulate biofilm technologies employ particles as the carriers for biomass attachment. The large specific surface area provided by carriers with small diameters will result in biomass accumulation and facilitate the enrichment of slow growth microorganisms (C. Nicolella et al., 2000). Besides, the suspension or fluidization of bioparticles increases the contact area between the wastewater and biomass, which increase the system nutrient removal efficiencies. These characteristics make particulate biofilm technologies outcompete the suspended growth system with the advantages of small footprint, high

loading rates, and low biomass yield (Boltz et al., 2010). There are many types of particulate biofilm reactors and various particles were used as the carriers in these bioreactors. The main bioreactors include airlift bioreactor, moving bed bioreactor (MBBR), and fluidized bed bioreactor (FBBR) (Guo et al., 2005; Nelson et al., 2017; Plattes et al., 2006).

Biofilm accumulation is a dynamic process including the adhesion, growth, and detachment processes, which is affected by several external aspects, such as the wastewater characteristics, the velocities of gas and liquid phases, shear stress implemented on bioparticles, filling ratio of particles, particle-particle collisions, and particle-wall collisions (Eldyasti et al., 2012a). The bonds of biomass depend on the extracellular polymeric substances (EPS) produced during the bioreactions (Li et al., 2008). However, the properties of carrier particles play significant roles for determining the initial biomass attachment and the strength between biofilm and carriers in the particulate biofilm reactors. The characteristics of carrier particles include size, shape, porosity, density, surface roughness. Besides, the selection of carrier particles also affect the initial investment and the stability of long-term running (Dempsey et al., 2005).

Various particles are chosen as the carriers for biofilm attachment in the particulate biofilm technologies. The carriers include organic, inorganic, and mixture materials. Bioparticles with high roughness, large specific surface area, high porosity, and coated inorganic materials are reported to benefit the biomass attachment (Eldyasti et al., 2012a). Table 2-1 summarizes the carrier particles used in the airlift reactor, MBBR, and FBBR systems. For most of carriers used in the airlift, MBBR, and inverse FBBR systems, the materials are organic due to the density lower than the density of water. In the conventional FBBR system, inorganic materials are usually used as the carriers due to the properties of easily acquired and high porosity (Wang et al., 2019; Zinatizadeh and Ghaytooli, 2015).

Table 2-1. Summary of carrier particles used in fixed-bed bioreactors

Bioreactor	Name	Material	Dimensions		Specific surface area (m^2/m^3)	References
			Length (mm)	Diameter (mm)		
Airlift	Expanded polystyrene	Expanded polystyrene		0.8-1.6	3750-7500	(Loh et al., 2005)
Airlift	Beads	Expanded polystyrene		1.0-1.18	5080-6000	(Loh and Liu, 2001)
Airlift	Basalt	Basalt		0.09-0.30		(Garrido et al., 1997)
MBBR	AnoxKaldnes™ K1	HDPE	7	9	500	(Barwal et al, 2014)
MBBR	AnoxKaldnes™ K2	HDPE	15	15	350	(Barwal et al, 2014)
MBBR	AnoxKaldnes™ K3	HDPE	12	25	500	(Barwal et al, 2014)
MBBR	AnoxKaldnes™ Natrix C2	HDPE	30	36	220	(Barwal et al, 2014)
MBBR	AnoxKaldnes™ Chip M	HDPE	2.2	48	1200	(Barwal et al, 2014)
MBBR	FLOCOR-RMP	PP	10	15	260	(Andreottola et al., 2000b)
MBBR	FLOCOR-RS	PP	35	35	230	(Andreottola et al., 2000a)
MBBR	Seimens-Biosphere	PE	9	13	800	(Barwal et al, 2014)
MBBR	Seimens-Spira 12	PE	12	12	650	(Barwal et al, 2014)

MBBR	Z400			0.4	30	0.0013 mm^2/carrier	(Piculell et al., 2016)
MBBR	Z50			0.05	30	0.0011 mm^2/carrier	(Piculell et al., 2016)
Conventional FBBR	Lava rock	Lava rock		0.3-1.0		9200	(Cui et al., 2004)
Conventional FBBR	Zeolite	Zeolite		0.4-0.7		1.85 m^2/g	(Andalib et al., 2014)
Conventional FBBR	Silica sand	Silica sand		0.2			(Sen and Dentel, 1998)
Conventional FBBR	Clay schists	Clay schists		5.0-7.0			(Gálvez et al., 2003)
Conventional FBBR	Maxi-blast plastic	Plastic		0.6-0.85		0.72 m^2/g	(Eldyasti et al., 2012a)
Conventional FBBR	Cylindrical PVC	PVC	2.54	3.68		1250	(Ulson et al., 2008)
Inverse FBBR	Perlite	Perlite		0.9		6200	(Garcia et al., 1998)
Inverse FBBR	Sepiolite	Sepiolite		0.25-0.6			(Arnaiz et al., 2006)
Inverse FBBR	Extendosphere	Silica		0.175		34200	(Buffière et al., 2000)

2.3.2 Airlift bioreactor

Airlift reactor is a multi-phase pneumatic agitated reactor. It is well recognized as an efficient contactor for the reactions of gas, liquid, and solid phases. Airlift reactors consist of four distinct functional sections-riser, downer, bottom gas distributor, and phase separator at the top (Zhang et al., 2017). The riser and downer are parallel in the vertical direction and connected. Different configurations are designed as the modification of traditional airlift reactors, including internal loop and external loop. geometry, operation, and hydrodynamic parameters are the main parameters to characterize different airlift reactors. The driving force of the airlift reactors is mainly the hydrostatic pressure difference at a steady state and the kinetic energy of rising bubbles. Liquid circulation is caused by the difference of fluid density between the riser and the downer. The higher gas holdup in the riser results in higher liquid circulation velocity, while the correlation is not linear (C. Nicolella et al., 2000). Two situations happen to the particles - staying in the downer and circulating with the circulation of liquid.

The density of particles used in the airlift bioreactor is lower than the density of wastewater. Airlift bioreactor has been applied for aerobic and anaerobic wastewater treatment. In the aerobic treatment system, air was used as the gas phase. The well mixing of wastewater and biomass ensures optimal contact efficiency (Chisti and Moo-yong, 1987). One of the commercial aerobic airlift bioreactors is named as CIRCOX (Figure 2-7), which has high nutrient loading of 4-10 kg COD/(m^3 d), high biomass concentration of 15-30 kg/m^3, and short hydraulic retention time (HRT) of 0.5-4 h (Nicolella et al., 2000). The high SRT enables specialized growing microbes to stay in the reactor, like the nitrifiers, anammox bacteria. In order to meet the stringent nitrogen discharge standards, a CIRCOX reactor in combination with a denitrifying CIRCOX reactor in pilot-scale was built up to treat the municipal wastewater at Zaandam, Netherlands. The carrier particles used in the CIRCOX process are basalts with diameter in the range of 90-300 μm (Frijters et al., 1997). TURBOFLO is an internal circulating airlift biofilm reactor with high-density polyethylene beads (size of 0.5-2.5 mm and density of 860 kg/m^3) as the carriers (Figure 2-8). Both the lab-scale and pilot-scale of TURBOFLO were successfully used for secondary and tertiary

wastewater treatment (Lazarova and Manem, 1996). In the anaerobic treatment system, nitrogen, self-produced gas or air are used as the gas phase, the anaerobic airlift bioreactors are usually applied to industrial wastewater treatment. The combination of anaerobic and aerobic airlift reactors are comprised of BIOPAQ-IC and CIRCOX technology (Figure 2-9), which was established at Grosch brewery, Enschede, Netherlands. The system achieved average 80% TCOD and 94% SCOD removal efficiencies at HRT of 2.2h and 1.3h in the BIOPAQ-IC and CIRCOX reactors, respectively. The wastewater treated in this technology was brewery wastewater, with a flow rate of 4200 m^3/d, TCOD of 2500 mg/L, TSS of 750 mg/L (Andalib, 2011). The other application of airlift bioreactor is external loop inversed bioreactor (Figure 2-10) with expanded polystyrene beads (diameter of 1.0-1.18 mm and density of 713 kg/m^3) as the carriers for immobilizing *Pseudomonas putida* ATCC11172 bacteria. This reactor is used to treat phenol wastewater with concentration of up to 3000 mg/L in batch mode, and found that phenol degradation started after 1-3 days (Loh and Liu, 2001).
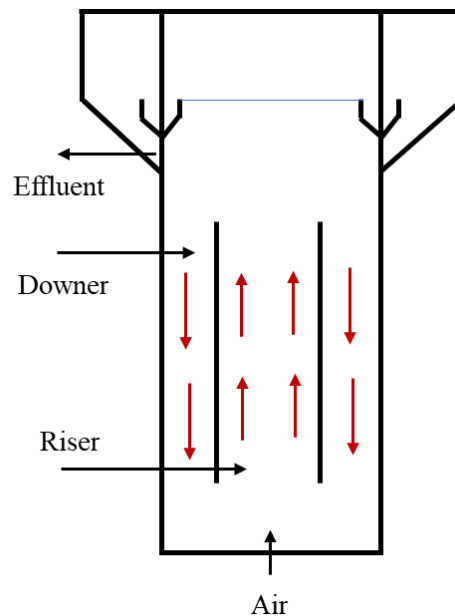
Figure 2-7. Schematic of CIRCOX airlift bioreactor (Frijters et al., 1997)
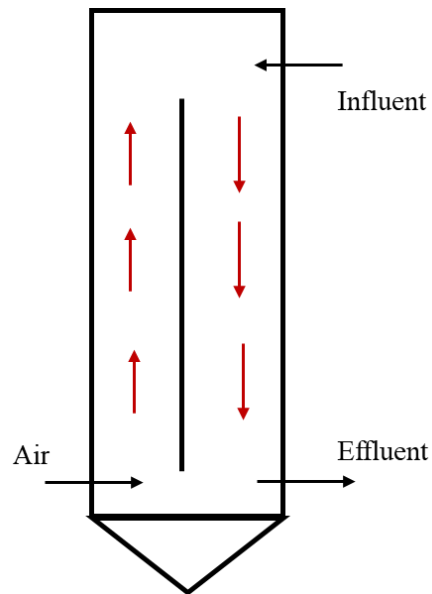
Figure 2-8. Schematic of TURBOFLO airlift bioreactor (Lazarova and Manem, 1996)
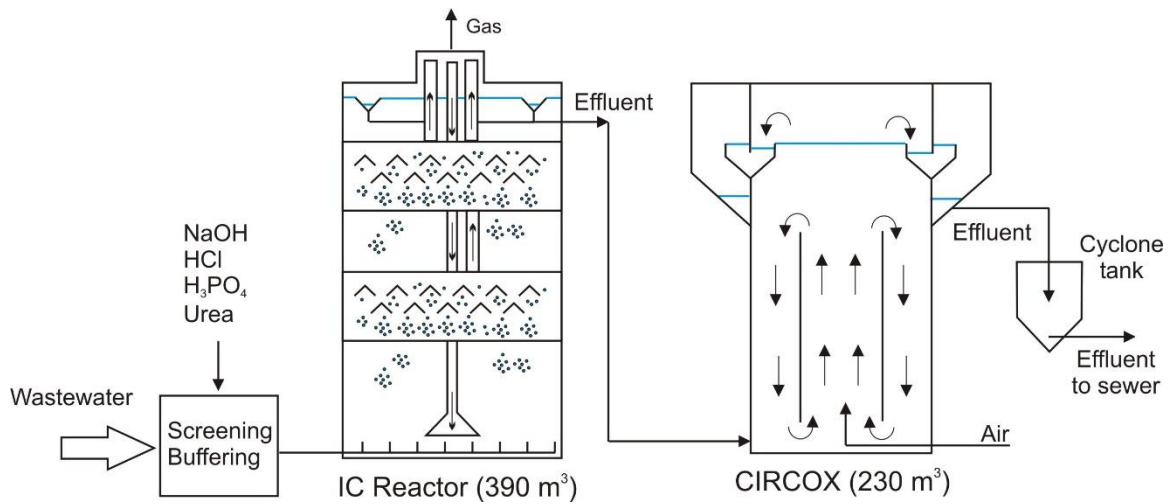
Figure 2-9. Schematic of BIOPAQ-IC and CIRCOX airlift bioreactor (Andalib, 2011)
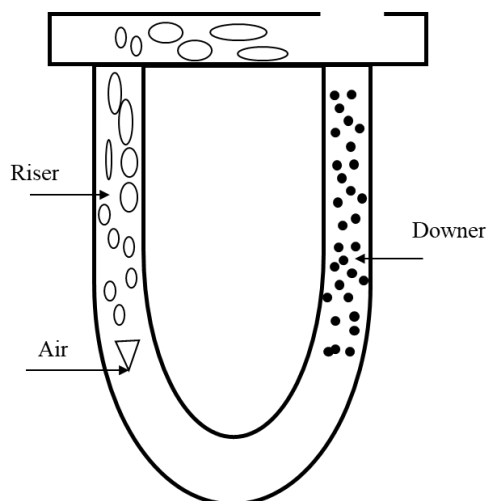
Figure 2-10. Schematic of external airlift bioreactor (Loh and Liu, 2001)

2.3.3 Moving bed bioreactor

Moving bed biofilm reactor (MBBR) is a type of biofilm wastewater treatment process that was first invented at Norwegian University of Science and Technology in the late 1980s (Kermani et al., 2008). MBBR systems incorporate the benefits of both attached and suspended growth systems. It has the advantages of compacted footprint, high biomass concentration, low biomass yield, no requirement for backwashing, and long sludge retention time. The key parameter of the MBBR technology is the carriers for biomass attachment. Unlike other particulate biofilm technologies, the carriers used in MBBR systems have hollow insides with the protection of walls. Microorganisms grow in the internal structures of the biocarriers, which degrade the pollutants (Ali Kawan et al., 2016). The fluidization methods of MBBR systems are shown in Figure 2-11. In the anaerobic or anoxic zones, the movement of carriers is aided by the mechanical stirring, while in the aerobic zone, the carriers move with the hydraulic directions caused by the gas distributors. In all MBBR systems, carriers move freely in the reactor and usually the shear force implemented on the carriers are relatively high, which result in that rare biomass grow on the out surface of the carriers (Barwal and Chaudhary, 2014).
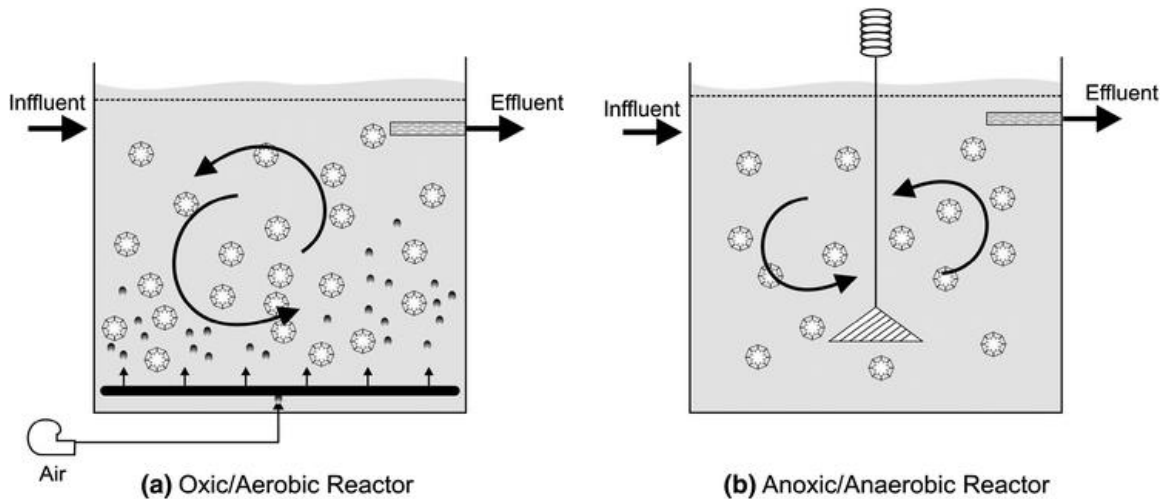
Figure 2-11. Fluidization methods of MBBR system (a) aeration, (b) mechanical stirring (Barwal and Chaudhary, 2014)

MBBR systems have been studied extensively over the past decades. Table 2-2 summarized the typical application of MBBR systems. As shown in Table 2-2, the successful application of MBBR systems in municipal and industrial wastewater treatment include paper industrial wastewater, sewage wastewater, phenolic wastewater, refinery wastewater, pharmaceutical wastewater, and dairy wastewater, etc. The feasibility of the combination MBBR system with the biological nutrient removal processes of carbon removal, nitrification, denitrification, partial nitrification, and anammox has been studied, which demonstrated MBBR system is a very efficient particulate biofilm technology. Presently, more than 400 large scale wastewater treatment plants employ MBBR system as their biological reaction processes.

Table 2-2. Summary of typical MBBR processes

Application	Process	treatment performance	References
Dairy wastewater	aerobic carbon removal	60%-85% COD removal at OLR of 12-21.6 kg COD/(m^3 d)	(Rusten et al., 1992)
Paper wastewater	aerobic carbon removal	70% COD removal at OLR of 25 kg COD/(m^3 d)	(Broch-Due et al., 1994)
Municipal wastewater	nitrification and aerobic carbon removal	76% TCOD and 92% NH$_3$-N removal at NLR of 0.12 kg N/(m^3 d)	(Andreottola et al., 2000b)
Cheese	aerobic carbon removal	87-97% COD removal at OLR of 3.3 kg COD/(m^3 d)	(Rusten et al., 1996)
Municipal wastewater	nitrification and denitrification	91% COD, 80% TKN, and 95% P removal at wide loading rates	(Ødegaard, 2006)
Municipal wastewater	simultaneous nitrification and denitrification	78% COD, 99% NH$_3$-N, and 42% TN removal at OLR of 1.7 kg COD/(m^3 d)	(Wang et al., 2006)
Municipal wastewater	nitrification and denitrification	96.9% COD, 84.6% TN, and 95.8% P removal at OLR of 0.5 kg COD/(m^3 d) and NLR of 25-125 g N/(m^3 d)	(Kermani et al., 2008)
synthetic wastewater	partial nitrification	91% ammonia removal and 90% nitrite accumulation at start-up period	(Liu et al., 2017)
synthetic wastewater	partial nitrification-anammox	ammonium conversion dropped from an average of 40 g N/(m^3 d) at 20 °C to about 15 g N/(m^3 d) at 10 °C.	(Gilbert et al., 2014)

2.3.4 Fluidized bed bioreactor

Fluidized bed bioreactor (FBBR) is the application of fluidized bed technology in the field of wastewater treatment for biological nutrient removal. Due to enhanced mass transfer between different phases after particles being fluidized, the investigation of fluidized bed bioreactors has gained numerous interests in the last several decades. Same as other particulate biofilm technologies, fluidized bed bioreactor requires particles to be the carriers for biofilm attachment, while the particles used in the fluidized bed bioreactors have smaller diameters than the particles used in the airlift bioreactors or MBBRs (Nelson et al., 2017). With liquid fluidization or bubble-induced fluidization, the particles distribute uniformly in the bioreactors, which can reduce the attrition between bioparticles, resulting in less biofilm detachment. Unlike the biofilm formed on MBBR carriers, the biofilm usually attach on the out surface of FBBR carriers (Bello et al., 2017). According to the density of carriers, fluidized bed bioreactors can be divided into two categories – conventional fluidized bed bioreactor and inverse fluidized bed bioreactor (Figure 2-12).
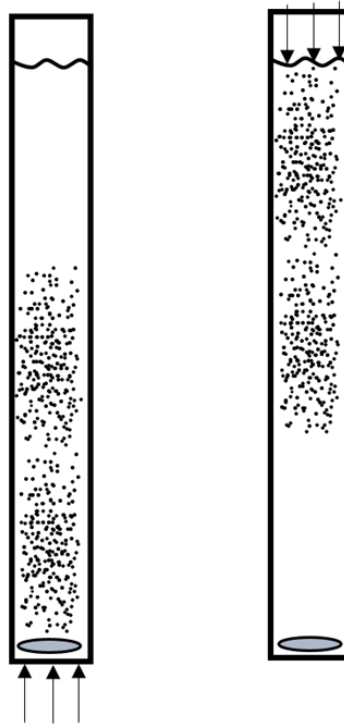
Figure 2-12. Compassion of conventional and inverse fluidized bed bioreactors

In the inverse fluidized bed bioreactors, the density of carriers is little lower than the density of water. The fluidization methods include bubble-induced in the aerobic zone and liquid fluidization in the anoxic/anaerobic zone. Most of the studies were carried out for high-strength organic wastewater under anaerobic conditions, which demonstrated the high COD removal efficiencies of inverse FBBR system at high organic loadings (Heijnen et al., 1989).

For the conventional FBBR system, the density of carriers is higher than the density of water. Upward-moving liquid is required to fluidize the carriers. The superficial liquid velocity should be operated higher than the minimum fluidized velocity of carriers for bed expansion and lower than the terminal settling velocity of carriers for prevention of particle entrainment, while in some cases for achieving particle exchanging of different environmental scenarios, the superficial liquid velocity should be higher than the terminal settling velocity, like the circulating fluidized bed bioreactor (CFBBR system) (Chowdhury et al., 2008; M. Li et al., 2012; Patel et al., 2006). For the early investigation of FBBR, Weber and his coworkers studied the physicochemical treatment of raw sewage with granular activated carbon as the carriers (Weber et al., 1978). CFBBR system has been studied over the last two decades by Dr. Zhu and Dr. Nakhla. It consists of two connected fluidized beds serve as anoxic zone and aerobic zone, respectively (Figure 2-13). Lava rock (diameter of 0.6-1.0 mm, true density of 2620 kg/m^3) and zeolite (diameter of 0.4-0.7 mm, true density of 2360 kg/m^3) were used as the carriers, which provided large specific surface area for biomass attachment (Nelson et al., 2017). Both the lab-scale and pilot-scale CFBBRs have demonstrated the high nutrient removal efficiencies. Without particle circulation between the anoxic and aerobic zones, the CFBBR system could achieve achieved more than 90% organic, 75-80% total nitrogen removal for municipal wastewater treatment at HRT of 2-3h, and additional 85% phosphorous removal with particle recirculation. The biomass yield in the CFBBR system is very low, as 0.07-0.16 g VSS/g COD. CFBRR system has been applied to treat municipal wastewater, landfill leachate, thin stillage, and primary sludge (Andalib et al., 2010; Eldyasti et al., 2010).
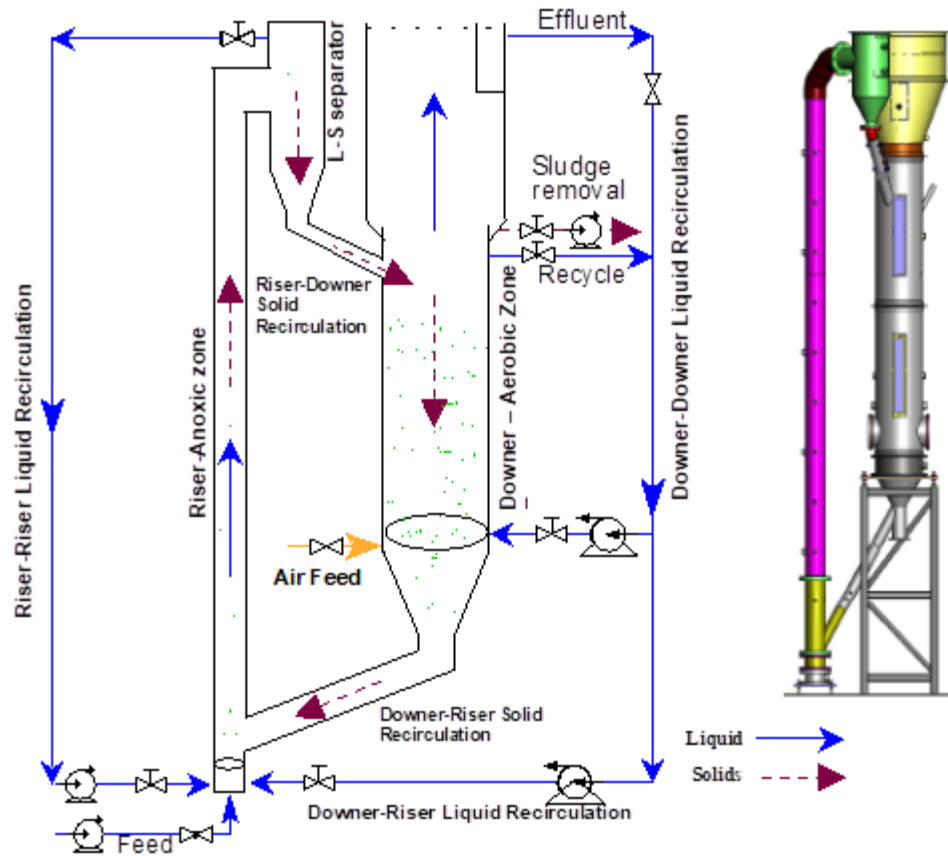
Figure 2-13. Schematic diagram of the CFBBR system (Andalib, 2011)

2.4 Mathematical modeling

Numerical analysis and modeling of biological nutrient removal (BNR) biofilm process have been studied over the last decades. The purpose of mathematical modeling is to improve the understanding of the general process and predict the system responses of certain circumstance. For modeling of the BNR process, activated sludge models (ASM1, ASM2, ASM3) proposed by International Water Association (IWA) have been widely adopted (Henze et al., 2000). In these models, the mass balance and stoichiometry of major components were considered, along with appropriate kinetics from the wastewater treatment plants were used for the Monod model. These ASM models include the processes of carbon oxidation, nitrification, denitrification, and biological phosphorus removal. ASM

models are applicable for complete mixed activated sludge systems, while mass transfer limitations should be considered for the BNR biofilm processes. Five mathematical classes have been published for biofilm models, including analytical, pseudo-analytical, one-dimensional numerical, two-dimensional numerical, and three-dimensional numerical. Among them, the one-dimensional numerical model is widely used in various user-friendly software due to the consideration of the balance between the simplicity and complexity of mechanistic approach (Gujer et al., 1999; Henze et al., 1999; Vanrolleghem et al., 1999).

In the one-dimensional numerical model, a set of mass balance equations for mixed-culture biofilms are developed to describe the progression of biofilm thickness, spatial distribution and development of particulate and dissolved components in the biofilm as a function of transport and transformation processes (Wanner and Reichert, 1996). Iteration is necessary to get the solution for these equations, which requires numerous computation capability. Currently, the popular software for biofilm model includes BioWin® (Envirosim Associates Ltd., Burlington, ON), AQUIFAS® (Aquaregen, Mountain View, CA), GPS-X® (Hydromantis Inc., Hamilton, ON), WEST® (Mostforwater, Belgium). Pro-2D® (CH2M HILL, Inc., Colorado, US), and STOAT® (WRC, Wiltshire, England). These one-dimensional models consider the mass flux, the competition of different microbial species for substrates, conversation laws, multiple diffusion layers inside the biofilms, and liquid boundary layers, while some processes are simplified, such as attachment and detachment rates. The operational conditions and hydrodynamic characteristics of reactors have great impacts on the overall performance of BNR biofilm systems (Chowdhury et al., 2010; Eldyasti et al., 2012b).

References

Ahn, J.H., Yu, R., Chandran, K., 2008. Distinctive microbial ecology and biokinetics of autotrophic ammonia and nitrite oxidation in a partial nitrification bioreactor. Biotechnol. Bioeng. 100, 1078–1087.

Ahn, Y.-H., 2006. Sustainable nitrogen elimination biotechnologies: A review. Process Biochem. 41, 1709–1721.

Albertson, O.E., Stensel, H.D., 1994. Aerated Anoxic Biological NdeN Process. Water Sci. Technol. 29, 167–176.

Ali Kawan, J., Abu Hasan, H., Jaafar, O., Suja, F., Bin Jaafar, O., Abd-rahman, R., 2016. 1098-1120 A Review on Sewage Treatment and Polishing using Moving. J. Eng. Sci. Technol. 11.

Andalib, M., 2011. Biological Nutrient Removal from Municipal and Industrial Wastewater Using a Twin Circulating Fluidized Bed Bioreactor. Electron. Thesis Diss. Repos. Western University.

Andalib, M., Elbeshbishy, E., Mustafa, N., Hafez, H., Nakhla, G., Zhu, J., 2014. Performance of an anaerobic fluidized bed bioreactor (AnFBR) for digestion of primary municipal wastewater treatment biosolids and bioethanol thin stillage. Renew. Energy 71, 276–285.

Andalib, M., Nakhla, G., Zhu, J., 2010. Dynamic testing of the twin circulating fluidized bed bioreactor (TCFBBR) for nutrient removal from municipal wastewater. Chem. Eng. J. 162, 616–625.

Andreottola, G., Foladori, P., Ragazzi, M., 2000a. Upgrading of a small wastewater treatment plant in a cold climate region using a moving bed biofilm reactor (MBBR) system. Water Sci. Technol. 41, 177–185.

Andreottola, G., Foladori, P., Ragazzi, M., Tatàno, F., 2000b. Experimental comparison between MBBR and activated sludge system for the treatment of municipal wastewater.

Water Sci. Technol. 41, 375–382.

Anthonisen, A.C., Loehr, R.C., Prakasam, T.B.S., Srinath, E.G., 1976. Inhibition of nitrification by ammonia and nitrous acid. J. Water Pollut. Control Fed. 835–852.

Arnaiz, C., Gutierrez, J.C., Lebrato, J., 2006. Support material selection for anaerobic fluidized bed reactors by phospholipid analysis. Biochem. Eng. J. 27, 240–245.

Bae, W., Baek, S., Chung, J., Lee, Y., 2001. Optimal operational factors for nitrite accumulation in batch reactors. Biodegradation 12, 359–366.

Balmelle, B., Nguyen, K.M., Capdeville, B., Cornier, J.C., Deguin, A., 1992. Study of Factors Controlling Nitrite Build-Up in Biological Processes for Water Nitrification. Water Sci. Technol. 26, 1017–1025.

Barnard, J.L., 1975. Biological nutrient removal without the addition of chemicals. Water Res. 9, 485–490.

Barwal, A., Chaudhary, R., 2014. To study the performance of biocarriers in moving bed biofilm reactor (MBBR) technology and kinetics of biofilm for retrofitting the existing aerobic treatment systems: a review. Rev. Environ. Sci. Bio/Technology 13, 285–299.

Beauchamp, E.G., Trevors, J.T., Paul, J.W., 1989. Carbon Sources for Bacterial Denitrification. Springer, New York, NY, pp. 113–142.

Begovich, J.M., Watson, J.S., 1978. An electroconductivity technique for the measurement of axial variation of holdups in three-phase fluidized beds. AIChE J. 24, 351–354.

Bello, M.M., Abdul Raman, A.A., Purushothaman, M., 2017. Applications of fluidized bed reactors in wastewater treatment – A review of the major design and operational parameters. J. Clean. Prod. 141, 1492–1514.

Blackburne, R., Yuan, Z., Keller, J., 2008. Partial nitrification to nitrite using low dissolved oxygen concentration as the main selection factor. Biodegradation 19, 303–312.

Boltz, J.P., Morgenroth, E., Sen, D., 2010. Mathematical modelling of biofilms and biofilm

reactors for engineering design. Water Sci. Technol. 62, 1821–1836.

Broch-Due, A., Andersen, R., Kristoffersen, O., 1994. Pilot plant experience with an aerobic moving bed biofilm reactor for treatment of NSSC wastewater. Water Sci. Technol. 29, 283–294.

Buffière, P., Bergeon, J.-P., Moletta, R., 2000. The inverse turbulent bed: a novel bioreactor for anaerobic treatment. Water Res. 34, 673–677.

Cervantes, F.J., 2009. Environmental technologies to treat nitrogen pollution. IWA publishing.

Cheng, Y., Zhu, J.-X.J., 2008. CFD Modelling and simulation of hydrodynamics in liquid-solid circulating fluidized beds. Can. J. Chem. Eng. 83, 177–185.

Chisti, M.Y., Moo-yong, M., 1987. Airlift reactors: characteristics, applications and desigen considersations. Chem. Eng. Commun. 60, 195–242.

Chowdhury, N., Nakhla, G., Sen, D., Zhu, J., 2010. Modeling biological nutrient removal in a liquid-solid circulating fluidized bed bioreactor. J. Chem. Technol. Biotechnol. 85, 1389–1401.

Chowdhury, N., Nakhla, G., Zhu, J., 2008. Load maximization of a liquid-solid circulating fluidized bed bioreactor for nitrogen removal from synthetic municipal wastewater. Chemosphere 71, 807–815.

Ciudad, G., Rubilar, O., Muñoz, P., Ruiz, G., Chamy, R., Vergara, C., Jeison, D., 2005. Partial nitrification of high ammonia concentration wastewater as a part of a shortcut biological nitrogen removal process. Process Biochem. 40, 1715–1719.

Comeau, Y., Hall, K.J., Hancock, R.E.W., Oldham, W.K., 1986. Biochemical model for enhanced biological phosphorus removal. Water Res. 20, 1511–1521.

Cui, Y., Nakhla, G., Zhu, J., Patel, A., 2004. Simultaneous carbon and nitrogen removal in anoxic-aerobic circulating fluidized bed biological reactor (CFBBR). Environ. Technol. 25,

699–712.

Dapena-Mora, A., Campos, J.., Mosquera-Corral, A., Jetten, M.S.., Méndez, R., 2004. Stability of the ANAMMOX process in a gas-lift reactor and a SBR. J. Biotechnol. 110, 159–170.

Darton, R.C., Harrison, D., 1976. Bubble wake structure in three-phase fluidization. Fluid. Technol. 1, 339–403.

Darton, R.C., Harrison, D., 1975. Gas and liquid hold-up in three-phase fluidisation. Chem. Eng. Sci. 30, 581–586.

Dempsey, M.J., Lannigan, K.C., Minall, R.J., 2005. Particulate-biofilm, expanded-bed technology for high-rate, low-cost wastewater treatment: Nitrification. Water Res. 39, 965–974.

Dosta, J., Fernández, I., Vázquez-Padín, J.R., Mosquera-Corral, A., Campos, J.L., Mata-Álvarez, J., Méndez, R., 2008. Short- and long-term effects of temperature on the Anammox process. J. Hazard. Mater. 154, 688–693.

Eddy, M., Burton, F., Tchobanoglous, G., Tsuchihashi, R., 2014. Wastewater engineering : treatment and resource recovery. McGraw-Hill Education.

Ekama, G.A., Siebritz, I.P., Marais, G.V.R., 1983. Considerations in the process design of nutrient removal activated sludge processes. Water Sci. Technol. 15, 283–318.

Ekama, G.A., Wentzel, M.C., 1999. Difficulties and developments in biological nutrient removal technology and modelling. Water Sci. Technol. 39, 1–11.

Eldyasti, A., Chowdhury, N., Nakhla, G., Zhu, J., 2010. Biological nutrient removal from leachate using a pilot liquid – solid circulating fluidized bed bioreactor (LSCFB). J. Hazard. Mater. 181, 289–297.

Eldyasti, A., Nakhla, G., Zhu, J., 2012a. Influence of particles properties on biofilm structure and energy consumption in denitrifying fluidized bed bioreactors (DFBBRs).

Bioresour. Technol. 126, 162–171.

Eldyasti, A., Nakhla, G., Zhu, J., 2012b. Development of a calibration protocol and identification of the most sensitive parameters for the particulate biofilm models used in biological wastewater treatment. Bioresour. Technol. 111, 111–121.

Epstein, N., 2002. Applications of liquid-solid fluidization. Int. J. Chem. React. Eng. 1.1

Epstein, N., 1981. Three-phase fluidization: some knowledge gaps. Can. J. Chem. Eng. 59, 649–657.

Ergun, 1952. Fluid flow through packed columns. Chem. Eng. Prog. 48, 89–94.

Fan, L.T., Kang, Y., Neogi, D., Yashima, M., 1993. Fractal analysis of fluidized particle behavior in liquid-solid fluidized beds. AIChE J. 39, 513–517.

Frijters, C.T.M.J., Eikelboorn, D.H., Mulder, A., Mulder, R., 1997. Treatment of municipal wastewater in a CIRCOX® airlift reactor with integrated denitrification. Water Sci. Technol. 36, 173–181.

Fuhs, G.W., Chen, M., 1975. Microbiological basis of phosphate removal in the activated sludge process for the treatment of wastewater. Microb. Ecol. 2, 119–138.

Gálvez, J.., Gómez, M.., Hontoria, E., González-López, J., 2003. Influence of hydraulic loading and air flowrate on urban wastewater nitrogen removal with a submerged fixed-film reactor. J. Hazard. Mater. 101, 219–229.

Garcia-Calderon, D., Buffiere, P., Moletta, R., Elmaleh, S., 1998. Anaerobic digestion of wine distillery wastewater in down-flow fluidized bed. Water Res. 32, 3593–3600.

Garrido, J.M., van Benthum, W.A.J., van Loosdrecht, M.C.M., Heijnen, J.J., 1997. Influence of dissolved oxygen concentration on nitrite accumulation in a biofilm airlift suspension reactor. Biotechnol. Bioeng. 53, 168–178.

Garside, J., Al-Dibouni, M.R., 1977. Velocity-voidage relationships for fluidization and sedimentation in solid-liquid systems. Ind. Eng. Chem., Process Des. Dev 16, 206–214.

Ge, S., Wang, S., Yang, X., Qiu, S., Li, B., Peng, Y., 2015. Detection of nitrifiers and evaluation of partial nitrification for wastewater treatment: A review. Chemosphere 140, 85–98.

Gerardi, M.H., 2002. Nitrification and denitrification in the activated sludge process. Wiley-Interscience.

Gilbert, E.M., Agrawal, S., Karst, S.M., Horn, H., Nielsen, P.H., Lackner, S., 2014. Low temperature partial nitritation/anammox in a moving bed biofilm reactor treating low strength wastewater. 48(15), 8784-8792

Grace, J.R., 1986. Contacting modes and behaviour classification of gas-solid and other two-phase suspensions. Can. J. Chem. Eng. 64, 353–363.

Grunditz, C., Dalhammar, G., 2001. Development of nitrification inhibition assays using pure cultures of nitrosomonas and nitrobacter. Water Res. 35, 433–440.

Gujer, W., Henze, M., Mino, T., Loosdrecht, M. van, 1999. Activated sludge model No. 3. Water Sci. Technol. 39, 183–193.

Guo, H., Zhou, J., Su, J., Zhang, Z., 2005. Integration of nitrification and denitrification in airlift bioreactor. Biochem. Eng. J. 23, 57–62.

He, S., Niu, Q., Ma, H., Zhang, Y., Li, Y.-Y., 2015. The treatment performance and the bacteria preservation of anammox: a review. Water, Air, Soil Pollut. 226, 163.

Heijnen, J.J., Mulder, A., Enger, W., Hoeks, F., 1989. Review on the application of anaerobic fluidized bed reactors in waste-water treatment. Chem. Eng. J. 41, B37–B50.

Henze, M., Gujer, W., Mino, T., Matsuo, T., Wentzel, M.C., Marais, G. v. R., Van Loosdrecht, M.C.M., 1999. Activated Sludge Model No.2d, ASM2D. Water Sci. Technol. 39, 165–182.

Henze, M., Gujer, W., Mino, T., van Loosdrecht, M.C.M., 2000. Activated sludge models ASM1, ASM2, ASM2d and ASM3. International water association (IWA) publishing.

Hu, Z., Chandran, K., Grasso, D., Smets, B.F., 2003. Impact of metal sorption and internalization on nitrification inhibition. 37(4), 728-734.

Hu, Z., Lotti, T., de Kreuk, M., Kleerebezem, R., van Loosdrecht, M., Kruit, J., Jetten, M.S.M., Kartal, B., 2013. Nitrogen removal by a nitritation-anammox bioreactor at low temperature. Appl. Environ. Microbiol. 79, 2807–12.

Hua, J., Lou, J., 2007. Numerical simulation of bubble rising in viscous liquid. J. Comput. Phys. 222, 769–795.

Ibrahim, M., Yusof, N., Mohd Yusoff, M.Z., Hassan, M.A., 2016. Enrichment of anaerobic ammonium oxidation (anammox) bacteria for short start-up of the anammox process: a review. Desalin. Water Treat. 57, 13958–13978.

Jetten, M.S.., Wagner, M., Fuerst, J., van Loosdrecht, M., Kuenen, G., Strous, M., 2001. Microbiology and application of the anaerobic ammonium oxidation ('anammox') process. Curr. Opin. Biotechnol. 12, 283–288.

Jin, R.-C., Yang, G.-F., Yu, J.-J., Zheng, P., 2012. The inhibition of the Anammox process: A review. Chem. Eng. J. 197, 67–79.

Jin, R., Hu, B., Zheng, P., Qaisar, M., Hu, A., Islam, E., 2008. Quantitative comparison of stability of ANAMMOX process in different reactor configurations. Bioresour. Technol. 99, 1603–1609.

Kermani, M., Bina, B., Movahedian, H., Amin, M.M., Nikaein, M., 2008. Application of moving bed biofilm process for biological organics and nutrients removal from municipal wastewater, American Journal of Environmental Sciences. 4, 675.

Kim, S.D., Kang, Y., 1997. Heat and mass transfer in three-phase fluidized-bed reactors—an overview. Chem. Eng. Sci. 52, 3639–3660.

Kuenen, J.G., 2008. Anammox bacteria: from discovery to application. Nat. Rev. Microbiol. 6, 320–326.

Kunii, D., Levenspiel, O., 2013. Fluidization Engineering. Elsevier. 2013

Lan, Q., Bassi, A., Zhu, J.-X. (Jesse), Margaritis, A., 2002. Continuous protein recovery from whey using liquid-solid circulating fluidized bed ion-exchange extraction. Biotechnol. Bioeng. 78, 157–163.

Lazarova, V., Manem, J., 1996. An innovative process for waste water treatment: The circulating floating bed reactor. Water Sci. Technol. 34, 89–99.

Li, H., Zhou, S., Ma, W., Huang, G., Xu, B., 2012. Fast start-up of ANAMMOX reactor: Operational strategy and some characteristics as indicators of reactor performance. Desalination 286, 436–441.

Li, M., Nakhla, G., Zhu, J., 2012. Simultaneous carbon and nitrogen removal with enhanced bioparticle circulation in a circulating fluidized bed biofilm reactor. Chem. Eng. J. 181, 35–44.

Li, T., Bai, R., Liu, J., 2008. Distribution and composition of extracellular polymeric substances in membrane-aerated biofilm. J. Biotechnol. 135, 52–57.

Liang, W., Zhang, S., Zhu, J.-X., Jin, Y., Zhiqing Yu, Wang, Z., 1997. Flow characteristics of the liquid–solid circulating fluidized bed. Powder Technol. 90, 95–102.

Liu, T., Mao, Y., Shi, Y., Quan, X., 2017. Start-up and bacterial community compositions of partial nitrification in moving bed biofilm reactor. Appl. Microbiol. Biotechnol. 101, 2563–2574.

Liu, X., Kim, M., Nakhla, G., 2017. A model for determination of operational conditions for successful shortcut nitrification. Environ. Sci. Pollut. Res. 24, 3539–3549.

Loh, K.-C., Liu, J., 2001. External loop inversed fluidized bed airlift bioreactor (EIFBAB) for treating high strength phenolic wastewater. Chem. Eng. Sci. 56, 6171–6176.

Mainstone, C.P., Parr, W., 2002. Phosphorus in rivers — ecology and management. Sci. Total Environ. 282–283, 25–47.

Marques, R., Santos, J., Nguyen, H., Carvalho, G., Noronha, J.P., Nielsen, P.H., Reis, M.A.M., Oehmen, A., 2017. Metabolism and ecological niche of Tetrasphaera and Ca. Accumulibacter in enhanced biological phosphorus removal. Water Res. 122, 159–171.

McIlroy, S.J., Starnawska, A., Starnawski, P., Saunders, A.M., Nierychlo, M., Nielsen, P.H., Nielsen, J.L., 2016. Identification of active denitrifiers in full-scale nutrient removal wastewater treatment systems. Environ. Microbiol. 18, 50–64.

Mulder, A., Graaf, A.A., Robertson, L.A., Kuenen, J.G., 1995. Anaerobic ammonium oxidation discovered in a denitrifying fluidized bed reactor. FEMS Microbiol. Ecol. 16, 177–184.

Mulder, J.W., van Loosdrecht, M.C.M., Hellinga, C., van Kempen, R., 2001. Full-scale application of the SHARON process for treatment of rejection water of digested sludge dewatering. Water Sci. Technol. 43, 127–134.

Muroyama, K., Fan, L.-S., 1985. Fundamentals of gas-liquid-solid fluidization. AIChE J. 31, 1–34.

Nelson, M.J., Nakhla, G., Zhu, J., 2017. Fluidized-bed bioreactor applications for biological wastewater treatment: a review of research and developments. Engineering 3, 330–342.

Ni, S.-Q., Lee, P.-H., Fessehaie, A., Gao, B.-Y., Sung, S., 2010. Enrichment and biofilm formation of Anammox bacteria in a non-woven membrane reactor. Bioresour. Technol. 101, 1792–1799.

Ni, S.-Q., Zhang, J., 2013. Anaerobic ammonium oxidation: from laboratory to full-scale application. Biomed Res. Int.

Nicolella, C., van Loosdrecht, M.C.M., Heijnen, J.J., 2000. Wastewater treatment with particulate biofilm reactors. J. Biotechnol. 80, 1–33.

Nicolella, Cristiano, VanLoosdrecht, M.C.M., Heijnen, S.J., 2000. Particle-based biofilm reactor technology. Trends Biotechnol. 18, 312–320.

Ødegaard, H., 2006. Innovations in wastewater treatment–the moving bed biofilm process. Water Sci. Technol. 53, 17–33.

Oehmen, A., Lemos, P.C., Carvalho, G., Yuan, Z., Keller, J., Blackall, L.L., Reis, M.A.M., 2007. Advances in enhanced biological phosphorus removal: From micro to macro scale. Water Res. 41, 2271–2300.

Pambrun, V., Paul, E., Spérandio, M., 2008. Control and modelling of partial nitrification of effluents with high ammonia concentrations in sequencing batch reactor. Chem. Eng. Process. Process Intensif. 47, 323–329.

Park, S., Bae, W., 2009. Modeling kinetics of ammonium oxidation and nitrite oxidation under simultaneous inhibition by free ammonia and free nitrous acid. Process Biochem. 44, 631–640.

Park, S., Bae, W., Rittmann, B.E., 2010. Operational boundaries for nitrite accumulation in nitrification based on minimum/maximum substrate concentrations that include effects of oxygen limitation, pH, and free Ammonia and free nitrous acid inhibition. Environ. Sci. Technol. 44, 335–342.

Patel, A., Zhu, J., Nakhla, G., 2006. Simultaneous carbon, nitrogen and phosphorous removal from municipal wastewater in a circulating fluidized bed bioreactor. Chemosphere 65, 1103–1112.

Peng, Y., Ma, Y., Wang, S., 2007. Denitrification potential enhancement by addition of external carbon sources in a pre-denitrification process. J. Environ. Sci. 19, 284–289.

Peng, Y., Zhu, G., 2006. Biological nitrogen removal with nitrification and denitrification via nitrite pathway. Appl. Microbiol. Biotechnol. 73, 15–26.

Picioreanu, C., van Loosdrecht, M.C.M., Heijnen, J.J., 1997. Modelling the effect of oxygen concentration on nitrite accumulation in a biofilm airlift suspension reactor. Water Sci. Technol. 36, 147–156.

Piculell, M., Suarez, C., Li, C., Christensson, M., Persson, F., Wagner, M., Hermansson,

M., Jönsson, K., Welander, T., 2016. The inhibitory effects of reject water on nitrifying populations grown at different biofilm thickness. Water Res. 104, 292–302.

Plattes, M., Henry, E., Schosseler, P.M., Weidenhaupt, A., 2006. Modelling and dynamic simulation of a moving bed bioreactor for the treatment of municipal wastewater. Biochem. Eng. J. 32, 61–68.

Prosser, J.I., 1990. Autotrophic nitrification in bacteria. Adv. Microb. Physiol. 30, 125–181.

Ramesh, K., Murugesan, T., 2002. Minimum fluidization velocity and gas holdup in gas-liquid-solid fluidized bed reactors. J. Chem. Technol. Biotechnol. 77, 129–136.

Richardson, J.F., Zaki, W.N., 1997. Sedimentation and fluidisation: Part I. Chem. Eng. Res. Des. 75, S82–S100.

Rittmann, B.E., McCarty, P.L., 2012. Environmental biotechnology: principles and applications. Tata McGraw-Hill Education.

Ruiz, G., Jeison, D., Chamy, R., 2003. Nitrification with high nitrite accumulation for the treatment of wastewater with high ammonia concentration. Water Res. 37, 1371–1377.

Rusten, B., Ødegaard, H., Lundar, A., 1992. Treatment of dairy wastewater in a novel moving bed biofilm reactor. Water Sci. Technol. 26, 703–711.

Rusten, B., Siljudalen, J.G., Strand, H., 1996. Upgrading of a biological-chemical treatment plant for cheese factory wastewater. Water Sci. Technol. 34, 41–49.

Sen, P., Dentel, S.K., 1998. Simultaneous nitrification-denitrification in a fluidized bed reactor. Water Sci. Technol. 38, 247–254.

Seviour, R.J., Mino, T., Onuki, M., 2003. The microbiology of biological phosphorus removal in activated sludge systems. FEMS Microbiol. Rev. 27, 99–127.

Shao, M.-F., Zhang, T., Fang, H.H.-P., 2010. Sulfur-driven autotrophic denitrification: diversity, biochemistry, and engineering applications. Appl. Microbiol. Biotechnol. 88,

1027–1042.

Sharma, B., Ahlert, R.C., 1977. Nitrification and nitrogen removal. Water Res. 11, 897–925.

Sinha, B., Annachhatre, A.P., 2007. Partial nitrification—operational parameters and microorganisms involved. Rev. Environ. Sci. Bio/Technology 6, 285–313.

Siripong, S., Rittmann, B.E., 2007. Diversity study of nitrifying bacteria in full-scale municipal wastewater treatment plants. Water Res. 41, 1110–1120.

Smith, V.H., Tilman, G.D., Nekola, J.C., 1999. Eutrophication: impacts of excess nutrient inputs on freshwater, marine, and terrestrial ecosystems. Environ. Pollut. 100, 179–196.

Song, G.-H., Bavarian, F., Fan, H.-S., Buttke, R.D., Peck, L.B., 1989. Hydrodynamics of three-phase fluidized bed containing cylindrical hydrotreating catalysts. Can. J. Chem. Eng. 67, 265–275.

Stenstrom, M.K., Poduska, R.A., 1980. The effect of dissolved oxygen concentration on nitrification. Water Res. 14, 643–649.

Tang, C.J., Zheng, P., Wang, C.H., Mahmood, Q., Zhang, J.Q., Chen, X.G., Zhang, L., Chen, J.W., 2011. Performance of high-loaded ANAMMOX UASB reactors containing granular sludge. Water Res. 45, 135–144.

Tokutomi, T., 2004. Operation of a nitrite-type airlift reactor at low DO concentration. Water Sci. Technol. 49, 81–88.

Ulson de Souza, A.A., Brandão, H.L., Zamporlini, I.M., Soares, H.M., Guelli Ulson de Souza, S.M. de A., 2008. Application of a fluidized bed bioreactor for cod reduction in textile industry effluents. Resour. Conserv. Recycl. 52, 511–521.

van Dongen, U., Jetten, M.S.M., van Loosdrecht, M.C.M., 2001. The SHARON®-Anammox® process for treatment of ammonium rich wastewater. Water Sci. Technol. 44, 153–160.

van Kempen, R., Mulder, J.W., Uijterlinde, C.A., Loosdrecht, M.C.M., 2001. Overview: full scale experience of the SHARON® process for treatment of rejection water of digested sludge dewatering. Water Sci. Technol. 44, 145–152.

Vanrolleghem, P.A., Spanjers, H., Petersen, B., Ginestet, P., Takacs, I., 1999. Estimating (combinations of) activated sludge model no. 1 parameters and components by respirometry. Water Sci. Technol. 39, 195–214.

Wagner, M., Rath, G., Koops, H.-P., Flood, J., Amann, R., 1996. In situ analysis of nitrifying bacteria in sewage treatment plants. Water Sci. Technol. 34, 237–244.

Wang, H., Kim, M., Li, K., Shao, Y., Zhu, J., Nakhla, G., 2019. Effective partial nitrification of ammonia in a fluidized bed bioreactor. Environ. Technol. 40, 94–101.

Wang, X., Hu, M., Xia, Y., Wen, X., Ding, K., 2012. Pyrosequencing analysis of bacterial diversity in 14 wastewater treatment systems in China. Appl. Environ. Microbiol. 78, 7042–7047.

Wang, X.J., Xia, S.Q., Chen, L., Zhao, J.F., Renault, N.J., Chovelon, J.M., 2006. Nutrients removal from municipal wastewater by chemical precipitation in a moving bed biofilm reactor. Process Biochem. 41, 824–828.

Wanner, O., Reichert, P., 1996. Mathematical modeling of mixed-culture biofilms. Biotechnol. Bioeng. 49, 172–184.

Weber, W.J., Pirbazari, M., Melson, G.L., 1978. Biological growth on activated carbon: an investigation by scanning electron microscopy. Environ. Sci. Technol. 12, 817–819.

Wen, C.Y., Yu, Y.H., 1966. A generalized method for predicting the minimum fluidization velocity. AIChE J. 12, 610–612.

Zanetti, L., Frison, N., Nota, E., Tomizioli, M., Bolzonella, D., Fatone, F., 2012. Progress in real-time control applied to biological nitrogen removal from wastewater. A short-review. Desalination 286, 1–7.

Zhang, J.-P., Epstein, N., Grace, J.R., 1998. Minimum fluidization velocities for gas—liquid—solid three-phase systems. Powder Technol. 100, 113–118.

Zhang, T., We, C., Ren, Y., Feng, C., Wu, H., 2017. Advances in airlift reactors: modified design and optimization of operation conditions. Rev. Chem. Eng. 33, 163–182.

Zheng, Y., Zhu, J.-X., Wen, J., Martin, S.A., Bassi, A.S., Margaritis, A., 1999. The axial hydrodynamic behavior in a liquid-solid circulating fluidized bed. Can. J. Chem. Eng. 77, 284–290.

Zhou, Y., Oehmen, A., Lim, M., Vadivelu, V., Ng, W.J., 2011. The role of nitrite and free nitrous acid (FNA) in wastewater treatment plants. Water Res. 45, 4672–4682.

Zhu, J.-X. (Jesse), Karamanev, D.G., Bassi, A.S., Zheng, Y., 2000. (Gas-)liquid-solid circulating fluidized beds and their potential applications to bioreactor engineering. Can. J. Chem. Eng. 78, 82-94.

Zinatizadeh, A.A.L., Ghaytooli, E., 2015. Simultaneous nitrogen and carbon removal from wastewater at different operating conditions in a moving bed biofilm reactor (MBBR): Process modeling and optimization. J. Taiwan Inst. Chem. Eng. 53, 98–111.

Chapter 3

Performance and Bacterial Community Structure of a Novel Inverse Fluidized Bed Bioreactor (IFBBR) Treating Synthetic Wastewater

3.1 Introduction

Biological nutrient removal (BNR) is a widely employed process in wastewater treatment plants (WWTPs). The conventional BNR process is the suspended growth activated sludge (Eddy et al., 2014). Recently, extensive researches have investigated the integration of BNR process with attached growth system to enhance nutrient removal, including rotating biological contactors (Pynaert et al., 2003), trickling filters (Zhang et al., 2015), sponge bioreactors (Xing et al., 2011), moving bed biofilm reactor (MBBR) (Casas et al., 2015), and fluidized bed bioreactor (FBBR) (Wang et al., 2019). In the FBBR systems, carrier particles with small diameter (0.6-4.0 mm) provide large specific surface area for biomass attachment, which makes the FBBR systems outcompete the other attached growth systems with the advantages of highly specialized biomass concentration, enhanced nutrient loading, small footprint occupying and reduced sludge handling cost (Chan et al., 2009; Eldyasti et al., 2010; Nelson et al., 2017).

Numerous studies have investigated the application of FBBR systems for wastewater treatment, either in aerobic, anoxic treatment or anaerobic digestion (Nelson et al., 2017). One type of FBBR systems, the circulating fluidized bed bioreactor (CFBBR), that has been widely reported for BNR, is comprised of two fluidized beds as anoxic riser and aerobic downer, respectively (Cui et al., 2004). The CFBBR was studied with municipal wastewater treatment at short hydraulic retention times (HRTs) of 2-3 hrs, and achieved more than 90% organic, 75-80% total nitrogen removal without particle recirculation and additional 85% phosphorous removal with particle recirculation. Besides, low observed biomass yields of 0.07-0.16 g VSS/g COD were reported for the CFBBR system (Li et al., 2012, 2013; Andalib et al., 2010; Chowdhury et al., 2008; Patel et al., 2006). The results

highlighted the advantages of integrated FBBR system as a continuous process, with distinguished nitrification and denitrification into two separate reactors. However, the carrier particles used in CFBBR system were heavy lava rock with true density of 2628 kg/m^3, which required liquid recirculation to fluidize the carriers and increased the overall energy consumption. It was the main hurdle for the industrial application of CFBBR (Nelson et al., 2017). The other type of FBBR systems, inverse fluidized bed bioreactors (IFBBRs), employ carriers with density slightly lower than the wastewater (Nikolov and Karamanev, 1987). It was reported that the energy consumption was reduced in IFBBRs compared to the traditional FBBRs, as the carriers were fluidized by the gas-induced agitation in the aerobic zone or down-flow liquid in the anaerobic/anoxic zone (Sur and Mukhopadhyay, 2017). The applications of IFBBR system for wastewater treatment are summarized in Table 3-1. Most of the studies were carried out for high-strength organic wastewater under anaerobic conditions. More than 75% COD removal was achieved at the volumetric OLRs of 0.5-70 kg COD/(m^3 d), except for the IFBBR operated at low temperature of 10℃, where 33%-69% COD removal was achieved at OLR of 0.5-5.0 kg COD/(m^3 d) (Bialek et al., 2014). For aerobic treatment, one paper revealed that stable complete nitrification achieved at NLR of 3.6 kg N/(m^3 d) (Bougard et al., 2006). As evident from previous studies, the IFBBR system was capable of handing high-strength organic wastewater at high loadings. However, all the applications were related to industrial wastewater and processed in one stage. Considering the advantages demonstrated by CFBBR, it's necessary to systematically investigate the IFBBRs as an integrated system for BNR from municipal wastewater treatment.

Table 3-1. Summary of various IFBBR systems

Wastewater	Particle properties	Reactor performance	References
Aerobic synthetic wastewater (250-2000 mg NH_3-N)	Extendospheres $d_p = 147$ μm, $\rho = 690$ kg/m^3	At 30°C, completed stable nitrification to nitrate at NLR of 3.6 kg N/(m^3 d). At 35°C, an immediate and durable nitrite accumulation occurred	(Bougard et al., 2006)
Anaerobic digestion wine distillery wastewater	Extendospheres $d_p = 175$ μm, $\rho = 690$ kg/m^3	75-85% carbon removal at OLR of 2-15 kg COD/(m^3 d).	(Buffiere et al., 2000)
Anaerobic digestion wine distillery wastewater	Ground perlite $d_p = 0.7$-1.0 mm, $\rho = 280$ kg/m^3	85% TOC removal at OLR of 4.5 kg COD/(m^3 d).	(GARCIA-CALDERON et al., 1998)
Anaerobic digestion distillery wastewater	Perlite particle $d_p = 1.0$ mm, $\rho = 205$ kg/m^3	84% COD removal at OLR of 35 kg COD/(m^3 d).	(Sowmeyan and Swaminathan, 2008)
Anaerobic digestion brewery wastewater	Extendospheres $d_p = 0.1$-0.4 mm, $\rho = 700$ kg/m^3 Triturated polyethylene $d_p = 0.1$-1.2 mm, $\rho = 930$ kg/m^3	>90% COD removal achieved in both IFBBRs. For Extendospheres, the OLR was 70 kg COD/(m^3 d). For polyethylene, the OLR was 10 kg COD/(m^3 d).	(Alvarado-Lassman et al., 2008)
Denitrification synthetic wastewater (490 mg/L nitrate, 180 mg/l phenol and sulfate)	Polyethylene $d_p = 0.4$ mm, $\rho = 267$ kg/m^3	Consumption efficiencies of phenol, sulfide and nitrate were 100%. The N_2 yield (g N_2/g NO_3-N) was 0.89	(Beristain-cardoso et al., 2009)
Anaerobic synthetic wastewater (2.5-3.5 g COD/L, 1.5-5.2 g/l sulfate)	Polyethylene $d_p = 0.4$ mm, $\rho = 267$ kg/m^3	COD removal of 93% and sulfate removal of 75% were reached at OLR of 5.2 kg COD/(m^3 d) and SLR of 7.3 kg SO$_4$/(m^3 d).	(Celis-García et al., 2007)

Aerobic digestion starch industry wastewater (2250-8910 mg/L COD)	Irregular polypropylene $\rho = 870$ kg/m^3	The optimum COD removal of 93.8% was achieved at OLR of 2.25 kg COD/(m^3 d).	(Rajasimman and Karthikeyan, 2007)
Cometabolic biotransformation phenolic wastewater (600-1600 mg/L phenol, 200 mg/L 4-chlorophenol)	Expanded polystyrene beads dp = 1.0-1.18 mm, $\rho =$ 713 kg/m^3	1600 mg/L of phenol and 200 mg/L of 4-cp were complete degraded at OLR of 0.48 kg COD/(m^3 d).	(Loh and Ranganath, 2005)
Anaerobic digestion dilute dairy wastewater (1.0-2.5 g/L COD)	Extendospheres dp = 0.07-2.0 mm, $\rho =$ 690 kg/m^3	33%-69% COD removal was reached at OLR of 0.5-5.0 kg COD/(m^3 d) at 10°C.	(Bialek et al., 2014)

In the wastewater treatment systems, the BNR performance relies on the bacterial communities and specific functional species present in the active biomass. For nitrogen removal, nitrification is a two-step process sequentially accomplished by ammonia-oxidizing bacteria (AOB) and nitrite-oxidizing bacteria (NOB) (Dionisi et al., 2002). The functional genera *Nitrosomonas* or *Nitrosospira* as AOB and *Nitrospira* as NOB were typically discovered in various WWTPs (Siripong and Rittmann, 2007). Denitrification is the sequential reduction of nitrate or nitrite to dinitrogen gas, via the gaseous intermediates nitric oxide and nitrous oxide (Betlach and Tiedje, 1981). The genera reported as denitrifiers were diverse, such as *Thauera*, *Azoarcus*, *Paracoccus*, *Hyphomicrobium*, and *Comamonas* (Liu et al., 2006; Wang et al., 2014). However, the populations and relative abundance of functional genera varied from studies. In a nitrifying FBBR, *Nitrosospira* was detected as the dominant AOB (Schramm et al., 1998), while in another nitrifying FBBR (Tsuneda et al., 2003), the dominant AOB were *Nitrosomonas*. Moreover, the bioreactor configurations and operational conditions have great influence on the diversity and structure of microbial communities. Bialek et al. (2012) tested the anaerobic microbial communities in an IFBBR and a granular sludge bed with the same operational conditions, observed <58% similarity between the two microbial cultures. By analyzing the microbial communities in activated sludge samples from 14 different WWTPs, wastewater characteristics were considered to have the greatest contribution to the bacterial community over other variances (Wang et al., 2012). Unlike other fixed-film technologies operated at high shear force, the paucity of knowledge on microbial community structures in nitrifying and denitrifying IFBBRs is evident. Thus, the information about the structure of microbial populations in the anoxic and aerobic IFBBRs is required for better understanding of reactor performance, leading to process optimization and efficient process design.

In this study, the integrated IFBBR system was run for 6 phases by increasing the carrier filling ratio and nutrient loading gradually, with high-strength and low-strength synthetic wastewater (SWW). The objectives were (i) to examine the general BNR performance of the integrated IFBBR system, (ii) to reveal the bacterial community structures, (iii) to elucidate its correlation with the reactor performance.

3.2 Materials and methods

The SMW used in this study was prepared daily with tap water combined with 300-700 mg COD/L using CH_3COONa, 30-70 mg N/L using NH_4Cl, 6 mg P/L using KH_2PO_4 and 200-400 mg $CaCO_3$/L using $NaHCO_3$. The trace metal solution, which was added to the feed at 1.5 mL/L, was composed of 15 mg EDTA/L, 0.43 mg $ZnSO_4 \cdot 7H_2O$/L, 0.24 mg $CoCl_2$/L, 0.99 mg $MnCl_2$/L, 0.25 mg $CuSO_4 \cdot H_2O$/L, 0.22 mg $NaNoO_4 \cdot H_2O$/L, 0.19 mg $NiCl \cdot 6H_2O$ /L, and 0.014 mg H_3BO_4/L. All the chemicals were purchased from VWR Canada.

3.2.1 Reactor description

The lab-scale integrated IFBBR system (Figure 3-1) is comprised of two 4-m high plexiglass columns with the water level kept at 3.6 m to avoid particle overflow from the top of the columns. The anoxic column (3.8 cm inner diameter (ID)) was operated similar to an airlift reactor, with slow coarse air bubbles (monitored by a rotameter (Fischer & Porter, Canada)) injected from the middle of a tube (1.2 cm ID) at the flow rate of 0.04-0.08 m^3/d. The liquid was driven by the rising bubbles to circulate between the tube and the anoxic column, which facilitated the fluidization of particles. The particles in the aerobic column (10 cm ID) were fluidized by the agitation from the fine bubble aerator (Xinggang Ltd, China), which was installed 20 cm above the bottom of the column. The air flow rate was monitored and controlled by a rotameter (Omega Engineering INC, USA) to maintain the fluidization and the dissolved oxygen (DO) above 1.5 mg/L. The synthetic wastewater was fed into the top of the anoxic column by a peristaltic pump (Masterflex I/P; Masterflex, Germany), went out of the anoxic zone from the bottom and then got into the top of the aerobic column through a tube connection. A water balance tank was used to balance the water level in the aerobic column, so the system effluent would flow out from the aerobic column automatically. In order to achieve denitrification, liquid recirculation from the aerobic zone to the anoxic zone was kept as 3-5 times the inflow, which was controlled by a centrifugal pump (MD-70RLT, Iwaki, Japan).

Inflow

Peristaltic
pump

Anoxic column

Aerobic column

Water
balance tank

Rotameter

Effluent

Centrifugal
pump

Aerator
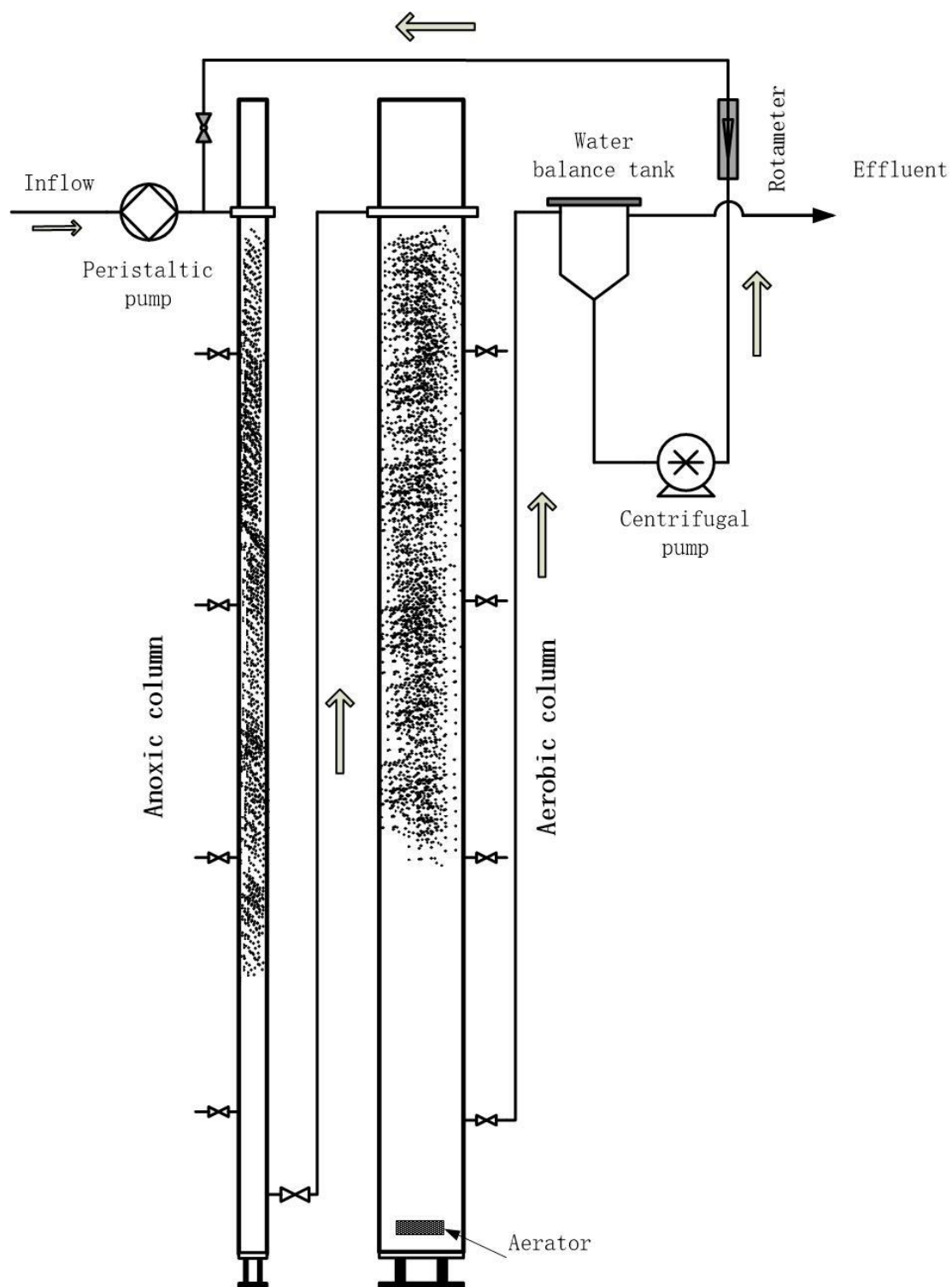
Figure 3-1. The configuration of the integrated IFBBR system

3.2.2 Experimental start-up and procedures

20 L return activated sludge (RAS) collected from the Adelaide Water Pollution Control Plant (London, Canada) was used as the seed sludge, with Total suspended solids (TSS) and Volatile suspended solids (VSS) concentrations of approximately 3900 and 3100 mg/L, respectively. To initiate biofilm formation, the particles were fluidized by controlling the airflow rate of 0.06 m^3/d in the anoxic zone and 0.82 m^3/d in the aerobic zone. The SMW and seed sludge were recirculated between two columns for 3 days to attach the bacteria on the particles' surface. After that, the system was continuously fed with SMW at the rate of 15 L/d for 3 weeks. Most of the particles in both columns were coated with biofilm. The average concentrations of biofilm in the anoxic zone and the aerobic zones were 17.2 and 6.4 mg VSS/g particle, respectively.

Activated carbon-coated polypropylene beads with average diameter of 3.2 mm (3.0-3.5 mm) and true density of 904 kg/m^3 were employed as the carriers for biofilm attachment. The total amount of particles used in the anoxic and aerobic columns in Phases I and II was 1.72 kg (2.8 L compacted bed volume), which were increased to 3.44 kg (5.6 L compacted bed volume) in Phase III. These particles were distributed 1/4 in the anoxic column and 3/4 in the aerobic column. The particles' distribution was determined based on the biomass specific nitrification rates (SNRs) of 0.09-0.14 g NH_3-N/(g VSS d) and the biomass specific denitrification rates (SDNRs) of 0.033-0.243 g NOx-N/(g VSS d) reported in the CFBBR system (Patel et al., 2006). In Phases IV to VI (Period II), 4.49 kg (7.3 L compacted bed volume) fresh particles were put into the aerobic column to make the filling ratio (compacted bed volume divided by total volume) as 40%, respectively. The detailed operational conditions are shown in Table 3-2.

Table 3-2. Operational conditions

		Phase I	Phase II	Phase III	Phase IV	Phase V	Phase VI
Influent flow (L/d)		15	22.5	45	120	160	210
Air flow (m^3/d)	Anoxic	0.04	0.03	0.03	0.03	0	0
	Aerobic	0.28	0.34	0.41	2.38	2.17	1.90
DO (mg/L)	Anoxic	0.3-0.5	0.3-0.6	0.1-0.3	0.21-0.42	0.09-0.25	0.05-0.12
	Aerobic	4.3-6.0	4.1-4.7	1.8-2.4	4.6-5.5	2.3-3.2	1.4-1.9
Particle weight (kg)	Anoxic	0.43	0.43	0.86	0.86	0.86	0.86
	Aerobic	1.29	1.29	2.58	7.07	7.07	7.07
HRT (h)	Anoxic	6.5	4.3	2.2	0.8	0.6	0.5
	Aerobic	45	30	15	5.6	4.2	3.2
EBCT (h) = $V_{compact}/Q_{in}$	Anoxic	1.12	0.75	0.75	0.34	0.26	0.19
	Aerobic	3.36	2.24	2.24	2.3	1.73	1.29
Average organic loading (kg COD/(m^3 d))		0.34	0.50	1.02	1.21	1.63	2.10
Average nitrogen loading (kg N/(m^3 d))		0.035	0.052	0.103	0.121	0.166	0.213
Average organic loading based on compacted bed volume (kg COD/(m^3 d))		3.86	5.70	5.80	2.89	3.89	5.01
Average nitrogen loading based on compacted bed volume (kg COD/(m^3 d))		0.392	0.583	0.582	0.289	0.396	0.507
Average attached biomass (mg VSS/g particle)	Anoxic	17.2	35.7	50.3	37.2	40.4	42.1
	Aerobic	7.64	9.87	10.2	3.36	3.96	5.90
Biomass (g VSS)	Anoxic	7.40	15.4	43.3	32.0	34.8	36.2
	Aerobic	9.87	12.7	26.3	23.8	28.0	41.7
F/M ratio (g COD/(g VSS d))	Anoxic	1.46	1.04	0.75	1.20	1.49	1.84
F/M ratio (g N/(g VSS d))	Aerobic	0.11	0.13	0.12	0.16	0.19	0.16

3.2.3 Analytical methods

Samples from the feed tank (influent), bottom of the anoxic column, and the final effluent were collected in airtight bottles and refrigerated at 4°C before analysis. Total and soluble chemical oxygen demand (TCOD and SCOD), NH_3-N, NO_2-N, NO_3-N were analyzed with Hach methods and testing kits (Odyssey DR3900, HACH). TSS and VSS were measured in accordance with Standard Methods no 2540D, 2540E, respectively (American Public Health Association, 2008). DO and temperature were measured onsite using Orion Star A323 (Thermo scientific, Oakwood, USA). For each phase, 6-10 bioparticles taken from different heights were observed to determine the biofilm thickness using the microscope (Mitutoya, Japan) coupled with a camera (Leica DC 300, Germany) at a magnification of 50X. Biofilm thickness was expressed as a range. Attached biomass on the particles were measured according to Standard Method no 2540G (American Public Health Association, 2008). Approximately 10 g bioparticles were taken from each column, suspended in 100 ml vials, and stirred on the stirring plate (PC-6200, Corning, USA) under 350 rpm for 2 hrs, then sonicated for 3 hrs at 30°C in an Aquasonic Sonicator (Changzhou, China) with a rated power of 45 watts. After sonication, the VSS content of the detached biomass was determined following Standard Methods no 2540E (American Public Health Association, 2008). The cleaned particles were dried naturally. Attached biomass was expressed as mg VSS/ g particle.

3.2.4 Batch tests

Batch tests were carried out to test the kinetics of the aerobic and anoxic attached biofilm, mainly focusing on the biomass SNR and SDNR. 0.5 L working volume BOD bottles equipped with magnetic stirrers were used as the batch reactors. The attached biofilm was detached by the sonication to reduce the substrate transfer limitations. For the SNR test of the aerobic biofilm, approximately 20 g bioparticles were taken to detach the biomass, the initial concentrations of solution were 30-65 mg N/L, 240-300 mg/L alkalinity as $CaCO_3$. DO was kept above 5 mg/L by the air diffuser (Xinggang Ltd, China). For the SDNR tests of the anoxic biofilm, approximately 10 g bioparticles were taken to detach the biomass,

the initial acetate COD was 250-350 mg/L and the NO_3-N was kept as 30-45 mg/L. The initial food-to-microorganism (F/M) ratios were determined by the nutrient loading and attached biomass in the IFBBR system.

3.2.5 16S rRNA sequencing analysis

Biomass samples of aerobic attached (H1) and anoxic attached (H2), aerobic effluent (H3) were collected from the IFBBR system during Phase VI on day 276, centrifuged with microcentrifuge (microcl 17, Thermo Scientific^{TM}, USA) under 23000 rpm. The concentrated samples were used for DNA extraction by FastDNA SPIN Kit for Soil (Omega, USA). The extracted DNA was evaluated on 1% (wt/vol) agarose gel and stored at -20°C until further use. The microbial community analysis was performed by amplifying the 16S v4 region using Forward primer 515F (GTGCCAGCMGCCGCGGTAA), and Reserve primer 805R (GGACTACHVGGGTWTCTAAT) with a 12nt barcode unique to each sample (Gloor et al., 2016, 2010).

The extracted DNA was amplified by the polymerase chain reaction (PCR) as follows: initial denaturation at 95°C for 3 mins, followed by 25 cycles of denaturing at 95 °C and annealing at 60°C for 30 secs, extension at 72°C for 30 secs, and extension hold at 72°C for 5 mins, final hold at 4°C. The PCR reaction mixture (100 μl) contained 10 ng DNA template, 10 µl of forward primer at 3.2 pMole/µl, 10 µl of reverse primer at 3.2 pMole/µl, and 20 µl Taq mastermix (Omega, USA). PCR products were submitted to the Robarts Research Institute (Western University, Canada) for sequencing and bioinformatic analysis. The demultiplexing and downstream bioinformatic was compiled using software R-3.5.2 with DADA2 package according to the online standard operation protocol (Callahan et al., 2016).

3.3 Results and discussions

3.3.1 Nutrient removal performance

3.3.1.1 Organic removal

The IFBBR system was tested with high strength SMW in Phases I-III and low strength SMW in Phases IV-VI to optimize the nutrient removal capabilities. Figure 3-2a shows the system performance with respect to the COD removal from SMW in different phases. In Period I, the influent TCOD was 716 ± 29 mg/L and influent SCOD was 695 ± 25 mg/L. More than 90% of the influent COD was removed at HRTs of 51.6, 34.4 and 17.2 hrs, respectively, with the average effluent TCOD less than 50 mg/L and effluent SCOD lower than 30 mg/L. There was almost no change with respect to the average effluent TCOD in this period, even though the organic loading rates (OLRs) based on the total volume increased from 0.34 to 1.02 kg COD/(m^3 d). These findings contradicted with the results from the CFBBR system that higher effluent TCOD would be observed at higher OLRs (Andalib et al., 2010; Chowdhury et al., 2008). The explanation for the relatively constant effluent TCOD in Period I was the presence of higher detached biomass despite the decreasing effluent SCOD. Typically, the biomass detachment rates increased with the increment of the total biomass and organic loadings. As shown in Table 3-2, the total attached biomass was 17.3 g VSS in Phase I and 69.6 g VSS in Phase III. The effluent VSS increased from 11.5 ± 4.8 mg/L in Phase I to 17.6 ± 6.5 mg/L in Phase III. Meanwhile, the abundant biomass in the system led to the average effluent SCOD dropping from 27 ± 11 mg/L to 17 ± 8 mg/L, while the TCOD remained almost the same through Phase I to Phase III.

In Period II (Phases IV to VI), the influent was switched to low strength SMW with average TCOD of 321 ± 18 mg/L and SCOD of 312 ± 16 mg/L. The inflow rates were maintained as 120 L/d, 160 L/d, and 210 L/d, corresponding to the HRTs (based on the total volume) of 6.4, 4.8, and 3.7 hrs, respectively. In order to provide enough DO in the aerobic zone and facilitate particle fluidization, the air flow rate in the aerobic zone was adjusted to 2.38 m^3/d in Phase IV. After biomass accumulated on the particles' surface, the air flow rate

was reduced to 2.17 m³/d in Phase V and further decreased to 1.90 m³/d in Phase VI. As shown in Table 3-2, the OLRs almost doubled from Phase IV to Phase VI, while the effluent VSS decreased from 29.8 ± 3.3 mg/L to 21.0 ± 6.1 mg/L. This phenomenon can be explained by the biofilm formation theory. In three-phase fluidized bed bioreactor, the bubble behavior is related to the air flow rate, the coalescence and breakup of bubbles would cause liquid disturbance and particle collision, which affects biofilm accumulation (Tavares et al., 1995). Thus, the detached biomass decreased with the decrease of air flow rate in Period II. More than 90% of the influent SCOD was removed. Both in Periods I and II, the effluent TCOD was <60 mg/L and effluent SCOD was <30 mg/L. It could be summarized that the integrated IFBBR system was very efficient with SCOD removal, while the effluent TCOD was affected by the effluent VSS, which could be minimized by clarification. The maximum volumetric OLR achieved in this study was 2.1 kg COD/(m³ d) with nitrification-denitrification process. There are studies reporting volumetric OLR of 2.5 kg COD/(m³ d) in CFBBR (DO ~6.4 mg/L) (Andalib et al., 2010), and 0.5 kg COD/(m³ d) in MBBR (DO >2.4 mg/L) (Kermani et al., 2008). Based on the particle surface area, the OLR was 4.1 kg COD/(m² d) in IFBBR, as compared with 0.75 kg COD/(m² d) in CFBBR and 3.1 kg COD/(m² d) in MBBR (Andalib et al., 2010; Kermani et al., 2008), which demonstrates that the integrated IFBBR system is a competitive technology with low DO concentration in the aerobic zone.

3.3.1.2 Nitrogen removal

The performance of the IFBBR system in terms of nitrogen removal is shown in Figure 3-2b, with respect to the temporal variations of the influent and effluent NH_3-N, effluent NO_2-N and NO_3-N. Table 3-3 summarizes the NH_3-N, NO_2-N and NO_3-N concentrations in the influent, anoxic effluent and system effluent. As this system was feed with SMW, the total nitrogen (TN) was not tested in this study. In Period I, there were negligible NO_2-N concentrations (<0.2 mg/L) in the influent, anoxic effluent and system effluent. Nitrification mainly happened in the aerobic zone where DO concentrations were kept as 1.3-6.0 mg/L. The effluent NH_3-N was lower than 2.0 mg/L at the steady-state phases even though the influent ammonia was 72.7 ± 3.9 mg/L in Period I and 32.1 ± 1.6 mg/L in Period II, corresponding to ammonia removal efficiencies >98.7% for the high strength

wastewater and >96.8% for the low strength wastewater. Based on the empty bed contact time (EBCT), the IFBBR system achieved the highest nitrogen loading rate (NLR) of 0.59 kg N/(m^3 d) in Phase III, which is higher than the NLR of 0.11 kg N/(m^3 d) reported in MBBR (Gong et al., 2012), but lower than the NLR of 1.26 kg N/(m^3 d) in CFBBR (Chowdhury et al., 2008). The aerobic biomass SNRs in the reactor were 0.14-0.26 g N/(g VSS d), while offline batch tests confirmed the biomass SNRs of aerobic attached biomass were 0.21-0.29 g N/(g VSS d). The relative agreement (<12% discrepancy) between online and offline biomass SNRs demonstrates that the aerobic biofilm thickness of 100-120 μm (Figure 3-3a) did not hinder nutrient diffusion. NOx-N produced in the aerobic zone was recycled to the anoxic zone at a recirculation-to-feed ratio of 3.1-5.4. The effluent NOx-N concentrations remained constant at 12.5 ± 1.3 mg/L in Period I and 6.0 ± 0.8 mg/L in Phases IV&V. In Phase VI, the effluent NOx-N increased to 7.3 ± 0.9 mg/L, higher than that in Phases IV&V. The increase of effluent NO$_X$-N was attributed to the incomplete denitrification of the recycled NOx-N in the anoxic zone with the average anoxic effluent NOx-N of 0.1 mg/L (Phase IV-V) versus 1.4 mg/L (Phase VI). In this study, although bioparticles in the anoxic zone were maximized at filling ratio of 50%, the ratio of particle mass in the anoxic zone to the aerobic zone was kept as low as 1:8 in Period II. The denitrified-nitrogen loading rates were 1.04-2.76 kg N/(m^3 d) based on the volume of the anoxic zone, which is higher than the loadings of 0.70-1.19 kg N/(m^3 d) reported in CFBBR (Andalib et al., 2010). Biomass SDNRs of the IFBBR system were 0.047-0.107 g N/(g VSS d), while offline batch tests demonstrated the biomass SDNRs of the anoxic attached biomass were in the range of 0.29-0.35 g N/(g VSS d). The difference between the online and offline biomass SDNRs was due to NOx-N diffusion limitation into the thick anoxic biofilm, which was up to 650 μm (Figure 3-3b).

Table 3-3. Water parameters

Parameter	Period I [a]							Period II [a]						
		Phase I		Phase II		Phase III			Phase IV		Phase V		Phase VI	
	Influent	Anoxic	Effluent[c]	Anoxic	Effluent[c]	Anoxic	Effluent[c]	Influent	Anoxic	Effluent[c]	Anoxic	Effluent[c]	Anoxic	Effluent[c]
pH	7.41±0.18	8.04±0.11	7.98±0.13	7.98±0.13	7.72±0.22	7.72±0.15	7.56±0.17	7.53±0.17	7.66±0.16	7.52±0.14	7.73±0.16	7.72±0.27	7.57±0.23	7.59±0.22
Alkalinity [b]	549±30	442±16	337±18	426±27	342±42	406±28	311±24	294±31	237±21	201±22	269±17	224±19	258±17	219±18
TCOD (mg/L)	716±29	118±21	40±16	128±12	47±8	133±12	43±12	321±18	79±8	52±10	78±14	47±7	70±9	41±8
SCOD (mg/L)	695±25	97±12	27±11	113±10	27±8	113±9	17±8	312±16	60±5	14±4	56±7	18±3	53±7	16±5
NH$_3$-N (mg/L)	72.7±3.9	14.7±1.3	0.5±0.3	14.4±1.5	0.7±0.5	14.6±0.7	0.9±0.5	32.1±1.6	6.4±0.5	0.9±0.2	7.2±0.9	1±0.3	6.9±0.4	0.8±0.3
NO$_3$-N (mg/L)	0.2±0.2	0.8±1.3	12.8±1.3	0.3±0.3	12.5±1.4	0.7±0.5	12.1±1.1	0.1±0.1	0±0	5.6±0.3	0.1±0.2	5.7±0.9	1.4±0.3	6.4±0.9
NO$_2$-N (mg/L)	—	—	—	—	—	—	—	0.04±0.14	0.1±0.04	0.33±0.23	0.17±0.37	0.36±0.31	0.18±0.12	0.89±0.29
TSS (mg/L)	10.1±4.7	15.1±4.4	19.5±7	15.9±6.2	20.8±5	18.5±9.2	26.6±7.8	4.7±3.3	17.3±11.6	39.7±6.8	23.2±5.7	28.5±5.9	17.4±4.1	25.7±6.1
VSS (mg/L)	5.7±3	10.5±4.5	11.5±4.8	11.5±4.5	13.7±3.6	11.2±5.5	17.6±6.5	3.1±2.4	10.9±6.2	29.8±3.3	18.7±5.7	22.8±5.1	14.3±3.6	21±6.1

a. Average ± SD (number of samples, 10-15)

b. As mg CaCO$_3$ equivalent/L.

c. Same as water characteristics of aerobic column.
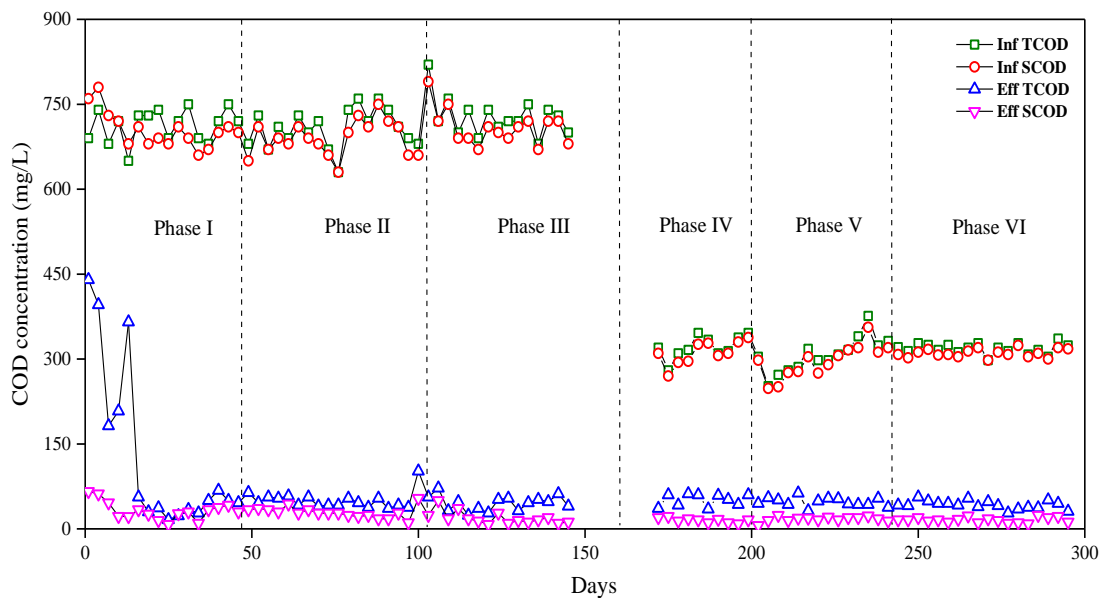
Figure 3-2a. COD removal performance in lab-scale IFBBR system
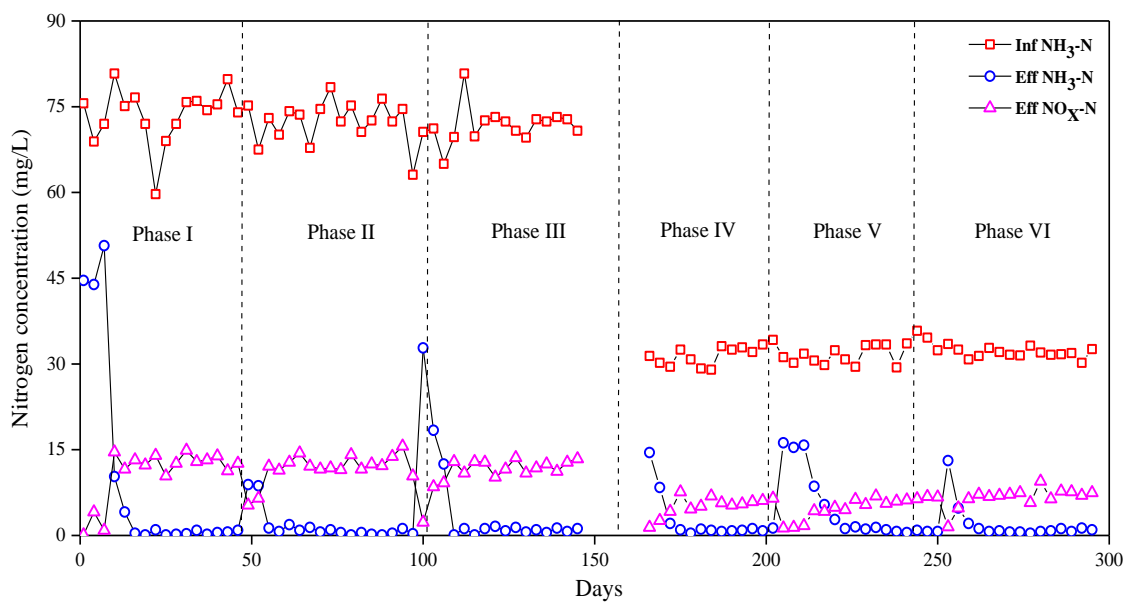
Figure 3-2b. Nitrogen removal performance in lab-scale IFBBR system
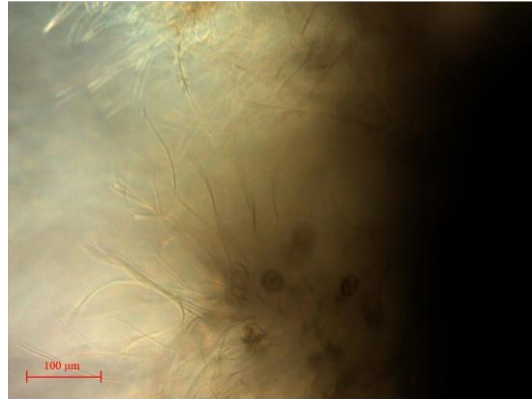
Figure 3-3a. The aerobic attached biofilm in Phase VI
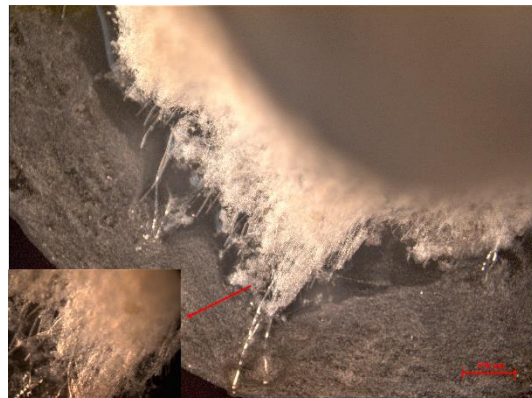
Figure 3-3b. The anoxic attached biofilm in Phase VI

3.3.1.3 Biomass yield

The observed sludge yield was calculated as the sum of the effluent biomass and biomass wasted divided by the SCOD consumed. The effluent solid concentrations in different phases are shown in Table 3-3. Figure 3-4 illustrates the linear regression between cumulative biomass and cumulative SCOD removal. Low biomass yields of 0.030, 0.043, 0.061, 0.101, 0.077 and 0.096 g VSS/g SCOD were achieved in Phases I to VI, respectively. As shown in Figure 3-5, the biomass yield of the IFBBR system was affected not only by the OLR, but also by the air flow rate. The correlation between biomass yield and OLR alone could not be determined. In Period I, the biomass yield increased from 0.030 to 0.061 g VSS/g SCOD with the increase of OLR from 0.34 to 1.02 kg/(m^3 d), while in Period II,

the biomass yield decreased from 0.101 g VSS/g SCOD in Phase VI (OLR of 1.2 kg/(m^3 d)) to 0.077 g VSS/g SCOD in Phase V (OLR of 1.6 kg/(m^3 d)), and then increased to 0.096 g VSS/g SCOD in Phase VI (OLR of 2.1 kg/(m^3 d)). Similarly, no correlation between biomass yield and air flow rate alone was observed. For example, the biomass yield increased with the increase of air flow rate from 0.28 to 0.41 m^3/d in Period I, while the biomass yield fluctuated with the reduction of air flow rate (2.38 m^3/d in Phase VI, 2.17 m^3/d in Phase V, and 1.90 m^3/d in Phase VI) in Period II. Compared with the activated sludge systems of 0.3 g VSS/g COD, the biomass yield of the IFBBR system was 70%-90% lower, which was attributed to the relatively long mean solids retention time (SRT) and the influent COD consumption in the anoxic zone. In other fluidized bed BNR processes, the biomass yields were reported as 0.06 g VSS/g COD at an OLR of 3 kg/(m^3 d) (Feng et al., 2008) and 0.081 g VSS/g COD at an OLR of 2.5 kg/(m^3 d) (Andalib et al., 2010), similar to the IFBBR system.
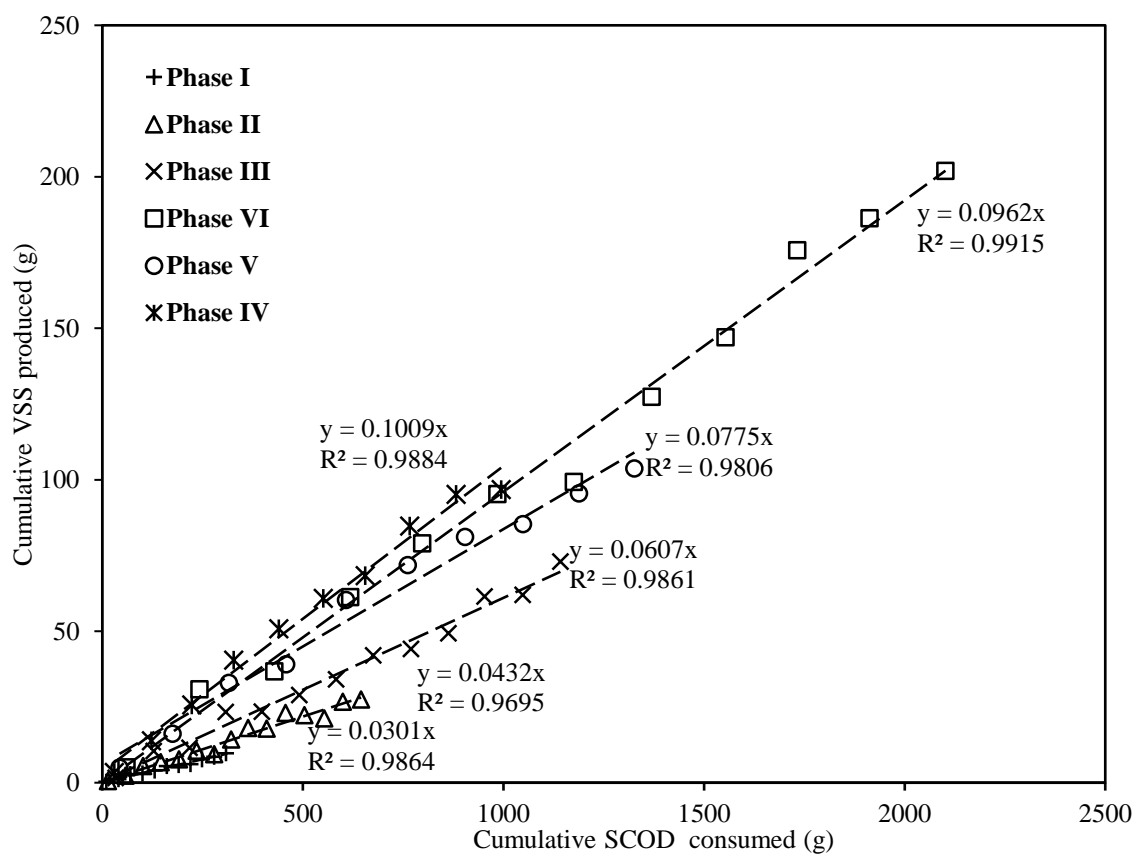
Figure 3-4. Biomass yield
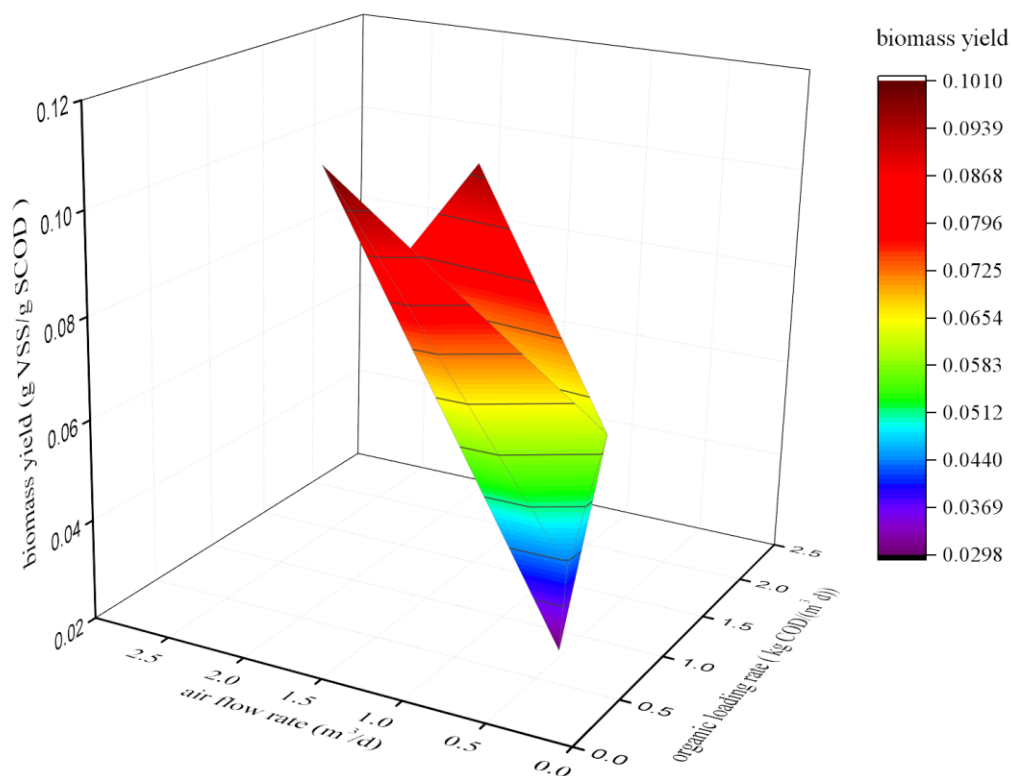
Figure 3-5. The effect of OLR and air flow rate on biomass yield

3.3.2 Mass balance

The steady-state mass balance for the anoxic and aerobic zones of IFBBR are presented in Table 3-4. The mass balance was based on the experimental data of the influent, anoxic and final effluent parameters, recirculation rates and the sludge wastage in each phase.

Anoxic COD consumption was observed to account for 31%-42% of the overall COD removal. The reaction happened in the anoxic zone was considered mainly as denitrification. According to Equation (3.1), the COD uptake rate for denitrification was calculated with the observed biomass yield and the nitrate consumption rate. As shown in Table 3-4, the COD removal by denitrification only accounted for 47.3%-62.9% of the COD consumed in the anoxic zone. Even with consideration of the aerobic COD removal in the anoxic zone due to DO in the influent and liquid recirculation, the actual and

theoretical COD consumption was not matched up. In addition, with 2.54-15.80 g/d alkalinity as $CaCO_3$ generated by denitrification of 0.71-3.87 g/d nitrate and 0.09-0.56 g/d nitrite in the anoxic zone, the alkalinity balance did not close in all phases. It was reported that thick anoxic biofilm favored the growth of sulfate-reducing bacteria (SRB) (Santegoeds et al., 1998). We assumed that the non-closure of COD and alkalinity in the anoxic zone was due to the presence of SRB in the anoxic biofilm. Thus, taking the sulfate reduction into consideration, where sulfate accepted eight elections to produce sulfide and 1 mg/L alkalinity as $CaCO_3$ was produced per 1 mg/L sulfate reduced (Equation (3.2)). With sulfate concentration of 36-84 mg/L (Andalib et al., 2010), the COD consumption by SRB could be estimated by the alkalinity balance resulting in COD closure in the anoxic zone of 86.6%-99.5%. Denitrification, aerobic COD oxidization, and sulfate reduction were the predominant processes occurring in the anoxic zone. For the aerobic zone, the ammonia nitrogen was converted to nitrate in Phases I-III and additionally to nitrite in Phases IV-VI. Some of the ammonia was also involved in biomass synthesis. The nitrogen and alkalinity closure in the aerobic zone were in the reasonable range of 85.6%-94.5% and 81.7-111.2%, respectively.

$$\frac{gSCOD}{gNO_3\text{-}N} = \frac{2.86}{1\text{-}1.42Y_{obs}} \tag{3.1}$$

$$SO_4^{2-} + CH_3COOH + 2H^+ \rightarrow HS^- + 2HCO_3^- + 3H^+ \tag{3.2}$$

Table 3-4. Mass balance

		Mass in influent [g/d]	Mass consumed [g/d] Anoxic	Mass consumed [g/d] Aerobic	Mass in effluent [g/d]	Mass wastage [g/d]	Closure [%]
Phase I	TCOD	10.80	4.31 $(2.04)^a (0.74)^b (1.12)^c$	5.71	0.60	0.18^i	90.4^f
	NH_3-N	1.10	0.03	1.05	0.01	0.01^j	85.6^g
	NO_3-N	0	0.71	-0.90	0.19		
	Alkalinity	8.72	-4.20 $(-2.54)^d$	7.87 $(6.43)^e$	5.05		81.7^h
Phase II	TCOD	15.96	5.79 $(3.14)^a (1.10)^b (0.77)^c$	8.66	1.05	0.47	86.6^f
	NH_3-N	1.63	0.07	1.51	0.02	0.03	91.4^g
	NO_3-N	0	1.10	-1.38	0.28		
	Alkalinity	12.01	-5.06 $(-3.93)^d$	9.38 $(9.84)^e$	7.70		105.0^h
Phase III	TCOD	32.47	10.15 $(6.38)^a (1.13)^b (2.58)^c$	18.88	1.92	1.52	99.5^f
	NH_3-N	3.26	0.14	2.96	0.04	0.11	86.7^g
	NO_3-N	0.01	2.04	-2.57	0.55		
	Alkalinity	24.24	-11.09 $(-7.28)^d$	21.34 $(18.36)^e$	14.00		86.1^h
Phase IV	TCOD	38.38	16.08 $(7.71)^a (5.23)^b (2.96)^c$	16.08	6.22	0	98.9^f
	NH_3-N	3.84	0.44	3.29	0.11	0	106.2^g
	NO_3-N	0.01	2.70	-3.35	0.67		
	NO_2-N	0.02	0.11	-0.14	0.04		
	Alkalinity	31.63	-14.00 $(-10.03)^d$	21.54 $(23.95)^e$	24.10		111.2^h

Phase V	TCOD	52.11	19.66 $(10.20)^a$ $(4.18)^b$ $(4.83)^c$	24.96	7.49	0	97.7^f
	NH_3-N	5.22	0.10	4.97	0.16	0	93.1^g
	NO_3-N	0.01	3.56	-4.47	0.92		
	NO_2-N	0	0.09	-0.15	0.06		
	Alkalinity	52.45	-19.87 $(-13.06)^d$	36.56 $(33.02)^e$	35.76		90.3^h
Phase VI	TCOD	66.64	26.93 $(12.79)^a$ $(4.39)^b$ $(8.37)^c$	29.01	8.56	2.14	94.9^f
	NH_3-N	6.70	0.11	6.26	0.18	0.15	94.5^g
	NO_3-N	0.03	3.87	-5.17	1.34		
	NO_2-N	0	0.56	-0.75	0.19		
	Alkalinity	61.20	-26.18 $(-15.80)^d$	41.39 $(42.26)^e$	45.99		102.1^h

a. SCOD consumption through denitrification based on Equation (3.1)

for example, Phase I $= \dfrac{2.86}{1-1.42\times0.030}$

b. Aerobic SCOD consumption in the anoxic zone

for example, Phase I $= \dfrac{\Delta O_2}{\Delta t} \times (1 - Y_H)^{-1} = (4 \times 5.6 + 6) \dfrac{mg}{L} \times 15 \dfrac{L}{d} \times (1-0.3)^{-1}$

c. SCOD consumed by SRB based on stoichiometry of Equation (3.2);

for example, Phase I $= (-2.54-(-4.20)) \dfrac{g\ SO_4^{2-}}{d} \times \dfrac{59\ g/mol\ CH_3COOH}{96\ g/mol\ SO_4^{2-}} \times \dfrac{1.1\ g\ COD}{1\ g\ CH_3COOH}$

d. Alkalinity generated in the anoxic zone by denitrification

for example, Phase I $= 0.71\ g\ N_{denitrified} \times 3.57 \dfrac{g\ Alk}{g\ N}$

d. Alkalinity consumed in the aerobic zone

for example, Phase I = -0.90 g $N_{nitrified} \times 7.14 \frac{g\ Alk}{g\ N}$

f. COD closure in the anoxic zone

for example, Phase I = (2.04 + 0.74 +1.12) / 4.31 × 100

g. Ammonia closure in the aerobic zone

for example, Phase I = -(-0.90) / 1.05 × 100

h. Alkalinity closure in the aerobic zone

for example, Phase I = (6.43) / 7.87 × 100

i and j. COD equivalent and nitrogen (N) content of 1 g biomass were as 1.42 and 0.1 g, respectively.

3.3.3 Energy consumption

When comparing different FBBR systems, energy consumption arising mainly from particle fluidization and aeration is an important parameter to be considered for industrial applications. For particle fluidization, the up or down flow liquid is required to overcome the pressure drop when the liquid velocity reaches the minimum fluidization velocity. As reported for the CFBBR system, the liquid recirculation was powered by the centrifugal pumps (Andalib et al., 2010; Cui et al., 2004; Nelson et al., 2017). With known liquid flow rate, the energy consumption for particle fluidization could be calculated based on Equation (3.3) (McCabe et al., 2005). It is worth noting that according to Bernouli's equation, the energy of centrifugal pumps depends on the pressure drop difference between the inlet and the outlet. Thus, the density difference (ρ_m - ρ_l) rather than the liquid density ρ_l is used in Equation (3.3). In some cases with particle density close to liquid density (Alvarado-Lassman et al., 2008; Bougard et al., 2006), the gas disturbance caused by aerators is enough to fluidize the particles. Aeration energy for blowers is computed according to Equation (3.4) (Eddy et al., 2014).

$$P_l = \frac{Q_l g h (\rho_m - \rho_l)}{\eta_p \times 3.6 \times 10^6} \tag{3.3}$$

$$P_g = \frac{Q_g T \times 8.314}{22.4 \times 0.283 \times \eta_b} \times \left[\left(\frac{P_2}{P_1} \right)^{0.283} - 1 \right] \times 2.78 \times 10^{-3} \tag{3.4}$$

The energy consumption of IFBBR in this study was calculated and compared with CFBBRs (all lab-scale nitrification-denitrification systems) (Andalib et al., 2010; Chowdhury et al., 2008). The operational conditions and energy consumption results are summarized in Table 3-5 and Figure 3-6. In the calculations, the pressure drops caused by the major and minor frictional losses in the pipelines were neglected due to different configurations. The theoretical COD (THCOD) loading was calculated as the sum of daily inflow TCOD and $4.57 \times NH_3$-N. As shown in Table 3-5, the IFBBR in Phase III treated similar amount of THCOD as CFBBR I, and the DO concentration was kept near 2.0 mg/L in both systems, the energy consumption for aeration was 0.11 (IFBBR I) versus 0.14 (CFBBR I) kWh/kg THCOD. However, the CFBBR system required additional liquid

recirculation for particle fluidization, which consumed 0.27 kWh/kg THCOD. When treating the same amount of THCOD, the energy consumption of CFBBR I was 3.8 times of that in IFBBR I. Similarly, the IFBBR in Phase VI (IFBBR II) treated almost the same amount of THCOD as CFBBR II, while DO was maintained as 1.6 ± 0.3 mg/L in IFBBR II versus 7 ± 0.3 mg/L in CFBBR II. The energy consumption for aeration was 0.27 (IFBBR II) versus 0.48 (CFBBR II) kWh/kg THCOD. Liquid recirculation consumed 0.12 kWh/kg THCOD for CFBBR II. The total energy consumption of CFBBR II was 2.3 times of that in IFBBR II. The analysis demonstrated that IFBBR system was superior to CFBBR system in terms of energy consumption. The advantage of IFBBR system was that it did not require additional liquid recirculation for particle fluidization and was run with low DO concentration in the aerobic zone.
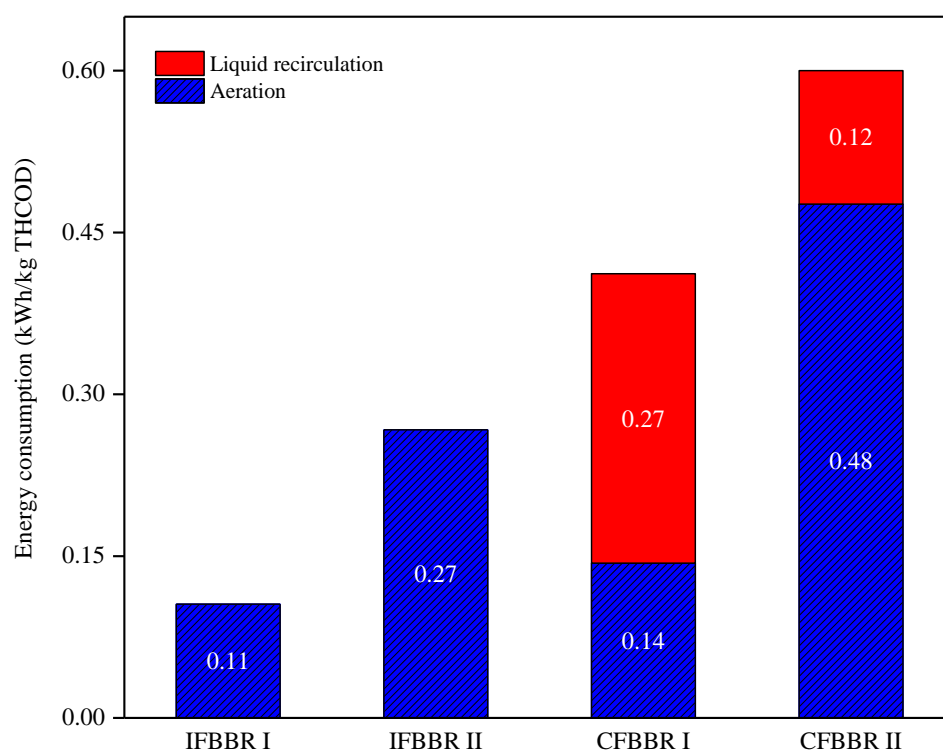
Figure 3-6. The comparison of energy consumption

Table 3-5. Summary of energy consumption in IFBBR and CFBBR systems

	IFBBR I (Phase III)		IFBBR II (Phase VI)		CFBBR I (Chowdhury et al., 2008)		CFBBR II (Andalib et al., 2010)	
	Anoxic	Aerobic	Anoxic	Aerobic	Anoxic	Aerobic	Anoxic	Aerobic
Operational conditions								
Air flow rate (m³/d)	0.03	0.34	—	1.90	—	0.315	—	3.23
Daily COD loading (g COD/d)	32.5		66.5		20.3		62.9	
Daily THCOD loading (g COD/d)	47.4		97.2		29.7		91.5	
DO (mg/L)	0.1-0.3	1.8-2.4	0.05-0.12	1.4-1.9	0.5	2.0	0.1	7.0
Particles	Polypropylene beads				Lava rock			
True density (kg/m³)	904				2628			
Particle weight (kg)	0.86	2.58	0.86	7.07	0.7	1.8	4.7	5.4
Energy consumption								
Aeration (kWh/kg THCOD)	0.11		0.27		0.14		0.48	
Liquid recirculation (kWh/kg THCOD)	—		—		0.27		0.12	
Total (kWh/kg THCOD)	0.11		0.27		0.41		0.60	

3.3.4 Bacterial community structure analysis

3.3.4.1 Phylum level

To investigate the microbial community structure of the attached and detached biomass in the IFBBR system, high-throughput Illumina Sequencing of 16S rRNA genes was performed for samples H1 (aerobic attached biofilm), H2 (anoxic attached biofilm) and H3 (aerobic effluent). 663090-981926 sequences were obtained and clustered to 809-1188 operational taxonomy units (OTUs) in this study. Of all the sequences, only 0.059-0.066% were not assigned to named phyla. Figure 3-7 summarizes the major phyla of each sample. The most abundant phylum was *Proteobacteria* with an average relative abundance (RA) of 50.08% (minimum RA of 35.53% in H3 and maximum RA of 59.38% in H2). The coincident overview of the prominent phylum *Proteobacteria* was found in various WWTPs and bioreactors within the range of 21-65% (Wagner and Loy, 2002; Yang et al., 2011; Zhang et al., 2012). The following dominant phyla were *Bacteroidetes* (mean 23.33%, 12.69%-29.00%), *Epsilonbacteraeota* (mean 17.96%, 1.97%-27.97%), *Firmicutes* (mean 4.89%, 0.88%-10.46%), *Verrucomicrobia* (mean 1.41%, 0.71%-2.09%). These top five phyla accounted for 97% of the total population and were ubiquitous in other systems (Juretschko et al., 2002; Wang et al., 2012). It is worth mentioning the *Epsilonbacteraeota* is a new phylum proposed in 2017 to include the known class *Epsilonproteobacteria* and the order *Desulfurellales* (Waite et al., 2017). One publication revealed *Epsilonbacteraeota* occupied 8.2%-46.6% of the total bacteria in an open-photobioreactor (García et al., 2019), while *Epsilonproteobacteria* was a common phylum reported in various WWTPs (McIlroy et al., 2016; Varela et al., 2014).
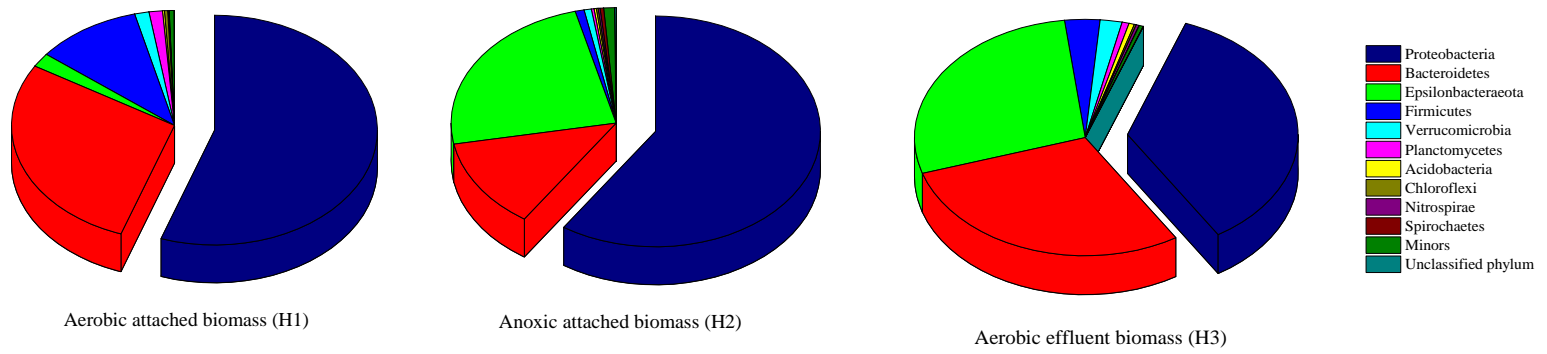
Figure 3-7. The dominant phyla in samples H1, H2 and H3

3.3.4.2 Identification of the core genera

Figure 3-8 shows the dominant genera involving different species. A large proportion of sequences (20%-32%) was not assigned to any genera for samples H1 to H3.

The aerobic attached biomass (Sample H1) potentially occurred under microaerobic conditions with bulk liquid DO of 1.4-1.9 mg/L in Phase VI. The relative abundance (RA) of functional genera nitrifiers AOB and NOB were 0.451% and 0.110%, respectively. The unexpected low abundance of AOB and NOB seems to conflict with the high ammonia removal rate in this system. However, similar phenomena were observed in other studies. The percentage of AOB varied from 0.29% to 0.64% in six full-scale wastewater treatment bioreactors (Zhang et al., 2011). By analyzing three samples taken from a municipal WWTP with anaerobic/anoxic/aerobic system, NOB in the activated sludge were in the range of 0.15%-1.17%, while AOB were hardly detected (Wang et al., 2016). Furthermore, the analysis of bacterial communities in an aerobic granular sludge system revealed that AOB were absent at the NLRs of 0.06-0.72 kg N/(m^3 d) (Zhao et al., 2013). Interestingly, the genera *Haliangium* and *Clostridium_sensu_stricto_13* exhibited RA of more than 10% in sample H1 while the RA was less than 2% in the other samples (H2 and H3). Some literature indicated that the aerobic heterotrophic genus *Haliangium* is capable of nitrite reduction (Wang et al., 2017; Zhou et al., 2014). Additionally, it belongs to the order *Myxobacteria* (slime bacteria) and was suggested as a significant contributor to biofilm formation (Wei et al., 2011). The high RA of *Haliangium* in H1 might be attributed to the nitrite produced in the aerobic column with low bulk DO concentration. The genus *Haliangium* also suppressed the growth of NOB as the competitor for nitrite, resulting in the low RA of NOB. The genus *Clostridium_sensu_stricto_13* is commonly considered as an anaerobic fermenter (Li et al., 2018). However, the presence of genus *Clostridium_sensu_stricto_13* in the aerobic zone with sodium acetate as the carbon source suggested that it had alternative function in this system. It was more reasonable to assign the genus *Clostridium_sensu_stricto_13* to denitrifiers, which were confirmed in several previous studies (Kostrytsia et al., 2018; Xu et al., 2017). The other dominant genera in sample H1 were also classified according to their functions, like the genera *Flavobacterium*

and *Ferruginibacter* which are heterotrophs (Benedict and Carlson, 1971; Liu et al., 2017). Even predators of other bacteria, like the genus *Bdellovibrio* (Rendulic et al., 2004) was found in sample H1 and accounted for 2.25% of the total population.

The top 5 genera in the anoxic attached biofilm (sample H2) were *Arcobacter*, *Zoogloea*, *Thiothrix*, *Dechlorobacter,* and *Acinetobacter*, which were commonly found in the WWTPs (Gao et al., 2016; Zhang et al., 2012). The genus *Arcobacter* was considered as nitrogen-fixing bacteria and dominated by two species, *Arcobacter aquimarinus* and *Arcobacter suis* (Biswas and Turner, 2012). *Zoogloea* is a genus facilitating flocs formation in the activated sludge system (Friedman and Dugan, 1968). The top 5 genera were assigned to denitrifiers except for the genus *Acinetobacter*, which was reported as polyphosphate-accumulating organisms (PAOs) (Wagner et al., 1994). The presence of AOB and NOB in sample H2 was unexpected, while the oxygen entrainment by the synthetic influent (DO ~6.0 mg/L) and the recycled flow from the aerobic zone (DO 1.4-1.9 mg/L) favored the growth of AOB and NOB. In addition, the genus *Chlorobium* was recognized as a sulfate-reducing bacteria (Kirchhoff and Truper, 1974), its relatively higher RA of 0.32% in sample H2 rather than in sample H1 (RA of 0.07%) justified the assumption of sulfate reduction occurring in the anoxic zone needed to close the COD balance.

The effluent biomass (sample H3) was the mixture of detached bacteria from the anoxic and aerobic attached biofilm. Microbial community in sample H3 covered most of the genera present in samples H1 and H2. The dominant genera in samples H1, H2, and H3 were classified into different microbial groups according to the functions reported in the literature (Appendix A). SRT represents the retention time of microbes in the system and is an important parameter for bioreactor design (Eddy et al., 2014). With the identification of genera in the attached and effluent biomass, the SRTs for various microbial groups were determined based on Equation (3.5) and listed in Table 3-6. Specifically, the aerobic SRTs of AOB and NOB were 8.2 days and 2.5 days, respectively. Compared with the system aerobic SRT of 7.1 days, the operational conditions of aerobic zone in Phase VI favored the growth of AOB over NOB. Although the SRT of NOB was as short as 2.5 days, NOB were not washed out due to the minimum SRT of NOB calculated as 1.7 days with

Equations (3.6) and (3.7) at the operational conditions of DO as 1.6 mg/L and NO_2-N as 0.9 mg/L. The kinetic parameters of μ_{max} and b used in Equations (3.6) and (3.7) were 1.0 d^{-1} and 0.17 d^{-1}, respectively (Eddy et al., 2014). Besides, the half-saturation constants $K_{O,NOB}$ of 0.13 mg/L and K_{NO_2} of 0.17 mg/L used in the equations were from the membrane bioreactor system with floc sizes of 100-300 µm (Manser et al., 2005), similar to the aerobic biofilm thickness in Phase VI. For the heterotrophs, both the total and aerobic SRTs of 12.9 and 6.0 days were almost the same as the system total and aerobic SRTs of 13.2 and 7.1 days (based on total VSS), indicating that the system SRT was mostly governed by the heterotrophs as the dominant genera in both anoxic and aerobic biofilms, which accounted for more than 51% of the total biomass.

$$SRT_{total} = \frac{RA_{an}M_{an}X_{an} + RA_{ae}M_{ae}X_{ae}}{RA_{eff}(Q_{eff}VSS_{eff} + X_{waste})} \tag{3.5a}$$

$$SRT_{aerobic} = \frac{RA_{ae}M_{ae}X_{ae}}{RA_{eff}(Q_{eff}VSS_{eff} + X_{waste})} \tag{3.5b}$$

$$\mu = \mu_{max} \frac{S_O}{K_{O,NOB} + S_O} \times \frac{S_{NO_2}}{K_{NO_2} + S_{NO_2}} \tag{3.6}$$

$$SRT_{min} = \frac{1}{\mu - b} \tag{3.7}$$
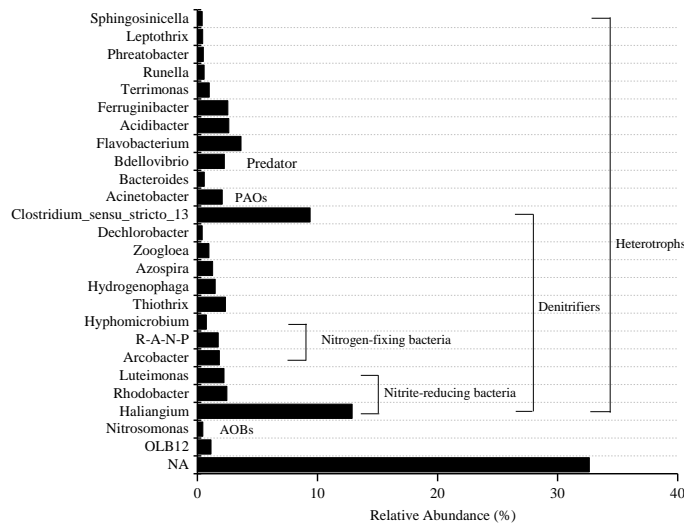
Figure 3-8a. Top 25 genera in aerobic attached biomass (H1)
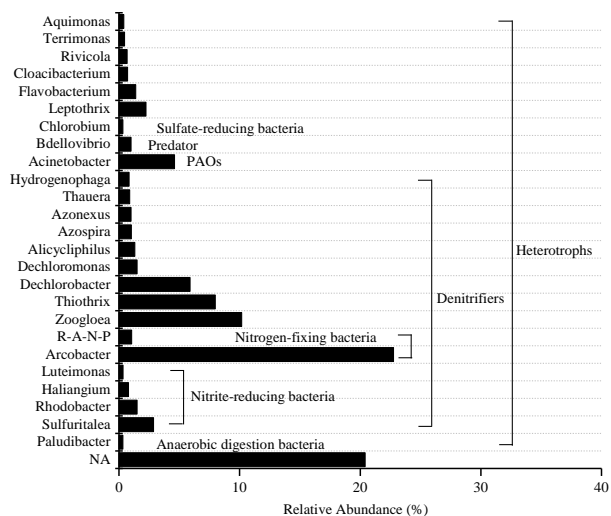
Figure 3-8b. Top 25 genera in anoxic attached biomass (H2)
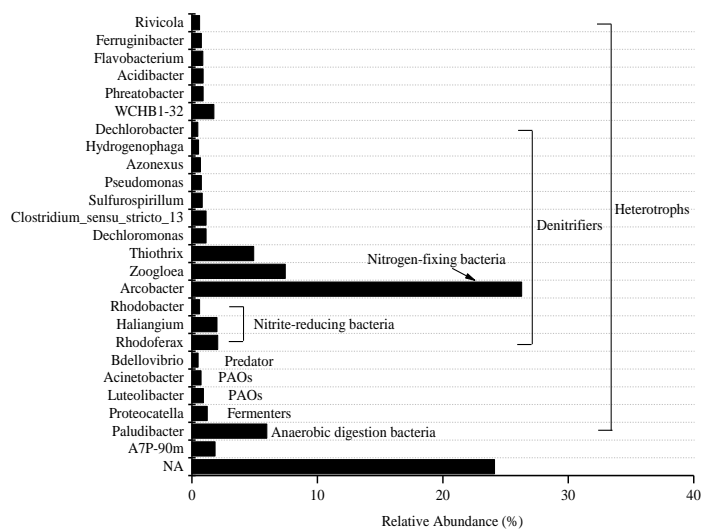
Figure 3-8c. Top 25 genera in aerobic effluent biomass (H3)

Table 3-6. SRTs of different functional species

	Relative abundance (%)			Total SRT (d)	Aerobic SRT (d)
	Aerobic	Anoxic	Effluent		
Nitrifiers (AOB and NOB)	0.56	0.38	0.70	9.1	5.7
AOB (*Nitrosomonas*)	0.45	0.18	0.39	11.0	8.2
NOB (*Nitrospira*)	0.11	0.20	0.30	6.6	2.5
Heterotrophs (Denitrifiers, foaming bacteria, fermenters etc.)	54.32	72.05	63.95	12.9	6.0
Denitrifiers (Nitrogen fixing bacteria, nitrite reducing bacteria etc.)	28.31	58.91	47.69	11.8	4.2
Nitrogen fixing bacteria (*Arcobacter, Hyphomicrobium, Rhodococcus* etc.)	4.32	23.81	26.28	6.7	1.2
Nitrite reducing bacteria (*Haliangium, Rhodobacter, Luteimonas* etc.)	17.55	5.49	4.67	33.7	26.7
Sulfate reducing bacteria (*Chlorobium*)	0.07	0.32	0.01	274.0	53.3
Total biomass based on VSS				13.2	7.1

3.4 Conclusions

The lab-scale integrated IFBBR system was operated at loading rates of 0.34-2.10 kg COD/(m^3 d) and 0.035-0.213 kg N/(m^3 d) to study nutrient removal efficiencies of the system. The principal findings of this study based on the synthetic wastewater used are:

(i) TCOD removal efficiencies of >84% were achieved, concomitantly with complete nitrification. The overall nitrogen removal efficiencies were >75%. Low biomass yields of 0.030-0.101 g VSS/g SCOD were observed.

(ii) The calculations of energy consumption for FBBR systems were proposed. The energy costs for this IFBBR system were 0.11 kWh/kg THCOD at OLR of 1.02 kg COD/(m^3 d) and 0.27 kWh/kg THCOD at OLR of 2.10 kg COD/(m^3 d).

(iii) Bacterial communities were consistent with other full-scale WWTPs, and the dominant phyla were *Proteobacteria, Bacteroidetes*, *Epsilonbacteraeota*, *Firmicutes*, and *Verrucomicrobia.*

(iv) The COD mass balance in the anoxic zone could only be closed with considering of sulfate reduction, which was confirmed with the presence of genus *Chlorobium* (sulfate-reducing bacteria) in the anoxic attached biofilm with the RA of 0.32%.

(v) The bacterial communities both in the anoxic biofilm and aerobic biofilm were dominant by heterotrophs. Total and aerobic SRTs of heterotrophs were consistent on the basis of VSS and microbial community.

References

Alvarado-Lassman, A., Rustrián, E., García-Alvarado, M.A., Rodríguez-Jiménez, G.C., Houbron, E., 2008. Brewery wastewater treatment using anaerobic inverse fluidized bed reactors. Bioresour. Technol. 99, 3009–3015.

American Public Health Association, 2008. Standard methods for the examination of water and wastewater.

Andalib, M., Nakhla, G., Zhu, J., 2010. Dynamic testing of the twin circulating fluidized bed bioreactor (TCFBBR) for nutrient removal from municipal wastewater. Chem. Eng. J. 162, 616–625.

Andalib, M., Nakhla, G., Zhu, J., 2010. Biological nutrient removal using a novel laboratory-scale twin fluidized-bed bioreactor. Chem. Eng. Technol. 33, 1125–1136.

Benedict, R.G., Carlson, D.A., 1971. Aerobic heterotrophic bacteria in activated sludge. Water Res. 5, 1023–1030.

Beristain-cardoso, R., Texier, A., Alpuche-Solis, A., Gomez, J., Razo-Flores, E., 2009. Phenol and sulfide oxidation in a denitrifying biofilm reactor and its microbial community analysis. Process Biochem. 44, 23–28.

Betlach, M.R., Tiedje, J.M., 1981. Kinetic explanation for accumulation of nitrite, nitric oxide, and nitrous oxide during bacterial denitrification. Appl. Environ. Microbiol. 42, 1074–1084.

Bialek, K., Cysneiros, D., Flaherty, V.O., 2014. Hydrolysis, acidification and methanogenesis during low-temperature anaerobic digestion of dilute dairy wastewater in an inverted fluidised bioreactor. Appl. Microbiol. Biotechnol. 98, 8737–8750.

Bialek, K., Kumar, A., Mahony, T., Lens, P.N.L., Flaherty, V.O., 2012. Microbial community structure and dynamics in anaerobic fluidized-bed and granular sludge-bed reactors : influence of operational temperature and reactor configuration. Microb. Biotechnol. 5, 738–752.

Biswas, K., Turner, S.J., 2012. Microbial community composition and dynamics of moving bed biofilm reactor systems treating municipal sewage. Appl. Environ. Microbiol. 78, 855–64.

Bougard, D., Bernet, N., Che, D., Delgene, J., 2006. Nitrification of a high-strength wastewater in an inverse turbulent bed reactor : Effect of temperature on nitrite accumulation. Process Biochem. 41, 106–113.

Buffiere, P., Bergeon, J.-P., Moletta, R., 2000. The inverse turbulent bed : a novel bioreactor for anaerobic treatment. water Res. 34, 673–677.

Callahan, B.J., McMurdie, P.J., Rosen, M.J., Han, A.W., Johnson, A.J.A., Holmes, S.P., 2016. DADA2: High-resolution sample inference from Illumina amplicon data. Nat. Methods 13, 581–583.

Casas, M.E., Chhetri, K.R., Ooi, G., Hansen, K.M.S., Litty, K., Christensson, M., Kragelund, C., Andersen, H.R., Bester, K., 2015. Biodegradation of pharmaceuticals in hospital wastewater by staged moving bed biofilm reactors (MBBR). water Res. 83, 293–302.

Celis-García, L.B., Razo-Flores, E., Monroy, O., 2007. Performance of a down-flow fluidized-bed reactor under sulfate reduction conditions using volatile fatty acids as electron donors. Biotechnol. Bioeng. 97, 771–779.

Chan, Y.J., Chong, M.F., Law, C.L., Hassell, D.G., 2009. A review on anaerobic – aerobic treatment of industrial and municipal wastewater. Chem. Eng. J. 155, 1–18.

Chowdhury, N., Nakhla, G., Zhu, J., 2008. Load maximization of a liquid-solid circulating fluidized bed bioreactor for nitrogen removal from synthetic municipal wastewater. Chemosphere 71, 807–815.

Cui, Y., Nakhla, G., Zhu, J., Patel, A., 2004. Simultaneous carbon and nitrogen removal in anoxic-aerobic circulating fluidized bed biological reactor (CFBBR). Environ. Technol. 25, 699–712.

Dionisi, H.M., Layton, A.C., Harms, G., Gregory, I.R., Robinson, K.G., Sayler, G.S., 2002. Quantification of Nitrosomonas oligotropha-like ammonia-oxidizing bacteria and Nitrospira spp. from full-scale wastewater treatment plants by competitive PCR. Appl. Environ. Microbiol. 68, 245–253.

Eddy, M., Burton, F., Tchobanoglous, G., Tsuchihashi, R., 2014. Wastewater engineering : treatment and resource recovery. McGraw-Hill Education.

Eldyasti, A., Chowdhury, N., Nakhla, G., Zhu, J., 2010. Biological nutrient removal from leachate using a pilot liquid – solid circulating fluidized bed bioreactor (LSCFB). J. Hazard. Mater. 181, 289–297.

Feng, Q., Yu, A., Chu, L., Xing, X.-H., 2008. Performance study of the reduction of excess sludge and simultaneous removal of organic carbon and nitrogen by a combination of fluidized- and fixed-bed bioreactors with different structured macroporous carriers. Biochem. Eng. J. 39, 344–352.

Friedman, B.A., Dugan, P.R., 1968. Identification of Zoogloea species and the relationship to zoogloeal matrix and floc formation. J. Bacteriol. 95, 1903–9.

Gao, P., Xu, W., Sontag, P., Li, X., Xue, G., Liu, T., Sun, W., 2016. Correlating microbial community compositions with environmental factors in activated sludge from four full-scale municipal wastewater treatment plants in Shanghai, China. Appl. Microbiol. Biotechnol. 100, 4663–4673.

GARCIA-CALDERON, D., Buffiere, P., Moletta, R., Elmaleh, S., 1998. Anaerobic digestion of wine distillery wastewater in down-flow fluidized bed. water Res. 32, 3593–3600.

García, D., de Godos, I., Domínguez, C., Turiel, S., Bolado, S., Muñoz, R., 2019. A systematic comparison of the potential of microalgae-bacteria and purple phototrophic bacteria consortia for the treatment of piggery wastewater. Bioresour. Technol. 276, 18–27.

Gloor, G.B., Hummelen, R., Macklaim, J.M., Dickson, R.J., Fernandes, A.D., MacPhee,

R., Reid, G., 2010. Microbiome profiling by Illumina sequencing of combinatorial sequence-tagged PCR products. PLoS One 5, e15406.

Gloor, G.B., Wu, J.R., Pawlowsky-Glahn, V., Egozcue, J.J., 2016. It's all relative: analyzing microbiome data as compositions. Ann. Epidemiol. 26, 322–329.

Gong, L., Jun, L., Yang, Q., Wang, S., Ma, B., Peng, Y., 2012. Biomass characteristics and simultaneous nitrification-denitrification under long sludge retention time in an integrated reactor treating rural domestic sewage. Bioresour. Technol. 119, 277–284.

Juretschko, S., Loy, A., Lehner, A., Wagner, M., 2002. The microbial community composition of a nitrifying-denitrifying activated sludge from an industrial sewage treatment plant analyzed by the full-cycle rRNA approach. Syst. Appl. Microbiol. 25, 84–99.

Kermani, M., Bina, B., Movahedian, H., Amin, M.M., Nikaein, M., 2008. Application of moving bed biofilm process for biological organics and nutrients removal from municipal wastewater, American Journal of Environmental Sciences.

Kirchhoff, J., Truper, H.G., 1974. Adenylylsulfate reductase of Chlorobium limicola. Arch. Microbiol. 100, 115–120.

Kostrytsia, A., Papirio, S., Morrison, L., Ijaz, U.Z., Collins, G., Lens, P.N.L., Esposito, G., 2018. Biokinetics of microbial consortia using biogenic sulfur as a novel electron donor for sustainable denitrification. Bioresour. Technol. 270, 359–367.

Li, M., Nakhla, G., Zhu, J., 2013. Impact of worm predation on pseudo-steady-state of the circulating fluidized bed biofilm reactor. Bioresour. Technol. 128, 281–289.

Li, M., Nakhla, G., Zhu, J., 2012. Simultaneous carbon and nitrogen removal with enhanced bioparticle circulation in a circulating fluidized bed biofilm reactor. Chem. Eng. J. 181, 35–44.

Li, W., Khalid, H., Zhu, Z., Zhang, R., Liu, G., Chen, C., Thorin, E., 2018. Methane production through anaerobic digestion: Participation and digestion characteristics of

cellulose, hemicellulose and lignin. Appl. Energy 226, 1219–1228.

Liu, B., Zhang, F., Feng, X., Liu, Y., Yan, X., Zhang, X., Wang, L., Zhao, L., 2006. Thauera and Azoarcus as functionally important genera in a denitrifying quinoline-removal bioreactor as revealed by microbial community structure comparison. FEMS Microbiol. Ecol. 55, 274–286.

Liu, T., Mao, Y., Shi, Y., Quan, X., 2017. Start-up and bacterial community compositions of partial nitrification in moving bed biofilm reactor. Appl. Microbiol. Biotechnol. 101, 2563–2574.

Loh, K., Ranganath, S., 2005. External-loop fluidized bed airlift bioreactor (EFBAB) for the cometabolic biotransformation of 4-chlorophenol (4-cp) in the presence of phenol. Chem. Eng. Sci. 60, 6313–6319.

Manser, R., Gujer, W., Siegrist, H., 2005. Consequences of mass transfer effects on the kinetics of nitrifiers. Water Res. 39, 4633–4642.

McCabe, W.L., Smith, J.C., Harriott, P., 2005. Unit operations of chemical engineering, Seventh edition. McGraw-Hill, Boston.

McIlroy, S.J., Starnawska, A., Starnawski, P., Saunders, A.M., Nierychlo, M., Nielsen, P.H., Nielsen, J.L., 2016. Identification of active denitrifiers in full-scale nutrient removal wastewater treatment systems. Environ. Microbiol. 18, 50–64.

Nelson, M.J., Nakhla, G., Zhu, J., 2017. Fluidized-bed bioreactor applications for biological wastewater treatment : a review of research and developments. Engineering 3, 330–342.

Nikolov, L., Karamanev, D., 1987. Experimental study of the inverse fluidized bed biofilm reactor. Can. J. Chem. Eng. 65, 214–217.

Patel, A., Zhu, J., Nakhla, G., 2006. Simultaneous carbon, nitrogen and phosphorous removal from municipal wastewater in a circulating fluidized bed bioreactor. Chemosphere 65, 1103–1112.

Pynaert, K., Smets, B.F., Wyffels, S., Beheydt, D., Siciliano, S.D., Verstraete, W., 2003. Characterization of an autotrophic nitrogen-removing biofilm from a highly loaded lab-scale rotating biological contactor. Appl. Environ. Microbiol. 69, 3626–3635.

Rajasimman, M., Karthikeyan, C., 2007. Aerobic digestion of starch wastewater in a fluidized bed bioreactor with low density biomass support. J. Hazard. Mater. 143, 82–86.

Rendulic, S., Jagtap, P., Rosinus, A., Eppinger, M., Baar, C., Lanz, C., Keller, H., Lambert, C., Evans, K.J., Goesmann, A., Meyer, F., Sockett, R.E., Schuster, S.C., 2004. A predator unmasked: life cycle of Bdellovibrio bacteriovorus from a genomic perspective. Science 303, 689–92.

Santegoeds, C.M., Ferdelman, T.G., Muyzer, G., de Beer D, D. de, 1998. Structural and functional dynamics of sulfate-reducing populations in bacterial biofilms. Appl. Environ. Microbiol. 64, 3731–9.

Schramm, A., Beer, D. de, Wagner, M., Amann, R., 1998. Identification and activities in situ of Nitrosospira and Nitrospira spp . as dominant populations in a nitrifying fluidized bed reactor. Appl. Environ. Microbiol. 64, 3480–3485.

Siripong, S., Rittmann, B.E., 2007. Diversity study of nitrifying bacteria in full-scale municipal wastewater treatment plants. water Res. 41, 1110–1120.

Sowmeyan, R., Swaminathan, G., 2008. Performance of inverse anaerobic fluidized bed reactor for treating high strength organic wastewater during start-up phase. Bioresour. Technol. 99, 6280–6284.

Sur, D.H., Mukhopadhyay, M., 2017. Process aspects of three-phase inverse fluidized bed bioreactor : A review. J. Environ. Chem. Eng. 5, 3518–3528.

Tavares, C.R.G., Sant'anna, G.L., Capdeville, B., 1995. The effect of air superficial velocity on biofilm accumulation in a three-phase fluidized-bed reactor. Water Res. 29, 2293–2298.

Tsuneda, S., Nagano, T., Hoshino, T., Ejiri, Y., Noda, N., Hirata, A., 2003.

Characterization of nitrifying granules produced in an aerobic upflow fluidized bed reactor. water Res. 37, 4965–4973.

Varela, A.R., André, S., Nunes, O.C., Manaia, C.M., 2014. Insights into the relationship between antimicrobial residues and bacterial populations in a hospital-urban wastewater treatment plant system. Water Res. 54, 327–336.

Wagner, M., Erhart, R., Manz, W., Amann, R., Lemmer, H., Wedi, D., Schleifer, K.H., 1994. Development of an rRNA-targeted oligonucleotide probe specific for the genus Acinetobacter and its application for in situ monitoring in activated sludge. Appl. Environ. Microbiol. 60, 792–800.

Wagner, M., Loy, A., 2002. Bacterial community composition and function in sewage treatment systems. Curr. Opin. Biotechnol. 13, 218–227.

Waite, D.W., Vanwonterghem, I., Rinke, C., Parks, D.H., Zhang, Y., Takai, K., Sievert, S.M., Simon, J., Campbell, B.J., Hanson, T.E., Woyke, T., Klotz, M.G., Hugenholtz, P., 2017. Comparative genomic analysis of the class Epsilonproteobacteria and proposed reclassification to Epsilonbacteraeota (phyl. nov.). Front. Microbiol. 8, 682.

Wang, H., Kim, M., Li, K., Shao, Y., Zhu, J., Nakhla, G., 2019. Effective partial nitrification of ammonia in a fluidized bed bioreactor. Environ. Technol. 40, 94–101.

Wang, P., Yu, Z., Qi, R., Zhang, H., 2016. Detailed comparison of bacterial communities during seasonal sludge bulking in a municipal wastewater treatment plant. Water Res. 105, 157–166.

Wang, X., Hu, M., Xia, Y., Wen, X., Ding, K., 2012. Pyrosequencing analysis of bacterial diversity in 14 wastewater treatment systems in China. Appl. Environ. Microbiol. 78, 7042–7047.

Wang, X., Zhao, Y., Li, X., Ren, Y., 2017. Performance evaluation of a microfiltration-osmotic membrane bioreactor (MF-OMBR) during removing silver nanoparticles from simulated wastewater. Chem. Eng. J. 313, 171–178.

Wang, Z., Zhang, X., Lu, X., Liu, B., Li, Y., Long, C., Li, A., 2014. Abundance and diversity of bacterial nitrifiers and denitrifiers and their functional genes in tannery wastewater treatment plants revealed by high-throughput sequencing. PLoS One 9, 1–19.

Wei, X., Pathak, D.T., Wall, D., 2011. Heterologous protein transfer within structured myxobacteria biofilms. Mol. Microbiol. 81, 315–326.

Xing, W., Ngo, H.H., Guo, W.S., Listowski, A., Cullum, P., 2011. Evaluation of an integrated sponge – granular activated carbon fluidized bed bioreactor for treating primary treated sewage effluent. Bioresour. Technol. 102, 5448–5453.

Xu, Dan, Xiao, E., Xu, P., Zhou, Y., He, F., Zhou, Q., Xu, Dong, Wu, Z., 2017. Performance and microbial communities of completely autotrophic denitrification in a bioelectrochemically-assisted constructed wetland system for nitrate removal. Bioresour. Technol. 228, 39–46.

Yang, C., Zhang, W., Liu, R., Li, Q., Li, B., Wang, S., Song, C., Qiao, C., Mulchandani, A., 2011. Phylogenetic diversity and metabolic potential of activated sludge microbial communities in full-scale wastewater treatment plants. Environ. Sci. Technol. 45, 7408–7415.

Zhang, T., Shao, M.-F., Ye, L., 2012. 454 Pyrosequencing reveals bacterial diversity of activated sludge from 14 sewage treatment plants. ISME J. 6, 1137–1147.

Zhang, T., Ye, L., Tong, A.H.Y., Shao, M.-F., Lok, S., 2011. Ammonia-oxidizing archaea and ammonia-oxidizing bacteria in six full-scale wastewater treatment bioreactors. Appl. Microbiol. Biotechnol. 91, 1215–1225.

Zhang, Y., Cheng, Y., Yang, C., Luo, W., Zeng, G., Lu, L., 2015. Performance of system consisting of vertical flow trickling filter and horizontal flow multi-soil-layering reactor for treatment of rural wastewater. Bioresour. Technol. 193, 424–432.

Zhao, Y., Huang, J., Zhao, H., Yang, H., 2013. Microbial community and N removal of aerobic granular sludge at high COD and N loading rates. Bioresour. Technol. 143, 439–446.

Zhou, Z., Qiao, W., Xing, C., Shen, X., Hu, D., Wang, L., 2014. A micro-aerobic hydrolysis process for sludge in situ reduction: Performance and microbial community structure. Bioresour. Technol. 173, 452–456.

Chapter 4

Inverse Fluidized Bed Bioreactor (IFBBR) for Municipal Wastewater Treatment – Performance and Modeling

4.1 Introduction

Recent environmental restrictions for wastewater discharges have been more stringent due to the continued population growth and the increasing awareness of surface water quality deterioration in many countries. The need for technological solutions to enhance nutrients (especially carbon and nitrogen) removal is becoming urgent (Grandclément et al., 2017). The attached growth biological treatment processes have gained interest and been proven to be economical and efficient (Dempsey et al., 2005). Numerous investigations have been published with fixed-biofilm technologies for wastewater treatment, such as rotating biological contactors (Hassard et al., 2015), trickling filters (Mann and Stephenson, 1997), sponge bioreactors (Nguyen et al., 2010), moving bed biofilm reactors (MBBRs) (Zekker et al., 2012), and circulating fluidized bed bioreactors (CFBBRs) (Cui et al., 2004).

Particularly, the MBBR is a highly effective biological treatment process, which has been developed and successfully running since the 1980s (Ødegaard, 2006). The basic principal of the MBBR process is that plastic carriers with biomass attachment are kept moving by the agitation caused by diffusers in the aerobic zone or by a mechanical stirrer in the anaerobic/anoxic zone, which eliminates the need for recycling of biological sludges (Kermani et al., 2008; Ødegaard et al., 1994). The hollow carriers are specially designed and provide high surface area (about 500 m^2/m^3) for biofilm attachment. Besides, the particles have the "walls" to protect the attached biomass from high shear force, which results in that MBBR favor the growth of slow-growth microorganisms such as nitrifiers in the aerobic bioreactors (Barwal and Chaudhary, 2014; Rusten et al., 2006, 1995). However, the carriers need patented special design for the "walls", which requires more initial capital investments. Meanwhile, the MBBR is usually operated at elevated DO level (3-7 mg/L) in the aerobic zone for the fluidization of carriers, which increases the

operational costs (Ali Kawan et al., 2016). The other emerging fixed-biofilm technology is circulating fluidized bed bioreactor (CFBBR). CFBBR has been tested for biological nutrient removal (BNR) for municipal wastewater in both lab- and pilot-scales (Chowdhury et al., 2009). The implement of denitrification and nitrification within the integrated anoxic riser and aerobic downer makes the CFBBR system outcompete with other processes (Nelson et al., 2017). In summary, CFBBR system achieved more than 90% organic, 75-80% total nitrogen removal without particles recirculation and additional 85% phosphorous removal with particles recirculation for municipal wastewater treatment at hydraulic retention time (HRT) of 2-3 hrs, with low observed biomass yield of 0.07-0.16 g VSS/g COD. Natural material i.e. lava rock, with small diameter (0.6-1.0 mm), large surface area (0.48 m^2/g particles) and heavy density (2628 kg/m^3), was used as the carriers for biomass growth in the CFBBR system (Andalib et al., 2010; Chowdhury et al., 2008; Islam et al., 2009; Li et al., 2012). Liquid recirculation was required in each column to fluidize the carriers. As reported, the energy consumption for liquid recirculation accounted for 65% of the overall energy utilization (Eldyasti et al., 2012a). To circumvent the drawbacks and combine the advantages of MBBR and CFBBR systems, integrated inverse fluidized bed bioreactor (IFBBR) was built and tested for BNR with synthetic acetate carbon-based wastewater.

With the development of fixed-biofilm treatment processes, mathematical biofilm models and numerical analysis have been studied by many researchers (Takács et al., 2007; Wanner and Reichert, 1996). There are several commercial user-friendly software with one-dimensional fully dynamic and steady-state biofilm model, such as AQUASIM (EAWAG, Switzerland), BioWin (Envirosim Associates Ltd., Burlington, ON), AQUIFAS (Aquaregen, Mountain View, CA), and WEST (Mostforwater, Belgium) (Andalib et al., 2011; Boltz et al., 2010; Wanner and Morgenroth, 2004). Among them, Biowin has been applied to simulate a pilot-scale CFBBR system with treating municipal wastewater and landfill leachate (Eldyasti et al., 2012b, 2011). The results proved the accuracy of Biowin for modeling of the CFBBR system. Using the calibrated model, the impact of different carbon to nitrogen ratios of the influent on system performance was predicted to provide guidance for CFBBR operation (Luo et al., 2019).

To further investigate the application of integrated IFBBR system for actual municipal wastewater treatment, sludge from the primary clarifier was added to the SMW to examine the BNR performance during the treatment of high particulate COD wastewater. Moreover, the short response of the IFBBR system to composition disturbances in the influent, particularly the organic shock loads, was studied. IFBBR model was built and calibrated with the experimental data using Biowin. The impact of operational conditions on system performance was predicted with the IFBBR model.

4.2 Materials and methods

The wastewater was prepared daily with tap water combined with 240 mg COD/L as CH_3COONa, 25 mg N/L as NH_4Cl, 3 mg P/L as KH_2PO_4 and 200 mg $CaCO_3$/L as $NaHCO_3$. The trace metal solution, which was added to the feed at 1.5 mL/L, was composed of 15 mg EDTA/L, 0.43 mg $ZnSO_4\cdot7H_2O$/L, 0.24 mg $CoCl_2$/L, 0.99 mg $MnCl_2$/L, 0.25 mg $CuSO_4\cdot H_2O$/L, 0.22 mg $NaNoO_4\cdot H_2O$/L, 0.19 mg $NiCl\cdot6H_2O$/L, and 0.014 mg H_3BO_4/L. The primary sludge taken from Adelaide Water Pollution Control Plant (London, Canada) was added into the synthetic wastewater at a flow-to-feed ratio of 1/140 for particulate COD. The TSS and VSS contents of the primary sludge were measured as 29200 and 18900 mg/L, respectively, as well as the TCOD and SCOD concentrations were approximately 37000 and 1600 mg/L, respectively.

4.2.1 Reactor description

Two 4-m high plexiglass columns were used as anoxic and aerobic zones, respectively, with a free board of 0.4 m at the top of both columns to avoid carrier overflow (Figure 4-1). The 3.8 cm inner diameter (ID) and 4.0 L anoxic column was operated as an inverse liquid-solid fluidized bed. The combination of liquid rate provided by inflow and recirculated flow from the aerobic zone was adequate to fluidize the carriers, where the inflow was controlled by a peristaltic pump (Masterflex I/P; Masterflex, Germany), and the liquid recirculation of 3.5-4.5 times inflow was controlled by a centrifugal pump (MD-70RLT, Iwaki, Japan). In the 10 cm ID and 28.3 L aerobic column, carriers were fluidized by the agitation from the fine bubble aerator (Xinggang Ltd, China). Bed was expanded to

3.3 m after fluidization. The aerator was installed 20 cm above the bottom of the aerobic column. To maintain carrier fluidization and the bulk liquid DO of > 1.8 mg/L, air flow rate of 2.10 m³/d was monitored and controlled by a rotameter (Omega Engineering INC, USA). Feed wastewater went through the anoxic zone from the top to the bottom, then got into the top of the aerobic zone, and finally treated effluent overflowed from the water balance tank. The detailed operational conditions and system dimensions are shown in Table 4-1.
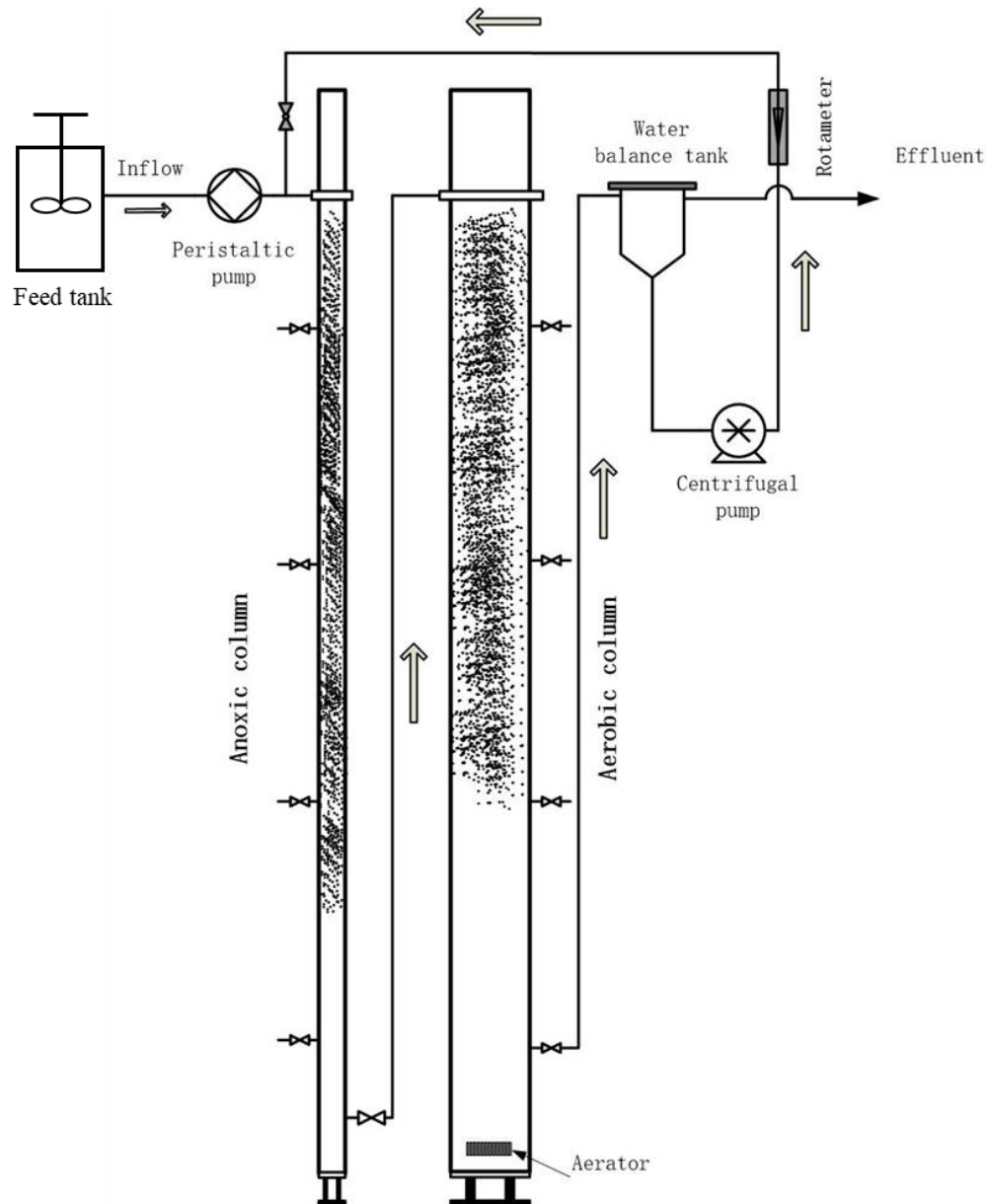
Figure 4-1. The schematic diagram of IFBBR system for municipal wastewater treatment

Table 4-1. Operational conditions

		Stable-state phase
Influent flow rate (L/d)		210 ± 5.2
Air flow rate (m^3/d)	Aerobic	2.31
DO (mg/L)	Anoxic	0.1-0.3
	Aerobic	1.8-2.4
Particles weight (kg)	Anoxic	1.05
	Aerobic	7.07
HRT (h)	Anoxic	0.5
	Aerobic	3.2
EBCT (h) = $V_{compact}/Q_{in}$	Anoxic	0.19
	Aerobic	1.29
Average organic loading (kg COD/(m^3 d))		2.77
Average nitrogen loading (kg N/(m^3 d))		0.26
Average organic loading based on compacted bed volume (kg COD/(m^3 d))		7.57
Average nitrogen loading based on compacted bed volume (kg N/(m^3 d))		0.71
Average attached biomass (mg VSS/g particle)	Anoxic	25.9
	Aerobic	6.5
Biomass (g VSS)	Anoxic	27.2
	Aerobic	46.0
F/M ratio (g COD/(g VSS d))	Anoxic	3.29
F/M ratio (g N/(g VSS d))	Aerobic	0.18

4.2.2 Reactor start-up

The carrier particles for biomass attachment are activated carbon-coated polypropylene beads with an average diameter of 3.2 mm (3.0-3.5 mm), true density of 904 kg/m^3, and specific surface area of 1890 m^2/kg. The amount of particles used in the anoxic and aerobic columns were 1.05 kg (2.0 L compacted bed volume) and 7.07 kg (11.5 L compacted bed volume), respectively. The experiment was performed as a continuous study for municipal wastewater treatment with high particulate COD in the IFBBR system. Biomass was well established on the particle surface after more than 230 days of stable operation with synthetic wastewater. Initially, the attached biomass was measured as 42.1 and 5.90 mg VSS/g particle in the anoxic and aerobic zones, respectively. The biomass specific nitrification rate (SNR) of the attached aerobic biomass was 0.24 $\pm$ 0.01 g N/(g VSS d), while the biomass specific denitrification rate (SDNR) of the attached anoxic biomass was 0.36 $\pm$ 0.03 g N/(g VSS d).

4.2.3 Batch tests

The biomass SNR of the aerobic attached biofilm and the biomass SDNR of the anoxic attached biofilm were measured using batch tests in the 0.5-L working volume BOD bottles equipped with magnetic stirrers once a week. In order to eliminate the substrate transfer limitations, attached biofilms were detached from the carriers by 3h sonication. Approximately 20 g bioparticles were used for the biomass SNR test of aerobic biofilm, at initial concentrations of 25-35 mg N/L, 200-250 mg/L alkalinity as CaCO$_3$. By injecting air in the BOD bottle with air diffuser (Xinggang Ltd, China), DO was kept above 5.0 mg/L through the test. For the SDNR tests of the anoxic biofilm, approximately 10 g bioparticles were used, with the initial acetate COD of 250-350 mg/L and the NO$_3$-N of 20-35 mg/L. The initial food-to-microorganism (F/M) ratios of batch tests were determined by the nutrient loading and attached biomass in the IFBBR system.

4.2.4 Analytical methods

Samples from the feed tank (influent), the bottom of the anoxic column, and the final effluent were collected at three days interval with airtight bottles, then refrigerated at 4°C

before analysis. Total suspended solids (TSS), volatile suspended solids (VSS) were analyzed with Standard Methods no 2540D, 2540E, respectively (American Public Health Association, 2008). The organic matter (TCOD and SCOD), various nitrogen (TN, NH_3-N, NO_2-N, NO_3-N) and phosphorus (TP and PO_4-P) were measured with testing kits provided by Hach company. Orion Star A323 (Thermo scientific, Oakwood, USA) were used to measure the DO and temperature in the bulk liquid. For the measurement of biofilm thickness, bioparticles suspended in water were observed with the microscope (Mitutoya, Japan) coupled with a camera (Leica DC 300, Germany) at a magnification of 50X. Approximately 10 g bioparticles from each column were taken to determine the amount of attached biomass and expressed as mg VSS/g particle. Bioparticles were suspended in a 100 ml vial with deionized water, stirred at speed of 350 rpm for 2 hrs on the stirring plate (PC-6200, Corning, USA). After sonication for 3 hrs at 30°C in an Aquasonic Sonicator (Changzhou, China), the amount of VSS was determined following Standard Methods no 2540 E. The clean particles were dried naturally and weighted.

4.2.5 Statistical analysis and modeling simulation

BioWin version 5.2 software (EnviroSim Associates Ltd. Canada) was used to simulate the IFBBR system with media bioreactor as the biological reactor. The simulated and experimental data were processed with Excel software.

4.3 Results and discussions

4.3.1 General performance

4.3.1.1 Nutrient removal

The COD removal performance is illustrated in Figure 4-2a and Table 4-2. The system was run at hydraulic retention time (HRT) of 3.7 hrs, with influent TCOD of 416 ± 21 mg/L and SCOD of 269 ± 23 mg/L, respectively. 87% TCOD removal efficiency was achieved at an organic loading rate (OLR) of 2.7 kg COD/(m^3 d). For the soluble COD, 94% SCOD removal efficiency was achieved with effluent SCOD of 16 ± 4 mg/L. Compared with the IFBBR system for synthetic wastewater treatment at the same inflow of 210 L/d, the OLR

increased 30% with more particulate COD in the influent, while the COD removal efficiency was similar as the previous study. Besides, the influent TSS and VSS were kept as 146 ± 17 and 95 ± 14 mg/L, respectively. An average effluent TSS of 37 mg/L was reached, corresponding to 75% suspended solids removal. The effluent TSS in this study was slightly higher than the effluent TSS of 26 mg/L for treating of the synthetic wastewater with almost no TSS in the influent. In the IFBBR system, the bioparticles with attached biomass floated in the top zone as the density was lower than the density of wastewater. Free board zone at the bottom provided an excellent settling region for the heavy organic matter settled. The daily sludge discharge was calculated as 2.1 g VSS/d, 40% larger than the sludge discharge of 1.5 g VSS/d for synthetic wastewater treatment. The extra sludge may be from the accumulation of nbVSS and more detached biomass in the system.

The performance of IFBBR system for nitrification and denitrification is presented in Figure 4-2b and Table 4-2. The nitrogen loading rate (NLR) was 0.26 g $N/(m^3$ d) with influent TN and NH_3-N of 39.8 ± 2.4 and 28.4 ± 1.6 mg/L, respectively. On average 73% total nitrogen removal was achieved with effluent TN of 10.7 ± 0.7 mg/L. Nitrification mainly occurred in the aerobic zone and DO was maintained as 2.1 mg/L, which may be not sufficient for full nitrification as the effluent NH_3-N was 1.3 ± 0.8 mg/L with NO_2-N generated. Ammonia was converted mainly to NO_3-N, with effluent NO_3-N and NO_2-N of 5.4 ± 0.7 and 0.51 ± 0.15 mg/L, respectively. The attached aerobic biomass was measured as 6.5 ± 0.8 mg VSS/ g particles. With known of the total amount of particles in the aerobic zone, the nitrification rate was calculated as 0.13 g N/(g VSS d). Batch tests were carried out to determine the biomass SNR of the attached aerobic biomass under DO concentration around 6.0 mg/L, the biomass SNR was 0.21 ± 0.04 g N/(g VSS d) based on four tests. The discrepancy (61%) between the online and offline biomass SNRs demonstrate that DO was affecting the nitrification performance in the aerobic biofilm as DO was maintained as 2.1 mg/L (online) versus >5.0 mg/L (offline). The NO_X-N produced was recirculated to the anoxic zone for denitrification with recirculation-inflow ratio of 3.5-4.5. Recirculated NO_X-N was not fully denitrified as the average anoxic effluent NO_X-N was 1.3 mg/L. The attached anoxic biomass was measured as 25.9 ± 4.5 g VSS/g particles, and the batch tests showed the SDNR of attached anoxic biomass was 0.41 ± 0.02 g N/(g VSS d). Compared

with the initial biomass characteristics, although the total amount of anoxic biomass decreased by 25% due to the impact of particulate organic matter, whereas the biomass SDNR increased by 14%. Based on the total amount of anoxic biomass, the online denitrification rate was 0.13 g N/(g VSS d). The discrepancy (215%) between the online and offline biomass SDNRs was attributed to mass transfer limitations, as the thickness of attached anoxic biofilm was observed to be 500-600 μm.

Figure 4-2c shows the TP and ortho-phosphates concentrations in the influent, anoxic effluent, and final effluent. As evident in Table 4-2, the initial ortho-phosphates concentration at the top of the anoxic zone was calculated as 2.26 mg/L based on the ortho-phosphates concentrations in the influent and final effluent of 3.7 mg/L and 1.9 mg/L, respectively. Compared with the ortho-phosphorus in the anoxic effluent of 2.4 mg/L, 0.14 mg/L ortho-phosphorus was released in the anoxic zone. Then extra phosphorus was absorbed for biomass synthesis as 0.5 mg/L ortho-phosphates was reduced in the aerobic zone. 48% overall phosphorus removal was achieved by biomass precipitation. The average phosphorus content in the effluent and discharge sludge was measured as 3.2 ± 0.1% by weight of TSS, which was in the range of P content in effluent biomass (1.7%-5.2%) observed in other FBBRs (Chowdhury et al., 2009), while higher than the P content of 1% in the conventional sludge (Eddy et al., 2014).

Table 4-2. Stable-state water characteristics

Water parameter	Influent	Anoxic	Effluent
pH	7.67±0.17	7.54±0.18	7.52±0.15
Alk (mg/L as $CaCO_3$)	257±18	219±18	187±22
TCOD (mg/L)	416±21	101±12	54±8
SCOD (mg/L)	269±23	45±9	16±4
TN (mg/L)	39.8±2.4	12.9±1.2	10.7±0.7
NH_3-N (mg/L)	28.4±1.6	6.9±0.8	1.3±0.8
NO_3-N (mg/L)	0.6±0.3	1.2±0.6	5.4±0.7
NO_2-N (mg/L)	—	0.12±0.1	0.51±0.15
TP (mg/L)	5.3±0.5	3.4±0.5	2.7±0.4
PO_4-P (mg/L)	3.7±0.4	2.4±0.3	1.9±0.4
TSS (mg/L)	146±17	53±9	37±5
VSS (mg/L)	95±14	39±8	28±6
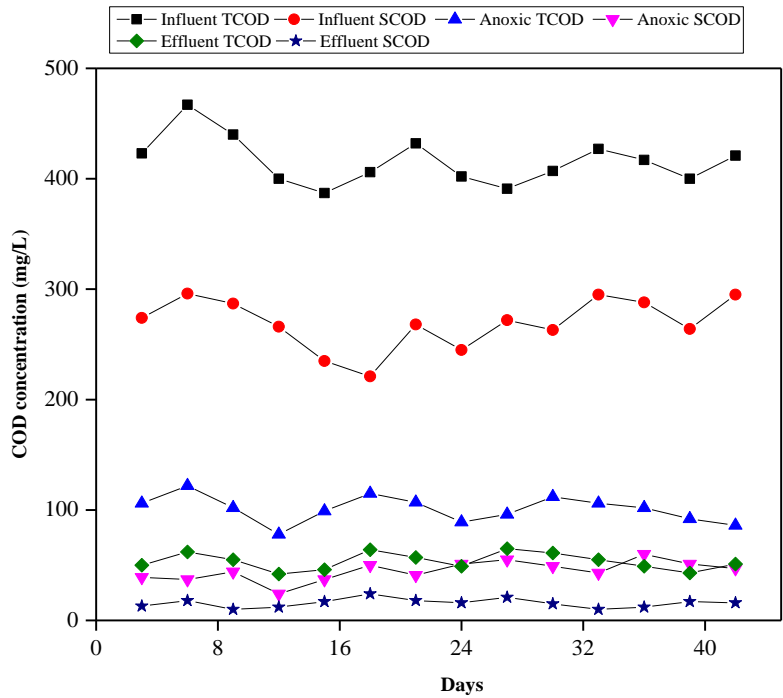
Figure 4-2a. COD concentrations in the influent, anoxic effluent and system effluent
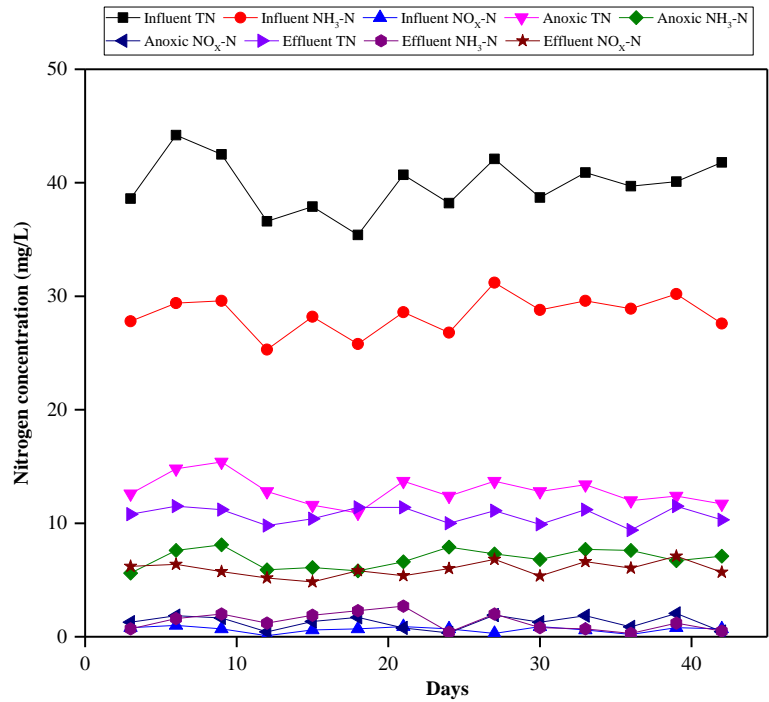
Figure 4-2b. Nitrogen concentrations in the influent, anoxic effluent and system effluent
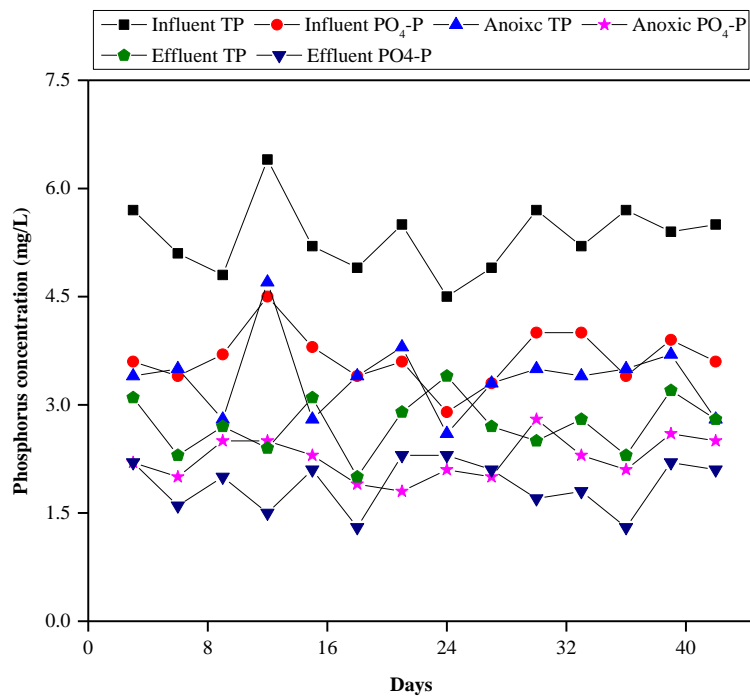
Figure 4-2c. Phosphorus concentrations in the influent, anoxic effluent and system effluent

4.3.1.2 Biomass yield

The observed sludge yield was calculated as the sum of the effluent biomass and the wasted sludge divided by the total COD consumed. An average of 2.1 g VSS/d sludge was wasted from the bottom of the aerobic zone, with final effluent VSS concentration of 28 ± 6 mg/L. The observed sludge yield was estimated as 0.15 g VSS/g COD based on Figure 4-3, which illustrates a linear regression of cumulative VSS produced versus cumulative COD removed. Sludge retention time (SRT) was calculated as 9.2 days based on Equation (4.1). As the biomass SNRs of aerobic attached biomass and effluent biomass were measured as 0.21 ± 0.04 g N/(g VSS d) and 0.04 ± 0.01 g N/(g VSS d), the system SRT was 48 days based on biomass SNR test. With a known system SRT, the theoretical biomass yield was found similar as the experimental value, computed as 0.18 g VSS/g COD according to Equation (4.2), where $Y = 0.36$ g VSS/g COD, $b = 0.15$ g VSS/(g VSS d), $f_d = 0.15$ g VSS/g VSS (Gerardi, 2002). Compared with the IFBBR system treating synthetic wastewater, the sludge yield increased by 46%, demonstrated the impact of high influent particulate COD.

$$SRT = \frac{M_{an}X_{an} + M_{ae}X_{ae}}{Q_{eff}VSS_{eff} + X_{waste}} \tag{4.1}$$

$$Y_{obs} = \frac{Y}{1+(b)SRT} + \frac{(f_d)(b)(Y)(SRT)}{1+(b)SRT} \tag{4.2}$$
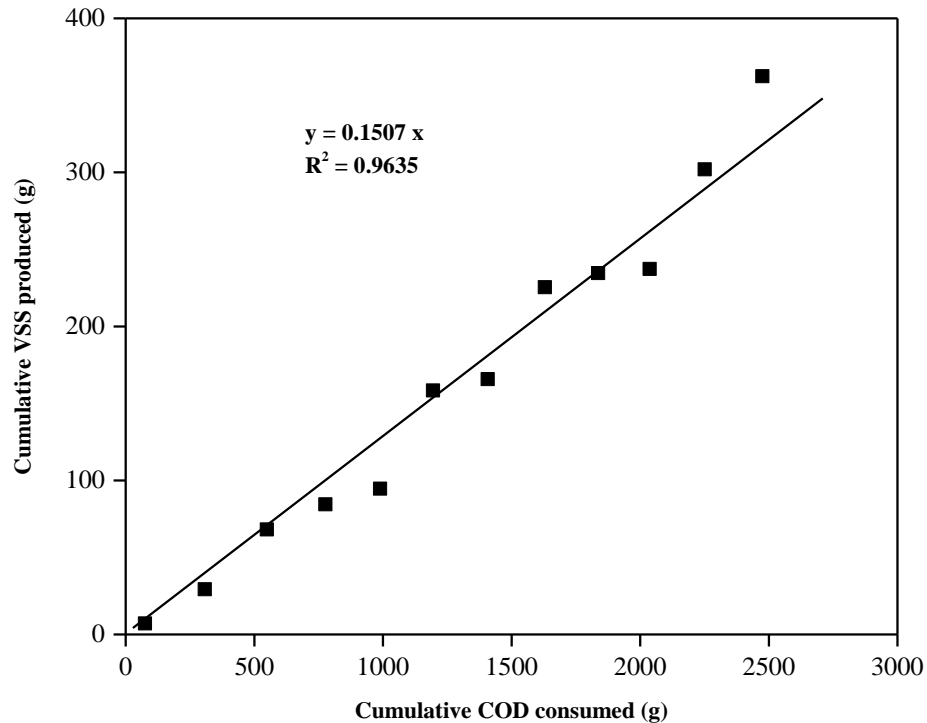
Figure 4-3. Biomass yield

4.3.1.3 Mass balance

Table 4-3 presents the detailed mass balance for COD, nitrogen, phosphorus, and alkalinity. The mass balance was based on experimental data of water characteristics in the influent, anoxic and final effluent, and the sludge wastage. The mass removal rates were calculated according to the difference between influent and effluent mass rates in each zone. For the values, positive represents removal while negative means generation.

As shown in Table 4-3, SCOD consumption in the anoxic zone accounted for 42% of overall SCOD removal. For anoxic COD closure, COD utilized for denitrification of 13.77

g was calculated based on Equation (4.3) with 3.79 g nitrate and nitrite reduced, while COD consumed aerobically in the anoxic zone was 2.94 g as the impact of inflow DO (~ 6mg/L) and liquid recirculation from the aerobic zone (DO 2.1 mg/L). The alkalinity balance in the anoxic zone did not close. The difference between the theoretical and actual alkalinity generation was used for the calculation of COD consumed by sulfate-reducing bacteria, as 4.08 g COD/d. The COD closure was 92.1% with consideration of denitrification, aerobic COD utilization, and sulfate reduction (Andalib, 2011; Anoop and Viraraghavan, 1997). The anoxic TCOD consumption accounted for only 36% of the overall TCOD removal, while 54% of influent TCOD was consumed in the aerobic zone. In this IFBBR system, the HRTs in the anoxic and aerobic zones were 0.5 hrs and 3.2 hrs, respectively. Longer HRT favored the breakdown of slowly biodegradable COD (Torrico et al., 2006). Besides, average 2.1 g VSS/d sludge was wasted from the bottom of the aerobic zone, which facilitated the particulate COD removal. Thus, it was reasonable that more TCOD was removed in the aerobic zone rather than in the anoxic zone.

Nitrification in the aerobic zone removed 5.89 g N/d of ammonia. As the DO concentration was kept as 2.1 mg/L, part of ammonia nitrogen was converted to nitrite. The nitrite and nitrate generation rates were 4.49 g N/d and 0.41 g N/d. The nitrogen mass balance closure in the aerobic zone was 86%, while the discrepancy may be due to denitrification in the aerobic zone. In the anoxic zone, the main reaction for nitrogen removal was denitrification, with 3.49 g NO_3-N/d consumed. Besides, 0.20 g NH_3-N/d was utilized for biomass synthesis. Alkalinity consumed in the aerobic zone was 33.6 g/d as $CaCO_3$, which was in 104% of the calculated alkalinity consumption based on NO_X-N generation. Phosphorus removal was mainly due to the biomass assimilation (Seviour et al., 2003). 0.13 g TP/d was released in the anoxic zone and 0.60 g TP/d was removed in the aerobic zone.

$$COD_{den} = \frac{2.86}{1-1.42 \times Y_{obs}}$$
(4.3)

Table 4-3. Mass balance for stable-state phase

	Mass in influent [g/d]	Mass consumed [g/d] Anoxic	Aerobic	Mass in effluent [g/d]	Mass wastage [g/d]	Percentage closure [%]
Alkalinity	53.21	-19.56	33.60	39.17		104.1[f]
		(-13.53)[a]	(34.99)[b]			
TCOD	87.30	26.34	46.74	11.24	2.98	
SCOD	56.54	22.58	30.68	3.29		92.1[g]
		(13.77)[c] (2.94)[d] (4.08)[e]				
TN	8.36	3.84	2.06	2.25	0.21	
NH$_3$-N	5.97	-0.20	5.89	0.27		
NO$_3$-N	0.14	3.49	-4.49	1.14		
NO$_2$-N	0.00	0.30	-0.41	0.11		
TP	1.12	-0.13	0.60	0.57	0.07	
PO$_4$-P	0.77	-0.01	0.38	0.40		

a. Alkalinity generated in the anoxic zone by denitrification

b. Alkalinity consumed in the aerobic zone

c. SCOD consumption through denitrification

d. Aerobic SCOD consumption in the anoxic zone

e. SCOD consumed by SRB

f. COD closure in the anoxic zone

g. Ammonia closure in the aerobic zone

4.3.2 Organic shock test

The organic shock test was conducted at the end of the experiment to examine the sensitivity of IFBBR system performance to influent organic variations. Sodium acetate was used as the carbon source, added into the feed to increase the influent COD from 380 mg/L to 810 mg/L and then 1320 mg/L, corresponding to an ultimate OLR of 8.7 kg COD/(m^3 d). As the objective was to simulate the short effect of organic shock on the nutrient removal, the duration of each test was maintained for 6.0 hrs, about 1.7 times of the mean system HRT. For the integrated IFBBR system, the organic loading increment affected the nitrification in the aerobic zone due to the competition between the heterotrophs and autotrophs for dissolved oxygen. As reported, nitrification only started after the SCOD concentration was lower than 20 mg/L (Eddy et al., 2014). Besides, the maximum specific growth rates of heterotrophs, ammonia-oxidizing bacteria (AOB) and nitrite-oxidizing bacteria (NOB) at 25°C are 3.2, 0.9 and 1.0 d^{-1}, respectively (Eddy et al., 2014; Liu et al., 2017). The lack of enough dissolved oxygen and abundance of substrate COD in the aerobic zone during the organic shock tests would facilitate the growth of heterotrophs over autotrophs, resulting in the domination of heterotrophs on the particle surface. As shown in Figure 4-4, the effluent SCOD increased from 12 mg/L to as high as 405 mg/L, with the SCOD removal efficiency dropped from 95% to 65%. Nitrification was adversely affected by the organic shock as well, with effluent ammonia increasing from 1.1 mg/L to 22.6 mg/L and the effluent nitrate dropping from 8.7 mg/L to 0.8 mg/L. For confirmation of the insufficient nitrification, the biomass SNRs were tested with DO of 6.0 mg/L and ammonia of 30 mg/L for the attached biomass taken at 1h, 7h, and 13h. It showed the biomass SNRs were 0.22 (1h), 0.19 (7h) and 0.15 (13h) g N/(g VSS d), respectively. Apparently, the biomass activity was hindered by 26% as the percentage of nitrifiers in the aerobic biomass decreased. The nitrifiers reduction may be attributed to the overgrowth of heterotrophs and the lack of dissolved oxygen. The initial DO in bulk liquid was measured as 2.0 mg/L, but it dropped to 0.64 mg/L at the end of the organic shock trial (t = 13h). Figure 4-4c shows the effluent suspended solids during the organic shock test. The higher detachment rate of the rapid-growth heterotrophs resulted in the effluent VSS increasing from 27 mg/L to 73 mg/L within 13h. 4h after the influent reverted back to normal, the

effluent SCOD dropped to 74 mg/L, and the effluent ammonia dropped to 17.4 mg/L. The recovery of approximately 80% COD removal and 40% NH_3-N removal capabilities demonstrated good system reestablishment, while the duration for the recovery of nitrification was longer than that for COD removal.
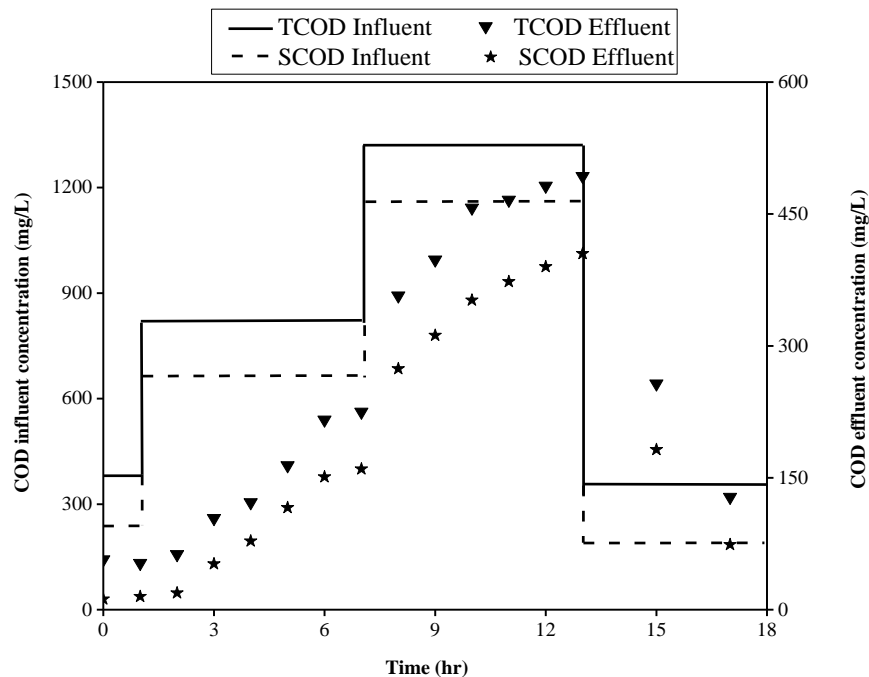
Figure 4-4a. COD variations during the organic shock test
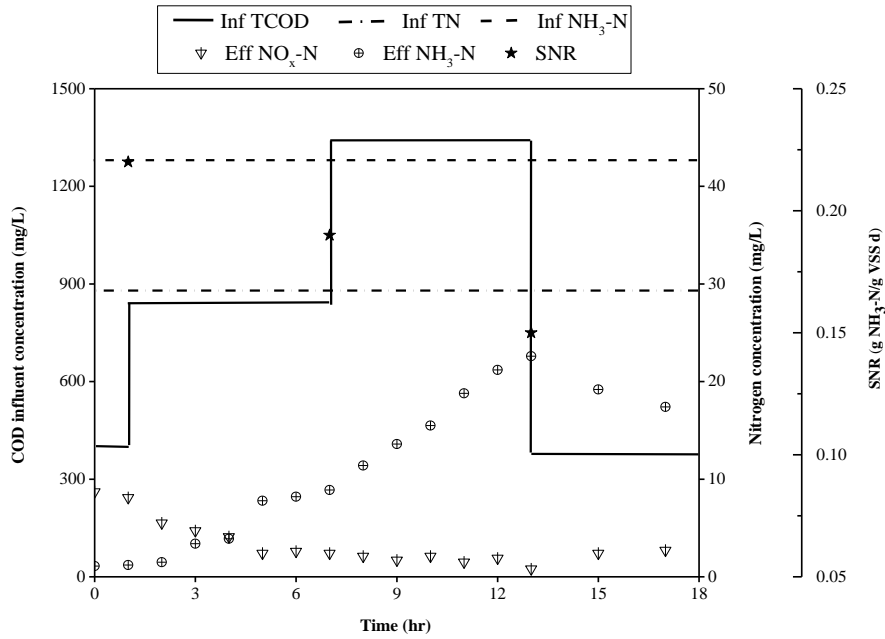
Figure 4-4b. Nitrogen variations during the organic shock test
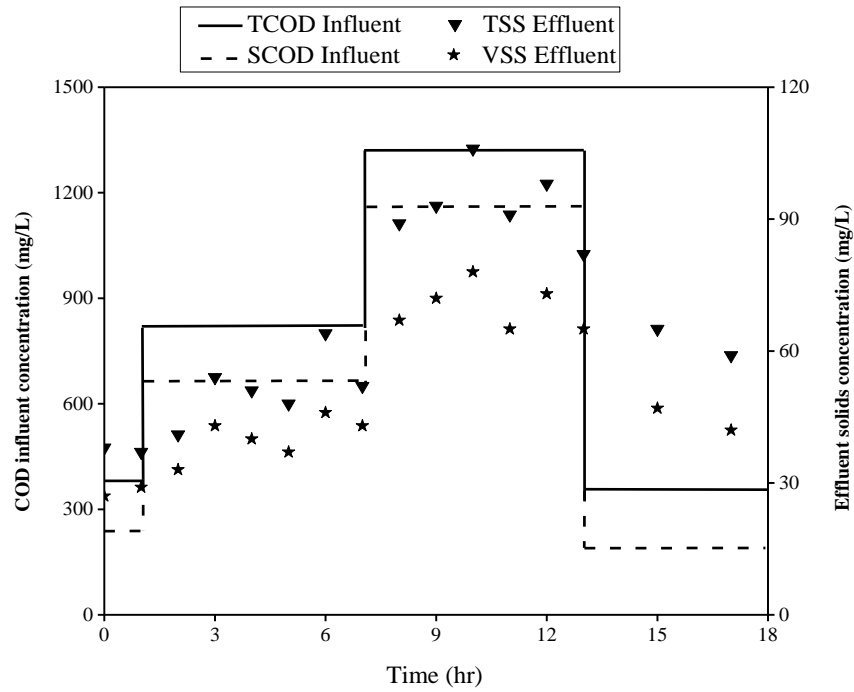
Figure 4-4c. Suspended solid variations during the organic shock test

4.3.3 Biowin simulation

Media bioreactor inside Biowin is a 1-D fully dynamic and steady-state configuration to simulate fixed biofilm systems. The mathematical model implemented for the media bioreactor developed by Reichert and Wanner (1997), includes diffusion of soluble and particulate components, a boundary layer between the biofilm surface and liquid followed Fick's law as the solute diffusion resistance, exchange of particulates due to detachment and attachment of solids (For details, refer to the Biowin 5.2 manual and the literature related to the model (Wanner and Reichert, 1996)). The spatial variations of SCOD and ammonia were measured in both the anoxic and aerobic column (Data shown in Figure B1, Appendix B). It is evident that there were no significant concentration gradients in both anoxic ad aerobic IFBBRs and hence they were modeled in Biowin as continuous stirred tank reactors. The procedures for simulating the IFBBR system include reactor arrangement (dimensions, influent characteristics and fractions), specification of the media surface area (area, volume, and filling ratio), and identification of biofilm parameters (detachment rate, boundary layer thickness, and biofilm layers). The fitting of this model to the experimental data was primarily by changing both the detachment rate and boundary layer thickness.

4.3.3.1 Reactor arrangement

The reactor arrangement for IFBBR system is shown in Figure 4-5. COD Influent specifier was used to simulate the influent. As the inflow setting is specified to several parameters (i.e. flow rate, TCOD, TKN, TP, and ISS), the various influent COD fractions were adjusted to match the measured parameters, i.e. SCOD, ammonia, TSS and VSS concentrations. The default and calibrated fractions are summarized in Table 4-4. Both anoxic and aerobic columns were simulated with media bioreactor, unaerated for the anoxic zone and constant DO of 2.1 mg/L for the aerobic zone. The volume, depth, and width of the media bioreactors were set as the actual configurations. The recirculated flow from the end of the aerobic zone was set as 4 times of the inflow, with the rest of aerobic effluent got into a clarifier, which was to simulate the free board of the aerobic column (cross-sectional area same as aerobic column and height of 0.3 m). Effluent specifier and sludge

specifier were connected to the clarifier to reveal the effluent characteristics and sludge wastage (Table 4-5).
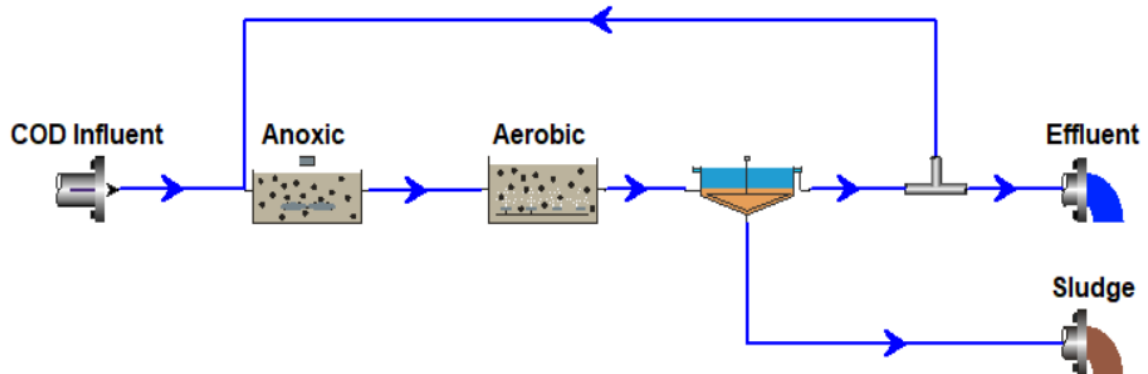
Figure 4-5. Binwin model arrangement for IFBBR system

4.3.3.2 Specific surface area

In the media bioreactor, the total amount of biofilm was related to the surface area for biofilm attachment. In Biowin, the characteristics of carriers were set based on three available parameters – specific area (m^2/m^3), specific volume (m^3/m^3) and % of reactor filled with media. Particle distribution, voidage, and density were not considered. The % of reactor filled with media was calculated as the compacted bed volume divided by the total volume, 50% for the anoxic zone and 40% for the aerobic zone. Specific volume (m^3/m^3) represents the bed voidage inside of the compacted bed volume, as 0.52 in both zones. Biofilm specific surface area (SSA) is the output of multiplying the reactor volume with the media fill fraction and the specific area. To match up the actual total surface area provided by carriers, the specific area was set as 989 m^2/m^3 for the anoxic zone and 1295 m^2/m^3 for the aerobic zone as calculated from Equation (4.4).

$$MA_m = VF_rA_s \tag{4.4}$$

4.3.3.3 Biofilm parameters

The attached biofilm activities in the fluidized bed are governed by the kinetic parameters as well as the hydrodynamic conditions. For the fixed biofilm model, biofilm thickness is

a function of bulk substrate concentrations, average biofilm VSS, and shear forces implied on biofilm. The kinetic parameters were set as default values, considering the anoxic and aerobic biofilm thickness was measured as 400-800 μm and 70-180 μm, respectively (>4 times observation). There are no direct correlations for calculating the biofilm thickness in the fluidized bed, especially for the three phases fluidized bed with strong disturbance (aerobic column). As suggested by Eldyasti et al. (2012b), the detachment rates of biofilm need to be calibrated by trial and error to fit the biofilm thickness with the actual ranges. The detachment rate for the anoxic and aerobic biofilm was finally set as 9×10^4 and 2×10^6 g/(m^3 d), respectively to replace the default value of 8×10^4 g/(m^3 d), which is explainable given that the shear force caused by gas disturbance and carriers attrition in the aerobic column was much higher than that in liquid fluidized bed of anoxic column. The simulated anoxic and aerobic biofilm thicknesses were 810 μm and 170 μm, respectively, within the observed experimental ranges of 400-800 μm (anoxic) and 70-180 μm (aerobic) (Shown in Figure B2, Appendix B). In addition, boundary layer thickness was the parameter affect mass transfer from the bulk liquid to the biofilm surface. After trial and error, the boundary layer was set as 40 μm instead of 100 μm in the aerobic column due to the high turbulence in the three-phase fluidized bed (Kim and Kang, 1997). Another adjustment is the biofilm layers, which was set as 2 instead of 3 for the aerobic biofilm, considering the thin aerobic attached biofilm. For the anoxic attached biofilm, the boundary layer thickness and the layers in the biofilm were set as default values.

4.3.3.4 Comparison of simulated and experimental data

Initially, the simulated COD influent should be set in agreement with the experimental data. After inputting the values for several parameters and adjusting the fractions, the experimental and simulated influent parameters are listed in Table 4-6. The average percentage error (APE) used to describe the discrepancy between simulated and experimental data was calculated as the summation of the absolute difference between the measured and simulated values divided by the measured values. For the inflow characteristics, the APEs of all parameters were within 4%. Subsequently, various aspects of process performance were predicted with steady-state Biowin model, with the comparison between model predictions and experimental data shown in Table 4-6. The

model predicted effluent quality well matched the experimental results, particularly the typical discharge standards i.e. TCOD, TN, NH_3, and TSS. The predicted system effluent TCOD of 53 mg/L, TN of 10.5 mg/L, NH_3-N of 1.3 mg/L, TSS of 36 mg/L were almost the same as these parameters in actual effluent. The difference between the simulated and experimental data for effluent NO_2-N and NO_3-N with APEs of 11% and 5%, respectively. Lower simulated NO_3-N was due to that the Biowin model considered more NO_3-N consumed by simultaneous nitrification and denitrification (SND) in the aerobic zone at a DO of 2.1 mg/L. It must be asserted that the 86% nitrogen balance closure in the aerobic zone potentially demonstrates the occurrence of SND. However, the effluent nitrogen was still in the reasonable agreement between simulated and experimental data with a maximum APE of 11%. For the anoxic zone, the simulated TN of 13.1 mg/L, NH_3-N of 7.0 mg/L and NO_3-N of 1.2 mg/L well matched the measured TN of 12.9 mg/L, NH_3-N of 6.9 mg/L and NO_3-N of 1.2 mg/L. Although the APE of NO_2-N was 23%, the simulated and measured NO_2-N concentrations were close, as 0.15 mg/L and 0.12 mg/L, respectively. For other parameters in the anoxic zone, TCOD and SCOD were overestimated with APE of 17% and 15%, respectively. Poor agreement between simulated and experimental TP and PO_4-P were generally observed. The difference was mainly due to the overestimation of phosphorus removal in the anoxic zone, as simulated TP of 2.6 mg/L and PO_4-P of 1.6 mg/L versus measured TP of 3.4 mg/L and PO_4-P of 2.4 mg/L. In the IFBBR system, phosphorus removal was achieved by biomass synthesis and subsequently discharge through the effluent VSS and wasted sludge. The average sludge wastage was measured as 2.1 g VSS/d, while the simulated sludge wastage was 2.7 g VSS/d, the overestimated sludge discharge from the system may result in the difference for TP and PO_4-P. The bad matching of TP and PO_4-P in the anoxic zone led to the underestimated system effluent TP and PO_4-P, even though the simulated phosphorus removal rate in the aerobic zone was same the calculated rate in the mass balance, as 0.60 g P/d. For the total attached biomass in the aerobic zone, the estimated value of 49.4 g VSS matched with the experimental value of 46.0 g VSS. However, the total attached biomass in the anoxic zone was underestimated of 26.6 g VSS as compared to the actual value of 33.1 g VSS, which may be the reason for the overestimated sludge discharge from the system. The estimated total biomass of 69.0 g VSS was similar to the experimental total biomass of 73.1 g VSS.

Table 4-4. Default and calibrated values for influent parameters

Fraction (abbreviation)	Unit	Default value	Input value
Readily biodegradable (Fbs)	g COD/g TCOD	0.27	**0.62**[1]
Acetate (Fac)	g COD/g rbCOD	0.15	**0.90**[1]
Non-colloidal slowly biodegradable (Fxsp)	g COD/g sbCOD	0.5	**1.00**[2]
Unbiodegradable soluble (Fus)	g COD/g TCOD	0.08	**0.02**[3]
Unbiodegradable particulate (Fup)	g COD/g TCOD	0.08	0.08
Ammonia (Fna)	gNH$_3$-N/g TKN	0.75	**0.73**[4a]
Particulate organic nitrogen (Fnox)	g N/g Organic N	0.25	0.25
Soluble unbiodegradable TKN (Fnus)	g N/g TKN	0.02	0.02
N:COD ratio for unbiodegradable part. COD (FupN)	g N/g COD	0.035	0.035
Phosphate (Fpo4)	g PO$_4$-P/g TP	0.75	**0.70**[4b]
P:COD ratio for influent unbiodegradable part. COD (FupP)	g P/g COD	0.011	0.011

1. These parameters were adjusted to match the influent acetate of around 240 mg/L (Page 99).

   As TCOD $\times$ Fbs $\times$ Fac = Acetate,

   416 mg TCOD/L (Ref to Table 4-6) $\times$ **0.62** $\times$ **0.90** = 232 mg acetate/L

2. All slowly biodegradable COD is from primary sludge, which is particulate. The parameter is adjusted to match the measured VSS. As TCOD $\times$ ((1- Fbs- Fus- Fup)$\times$ Fxsp + Fup $\times$ 0.5) $\div$ 1.42 = VSS,

   416 mg TCOD/L $\times$ ((1 - 0.62 – 0.02 - 0.08) $\times$ **1.00** + 0.08 $\times$ 0.5) $\div$ 1.42 mg VSS/ mg COD = 94 mg VSS/L (Measured as 95 mg/L, ref to Table 4-6).

3. Unbiodegradable soluble COD is from primary sludge, this parameter is adjusted to match the measured SCOD. As TCOD $\times$ (Fbs + Fus) = SCOD,

   416 mg TCOD/L $\times$ (**0.02** + 0.62) = 266 mg SCOD/L (Measured as 261 mg/L, ref to Table 4-6).

4. Based on the tests.

   (4a) 38.8 mg TKN/L $\times$ **0.73** = 28.3 mg NH$_3$-N/L (Ref to Table 4-6); (4b) 5.3 mg TP/L $\times$ **0.70** = 3.7 mg PO$_4$-P/L (Ref to Table 4-6).

Table 4-5. The dimensions of configurations and calibrated parameters

Configurations	Depth[1] (m)	Width[2] (m)	Volume[2] (L)	Specific area[3] (m²/m³)	Specific volume[4] (m³/m³)	Filling ratio[5] (%)	Biofilm layers	Boundary layer thickness (μm)
Anoxic	3.6[1a]	0.04	4.0	989[3a]	0.52	50[5a]	3[6]	100[6]
Aerobic	3.3[1b]	0.1	25.9	1295[3b]	0.52	40[5b]	2[7]	40[7]
Clarifier	0.3[1c]	0.1	2.4					

1. Same as (1a) anoxic column height, (1b) expended bed height in aerobic column, and (1c) free board height in aerobic column.

2. Same as column diameter and volume. (Section 4.2.1, page 99)

3. Calculated as total particle surface area divided by total volume and filling ratio. (Section 4.2.2, page 102)

   Surface are per g particle was estimated as: $\pi D^2 \div (\pi D^3/6) \times \rho \times \phi = 6 \div 3.2 \times 10^{-3}$ mm $\div 904$ kg/m³ $\times 0.91 = 1.89$ m²/kg

   (3a) 1.05 kg $\times$ 1.89 m²/kg $\div 4.0 \times 10^{-3}$ m² $\div 0.50 = 989$ m²/m³; (3b) 7.07 kg $\times$ 1.89 m²/kg $\div 25.9 \times 10^{-3}$ m² $\div 0.40 = 1295$ m²/m³.

4. As particle actual volume divided by compacted bed volume (commonly as 0.52).

5. Same as actual filling ratio (compacted bed volume/total bed volume). (Section 4.2.2, page 102)

   (5a) 2.0 L/4.0 L = 0.5; (5b) 11.5 L/(25.9+2.4) L = 0.4.

6. Default values, as thick anoxic biofilm (400-800 μm) and less turbulence in liquid-solid fluidized bed (Anoxic column).

7. By trial and error, as thin aerobic biofilm (70-180 μm) and high turbulence in gas-liquid-solid fluidized bed (Aerobic column).

   Data are shown in Figure B3, Appendix B.

Table 4-6. Comparison of experimental and simulated water characteristics

Parameter	Influent			Anoxic			Effluent		
	Experimental	Simulated	APE%	Experimental	Simulated	APE%	Experimental	Simulated	APE%
TCOD (mg/L)	416±21	416[1]	0	101±12	118	16.9	54±8	53	1.6
SCOD (mg/L)	269±23	266[2]	1.1	45±9	51	14.8	16±4	14	10.5
TN (mg/L)	39.8±2.4	39.8[2]	2.5	12.9±1.2	13.1	1.8	10.7±0.7	10.5	1.6
NH$_3$-N (mg/L)	28.4±1.6	28.3[2]	0.3	6.9±0.8	7.0	0.8	1.3±0.8	1.3	2.8
NO$_3$-N (mg/L)	0.6±0.3	0		1.2±0.6	1.2	0	5.4±0.7	5.2	5.1
NO$_2$-N (mg/L)	0	0		0.12±0.1	0.15	22.8	0.51±0.15	0.57	11.5
TP (mg/L)	5.3±0.5	5.3[1]	0	3.4±0.5	2.6	22.6	2.7±0.4	1.9	29.6
PO$_4$-P (mg/L)	3.7±0.4	3.7[2]	1.6	2.4±0.3	1.6	28.7	1.9±0.4	1.2	35.5
TSS (mg/L)	146±17	141[1]	3.2	53±9	61	15.2	37±5	36	1.8
VSS (mg/L)	95±14	94[2]	0.7	39±8	43	11.6	28±6	26	5.6
Biofilm thickness				400-800	810		70-180	170	
Total biomass (g)				33.1	26.6	19.5	46.0	49.4	7.4
Attached biomass (mgVSS/g particle)				31.5	25.4[(3a)]	19.5	6.5	6.9[(3b)]	7.4

1. Input numbers for COD Influent Specifier.

2. Based on Table 4-4.

3. (3a) 26.6 g VSS ÷ 1.05 kg particles = 25.4 mg VSS/g particle; (3a) 49.4 g VSS ÷ 7.07 kg particles = 6.9 mg VSS/g particle

4.3.3.5 Prediction of the maximum flow rate

Under the experimental conditions, the Biowin model excellently predicted the effluent nutrient concentrations except for the phosphorus. In application, the model could be used to predict the maximum flow rate (Q_{max}) by monitoring the effluent qualities. The discharge standards related to nitrogen for wastewater treatment plant were as TN of 15 mg/L and NH_3-N of 5 mg/L (Jin et al., 2014). By setting the limitations for effluent nitrogen and increasing the inflow rate, the Q_{max} for IFBBR system under the operational conditions was predicted, as shown in Figure 4-6. With the increment of inflow rate, the effluent NH_3-N initially reached to the limitation at the flow rate of 310 L/d, which meant the IFBBR system should be operated under the Q_{max} of 310 L/d. In addition, the DO concentration has great impacts on nutrient removal and could be adjusted during the operation. For guidance, the impact of DO concentration in the aerobic zone on system performance was studied by exploring the Q_{max}. The Q_{max} was predicted as 420 L/d, 520 L/d and 630 L/d, respectively with DO in the aerobic zone set as 3.0 mg/L, 4.0 mg/L, and 5.0 mg/L, respectively. Effluent TN reached the limit initially at all the scenarios. In the IFBBR system, nitrification mainly happened in the aerobic zone, while denitrification mainly occurred in the anoxic zone. Although the ammonia removal rate increased with the increment of DO, the effluent TN was out of control due to the limited capability of denitrification in the anoxic zone.
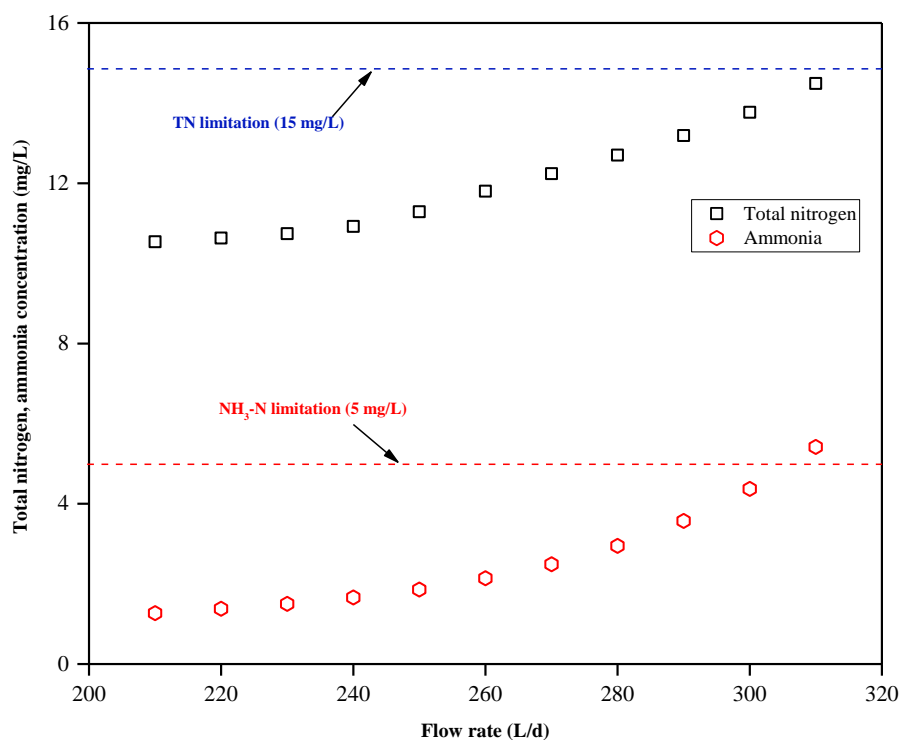
Figure 4-6. The impact of flow rate on effluent TN and NH₃-N concentrations

4.4 Conclusions

The lab scale integrated IFBBR system was operated to study the biological nutrient removal treating syntenic wastewater with high particulate COD, at an organic loading rate of 2.7 kg $COD/(m^3 d)$. 87% organic matter, 73% nitrogen, and 48% phosphorus were removed at HRT of 3.7 hrs. The mass balance showed that 36% of overall TCOD removal was achieved in the anoxic zone with NO_X-N denitrification, aerobic utilization, and sulfate reduction, while most of the ammonia was nitrified in the aerobic zone. Phosphorus was released in the anoxic zone and absorbed in the aerobic zone. Low biomass yield of 0.15 g VSS/ g COD was achieved. Organic shock test was conducted to examine the sensitivities of the IFBBR system with the response to the short variance of influent COD. The results showed the system has the good self-recovery ability, while reestablishment of COD

removal capability is superior to nitrification. A model of the IFBBR system was built in Biowin, calibrated with the stable state experimental data from the anoxic zone and aerobic zone, respectively. The IFBBR model simulated efficiently the carbon and nitrogen concentrations with APE of <17%, while the effluent phosphorus was underestimated due to overprediction of sludge discharge. With the calculated model, the maximum loading rate under the experimental operational conditions and the impact of DO in the aerobic zone on the maximum loading rate were predicted, which provided guidance for the operation of IFBBR system.

References

Ali Kawan, J., Abu Hasan, H., Jaafar, O., Suja, F., Bin Jaafar, O., Abd-rahman, R., 2016. A Review on Sewage Treatment and Polishing using Moving. J. Eng. Sci. Technol. 11, 1098–1120.

American Public Health Association, 2008. Standard methods for the examination of water and wastewater.

Andalib, M., 2011. Biological nutrient removal from municipal and industrial wastewater using a twin circulating fluidized bed bioreactor. Electron. Thesis Diss. Repos. Western University.

Andalib, M., Nakhla, G., Sen, D., Zhu, J., 2011. Evaluation of biological nutrient removal from wastewater by Twin Circulating Fluidized Bed Bioreactor (TCFBBR) using a predictive fluidization model and AQUIFAS APP. Bioresour. Technol. 102, 2400–2410.

Andalib, M., Nakhla, G., Zhu, J., 2010. Dynamic testing of the twin circulating fluidized bed bioreactor (TCFBBR) for nutrient removal from municipal wastewater. Chem. Eng. J. 162, 616–625.

Anoop, K., Viraraghavan, T., 1997. Nitrate removal from drinking water-review. J. Environ. Eng. 123, 371–380.

Barwal, A., Chaudhary, R., 2014. To study the performance of biocarriers in moving bed biofilm reactor (MBBR) technology and kinetics of biofilm for retrofitting the existing aerobic treatment systems: a review. Rev. Environ. Sci. Bio/Technology 13, 285–299.

Boltz, J.P., Morgenroth, E., Sen, D., 2010. Mathematical modelling of biofilms and biofilm reactors for engineering design. Water Sci. Technol. 62, 1821–1836.

Chowdhury, N., Nakhla, G., Zhu, J., 2008. Load maximization of a liquid-solid circulating fluidized bed bioreactor for nitrogen removal from synthetic municipal wastewater. Chemosphere 71, 807–815.

Chowdhury, N., Zhu, J., Nakhla, G., Patel, A., Islam, M., 2009. A novel liquid-aolid circulating fluidized-bed bioreactor for biological nutrient removal from municipal wastewater. Chem. Eng. Technol. 32, 364–372.

Cui, Y., Nakhla, G., Zhu, J., Patel, A., 2004. Simultaneous carbon and nitrogen removal in anoxic-aerobic circulating fluidized bed biological reactor (CFBBR). Environ. Technol. 25, 699–712.

Dempsey, M.J., Lannigan, K.C., Minall, R.J., 2005. Particulate-biofilm, expanded-bed technology for high-rate, low-cost wastewater treatment: Nitrification. Water Res. 39, 965–974.

Eddy, M., Burton, F., Tchobanoglous, G., Tsuchihashi, R., 2014. Wastewater engineering : treatment and resource recovery. McGraw-Hill Education.

Eldyasti, A., Andalib, M., Hafez, H., Nakhla, G., Zhu, J., 2011. Comparative modeling of biological nutrient removal from landfill leachate using a circulating fluidized bed bioreactor (CFBBR). J. Hazard. Mater. 187, 140–149.

Eldyasti, A., Nakhla, G., Zhu, J., 2012a. Influence of particles properties on biofilm structure and energy consumption in denitrifying fluidized bed bioreactors (DFBBRs). Bioresour. Technol. 126, 162–171.

Eldyasti, A., Nakhla, G., Zhu, J., 2012b. Development of a calibration protocol and identification of the most sensitive parameters for the particulate biofilm models used in biological wastewater treatment. Bioresour. Technol. 111, 111–121.

Gerardi, M.H., 2002. Nitrification and denitrification in the activated sludge process. Wiley-Interscience.

Grandclément, C., Seyssiecq, I., Piram, A., Wong-Wah-Chung, P., Vanot, G., Tiliacos, N., Roche, N., Doumenq, P., 2017. From the conventional biological wastewater treatment to hybrid processes, the evaluation of organic micropollutant removal: A review. Water Res. 111, 297–317.

Hassard, F., Biddle, J., Cartmell, E., Jefferson, B., Tyrrel, S., Stephenson, T., 2015. Rotating biological contactors for wastewater treatment – A review. Process Saf. Environ. Prot. 94, 285–306.

Islam, M., George, N., Zhu, J., Chowdhury, N., 2009. Impact of carbon to nitrogen ratio on nutrient removal in a liquid–solid circulating fluidized bed bioreactor (LSCFB). Process Biochem. 44, 578–583.

Jin, L., Zhang, G., Tian, H., 2014. Current state of sewage treatment in China. Water Res. 66, 85–98.

Kermani, M., Bina, B., Movahedian, H., Amin, M.M., Nikaein, M., 2008. Application of moving bed biofilm process for biological organics and nutrients removal from municipal wastewater, American Journal of Environmental Sciences.

Kim, S.D., Kang, Y., 1997. Heat and mass transfer in three-phase fluidized-bed reactors—an overview. Chem. Eng. Sci. 52, 3639–3660.

Li, M., Nakhla, G., Zhu, J., 2012. Simultaneous carbon and nitrogen removal with enhanced bioparticle circulation in a circulating fluidized bed biofilm reactor. Chem. Eng. J. 181, 35–

Liu, X., Kim, M., Nakhla, G., 2017. A model for determination of operational conditions for successful shortcut nitrification. Environ. Sci. Pollut. Res. 24, 3539–3549.

Luo, J., Li, W., Shao, Y., Nakhla, G., Zhu, J., 2019. Method for Determining the Hydraulic-Retention Time and Operating Conditions of a Circulating-Fluidized-Bed Bioreactor with Composition Disturbances. Ind. Eng. Chem. Res. 58, 2113–2124.

Mann, A.T., Stephenson, T., 1997. Modelling biological aerated filters for wastewater treatment. Water Res. 31, 2443–2448.

Nelson, M.J., Nakhla, G., Zhu, J., 2017. Fluidized-bed bioreactor applications for biological wastewater treatment : a review of research and developments. Engineering 3, 330–342.

Nguyen, T.T., Ngo, H.H., Guo, W., Johnston, A., Listowski, A., 2010. Effects of sponge size and type on the performance of an up-flow sponge bioreactor in primary treated sewage effluent treatment. Bioresour. Technol. 101, 1416–1420.

Ødegaard, H., 2006. Innovations in wastewater treatment: –the moving bed biofilm process. Water Sci. Technol. 53, 17–33.

Ødegaard, H., Rusten, B., Westrum, T., 1994. A new moving bed biofilm reactor - applications and results. water Sci. Technol. 29, 157–165.

Reichert, P., Wanner, O., 1997. Movement of solids in biofilms: Significance of liquid phase transport. Water Sci. Technol. 36, 321–328.

Rusten, B., Eikebrokk, B., Ulgenes, Y., Lygren, E., 2006. Design and operations of the Kaldnes moving bed biofilm reactors. Aquac. Eng. 34, 322–331.

Rusten, B., Lars, J.H., Hallvard, Ø., 1995. Nitrification of municipal wastewater in moving-bed biofilm reactors. Water Environ. Res. 67, 75–86.

Seviour, R.J., Mino, T., Onuki, M., 2003. The microbiology of biological phosphorus removal in activated sludge systems. FEMS Microbiol. Rev. 27, 99–127.

Takács, I., Bye, C.M., Chapman, K., Dold, P.L., Fairlamb, P.M., Jones, R.M., 2007. A biofilm model for engineering design. Water Sci. Technol. 55, 329–336.

Torrico, V., Kuba, T., Kusuda, T., 2006. Effect of particulate biodegradable COD in a post-denitrification enhanced biological phosphorus removal system. J. Environ. Sci. Heal. Part A 41, 1715–1728.

Wanner, O., Morgenroth, E., 2004. Biofilm modeling with AQUASIM. Water Sci. Technol. 49, 137–144.

Wanner, O., Reichert, P., 1996. Mathematical modeling of mixed-culture biofilms. Biotechnol. Bioeng. 49, 172–184.

Zekker, I., Rikmann, E., Tenno, Toomas, Lemmiksoo, V., Menert, A., Loorits, L.,

Vabamäe, P., Tomingas, M., Tenno, Taavo, 2012. Anammox enrichment from reject water on blank biofilm carriers and carriers containing nitrifying biomass: operation of two moving bed biofilm reactors (MBBR). Biodegradation 23, 547–560.

Chapter 5

Minimum Fluidization Velocity of Carrier Particles in the (Gas-)Liquid-Solid Fluidized Bed

5.1 Introduction

The fluidization of particles provides advantages for the gas-liquid-solid (three-phase) fluidized bed over the fixed-bed technology, such as improved interphase contact efficiencies, enhanced heat and mass transfer, and uniform bed temperature (Kim and Kang, 1997; Schügerl, 1997; Zhu et al., 2000). Depending on particle density (higher or lower than liquid), three-phase fluidized beds are divided into two categories - conventional fluidized bed and inverse fluidized bed (Buffière and Moletta, 1999; Jena et al., 2008). In the conventional fluidized bed, particles are fluidized by the concurrent upflow of gas and liquid, while fluidization is achieved by the downflow of liquid with upflow of gas in the inverse fluidized bed. Three-phase fluidized beds have been applied to many industrial processes over the last several decades, i.e. aerobic wastewater treatment, fermentation process, coal cracking process, and catalytic hydrogenation of petroleum products (Andalib et al., 2010; Kim et al., 1972; Neogi et al., 1986; Ryhiner et al., 1988; Wu et al., 2003).

In the aerobic fluidized bed wastewater treatment system, particles provide large surface area for biomass attachment. When choosing particles as the biomass carriers, there are several factors need to be considered i.e. particle diameter, density, porosity, surface roughness, and cracking resistance (Eldyasti et al., 2012). These parameters play a significant role in determining biomass adhesion and detachment rates, which further influence overall system performance (Tang and Fan, 1989). In addition, bioparticle properties affect the operational cost significantly as liquid circulation is required to fluidize the particles (Balaguer et al., 1997). Various particles have been reported as the carriers in the fluidized bed bioreactors, such as plastic beads, sand, lava rock, zeolite, raw clay, and resin (Celis-García et al., 2007; Li et al., 2013; Maqueda et al., 1992; Mustafa et al., 2014; Patel et al., 2006). These experiments mainly focused on the system biological

nutrient removal performance, rarely paid attention to the fluidization energy consumption for long-term running. The biochemical reaction of carbon and nitrogen oxidation is achieved on the surface of the solid phase, which requires oxygen transfer from the gas phase to the liquid phase, then to the solid phase (Swain et al., 2018). For certain amount of nutrient loading, the oxygen requirement is within the specified range. The air flow rate under the operational conditions could be confirmed by considering two factors - carrier fluidization and enough oxygen supply (Nelson et al., 2017). With the consideration of proper system design and operation, it's essential to investigate fluidization hydrodynamics of carrier particles under certain gas flow rates in the (gas-)liquid-solid fluidized bed.

Minimum fluidization velocity is recognized as one of the most important hydrodynamic parameters for particles. It is the superficial liquid velocity at which the particles become fluidized at a given superficial gas velocity. Above the minimum fluidization velocity, the phase holdup gradients are minimized and the contact area among the three phases are maximized, which benefits the heat and mass transfer for the reaction process (Kim et al., 1975; Lippens and Mulder, 1993; Renganathan and Krishnaiah, 2008). Thus, in a three-phase fluidized bed bioreactor, the liquid velocity usually is kept slightly higher than the minimum fluidization velocity to maintain bed expansion for the purpose of saving energy (Nelson et al., 2017). The definition of a gas-liquid-solid bed as fluidized is when the properties of three-phase mixture are same as the homogeneous fluid and the bed pressure drop is directly related to the average density of mixture (Briens et al., 1997a). Visual observation and bed pressure measurement are the general methods to measure the minimum fluidization velocity (Begovich and Watson, 1978). Although some researchers relied on visual observation to determine the minimum fluidization velocity by acquiring the point where the fixed bed begins to expend (Briens et al., 1997b), it's not a reliable method as gas penetration would cause disturbance inside of the bed, which results in subjective errors (Ramesh and Murugesan, 2002). Besides, bed contraction before incipient fluidization was reported in the literature (Epstein, 1976), which made it harder to determine the critical point at minimum fluidization. Bed pressure measurement is the common and reliable method to determine the minimum fluidization velocity in the liquid-solid fluidized bed. At low gas velocities (<0.2 m/s) without gas invasion into the manometers, bed pressure measurement accurately reflects the pressures at different axial

ports. The minimum fluidization velocity could be obtained by corresponding it to the intersection point of two linear regression lines in plot of pressure drop through the bed versus superficial liquid velocity (Zhang, 1996).

The carrier particles used in the three-phase fluidized bed bioreactors usually have small diameters and the densities near the water density, while the information about the minimum fluidization velocities of these particles is insufficient. For the propose of applying to wastewater treatment, it's necessary to explore the hydrodynamic properties of carrier particles to provide guidance for the system operation, and minimum fluidization velocity is also related to the energy consumption of fluidization. The objective of this research is to determine the minimum fluidization velocities of four particles used as biomass carriers in (gas-) liquid-solid fluidized bed and evaluate the experimental results with the values calculated based on the semiempirical equations, to provide extended data to the (two-) three-phase fluidized bed for better understanding of the carrier hydrodynamic characters.

5.2 Experimental apparatus and materials

5.2.1 Experimental apparatus

The experimental apparatus for the three-phase fluidized bed system is shown in Figure 5-1. A cylindrical plexiglass column with an inner diameter of 12.7 cm, a maximum height of 4.2 m and a wall thickness of 1 cm was used for this study. Liquid was recirculated from the top to the bottom of the column by a centrifugal pump (WMD-100RT, Iwaki, Japan) for particle fluidization with a 45 L bucket as the buffer tank. The liquid distributor with 10% opening ratio of 1.5 mm diameter holes located at 20 cm above the bottom of the column. A screen was installed on top of the liquid distributor to prevent particles falling into the plenum chamber. Air as gas phase was introduced into the bottom of the column through a fine bubble aerator, which was installed 10 cm higher than the liquid distributor. The initial diameter of bubbles coming out from the aerator was observed as approximately 1 mm. Gas and liquid flows were maintained upward and cocurrent in this study. The flow rates of gas and liquid were both controlled by valves and measured by the pre-calibrated

gas flowmeter (LZB-4, Yuanda, China) and liquid flowmeter (LZT-10, Yuanda, China), respectively. All the experiments were carried out at room temperature of $24 \pm 2°C$. Six U-tube manometers were connected to different ports and used to measure the pressures, which located along the column at heights of 30 cm, 56 cm, 82 cm, 108 cm, 134 cm, and 160 cm, respectively.

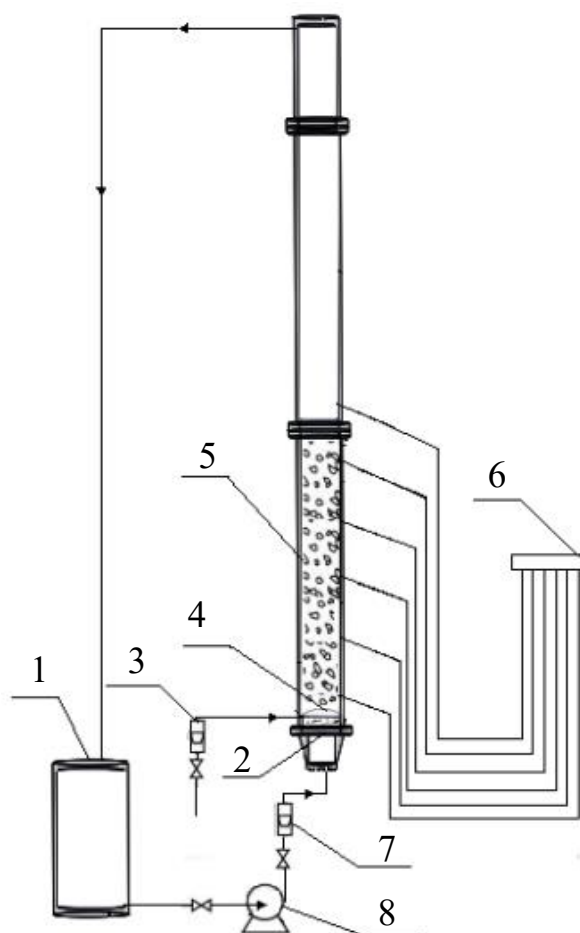**Figure 5-1.** Schematic diagram of the experimental apparatus. (1) Liquid bucket; (2) Liquid distributor; (3) Gas flowmeter; (4) Gas distributor; (5) Cylindrical column; (6) Manometers; (7) Liquid flowmeter; (8) Centrifugal pump.

5.2.2 Experimental materials

In order to investigate the impact of particle density and mean diameter on minimum fluidization velocity, four spherical carriers were chosen as the particles used in this

research, namely L-HDPE (size 1500-1900 μm), S-HDPE (size 700-1200 μm), pottery (size 700-1200 μm), and zeolite (size 700-1200 μm). The particles were picked out with sieves, then the diameters were determined. Particle densities were provided by the manufacturer and confirmed with the water displacement method, in which the particle volume was obtained by displaced water volume when the particles were placed into a beaker filled with water. The true densities of L-HDPE, S-HDPE, pottery, and zeolite were 1390 kg/m^3, 1390 kg/m^3, 2160 kg/m^3, and 1740 kg/m^3, respectively. The properties of these four particles were summarized in Table 5-1.

Table 5-1. The properties of experimental materials

Particle properties	L-HDPE	S-HDPE	Pottery	Zeolite
Particle size range (μm)	1500-1900	700-1200	700-1200	700-1200
Sauter mean diameter (μm)	1720	945	930	940
Particle true density (kg/m^3)	1390	1390	2160	1740

5.2.3 Experimental procedures

Gas velocity was chosen with the range of 0-12.4 mm/s considering the air flow rates requested by the bioreaction in the aerobic wastewater treatment system (Andalib, 2011; Chowdhury et al., 2008). For each case at the certain gas flow rate, initially the bed was fully fluidized and then superficial liquid velocity was decreased gradually until zero. The corresponding manometer readings were noted, and the pressure drop was calculated. The minimum fluidization velocity was obtained from the curve of pressure drop versus liquid velocity. With gas velocity of 0 mm/s, the carrier particles in the liquid-solid fluidized bed were studied firstly. After fully understanding of the fluidization characters of four carrier particles in the liquid-solid fluidized bed, gas was introduced to the system and the system became a three-phase fluidized bed. The hydrodynamics of each carrier particle was studied under gas velocities of 1.6 mm/s, 3.1 mm/s, 6.2 mm/s, 9.3 mm/s and 12.4 mm/s, respectively. After finishing one kind of particles, the column was cleaned thoroughly, and same produces were repeated for each kind of carrier particles.

5.3 Results and discussions

5.3.1 Flow regimes of three-phase fluidized bed

Three flow regimes were observed with decreasing of the superficial liquid velocity at certain superficial gas velocity. The three flow regimes were fluidized bed, gas agitated bed, and compacted bed.

For the particles in a three-phase fluidized bed, the force balance was achieved in the fluidized bed regime. The decrease of superficial fluid velocity resulted in the reduction of bed expansion as to keep the same drag force exerted on the particles at an upward axial direction in the reactor. Continuous position shifts of particles were observed, which indicated the good fluidization of bed at high liquid velocities. A radical bed hydrodynamics was observed with further decreasing of the superficial liquid velocity. Particles did not move smoothly and continuously as the behaviors in the fluidized bed regime. Instead, the agitation of gas bubbles caused the intermittent movement of particles, which was named as gas agitated bed regime. At low liquid velocities, the particles packed uniformly and became compacted bed. Although some movements of particles were observed due to the small agitation caused by gas bubbles, no continuously vertical or horizontal position shifts of particles were exhibited in this compacted bed regime. The minimum fluidization velocity was considered as the critical transition liquid velocity between the gas agitated regime and the compacted bed regime. The three regimes were also observed with the increase of superficial liquid velocity from the compacted bed state. Besides, bed contraction was exhibited before the incipient fluidization as the bed height decreased initially and then expended with the increase of superficial liquid velocity. Same phenomena were also reported by other studies and explained by the existence of bubble wakes (Epstein, 1981, 1976).

5.3.2 Minimum fluidization velocity in the liquid-solid fluidized bed

5.3.2.1 Experimental results

When superficial gas velocity equals zero, the three-phase fluidized bed turned into the liquid-solid fluidized bed. Figure 5-2 shows the pressure drop versus superficial liquid velocity of four carrier particles and the minimum fluidization velocities were summarized in Table 5-2. As obvious from the data for L-HDPE and S-HDPE with the same density, the minimum fluidization velocity decreased with the reduction of diameter. For the carrier particles of S-HDPE, pottery, and zeolite with the same size distribution, the minimum fluidization velocity increased with the increase of density. The results indicated that when selecting the carriers for biofilm attachment, particles with small diameter and low density have the lowest minimum fluidization velocity, which may contribute to reduce the overall fluidization energy consumption.
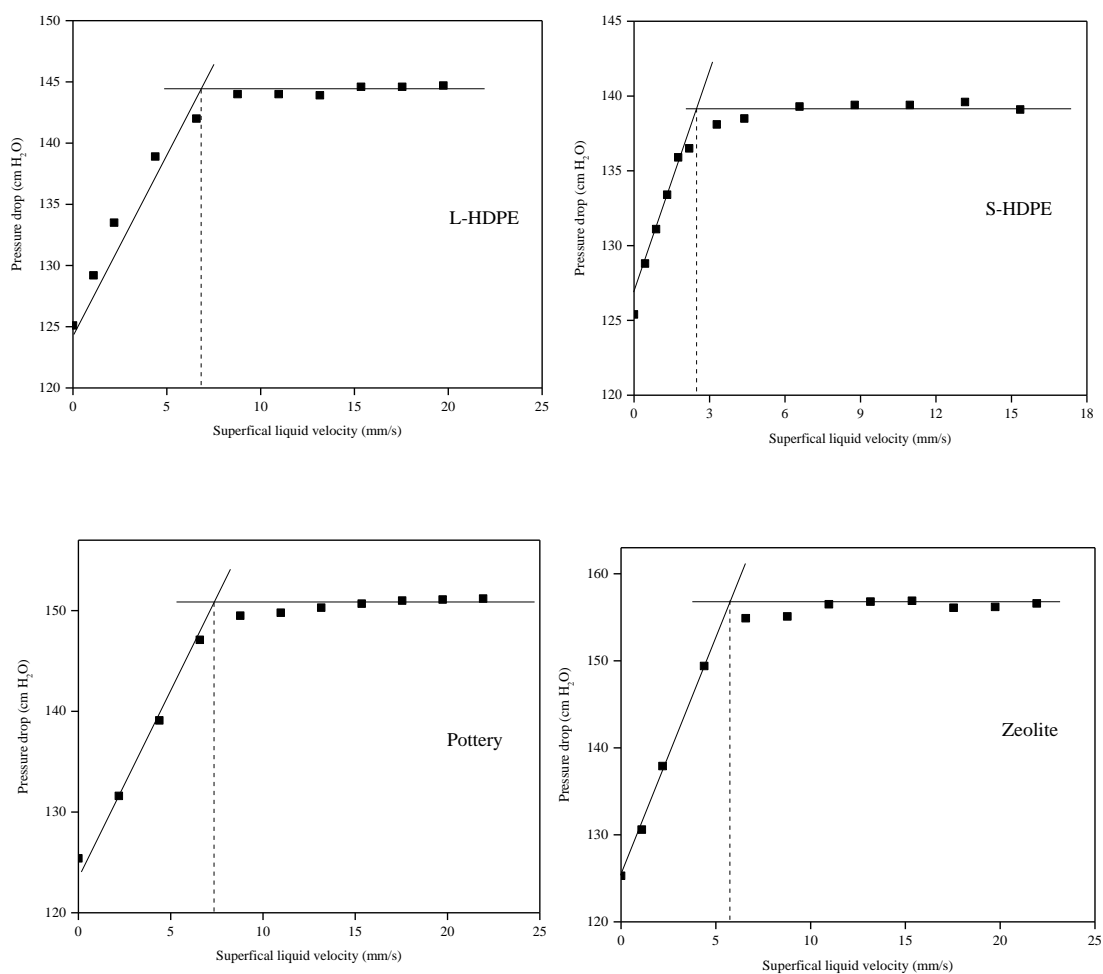
Figure 5-2. U_{mf} of carrier particles L-HDPE, S-HDPE, Pottery and Zeolite at the superficial gas velocity of 0 mm/s

5.3.2.2 Theory and prediction of minimum fluidization velocity

Minimum fluidization velocity is considered as the critical point where the pressure drop across the fluidized bed is equal to the weight of fluid and solid phases per unit area of the cross-section. Thus, the pressure drop is written as:

$$\Delta P = W_{bed}/A = gH((1 - \varepsilon)\rho_s + \varepsilon\rho_f) \tag{5.1}$$

The pressure drop through the compacted bed can be derived from a force balance on the continuous phase,

$$\Delta P = \Sigma F/A_f \tag{5.2}$$

The particles in the compacted bed have a random orientation, on average the cross-sectional area occupied by the continuous phase is:

$$A_f = \varepsilon A \tag{5.3}$$

ΣF is the sum of forces acting on the continuous phase, which include the fluid weight and the frictional force of solids on fluid. The friction of solids on fluid is the opposite direction of the friction of fluid on solids. Then, ΣF is written as:

$$\Sigma F = \rho_f g \varepsilon V + \Delta F \tag{5.4}$$

Therefore, the total bed pressure drop per unit bed height is given as:

$$\Delta P/H = (\rho_f g \varepsilon V + \Delta F)/(\varepsilon A H) = \rho_f g - \Delta P_f/H \tag{5.5}$$

where $-\Delta P_f/H = \Delta F/\varepsilon A$ is the frictional pressure drop per unit of bed height.

The frictional pressure drop ΔF on the solids results from the combination of skin friction (F_s) and form drag (F_f). As proposed by Ergun (1952) (Ergun, 1952), skin friction is the friction of the fluid on the surface of solid, form drag is caused by the "twists and turns" as well as the successive expansions and contractions that the fluids have to go through. F_s and F_f are written as:

$$F_s = k_1 \mu U_f \Delta S / (\varepsilon D_H) \tag{5.6}$$

$$F_f = k_2 U_f^2 \Delta S / \varepsilon^2 \tag{5.7}$$

For multisize non-spherical particles, the fluid-solid contact area or wetted surface (ΔS) in the compacted bed is defined by:

$$\Delta S = 6(1 - \varepsilon) AL / (\emptyset D_m) \tag{5.8}$$

Hydraulic diameter (D_H) is 4 times of fluid volume divided by wetted surface,

$$D_H = 4 (\varepsilon AL) / \Delta S = (2/3) \, \emptyset D_m \varepsilon / (1 - \varepsilon) \tag{5.9}$$

Then, the frictional pressure drop per unit of bed height is deduced as:

$$-\Delta P_f / H = k_1' \mu U_f (1 - \varepsilon)^2 / (\varepsilon^3 \emptyset^2 d_m^2) + k_2' \rho_f U_f^2 (1 - \varepsilon) / (\varepsilon^3 \emptyset d_m) \tag{5.10}$$

The minimum fluidization velocity (U_{mf}) could be solved by combining Equations (5.1), (5.5) and (5.10), which is written as:

$$C_1 U_{mf} + C_2 U_{mf}^2 = g(1 - \varepsilon_{mf})(\rho_s - \rho_f) \tag{5.11}$$

Where

$$C_1 = k_1' \mu (1 - \varepsilon_{mf})^2 / (\varepsilon_{mf}^3 \emptyset^2 d_m^2) \tag{5.12}$$

And

$$C_2 = k_2' \rho_f (1 - \varepsilon_{mf}) / (\varepsilon_{mf}^3 \emptyset d_m) \tag{5.13}$$

Various values have been proposed for the empirical constants k_1' and k_2'. The most commonly used values for these constants as k_1' of 150 and k_2' of 1.75 were introduced by Ergun (Ergun, 1952), with fitting the correlation with 640 experimental data. The bed voidage at minimum fluidization condition (ε_{mf}) can be estimated by the equations of Wen and Yu (Wen and Yu, 1966),

$$(1 - \varepsilon_{mf})/(\varepsilon_{mf}^3 \emptyset^2) = 11 \tag{5.14}$$

$$1/(\varepsilon_{mf}^3 \emptyset) = 14 \tag{5.15}$$

The minimum fluidization velocity for liquid-solid fluidized bed is estimated by Equation (5.11) and compared with current experimental data in Figure 5-3. The average percentage errors of experimental and estimated values were within 25%. The reasonable agreement suggested that the Ergun equation along with Wen and Yu equations are applicable to predict the minimum fluidization velocities of carrier particles with different densities and diameters in the liquid-solid fluidized bed.
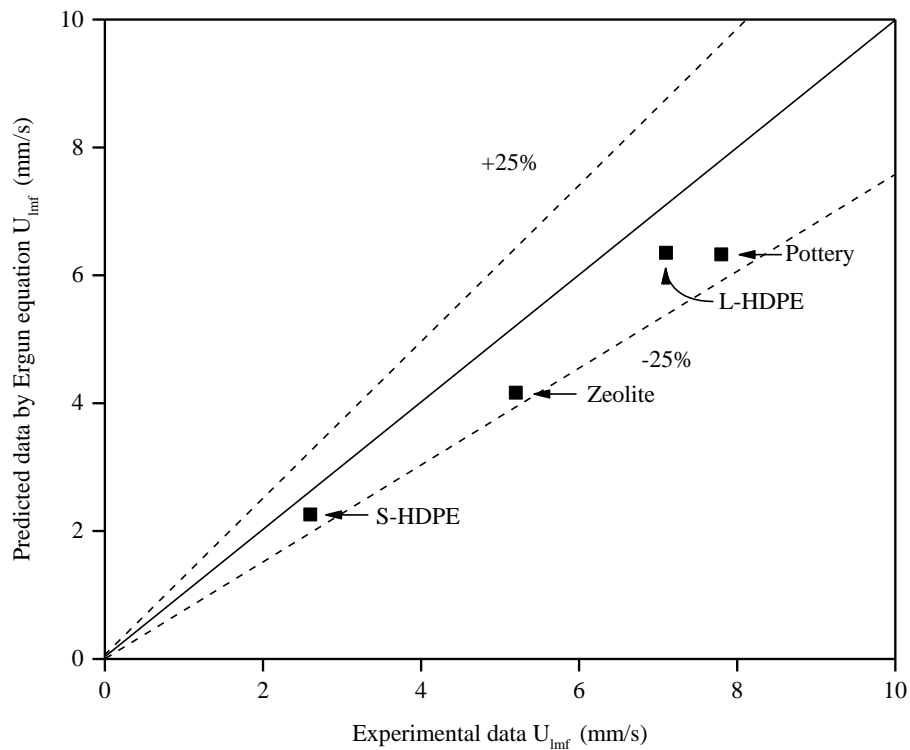
Figure 5-3. Comparison of U_{mf} between the experimental and calculated data by Ergun equation for different carrier particles at gas velocity of 0 mm/s

Table 5-2. The U_{mf} from the experiment and prediction by Ergun equation

	Experimental U_{mf} (mm/s)	Predicted by Ergun equation U_{mf} (mm/s)	APE (%)
L-HDPE	7.1	6.4	11
S-HDPE	2.6	2.3	13
Pottery	7.8	6.3	19
Zeolite	5.2	4.2	20

5.3.3 Minimum fluidization velocity in the gas-liquid-solid fluidized bed

5.3.3.1 Experimental results

The pressure drop of four carrier particles was measured under five different gas velocities of 1.6 mm/s, 3.1 mm/d, 6.2 mm/s, 9.3 mm/s, and 12.4 mm/s, respectively. By plotting the pressure drop versus superficial liquid velocity, the minimum fluidization velocity was read at the intersection of two linear lines, as shown in Appendix C. Unlike the pressure drop with almost same values (flat line) after incipient fluidization in the liquid-solid fluidized beds, there were decreased points at the high superficial liquid velocities in the three-phase fluidized beds. The reason for the decreased points is that the highest port of pressure measurement was at 1.6 m, while the water level in the column was maintained at around 3.5 m. Particle entrainment above highest pressure measurement port was observed during the experiments, which resulted in the decreased points at high superficial liquid velocities. Especially at relatively high gas velocities, the declining trend of pressure drop became more obvious with more particles entrained by bubble wakes. The minimum fluidization velocities of four carrier particles were summarized in Table 5-3 and Figure 5-4. The same trend was observed as in the liquid-solid fluidized beds that the minimum fluidization velocity decreased with the decrease of particle density as well as diameter at certain superficial gas velocity. Meanwhile, the minimum fluidization velocity decreased with the increase of superficial gas velocity, while the decreasing trend was leveled off at high superficial gas velocities.
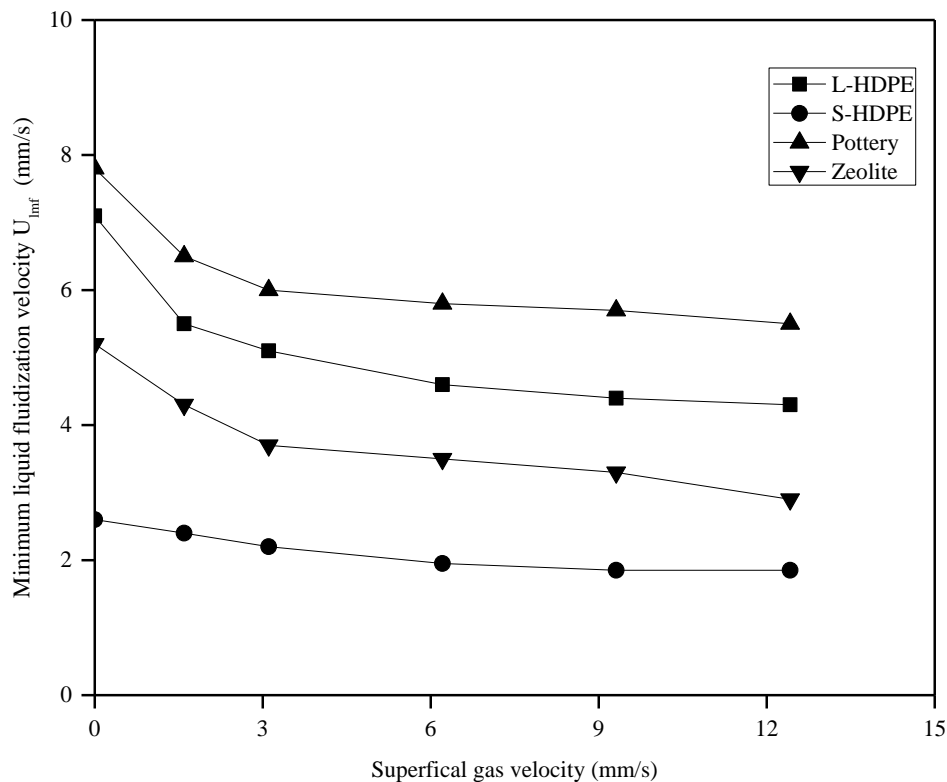
Figure 5-4. U_{mf} of four carrier particles at superficial gas velocities in the range of 0-12.4 mm/s

5.3.3.2 Theory and prediction of minimum fluidization velocity

Two semiempirical models developed by Song et al. (1989) and Zhang et al. (1998) were selected to predict the minimum fluidization velocity in the three-phase fluidized beds. Both models showed good agreement between the predicted and experimental data in the previous literature.

In the model of Song et al. (1989), the gas and liquid phases are considered as one-dimensional flows separately. There is no direct contact between the gas and solid phases and solid particles are completely wetted by liquid. Thus, the system is separated as three distinguished regions that the gas phase is in the central region and the solid phase is in the wall region as well as the liquid phase is between them.

The total pressure drop at minimum fluidization condition equals to the total bed weight per unit area of the cross-section and can be written as:

$$-\Delta P = W_{bed}/A = gH(\varepsilon_s \rho_s + \varepsilon_l \rho_l + \varepsilon_g \rho_g) \tag{5.16}$$

The pressure drop through the three-phase compacted bed can be derived from the continuous phase,

$$-\Delta P = (1 - \alpha)\rho_l gH + \alpha \rho_g gH + (1 - \alpha)(-\Delta P_F) \tag{5.17}$$

Where α is defined as the ratio of gas holdup to total fluid volume fraction,

$$\alpha = \varepsilon_g/(\varepsilon_g + \varepsilon_l) \tag{5.18}$$

And the frictional pressure loss $(-\Delta P_F)$ is between the liquid and the solid phases, which is expressed as:

$$-\Delta P_F = 4f_c\left(\frac{1}{D_e}\right)\left[\frac{1}{2}\rho_l\left(\frac{U_l}{\varepsilon_l}\right)^2\right]H \tag{5.19}$$

The equivalent diameter (D_H) of the channel for liquid flow is written as:

$$D_e = \frac{2(1-\varepsilon_s)}{3\varepsilon_s}(1 - \sqrt{\alpha})\emptyset d_m \tag{5.20}$$

The friction factor f_c can be replaced by the friction factor in the liquid-solid fluidized bed based on the assumption that solid particles are wetted by the liquid and Ergun equation is used to calculate f_c,

$$f_c = 0.583 + \frac{33.3}{Re_l'} \tag{5.21}$$

And the modified Reynolds number Re_l' is:

$$Re_l' = \frac{D_e \rho_l U_l}{\mu_l \varepsilon_l} \tag{5.22}$$

Combining Equations (5.16) with (5.17) and (5.19), one equation to calculate the minimum fluidization velocity was obtained,

$$(1 - \alpha_{mf})\{4f_c \left(\frac{1}{D_e}\right)[\frac{1}{2}\rho_l(\frac{U_{lmf}}{(1 - \alpha_{mf})\varepsilon_{mf}})^2]\} + (1 - \alpha_{mf})\rho_l g =$$

$$[(1 - \alpha_{mf})\varepsilon_{mf}\rho_l + (1 - \varepsilon_{mf})\rho_s]g \qquad (5.23)$$

Note that gas density is assumed small compared to the liquid and particle densities and negligible in the above equation. The bed voidage (ε_{mf}) at incipient fluidization is estimated from Equations (5.14) and (5.15) proposed by Wen and Yu (1966).

The minimum fluidization velocity can be calculated iteratively from Equation (5.23). An alternative empirical equation was then proposed by Song et al. (1989),

$$\frac{U_{lmf}}{U'_{lmf}} = 1 - 376 \, U_g^{0.327}\mu_l^{0.227}d_m^{0.213}(\rho_s - \rho_l)^{-0.423} \qquad (5.24)$$

Where U'_{lmf} is the minimum fluidization velocity at superficial gas velocity equals zero and can be calculated by Wen and Yu equations (Wen and Yu, 1966).

The prediction of minimum fluidization velocities for these four carrier particles by the model of Song et al. (1989) is shown in Table 5-3. Good agreement is obtained with the experimental data. Most of the differences between the estimated and experimental data are within 25%. The highest accuracy of model prediction is for particle L-HDPE with the largest diameter, while the lowest accuracy is for particle S-HDPE. It showed the model of Song et al. (1989) is suitable for prediction of the minimum fluidization velocity for the carrier particles studied in this experiment.
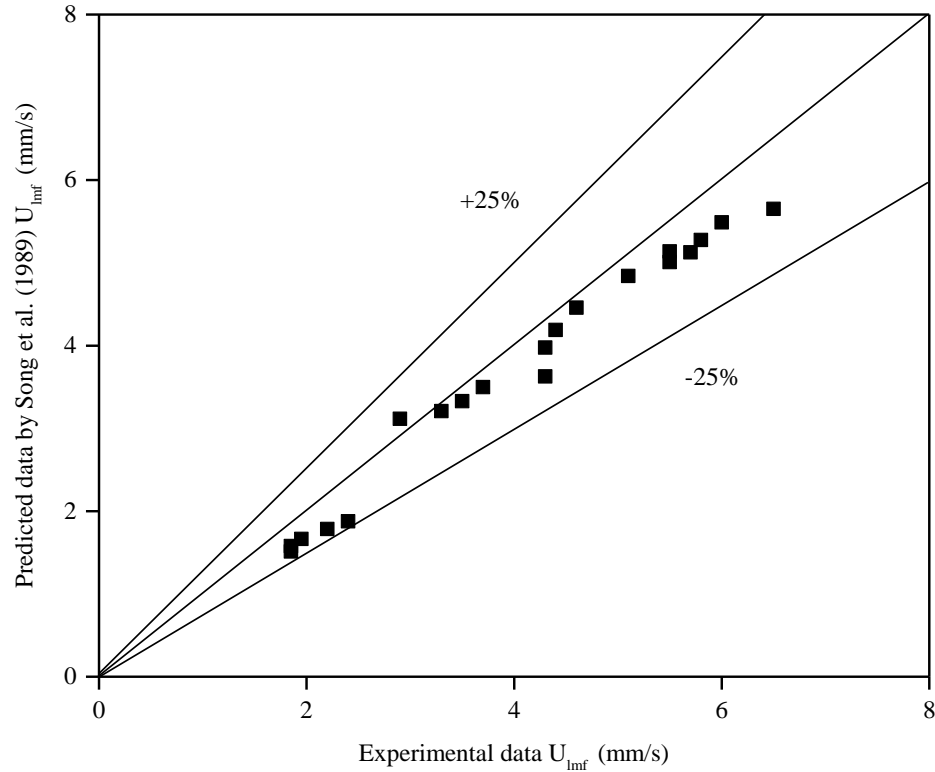
Figure 5-5. Comparison of U_{mf} between the experimental and calculated data by the model of Song et al. (1989) for carrier particles at different gas velocities

The second model used to predict the minimum fluidization velocity is proposed by Zhang et al. (1998), which is named gas-perturbed liquid model. This model was examined with 264 data points and had shown the quite well-matched prediction. The basic assumptions are that the particles are fully supported by the liquid and bubble-induced flow is ignored. The role of the gas phase is to occupy the space in the liquid phase and hence to increase the superficial liquid velocity. Thus, the hydraulic diameter of the liquid channel is derived as:

$$D_H = \frac{\emptyset d_m \varepsilon_l}{6(1-\varepsilon)} \qquad (5.25)$$

In this model, the liquid-buoyed weight per unit bed volume is equated to the frictional pressure gradient given in Ergun equation (Ergun, 1952) for the incipient fluidization in the liquid-solid fluidized bed. The equation is expressed

$$-\left(\frac{dP}{dZ}\right) = (1-\varepsilon)(\rho_s - \rho_l)g = 150\frac{\mu_l(\frac{U_l}{1-\varepsilon_g})(\frac{\varepsilon_s}{1-\varepsilon_g})^2}{\emptyset^2 d_m^2(\frac{\varepsilon_l}{1-\varepsilon_g})^3} + 1.75\frac{\rho_l(\frac{U_l}{1-\varepsilon_g})^2(\frac{\varepsilon_s}{1-\varepsilon_g})}{\emptyset d_m(\frac{\varepsilon_l}{1-\varepsilon_g})^3} \tag{5.26}$$

By introducing Reynolds number (Re_{mf}) and Archimedes number (Ar), Equation (5.26) becomes,

$$Re_{lmf} = \sqrt{[150(1-\varepsilon_{mf})/3.5\emptyset]^2 + \varepsilon_{mf}^3(1-\alpha_{mf})^3 Ar_l/1.75} - 150(1-\varepsilon_{mf})/3.5\emptyset \tag{5.27}$$

With

$$Re_{lmf} = \frac{\rho_l d_m U_{lmf}}{\mu_l} \tag{5.28}$$

And

$$Ar_l = \frac{\rho_l(\rho_s - \rho_l)g d_m^3}{\mu_l^2} \tag{5.29}$$

The fraction of gas hold up in total fluid (gas and liquid) at incipient fluidization (α_{mf}) can be calculated from an empirical equation from Yang et al. (1993), which is written as:

$$\alpha_{mf} = \frac{0.16 U_g}{\varepsilon_{mf}(U_g + U_{lmf})} \tag{5.30}$$

The application of Equation (5.30) is in the range of

$$U_g/(U_g + U_l) \leq 0.93 \tag{5.31}$$

The minimum liquid fluidization velocities of different carrier particles are predicted with the model of Zhang et al. (1998) and the results are summarized in Table 5-3. As shown in Figure 5-6, the gas perturbed model underestimates the experimental data at all the gas velocities. Especially for the S-HDPE with small diameter and density, the errors are even larger than 58%. Besides, at high superficial gas velocities, the deviation between the predicted and experimental data are more widely. The possible reason for the large error is that the basic assumption of the role of the gas phase is to occupy the space in the liquid

phase, which resulted to increase the superficial liquid velocity and underestimated the required velocity for fluidization. In addition, although the correlations by Zhang et al. (1998) was examined with particle diameters of 1.0-6.1 mm, most of the data were from the experiments with particle sizes of 3-6 mm. In all, the gas perturbed model is not applicable to predict the minimum fluidization velocities of carrier particles in this experiment.
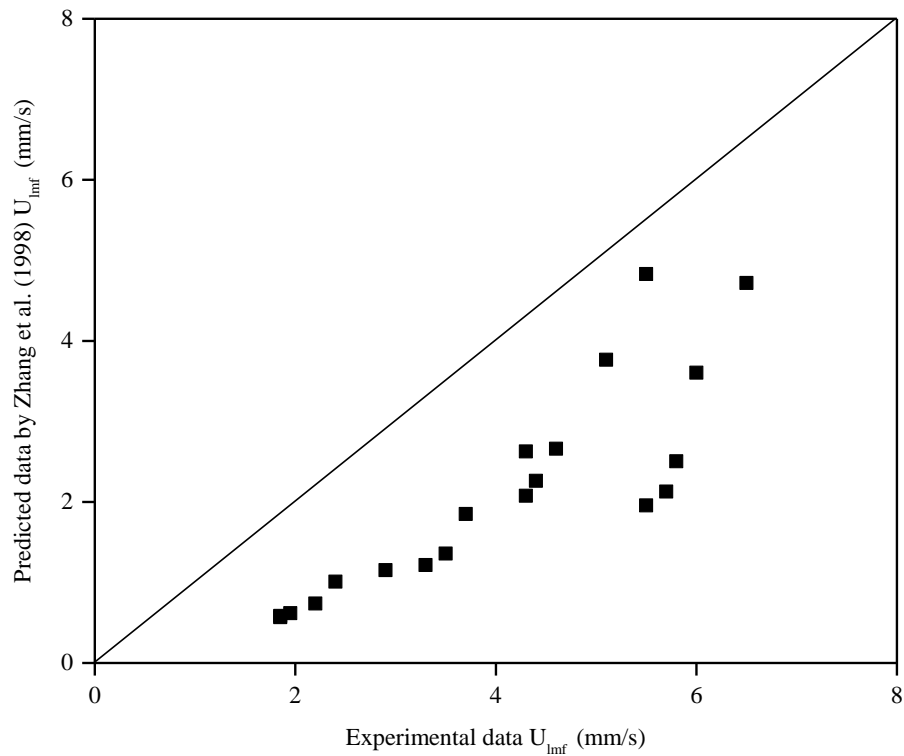
Figure 5-6. Comparison of U_{mf} between the experimental and calculated data by the model of Zhang et al. (1998) for carrier particles at different gas velocities

Table 5-3. Comparison of experimental and predicted U_{mf} in the three-phase fluidized bed

	Particle / Ug	1.6 mm/s	3.1 mm/s	6.2 mm/s	9.3 mm/s	12.4 mm/s
Experimental U_{mf} (mm/s)	L-HDPE	5.5	5.1	4.6	4.4	4.3
	S-HDPE	2.4	2.2	2.0	1.9	1.9
	Pottery	6.5	6.0	5.8	5.7	5.5
	Zeolite	4.3	3.7	3.5	3.3	3.2
Predicted U_{mf} (mm/s) by the model of Song et al. (1989)	L-HDPE	5.1	4.8	4.5	4.2	4.0
	S-HDPE	1.9	1.8	1.7	1.6	1.5
	Pottery	5.7	5.5	5.3	5.1	5.0
	Zeolite	3.6	3.5	3.3	3.2	3.1
Predicted U_{mf} (mm/s) by the model of Zhang et al. (1998)	L-HDPE	4.8	3.8	2.7	2.3	2.1
	S-HDPE	1.0	0.7	0.6	0.6	0.6
	Pottery	4.7	3.6	2.5	2.1	2.0
	Zeolite	2.6	1.9	1.4	1.2	1.2
APE (%) by the model of Song et al. (1989)	L-HDPE	22	19	15	15	18
	S-HDPE	13	9	9	10	9
	Pottery	16	5	5	3	-7
	Zeolite	7	5	3	5	3
APE (%) by the model of Zhang et al. (1998)	L-HDPE	12	26	42	49	52
	S-HDPE	58	66	68	68	69
	Pottery	27	40	57	63	64
	Zeolite	39	50	61	63	62

5.4 Conclusions

Knowledge of the minimum fluidization velocity of carrier particles is crucial for the design and operation of (gas-)liquid-solid fluidized bed wastewater treatment system. The minimum fluidization velocities of carriers L-HDPE, S-HDPE, pottery, and zeolite were experimentally determined. It was observed that in the (gas-)liquid-solid fluidized beds, minimum fluidization velocity increased with the increase of particle density and diameter. Besides, the minimum fluidization velocity decreased with the increase of superficial gas velocity, while the decreasing trend was leveled off at high superficial gas velocities. The well agreement of experimental and predicted data by Ergun equation (Ergun, 1952) demonstrated that Ergun equation (Ergun, 1952) is capable to predict the minimum fluidization velocities in the liquid-solid fluidized bed. For carrier particles in the gas-liquid-solid fluidized bed, the model of Song et al. (1989) predicted minimum fluidization velocity better than the model of Zhang et al. (1998). The bad agreement of experimental and predicted data by the model of Zhang et al. (1998) may due to the assumption that he role of the gas phase is to occupy the space in the liquid phase.

References

Andalib, M., 2011. Biological nutrient removal from municipal and industrial wastewater using a twin circulating fluidized bed bioreactor. Electron. Thesis Diss. Repos. Western University.

Andalib, M., Nakhla, G., Zhu, J., 2010. Dynamic testing of the twin circulating fluidized bed bioreactor (TCFBBR) for nutrient removal from municipal wastewater. Chem. Eng. J. 162, 616–625.

Balaguer, M.D., Vicent, M.T., Parfs, J.M., 1997. A comparison of different support materials in anaerobic fluidized bed reactors for the treatment of Vinasse. Environ. Technol. 18, 539–544.

Begovich, J.M., Watson, J.S. (Eds.), 1978. Hydrodynamic characteristics of three-phase fluidized beds in Fluidization. Cambridge University Press, Cambridge.

Briens, L. A., Briens, C.L., Margaritis, A., Hay, J., 1997a. Minimum liquid fluidization velocity in gas-liquid-solid fluidized beds. AIChE J. 43, 1180–1189.

Briens, L.A., Briens, C.L., Margaritis, A., Hay, J., 1997b. Minimum liquid fluidization velocity in gas-liquid-solid fluidized beds of low-density particles. Chem. Eng. Sci. 52, 4231–4238.

Buffière, P., Moletta, R., 1999. Some hydrodynamic characteristics of inverse three phase fluidized-bed reactors. Chem. Eng. Sci. 54, 1233–1242.

Celis-García, L.B., Razo-Flores, E., Monroy, O., 2007. Performance of a down-flow fluidized bed reactor under sulfate reduction conditions using volatile fatty acids as electron donors. Biotechnol. Bioeng. 97, 771–779.

Chowdhury, N., Nakhla, G., Zhu, J., 2008. Load maximization of a liquid-solid circulating fluidized bed bioreactor for nitrogen removal from synthetic municipal wastewater. Chemosphere 71, 807–815.

Eldyasti, A., Nakhla, G., Zhu, J., 2012. Influence of particles properties on biofilm structure and energy consumption in denitrifying fluidized bed bioreactors (DFBBRs). Bioresour. Technol. 126, 162–171.

Epstein, N., 1981. Three-phase fluidization: Some knowledge gaps. Can. J. Chem. Eng. 59, 649–657.

Epstein, N., 1976. Criterion for initial contraction or expansion of three-phase fluidized beds. Can. J. Chem. Eng. 54, 259–263.

Ergun, 1952. Fluid flow through packed columns. Chem. Eng. Prog. 48, 89–94.

Jena, H.M., Sahoo, B.K., Roy, G.K., Meikap, B.C., 2008. Characterization of hydrodynamic properties of a gas–liquid–solid three-phase fluidized bed with regular shape spherical glass bead particles. Chem. Eng. J. 145, 50–56.

Kim, S.D., Baker, C.G.I., Bergougnou, M.A., 1975. Phase holdup characteristics of three phase fluidized beds. Can. J. Chem. Eng. 53, 134–139.

Kim, S.D., Baker, C.G.J., Bergougnou, M.A., 1972. Hold-up and axial mixing characteristics of two and three phase fluidized beds. Can. J. Chem. Eng. 50, 695–701.

Kim, S.D., Kang, Y., 1997. Heat and mass transfer in three-phase fluidized-bed reactors—an overview. Chem. Eng. Sci. 52, 3639–3660.

Li, M., Nakhla, G., Zhu, J., 2013. Impact of worm predation on pseudo-steady-state of the circulating fluidized bed biofilm reactor. Bioresour. Technol. 128, 281–289.

Lippens, B.C., Mulder, J., 1993. Prediction of the minimum fluidization velocity. Powder Technol. 75, 67–78.

Maqueda, C., Pérez Rodríguez, J.L., Lebrato, J., 1992. Fresenius environmental bulletin., Fresenius Environmental Bulletin. Birkhäuser Verlag.

Mustafa, N., Elbeshbishy, E., Nakhla, G., Zhu, J., 2014. Anaerobic digestion of municipal wastewater sludges using anaerobic fluidized bed bioreactor. Bioresour. Technol. 172,

461–466.

Nelson, M.J., Nakhla, G., Zhu, J., 2017. Fluidized-bed bioreactor applications for biological wastewater treatment: a review of research and developments. Engineering 3, 330–342.

Neogi, D., Chang, C.C., Walawender, W.P., Fan, L.T., 1986. Study of coal gasification in an experimental fluidized bed reactor. AIChE J. 32, 17–28.

Patel, A., Zhu, J., Nakhla, G., 2006. Simultaneous carbon, nitrogen and phosphorous removal from municipal wastewater in a circulating fluidized bed bioreactor. Chemosphere 65, 1103–1112.

Ramesh, K., Murugesan, T., 2002. Minimum fluidization velocity and gas holdup in gas-liquid-solid fluidized bed reactors. J. Chem. Technol. Biotechnol. 77, 129–136.

Renganathan, T., Krishnaiah, K., 2008. Prediction of minimum fluidization velocity in two and three phase inverse fluidized beds. Can. J. Chem. Eng. 81, 853–860.

Ryhiner, G., Petrozzi, S., Dunn, I.J., 1988. Operation of a three-phase biofilm fluidized sand bed reactor for aerobic wastewater treatment. Biotechnol. Bioeng. 32, 677–688.

Schügerl, K., 1997. Three-phase-biofluidization—Application of three-phase fluidization in the biotechnology—A review. Chem. Eng. Sci. 52, 3661–3668.

Song, G.-H., Bavarian, F., Fan, H.-S., Buttke, R.D., Peck, L.B., 1989. Hydrodynamics of three-phase fluidized bed containing cylindrical hydrotreating catalysts. Can. J. Chem. Eng. 67, 265–275.

Swain, A.K., Sahoo, A., Jena, H.M., Patra, H., 2018. Industrial wastewater treatment by Aerobic Inverse Fluidized Bed Biofilm Reactors (AIFBBRs): A review. J. Water Process Eng. 23, 61–74.

Tang, W.-T., Fan, L.-S., 1989. Hydrodynamics of a three-phase fluidized bed containing low-density particles. AIChE J. 35, 355–364.

Wen, C.Y., Yu, Y.H., 1966. A generalized method for predicting the minimum Fluidization velocity. AIChE J. 12, 610–612.

Wu, S.-Y., Lin, C.-N., Chang, J.-S., 2003. Hydrogen production with immobilized sewage sludge in three-phase fluidized-bed bioreactors. Biotechnol. Prog. 19, 828–832.

Yang, X., Euzen, J., Wild, G., 1993. Study of liquid retention in fixed-bed reactors with upward flow of gas and liquid. Int. Chem. Eng. (A Q. J. Transl. from Russ. East. Eur. Asia) 33.

Zhang, J.-P., Epstein, N., Grace, J.R., 1998. Minimum fluidization velocities for gas—liquid—solid three-phase systems. Powder Technol. 100, 113–118.

Zhang, J., 1996. Bubble columns and three-phase fluidized beds : flow regimes and bubble characteristics. University of British Columbia.

Zhu, J.-X. (Jesse), Karamanev, D.G., Bassi, A.S., Zheng, Y., 2000. (Gas-)liquid-solid circulating fluidized beds and their potential applications to bioreactor engineering. Can. J. Chem. Eng. 78, 82–94.

Chapter 6

Effective Partial Nitrification of Ammonia in a Fluidized Bed Bioreactor

6.1 Introduction

Combining partial nitrification with ANAMMOX process is a promising biological process for nitrogen removal from ammonia-rich wastewater. For this technology, ammonia is converted to NO_2-N by the first step of nitrification rather than NO_3-N, then reduced to gaseous N_2 by residual NH_4-N. In contrast to the conventional nitrification/denitrification process, approximately 25% oxygen and 40% denitrification carbon could be saved (Turk and Mavinic, 1987). The SHARON® (Single reactor system for High Activity Ammonium Removal Over Nitrite) technology developed by Delft University of Technology in 1998 demonstrated the feasibility and economic advantages of this combined process (Hellinga et al., 1998).

Partial nitrification (PN) is the first step for the whole nitrification process and can be achieved by enriching ammonia-oxidizing bacteria (AOB) and inhibiting the growth of nitrite-oxidizing bacteria (NOB). Several studies have investigated the critical conditions required for PN process, such as free ammonia (FA), alkalinity, pH, dissolved oxygen concentration (DO) and temperature (Ge et al., 2015; Kinh et al., 2017; Sinha and Annachhatre, 2007). Usually, pH is maintained at 7.5 to 8.5 for nitrite accumulation (Peng and Zhu, 2006). It has been reported that NOB activity is inhibited at FA concentration of 0.1-1.0 mg/L (Abeling and Seyfried, 1992), while the tolerance FA concentration of AOB is in the range of 10-150 mg N/L at 30˚C (Anthonisen et al., 1976). The Monod half-saturation constant of DO (K_o) for AOB and NOB are 0.3 mg O_2/L and 1.1 mg O_2/L at 30˚C (Wiesmann, 1994). Similarly, Grunditz and Dalhammar (2001) concluded that the optimum temperature for AOB (*Nitrosomonas*) is 35˚C.

Various partial nitrification studies summarized in Table 6-1 present different nitrogen removal performance of membrane bioreactors, sequencing batch reactors, and biofilm

reactors with a wide range of nitrogen removal efficiencies from <50% to >99% at influent ammonium concentrations of 43 mg/L to 1400 mg/L (Dosta et al., 2015; Tokutomi et al., 2010; Zhang et al., 2015). Influent nitrogen loading rates tested in the aforementioned studies varied from <1 kg N/(m^3 d) to 5.9 kg N/(m^3 d) with mostly less than 2 kg N/(m^3 d) while the nitrogen removal rates also ranged from 0.4 kg N/(m^3 d) to 3 kg N/(m^3 d). It should be noted that the 5.9 kg N/(m^3 d) reported in Zhang et al. (2011) was tested one day; hence, stable operation at such high loading was not sustained. High nitrogen removal efficiencies with high influent concentrations and/or high nitrogen loadings were shown for airlift reactors (Chai et al., 2015), granular bioreactor (Soliman and Eldyasti, 2016) and biofilm media reactors (Zhang et al., 2011), possibly indicating that these technologies may outcompete CSTR for partial nitrification of higher ammonia concentrations. Of the aforementioned studies, few showed the effluent NO_2-N/NH_4-N ratio of 1.0-1.3 (Dosta et al., 2015; Zhang et al., 2011, Zhang et al., 2015) which is close to the stoichiometric ratio of 1.3 for the influent of anammox systems.

Table 6-1. Comparison of different PN processes

Bioreactor configuration	wastewater	Influent ammonia (mg N/L)	DO (mg/L)	Temp (°C)	Ammonia Loading Rate kg/(m³ d)	Ammonia Removal Efficiency (%)	NO$_2$-N /NO$_x$-N (%)	NO$_2$-N /NH$_4$-N	References
DHS (down-flow hanging sponge reactor)	Synthetic	100	0.42	30	1.46	42	>95	0.69	(Chuang et al., 2007)
FBBNR (fluidized-bed biofilm nitritation reactors)	Synthetic	250	2.5	21±1	0.9	99.2	74	71.4	(Aslan and Dahab, 2008)
Airlift-fluidized bed reactor	Synthetic	1243	3.0-3.8	30	2.6	68	99	2.12	(Tokutomi et al., 2010)
Swim-bed reactor	Digester supernatant	800-1000	Nearly 0	28 ± 1	3.0-5.9 [2]	52.5	>99.9	1.11	(Zhang et al., 2011)
Up-flow bioreactor	Synthetic	150	-	35	1.76	63.6		1.20±0.33	(Okabe et al., 2011)
MBMBR (moving bed membrane bioreactor)	Synthetic	42.8	-	25	-	87.8 (TN)	79.4	5.71	(Yang and Yang, 2011)
MBR (membrane bioreactor)	Synthetic	200	0.15	25±0.5	0.7	55	>99.9	1.1-1.3	(Zhang et al., 2015)
Airlift reactor	Synthetic	1400	2.2	35 ± 2	2.1	91	80	8.1	(Chai et al., 2015)
Granular sludge SBR	Digester supernatant	740 ± 40	-	30	3.1	50 ± 6.4	50	1.0	(Dosta et al., 2015)
Granular sludge SBR	Synthetic	990 ± 4.1	0.6-1.2	31	1.2	98.6	93.1	63.1	(Soliman and Eldyasti, 2016)
CSTR	Pretreated Water[1]	98.8 ±4.1	>2.0	23.9±0.9	0.10 ± 0.01	49.7	98.4	0.96	(Durán et al., 2014)

1. Pretreated in an aerobic granular pilot plant, characterized by low organic matter and relatively high ammonia content.

2. 5.9 kg/(m³·d) was applied for one day.

Fluidized bed bioreactor processes (FBBR) have been applied for wastewater treatment field for decades (Rabah and Dahab, 2004a). Both laboratory and pilot-scale studies demonstrated the high efficiency of FBBR such as shortened HRTs i.e. 1/8 of the conventional suspended system with the same capability, less space occupation, high biomass concentration, and remarkable low observed sludge yields (Andalib et al., 2010; Chowdhury et al., 2009; Cui et al., 2004). The FBBR system is particularly suitable for high nitrogen loadings with high influent concentrations. For example, the fluidized bed biofilm reactor achieved a nitrate removal efficiency of 99.8% at the nitrogen loading rate of 6.3 kg N/(m^3 d) with influent NO_3-N of 1000 mg/L (Rabah and Dahab, 2004b). The stability of such system also provides favorable conditions for slow growing microorganisms, such as AOB species.

Despite the excellent wastewater/solids treatment capacity of the fluidized bed process, few studies were conducted on the application of fluidized bed bioreactor to partial nitrification. For instance, Aslan and Dahab, (2008) who operated a fluidized bed system treating influent NH_4-N of 250 mg/L at 21°C and DO of 1.5-2.5 mg/L reported average ammonia removal efficiency of 99.2% at a nitrogen loading rate (NLR) of 0.9 kg N/(m^3 d) with high effluent NO_3-N concentration of 64 mg/L. Although the aforementioned study demonstrated the application of fluidized bed systems for PN processes, the operational conditions were not optimized in terms of high loading rates and proper effluent NO_2-N/NH_4-N ratio of 1.0-1.3. Particularly, the nitrogen loading of 0.9 kg N/(m^3 d) was lower than for other biofilm systems showing >2 kg N/(m^3 d) (Table 6-1); thus, the advantages of the FBBR technology for PN were not clearly demonstrated. In order to explore the feasibility of FBBR to PN/anammox processes as a promising second-generation biological nutrient removal process, it is essential to optimize the operation conditions.

This study operated a fluidized bed process to optimize operational conditions for PN processes treating different influent nitrogen loadings of 1.2-4.8 kg N/(m^3 d). The main objective of this research was to achieve stable partial nitrification of the ammonia-rich water in a FBBR system with nitrite to ammonia ratio of 1.3:1 of effluent at limiting dissolved oxygen (DO), and alkalinity concentrations. The effluent of partial nitrification

fluidized bed bioreactor (PNFBR) is optimized for further nitrogen removal in an anammox process. To the best of our knowledge, this study is the first report of high rate partial nitrification performance using a fluidized bed process.

6.2 Materials and methods

6.2.1 System configuration and startup

A lab-scale PNFBR (Figure 6-1) was fabricated using a 10.4 L cylindrical Plexiglass column with a height of 1.7 m and a diameter of 8.9 cm. A 4-L water level balancing tank was attached to the column to facilitate the liquid recirculation for fluidization. In addition, aeration was supplied from the top of the column and a separator was used to stabilize the PNFBR by preventing air entering and damaging the circulating pump. A 40L container was used as a feeding tank, from which influent was pumped to the bottom of the column by a peristaltic pump. The PNFBR dimensions are summarized in the Table 6-2.
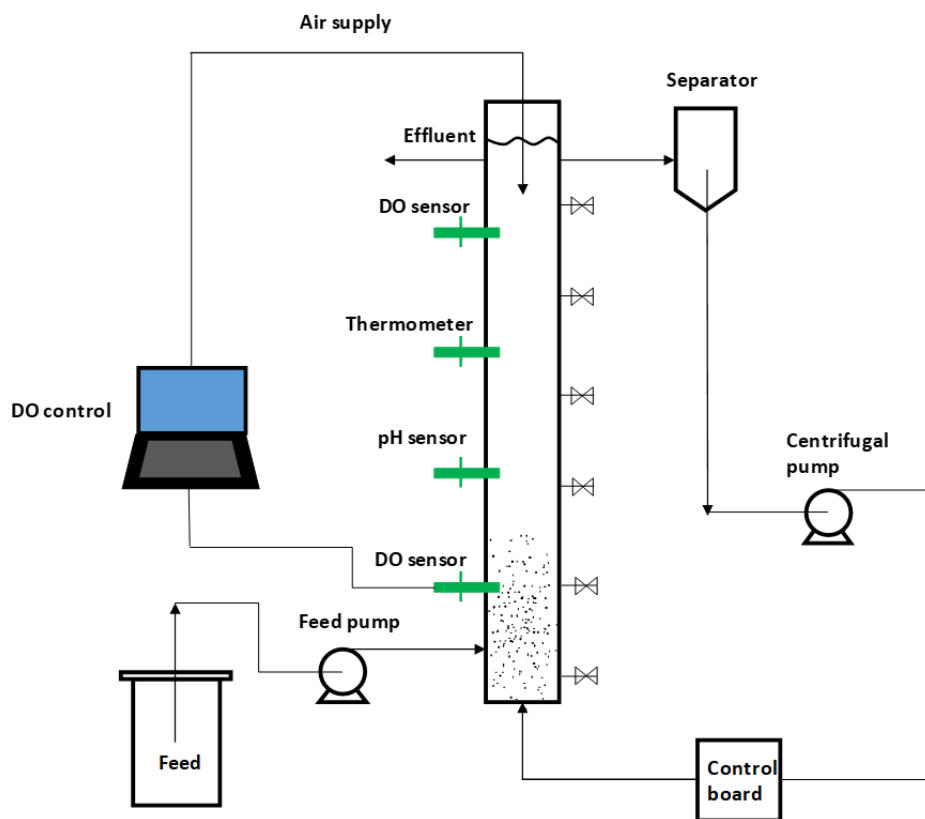

Figure 6-1. The schematic diagram of partial nitrification fluidized bed bioreactor

Approximately 2 kg of HDPE particles with a range of diameters of 600-850 μm were added into the reactor, and compacted to a volume of 2.5 L. The detailed media characteristics are presented in Table 6-2. The system was operated at 35°C controlled by a water bath system (VWR® Heated Circulating Bath, VWR International, Mississauga, Canada). On-line dissolved oxygen probes (ENV-40-DO, Atlas Scientific LLC, New York, USA) were placed at the top and bottom of the reactor and connected to a dissolved oxygen control system. Oxygen was provided from an air line with a fine bubble air diffuser on the top of the reactor, at an airflow rate of about 0.9 SCFH to maintain an average DO concentration of approximately 1.3 mg/L in the reactor. A pH sensor (ENV-40-pH, Atlas Scientific LLC, New York, USA) was placed at the middle of the reactor to monitor pH, which was in the range of 7.5-8.0.

The seed sludge for the PNFBR was return activated sludge (RAS) collected from the Adelaide Water Pollution Control Plant (London, Canada), and subsequently enriched for AOB in a 20-L mechanically mixed batch reactor for 30 days at a DO concentration of 2.0 mg/L, temperature of 35°C and pH of 8.0. After stopping mixing and aeration for 1 hr, 10 L of the reactor supernatant were withdrawn daily and replaced with a synthetic solution with the following components of 100 mg NH_4-N/L, 500 mg $CaCO_3$/L and trace metal solution. After 30 days, this AOB enriched culture had a respectable specific ammonia oxidation rate of 0.1 g NH_4-N/(g VSS h) with a nitrite conversion ratio of 60%. Subsequently, the PNFBR was seeded with 10L of the cultivated sludge. In order to enhance biomass attachment from the bulk liquid to the particle surface, the seed sludge was recirculated in the column for 2 days. Thereafter, the inflow was continuously fed to the PNFBR at a rate of 30 L/day.

6.2.2 Influent composition

The inflow used in this study consisted of 100-400 mg N/L using NH_4Cl, 500-2000 mg $CaCO_3$/L using $NaHCO_3$, 0.025 mg KH_2PO_4/L, 0.14 mg $CaCl_2$·$2H_2O$/L, and 0.3 mg $MgSO_4$/L. The trace metal solution, which was added to the feed at 1.5 mL/L, was composed of 15 mg EDTA/L, 0.43 mg $ZnSO_4$·$7H_2O$/L, 0.24 mg $CoCl_2$/L, 0.99 mg

MnCl$_2$/L, 0.25 mg CuSO$_4$·H$_2$O/L, 0.22 mg NaN$_0$O$_4$·H$_2$O/L, 0.19 mg NiCl·6H$_2$O /L, and 0.014 mg H$_3$BO$_4$/L.

Table 6-2. PNFBR parameters and media characteristics

Parameter	Value
PNFBR	
Total Reactor Volume	14.4 L
Column Volume	10.4 L
Compacted Bed Volume	2.5 L
Column Diameter	8.9 cm
DO	1.3-1.7 mg/L
Temperature	35 ˚C
pH	7.5-8.0
EBCT	2.0-2.7 h
Loading rate	22.5-30 L/d
Q$_R$	2.5-3 LPM
Bed Expansion*	20%
Concentration of Feed	100-400 mg NH$_4$-N/L
Alkalinity/NH$_4$-N ratio	5
Media characteristics	
Type	HDPE
Weight	2 kg
Diameter	600-850 μm
Voidage	48-52%
Specific surface area	4600 m^2/m^3
Wet bulk density	1230 kg/m^3

 * Calculated based on equation: Bed expansion (%) = (expanded bed volume −

compacted bed volume)/(compacted bed volume)

6.2.3 System operation

The operation of the PNFBR included five different phases over a period of 153 days i.e. phase 1 (36 days), phase 2 (31 days), phase 3 (26 days), phase 4 (16 days) and phase 5 (14 days) with different operational conditions in each phase. The feeding rates were 30 L/d for phases 1 through 3 and 22.5 L/d for phase 4 and phase 5, corresponding to EBCTs, calculated based as the product of compacted bed volume divided by inflow rate, of 2 hrs (phase 1-3) and 2.7 hrs (phase 4, 5). Influent nitrogen concentrations were 100 mg/L (phase 1), 200 mg/L (phase 2), 300 mg/L (phase 4) and 400 mg/L (phase 3, 5). Influent alkalinity was added based on an alkalinity-to-nitrogen mass ratio of 5:1. The recirculation liquid flow rates and corresponding superficial liquid velocities (the liquid flow rates divided by the cross area) were 3 L/min and 8.0×10^{-3} m/s for phases 1 and 2, 2.7 L/min and 7.3×10^{-3} m/s for phase 3, 2.5 L/min and 6.7×10^{-3} m/s for phases 4 and 5. The temperature was maintained at 35 ºC in all phases while DO concentrations were maintained around 1.3 mg/L but slightly varied i.e. 1.30 ± 0.20 mg/L (phase 1, 2, 4 and 5) and 1.71 ± 0.20 mg/L (phase 3).

6.2.4 Analysis

The influent and effluent samples were collected daily and analyzed for various water quality parameters including ammonia (NH_4-N), nitrite (NO_2-N), nitrate (NO_3-N), and alkalinity. Nitrogen compounds and alkalinity were measured using Hach Methods and Standard Methods (American Public Health Association, 2008), respectively. Additionally, biomass attachment was measured and recorded every two weeks. In order to measure the biomass attachment, approximately 10 g media were collected from the PNFBR and sonicated (Model 75HT, ETL Laboratory Investigating Inc., New York) for 3 hours at 30 ˚C to detach the biomass from the particles. The VSS content of the detached biomass was measured using standard methods APHA (American Public Health Association, 2008). The dry mass of the particles was also determined after drying at room temperature for 1-2 days.

6.2.5 Batch tests

Batch tests were carried out during the first and last phases of this study to determine the biomass specific nitrification rates (SNR) of the attached biomass. 0.5 L batch reactors equipped with magnetic stirrer and air diffuser (to maintain DO around 5 mg/L) were employed to examine the maximum reaction rate. The initial food-to-microorganism (S_0/X) ratio was calculated based on the nitrogen loading and biomass in the PNFBR. Alkalinity-to-ammonia ratio was maintained at 5:1 by using $NaHCO_3$. During the test, samples were taken at 0.5h intervals until the measured ammonia concentration decreased to near 0. Ammonia, nitrate and nitrite concentrations were tested for each sample.

6.2.6 Statistical analysis

T-tests were conducted using the unequal variances in an Excel software to assess the statistical significance of the observed differences at the 95% confidence level.

6.3 Results and discussions

6.3.1 System performance

Performance results for the five different phases (Table 6-3) showed that ammonia removal efficiencies of 57.2% in phase 1, 54.0% in phase 2, 46.0% in phase 3, 69.3% in phase 4, and 57.1% in phase 5, respectively. T-tests indicated that the observed differences in ammonia removal efficiencies between different phases were statistically significant ($p < 0.05$) except phase 1 versus phase 2 and phase 1 versus phase 5. The low ammonia removal efficiency in phase 3 clearly identifies the limiting nitrogen loading of this system for PN, and the optimal effluent NO_2-N/NH_4-N for anammox was not achieved. In phase 4, the influent ammonia concentration was reduced to 300 mg/L and EBCT of 2.7 hrs to optimize the effluent NO_2-N/NH_4-N ratio. However, NO_2-N/NH_4-N stabilized at 1.9 while the washout of NOB was sustained. In phase 5, the EBCT was fixed at 2.7 hrs and influent ammonia concentration was increased to 400 mg/L to identify the maximum nitrogen loading of this system for effluent NO_2-N/NH_4-N ratio of 1.0-1.3.

The ammonia oxidation efficiency (%AOE) was estimated by dividing the sum of effluent nitrite and nitrate concentrations by influent ammonia concentration (shown as Equation (6.1)). Similarly, the nitrite oxidation efficiency (%NOE) was obtained by dividing effluent nitrate concentration by the sum of effluent nitrite and nitrate levels (shown as Equation (6.2)). The calculated AOE and NOE were 46% and 16% for phase 1, 48% and 10% for phase 2, 43% and 6.0% for phase 3, 64% and 6.8% for phase 4, and 57% and 6.8% for phase 5. T-tests indicated that differences in AOE between the five phases except for the difference between phase 1 and phase 3 were statistically significant ($p < 0.05$). Likewise, the differences in NOE values between the five phases were statistically significant ($p < 0.05$).

$$\text{AOE (\%)} = \frac{\text{effluent } NO_2-N + NO_3-N}{\text{influent } NH_4-N} \times 100 \qquad (6.1)$$

$$\text{NOE (\%)} = \frac{\text{effluent } NO_3-N}{\text{effluent } NO_2-N + NO_3-N} \times 100 \qquad (6.2)$$

Scrutiny of the data indicated that the average effluent NO_2-N/NH_4-N ratio varied widely between the different phases i.e. 0.99 (phase 1), 1.02 (phase 2), 0.75 (phase 3), 1.9 (phase 4) and 1.27 (phase 5). T-tests indicated that differences in NO_2-N/NH_4-N ratios between the different phases were statistically significant except between phase 1 and phase 2 ($p < 0.05$). Similarly, alkalinity consumption per NH_4-N conversion were 5.2 (phase 1), 5.6 (phase 2), 5.1 (phase 3), 4.9 (phase 4) and 4.6 (phase 5). However, the differences of the ratios between the five phases were not statistically significant ($p > 0.05$).

Table 6-3. Operational conditions and performance data of the PNFBR

Parameter	Unit	Phase 1	Phase 2	Phase 3	Phase 4	Phase 5
NH$_4$-N-In	mg/L	99.0±2.1	200±5.1	399±6.0	300± 1.8	400±7.9
NH$_4$-N-Eff	mg/L	42.0±10.5	92±11.8	216±22.1	92±11.4	166±5.8
NO$_2$-N	mg/L	38.1±8.3	91.7±10.1	159±25.0	180±13.3	212±8.7
NO$_3$-N	mg/L	7.3±1.8	9.8±2.1	10±1.6	11.6±1.1	15.4±1.7
NO$_2$/NH$_4$ in effluent	-	0.99	1.02	0.75	1.9	1.27
Free ammonia	mg N/L	5.3	11.4	27.3	12.5	16.9
NLR	kg NH$_4$-N/m^3·d	1.2	2.4	4.8	2.7	3.6
DO	mg/L	1.31±0.20	1.29±0.20	1.71±0.35	1.31±0.32	1.30±0.25
pH	-	-	8.04±0.04	8.09±0.20	8.01±0.14	7.97±0.18
EBCT	hours	2.0	2.0	2.0	2.7	2.7
T	°C	35	35	35	35	35
Alkalinity Consumption	mg CaCO$_3$/L	271 ± 66	609 ± 101	888 ± 164	1010±174	1090±190
△Alkalinity/NH$_4$	-	5.2	5.6	5.1	4.9	4.6
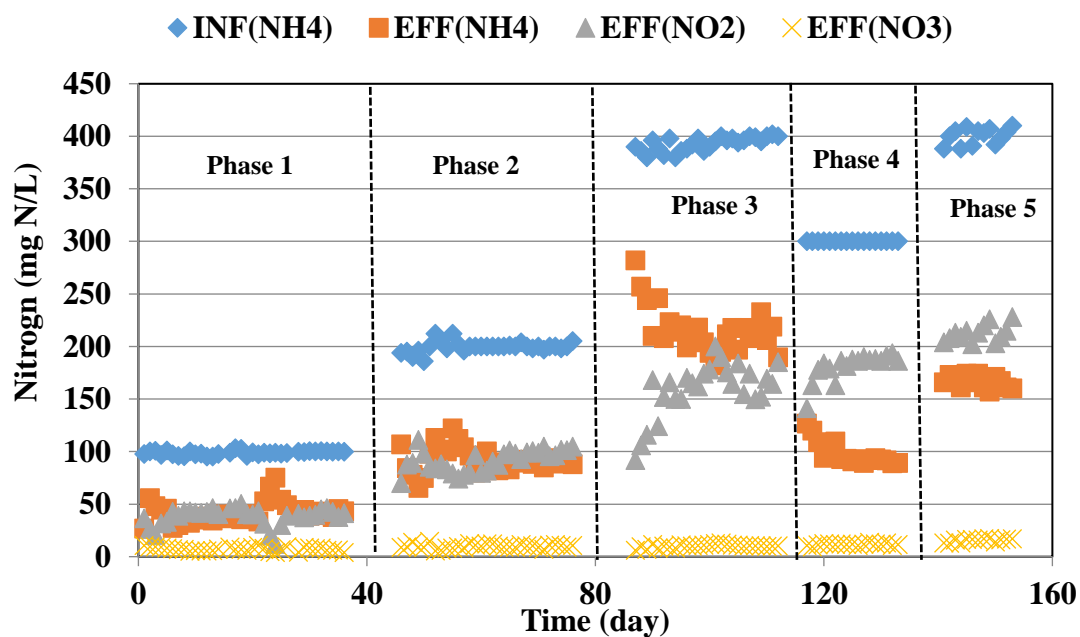
Figure 6-2. Influent and effluent nitrogen concentrations during different phases

6.3.2 Biofilm activity tests

Biomass tests showed that the attached biomass on bioparticles increased from 1.5 mg VSS/g dry particle in phase 1 to 2.3 mg VSS/g dry particle in phase 5, i.e. a 53.3% increase. In order to examine the activity of AOB and NOB, biomass SNR tests were conducted (Table 6-4). Most of the ammonia was converted to nitrite (90%) instead of nitrate (10%), which implied that AOB population was much larger than NOB population. Biomass SNR values show that AOB activity almost remained the same i.e. varying from 0.188 to 0.198 g NH_4-N/(g VSS h) while NOB activity stayed the same at 0.026 g NO_3-N/(g VSS h), indicating that NOB growth on the bioparticles was effectively suppressed in both phases 1 and 5. Based on the analysis of biomass tests and SNR tests, the maximum nitrite conversion rates (NriCR) were 10.7 g N/d (Phase 1) and 17.6 g N/d (Phase 5), while the maximum nitrate conversion rates (NraCR) were 1.87g N/d (Phase 1) and 2.87 g N/d (Phase 5). However, the actual NriCR in the reactor were 1.14 g N/d (Phase 1) and 4.77 g N/d (Phase 5), while the actual NraCR were 0.22 g N/d (Phase 1) and 0.34 g N/d (Phase 5). Based on the data presented in Table 6-4, the actual ammonia removal rates were only 12.6% and 24.2% of the maximum in phase 1 and 5. The discrepancies could be caused by the limitation of oxygen diffusion into the biofilm.

In comparison with literature data, the biomass SNR value of 3.74 g N/(g VSS d) in this study is much higher than those reported in previous biofilm systems such as 0.35 g N/(g VSS d) (Okabe et al., 2011) and 0.12 g N/(g VSS d) (Chuang et al., 2007) obtained from the systems using nonwoven fabric sheets ($4.0 \times 4.0 \times 0.8$ cm per sheet) and sponge material ($2.8 \times 2.8 \times 4$ cm in size), respectively, indicating the highly efficient PN performance of the PNFBR.

Table 6-4. Biomass specific ammonia uptake, nitritation and nitratation rates

	Phase 1	Phase 5
Samples Weight	12 g dry particles	8.25 g dry particles
Concentration (mg VSS/g particles)	1.5	2.3
Reactor Volume (ml)	500	
rNH₄-N g NH₄-N/(g VSS h)	0.188	0.198
Overall attached nitrification rate g NH₄-N/d	13.5	21.8
rNO₂-N g NO₂-N/(g VSS h)	0.149	0.159
Overall attached nitrite produced rate g NO₂-N/d	10.7	17.6
rNO₃-N g NO₃-N/(g VSS h)	0.027	0.026
Overall attached nitrate produced rate g NO₃-N/d	1.87	2.87
Bioreactor ammonia removal rate g NH₄-N/d	1.70	5.27
Bioreactor nitrite produced rate g NO₂-N/d	1.14	4.77
Bioreactor nitrate produced rate g NO₃-N/d	0.22	0.34

6.4 Partial nitrification loading

The SHARON® process is one of the established partial nitrification technologies. The full-scale SHARON® reactor (1800 m^3 continuous stirred tank reactor (CSTR)) was built to treat reject water at 35 ˚C and an SRT of 2.5 days with the nitrite/ammonium ratio in the effluent of 1.1 and ammonium conversion ratio of 53% at the NLR of 0.5 kg N/(m^3 d) (Mulder et al., 2001). However, while short SRT of SHARON process at high temperature promotes the selective growth of AOB, NLR of the system is limited by the growth rate of

AOB. In the present study, similar effluent qualities to the aforementioned SHARON[®] process were achieved at the NLR of 3.6 kg N/(m^3 d), indicating that the treatment capability was about 7 times more than the SHARON[®] process due to the advantages of fluidized bed bioreactor over CSTR. For another PN process - CANON(Completely autotrophic nitrogen removal over nitrite), 89% of TN and 98% of NH$_4$-N were removed at the NLR of 0.9 kg N/(m^3 d) during treatment of optoelectronic wastewater with an influent ammonia of 3712 ± 120 mg/L at temperature of 37 ℃, which means the ammonia nitrogen removal rate (NRR) was about half of the maximum NRR of this PNFBR system (Daverey et al., 2013). Additionally, although the nitrogen loading based on media surface area in this study, of 1.45 g N/(m^2 d), is similar to the previous fluidized bed PN study of 1.65 g N/(m^2 d) (Aslan and Dahab, 2008) and the moving-bed PN reactor of 1.5 g N/(m^2 d) (Szatkowska et al., 2007), the effluent NO$_2$-N/NH$_4$-N ratio of 1.27 in this study was more applicable to ANAMMOX process.

The relationship between the NRR and NLR is shown in Figure 6-3. NRR increased linearly from 0.72 to 2.16 kg N/(m^3 d) with the increase of NLR from 1.2 to 3.6 kg N/(m^3 d), and then remained constant at 2.16 kg N/(m^3 d) for NLR in the range of 3.6-4.8 kg N/(m^3 d), indicating that NRR reached maximum at NLR of 3.6 kg N/(m^3 d). Compared with other biofilm-type systems, Okabe et al., (2011) who performed PN in an up-flow bioreactor at the NLR of 1.76 kg N/(m^3 d) reported similar effluent NO$_2$-N/NH$_4$-N ratios to this study and NRR of 1.1 kg N/(m^3 d). Tokutomi et al., (2010) who operated an airlift-fluidized bed reactor at the NLR of 2.6 kg N/(m^3 d) with high inorganic carbon concentration in the influent also reported the maximum NH$_4$-N removal efficiency of 68% and NRR of 1.77 kg N/(m^3 d). Similarly, Chuang et al., (2007) who tested a down-flow hanging sponge reactor at the NLR of 1.46 kg N/(m^3 d) presented NRR of 0.61 kg N/(m^3 d) with NH$_4$-N removal efficiency of 42%. The NRR values of these three previous biofilm reactor studies (0.61-1.77 kg N/(m^3 d)) are lower than the maximum NRR of 2.16 kg N/(m^3 d) in this study, indicating better performance of PNFBR system than other biofilm processes. Furthermore, as shown in Table 6-1, the maximum NRR of 2.16 kg N/(m^3 d) observed in this study is higher than those observed with granular sludge i.e. 1.2 kg N/(m^3 d) for synthetic wastewater (Soliman and Eldyasti, 2016), and the 1.6 kg N/(m^3 d) for

digester supernatant (Dosta et al., 2015), as well as the 1.8 kg N/(m^3 d) observed in an airlift reactor (Chai et al., 2015).
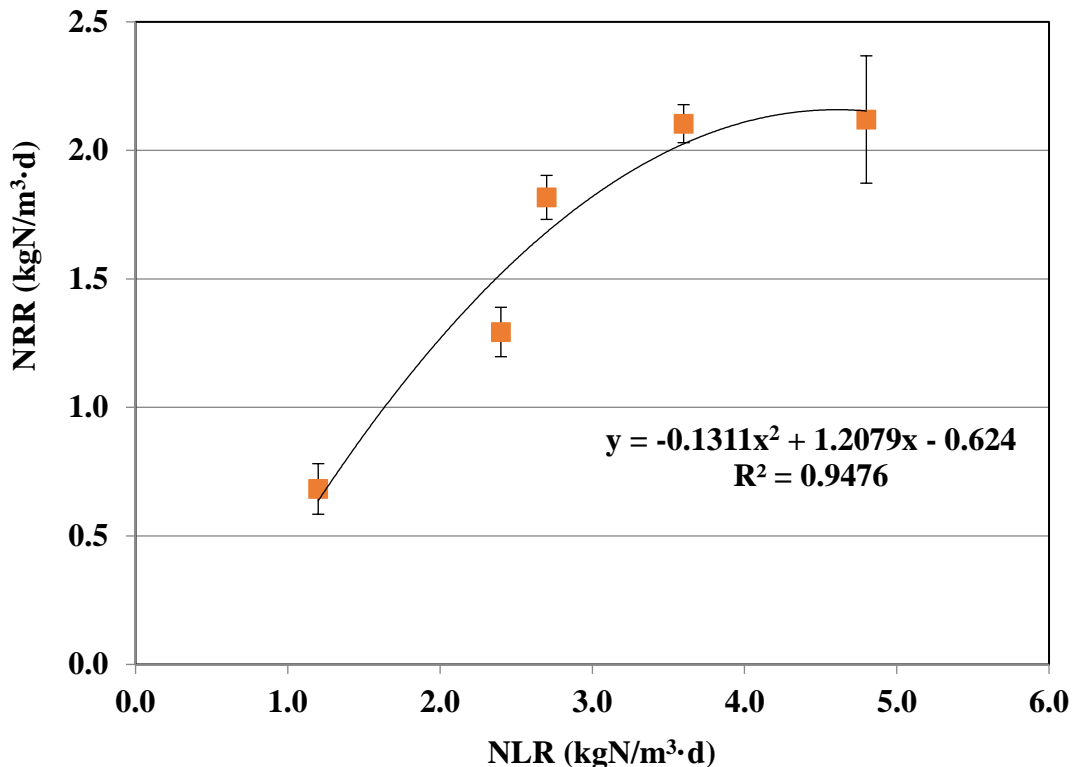

Figure 6-3. Relationship between NLR and NRR

Several factors impacting partial nitrification were examined such as FA, DO, influent alkalinity-to-ammonia ratio. It has been reported that AOB and NOB are inhibited at FA concentrations of 10-150 mg/L and 0.1-1.0 mg/L, respectively (Abeling and Seyfried, 1992; Anthonisen et al., 1976). Chung et al., (2006) also reported that FA concentration of 5-10 mg/L is necessary for partial nitrification. FA concentration in this study can be calculated according to Equation (6.3) (Anthonisen et al., 1976).

$$FA(mg/L) = \frac{17}{14} \frac{\sum NH_4-N\left(\frac{mg}{L}\right) \times 10^{pH}}{(k\_b/k\_w) + 10^{pH}}$$ (6.3)

Where

$$\frac{k_b}{k_w} = e^{6344/(273+T)}$$

Given that the PNFBR was operated at a pH of 7.5-8.0 and a temperature of 35˚C, the estimated average FA concentrations were 5.3 mg/L (phase 1), 11.4 mg/L (phase 2), 27.3 mg/L (phase 3), 12.5 mg/L (phase 4) and 21.2 mg/L (phase 5), indicating that FA levels fell within the inhibition range for NOB.

A model prediction of AOB and NOB activity was undertaken to estimate partial nitrification performance at the operational conditions of the PNFBR. The model developed by Liu et al. (2017) determines the minimum DO concentrations for AOB and NOB growth as a function of temperature, pH, NH_4-N, NO_2-N, and SRT to reflect the FA and FNA impact on the nitrifiers' activity. For the model estimation, kinetic values of AOB and NOB at 20 °C were also adopted from Liu et al. (2017). The half substrate saturation coefficient (K_s) is 0.75 mg N/L for AOB and 2.7 mg N/L for NOB while K_o is 0.51 mg/L for AOB and 1.98 mg/L for NOB. Similarly, maximum growth rate (μ_{max}) is 0.9 d^{-1} (AOB) and 1.0 d^{-1} (NOB) and decay coefficient (b) is 0.17 d^{-1} for both AOB and NOB. Different temperature correction factors for K_s, μ_{max}, and b were also used i.e. 1.029 (AOB and NOB) for K_s, 1.072 (AOB) and 1.063 (NOB) for μ_{max} and 1.04 (AOB and NOB) for b. Given that the operational conditions of the five phases (Table 6-3) were 42-216 mg NH_4-N/L, 38-212 mg NO_2-N/L, pH of 8, temperature of 35 ˚C, SRT of 51 days, the minimum DO concentrations for AOB were estimated at 0.15-0.51 mg/L. Furthermore, NOB would be suppressed in all phases due to decay and washout rate greater than the growth rate (Liu et al., 2017). However, it should also be noted that the estimated minimum DO should be DO concentrations within the biofilms while this study observed bulk DO only. Nonetheless, the model estimation indicates that the operational conditions in the fluidized bed system promote AOB activity over NOB.

The Monod half-saturation constant of DO for AOB and NOB are 0.3 mg O_2/L and 1.1 mg O_2/L at 30˚C, respectively (Grunditz and Dalhammar, 2001). Since the half-saturation DO concentration is much larger for NOB than AOB, NOB's activity dropped significantly at low DO conditions. Nitrite accumulation is more feasible when DO decreases below 1 mg/L, whereas when DO is greater than 1 mg/L, the activity of NOB begins to recover (Chuang et al., 2007; Sliekers et al., 2005). The DO concentration of this study was maintained around 1.3 mg/L except phase 3 (1.7 mg/L). Under the DO conditions, NO_2-N

accumulation and partial nitrification were still achieved, with lower NH$_4$-N conversion ratio. Considering that oxygen penetration decreases over the depth of biofilm and the typical slow growth NOB are in the inner layer of the biofilm, the ambient DO of 1.3 mg/L in this study did not promote NOB activity.

Influent alkalinity-to-ammonia ratio also played a role of stable partial nitrification. The ratio in this study was maintained at 5, close to the optimum ratio of 4.8 reported by Zhang et al., (2011) who tested PN performance at an NLR of 3.0-5.9 kg N/(m^3 d) at different alkalinity-to-ammonia ratios of 4.6-7.1. Additionally, since alkalinity also provides inorganic carbon source to both AOB and NOB, the low influent alkalinity-to-ammonia ratio in this study also contributed to effectively generate a NO$_2$-N/NH$_4$-N ratio of 1.27 through selectively enhancing AOB activity and suppressing NOB activity. Overall, the operational conditions in this study i.e. pH 8.0, 35 ˚C, high FA, alkalinity-to-ammonia ratio of 5, and DO of 1.3 mg/L were effective for successful PNFBR performance at NLR of 3.6 kg N/(m^3 d).

6.5 Conclusions

Partial nitrification of ammonia in a fluidized bed bioreactor was successfully achieved at high NLR of 4.8 kg N/(m^3 d) at pH of 8.0, temperature of 35˚C, and DO of 1.3 mg/L, demonstrating the feasibility of PN in PNFBR. Particularly, stable effluent NO$_2$-N/NH$_4$-N ratio of 1.27, which meets the required influent quality for the ANAMMOX process, was achieved at the NLR of 3.6 kg N/(m^3 d). The maximum ammonia nitrogen removal rate of the PNFBR system was 2.16 kg N/(m^3 d). Simulation using literature models confirmed that the operational conditions of PNFBR were effective for partial nitrification. High free ammonia and low influent alkalinity-to-ammonia seem to be the key factors for AOB accumulation and NOB inactivation in PNFBR system.

References

Abeling, U., Seyfried, C.F., 1992. Anaerobic-Aerobic Treatment of High-Strength Ammonium Wastewater - Nitrogen Removal via Nitrite. Water Sci. Technol. 26, 1007–1015.

American Public Health Association, 2008. Standard methods for the examination of water and wastewater.

Andalib, M., Nakhla, G., Zhu, J., 2010. Dynamic testing of the twin circulating fluidized bed bioreactor (TCFBBR) for nutrient removal from municipal wastewater. Chem. Eng. J. 162, 616–625.

Anthonisen, A.C., Loehr, R.C., Prakasam, T.B.S., Srinath, E.G., 1976. Inhibition of nitrification by ammonia and nitrous acid. J. (Water Pollut. Control Fed). 835–852.

Aslan, S., Dahab, M., 2008. Nitritation and denitritation of ammonium-rich wastewater using fluidized-bed biofilm reactors. J. Hazard. Mater. 156, 56–63.

Chai, L.-Y., Ali, M., Min, X.-B., Song, Y.-X., Tang, C.-J., Wang, H.-Y., Yu, C., Yang, Z.-H., 2015. Partial nitrification in an air-lift reactor with long-term feeding of increasing ammonium concentrations. Bioresour. Technol. 185, 134–142.

Chowdhury, N., Zhu, J., Nakhla, G., Patel, A., Islam, M., 2009. A novel liquid-solid circulating fluidized-bed bioreactor for biological nutrient removal from municipal wastewater. Chem. Eng. Technol. 32, 364–372.

Chuang, H.-P., Ohashi, A., Imachi, H., Tandukar, M., Harada, H., 2007. Effective partial nitrification to nitrite by down-flow hanging sponge reactor under limited oxygen condition. Water Res. 41, 295–302.

Chung, J., Shim, H., Park, S.-J., Kim, S.-J., Bae, W., 2006. Optimization of free ammonia concentration for nitrite accumulation in shortcut biological nitrogen removal process. Bioprocess Biosyst. Eng. 28, 275–282.

Cui, Y., Nakhla, G., Zhu, J., Patel, A., 2004. Simultaneous carbon and nitrogen removal in anoxic-aerobic circulating fluidized bed biological reactor (CFBBR). Environ. Technol. 25, 699–712.

Daverey, A., Su, S. H., Huang, Y. T., Chen, S. S., Sung, S., Lin, J. G., 2013. Partial nitrification and anammox process: a method for high strength optoelectronic industrial wastewater treatment. Water Res, 47, 2929-2937.

Dosta, J., Vila, J., Sancho, I., Basset, N., Grifoll, M., Mata-Álvarez, J., 2015. Two-step partial nitritation/Anammox process in granulation reactors: Start-up operation and microbial characterization. J. Environ. Manage. 164, 196–205.

Durán, U., Val del Río, A., Campos, J.L., Mosquera-Corral, A., Méndez, R., 2014. Enhanced ammonia removal at room temperature by pH controlled partial nitrification and subsequent anaerobic ammonium oxidation. Environ. Technol. 35, 383–390.

Ge, S., Wang, S., Yang, X., Qiu, S., Li, B., Peng, Y., 2015. Detection of nitrifiers and evaluation of partial nitrification for wastewater treatment: A review. Chemosphere 140, 85–98.

Grunditz, C., Dalhammar, G., 2001. Development of nitrification inhibition assays using pure cultures of nitrosomonas and nitrobacter. Water Res. 35, 433–440.

Hellinga, C., Schellen, A.A.J.C., Mulder, J.W., van Loosdrecht, M.C.M., Heijnen, J.J., 1998. The sharon process: An innovative method for nitrogen removal from ammonium-rich waste water. Water Sci. Technol. 37, 135–142.

Kinh, C.T., Ahn, J., Suenaga, T., Sittivorakulpong, N., Noophan, P., Hori, T., Riya, S., Hosomi, M., Terada, A., 2017. Free nitrous acid and pH determine the predominant ammonia-oxidizing bacteria and amount of N2O in a partial nitrifying reactor. Appl. Microbiol. Biotechnol. 101, 1673–1683.

Liu, X., Kim, M., Nakhla, G., 2017. A model for determination of operational conditions for successful shortcut nitrification. Environ. Sci. Pollut. Res. 24, 3539–3549.

Mulder, J.W., van Loosdrecht, M.C.M., Hellinga, C., van Kempen, R., 2001. Full-scale application of the SHARON process for treatment of rejection water of digested sludge dewatering. Water Sci. Technol. 43, 127–134.

Okabe, S., Oshiki, M., Takahashi, Y., Satoh, H., 2011. Development of long-term stable partial nitrification and subsequent anammox process. Bioresour. Technol. 102, 6801–6807.

Peng, Y., Zhu, G., 2006. Biological nitrogen removal with nitrification and denitrification via nitrite pathway. Appl. Microbiol. Biotechnol. 73, 15–26.

Rabah, F.K.J., Dahab, M.F., 2004a. Biofilm and biomass characteristics in high-performance fluidized-bed biofilm reactors. Water Res. 38, 4262–4270.

Rabah, F.K.J., Dahab, M.F., 2004b. Nitrate removal characteristics of high performance fluidized-bed biofilm reactors. Water Res. 38, 3719–3728.

Sinha, B., Annachhatre, A.P., 2007. Partial nitrification—operational parameters and microorganisms involved. Rev. Environ. Sci. Bio/Technology 6, 285–313.

Sliekers, A.O., Haaijer, S.C.M., Stafsnes, M.H., Kuenen, J.G., Jetten, M.S.M., 2005. Competition and coexistence of aerobic ammonium- and nitrite-oxidizing bacteria at low oxygen concentrations. Appl. Microbiol. Biotechnol. 68, 808–817.

Soliman, M., Eldyasti, A., 2016. Development of partial nitrification as a first step of nitrite shunt process in a Sequential Batch Reactor (SBR) using Ammonium Oxidizing Bacteria (AOB) controlled by mixing regime. Bioresour. Technol. 221, 85–95.

Szatkowska, B., Cema, G., Plaza, E., Trela, J., Hultman, B., 2007. A one-stage system with partial nitritation and Anammox processes in the moving-bed biofilm reactor. Water Sci. Technol. 55, 19–26.

Tokutomi, T., Shibayama, C., Soda, S., Ike, M., 2010. A novel control method for nitritation: The domination of ammonia-oxidizing bacteria by high concentrations of inorganic carbon in an airlift-fluidized bed reactor. Water Res. 44, 4195–4203.

Turk, O., Mavinic, D.S., 1987. Benefits of using selective inhibition to remove nitrogen from highly nitrogenous wastes. Environ. Technol. Lett. 8, 419–426.

Wiesmann, U., 1994. Biological nitrogen removal from wastewater. Springer, Berlin, Heidelberg, pp. 113–154.

Yang, S., Yang, F., 2011. Nitrogen removal via short-cut simultaneous nitrification and denitrification in an intermittently aerated moving bed membrane bioreactor. J. Hazard. Mater. 195, 318–323.

Zhang, L., Yang, J., Hira, D., Fujii, T., Furukawa, K., 2011. High-rate partial nitrification treatment of reject water as a pretreatment for anaerobic ammonium oxidation (anammox). Bioresour. Technol. 102, 3761–3767.

Zhang, X., Li, D., Liang, Y., Zeng, H., He, Y., Fan, D., Zhang, J., 2015. Start-up, influence factors, and the microbial characteristics of partial nitrification in membrane bioreactor. Desalin. Water Treat. 54, 581–589.

Chapter 7

Conclusions and Recommendations

7.1 Conclusions

The aim of this work is to develop new processes for nutrient removal from wastewater in the fluidized bed bioreactors with consideration of reducing the overall energy consumption. The principal findings of this study were:

1. A lab-scale integrated anoxic and aerobic zones inverse fluidized bed bioreactor (IFBBR) system with carbon-coated polypropylene beads as carries was operated to test the biological nutrient removal efficiencies for synthetic wastewater. The system achieved >84% TCOD removal and complete nitrification with >75% total nitrogen removal, as well as low biomass yields. The energy consumption was calculated for the IFBBR system and compared with the CFBBR system, the results showed 59% less energy consumption of IFBBR system than CFBBR system was achieved at organic loading rate (OLR) of 1.02-2.10 kg COD/(m^3 d). Bacterial community structure was analyzed for the attached and effluent biomass and a new method to calculate system sludge retention time (SRT) was proposed. Biomass in both anoxic and aerobic zones were dominant by heterotrophs. The presence of genus *Chlorobium* as sulfate-reducing bacteria in the anoxic attached biomass confirmed the reaction of sulfate reduction in the anoxic zone.

2. The BNR performance of this lab-scale integrated IFBBR system was studied with treating synthetic wastewater of high particulate COD. 87% organic matter, 73% nitrogen, and 48% phosphorus removal were achieved at OLR of 2.8 kg COD/(m^3 d) and nitrogen loading rate (NLR) of 0.26 kg N/(m^3 d). The organic shock test was conducted to examine the system sustainability with short term response to the disturbance of influent COD. About 75% loss of nitrification efficiency was observed during the carbon shock test due to DO limitations, high COD concentrations, and washout of nitrifiers in the aerobic zone. The calibrated IFBBR model built in Biowin was applied to predict the water qualities in the anoxic and

aerobic zones, respectively. The model could predict the TCOD, SCOD, NH_4-N, NO_2-N, NO_3-N and TN with the average percent error (APE) of 15%, while underestimated the TP and PO_4-P. The maximum flow rate under the operational conditions was predicted as 300 L/d by the calibrated model with setting of the effluent standards, and the impact of DO on the system performance was predicted with the IFBBR model.

3. Four carrier particles of L-HDPE, S-HDPE, pottery, and zeolite were chosen to study the impact of diameter and density on the minimum fluidization velocity in the liquid-solid and gas-liquid-solid fluidized bed. The results showed S-HDPE particles have the lowest minimum fluidization velocity under certain gas velocities. S-HDPE was selected as the carrier particles for biomass attachment in the partial nitrification fluidized bed. Partial nitrification was successfully achieved in the fluidized bed bioreactor with the suppression of the nitrite-oxidizing bacteria growth, and the highest NLR was 4.8 kg N/(m^3 d). Stable effluent with NO_2-N/NH_4-N ratio of 1.27 at NLR of 3.6 kg N/(m^3 d) can be used as the influent of the anaerobic ammonium oxidation (ANAMMOX) process. The maximum ammonia removal rate of this process was 2.16 kg N/(m^3 d) with effluent nitrate concentration of <15 mg/L.

7.2 Recommendations

Based on the findings of this research, future research should address the following areas:

1. The properties of carrier particles are critical parameters that affect the performance of fluidized bed bioreactor system. Although in this work, different particles were chosen as carriers for biomass attachment, the impacts of particle properties (including surface roughness, diameter, density, and porosity) on biofilm were not studied systemically and no correlations were developed as guidance for the selection of carrier particles.

2. In the inverse three-phase fluidized bed bioreactor with gas phase as the driven for particle fluidization, the mechanism of biofilm attachment and detachment has not

been studied thoroughly, and the impacts of hydrodynamics on biofilm has not been quantified.

3. For modelling of the fluidized bed bioreactor system in future work, it is recommended to link the kinetics of bioreactions, biofilm diffusion mechanisms, along with the hydrodynamics of fluidized bed to built up the comprehensive model.

4. In this work, the first step of partial nitrification-denitrification/anammox process has been accomplished in the fluidized bed bioreactor. It is recommended to continue the study of the denitrification or anammox process in the fluidized bed bioreactor.

5. Temperature would have a significant impact on the process performance. It is meaningful to investigate the system performance at low temperature (e.g. <8 °C) to explore the feasibility of applying the fluidized bed bioreactor technology in Canada, especially the north of Canada.

Appendices

Appendix A. The function of Top 25 genera in samples H1, H2 and H3 (Chapter 3)

Table A1. Top 25 genera of aerobic attached biomass (Sample H1)

Genus	Relative Abundance	Function	References
NA	32.64		
Haliangium	12.88	nitrite-reducing bacteria	(McIlroy et al., 2016)
Clostridium_sensu_stricto_13	9.39	denitrifiers	(Kostrytsia et al., 2018)
Flavobacterium	3.63	heterotrophs	(Benedict and Carlson, 1971)
Acidibacter	2.62	heterotrophs	(Gao et al., 2019)
Ferruginibacter	2.53	heterotrophs	(Liu et al., 2017)
Rhodobacter	2.46	nitrite-reducing bacteria	(Tosques et al., 1997)
Thiothrix	2.33	denitrifiers	(Peng et al., 2014)
Bdellovibrio	2.25	predator	(Rendulic et al., 2004)
Luteimonas	2.21	nitrite-reducing bacteria	(Qian et al., 2017)
Acinetobacter	2.07	PAOs	(Cloete and Steyn, 1988)
Arcobacter	1.83	nitrogen-fixing bacteria	(Collado and Figueras, 2011)
Rhizobium-Allorhizobium-Neorhizobium-Pararhizobium (R-A-N-P)	1.74	nitrogen-fixing bacteria	(de Lajudie et al., 1998)
Hydrogenophaga	1.48	denitrifiers	(Visvanathan et al., 2008)
Azospira	1.27	denitrifiers	(Rossi et al., 2014)
OLB12	1.14		
Terrimonas	0.98	heterotrophs	(Shi et al., 2019)
Zoogloea	0.96	denitrifiers	(Strand et al., 1988)
Hyphomicrobium	0.75	nitrogen-fixing bacteria	(Layton et al., 2000)
Bacteroides	0.57	heterotrophs	(Grenier and Mayrand, 1987)
Runella	0.56	heterotrophs	(Horsnell et al., 1991)

Phreatobacter	0.5	heterotrophs	(Toth et al., 2014)
Nitrosomonas	0.45	AOB	(Stein et al., 2007)
Leptothrix	0.44	heterotrophs	(Johnson et al., 1992)
Sphingosinicella	0.4	heterotrophs	(Geueke et al., 2007)
Dechlorobacter	0.4	denitrifiers	(Han et al., 2018)
Specific genus			
Nitrospira	0.11	NOB	(Cébron and Garnier, 2005)
Chlorobium	0.07	Sulfate reducing bacteria	(Kirchhoff and Truper, 1974)

Table A2. Top 25 genera of anoxic attached biomass (Sample H2)

Genus	Relative Abundance	Function	References
Arcobacter	22.76	nitrogen-fixing bacteria	(Collado and Figueras, 2011)
NA	20.40		
Zoogloea	10.18	denitrifiers	(Strand et al., 1988)
Thiothrix	7.98	denitrifiers	(Peng et al., 2014)
Dechlorobacter	5.89	denitrifiers	(Han et al., 2018)
Acinetobacter	4.60	PAOs	(Cloete and Steyn, 1988)
Sulfuritalea	2.87	nitrite-reducing bacteria	(McIlroy et al., 2016)
Leptothrix	2.24	heterotrophs	(Johnson et al., 1992)
Dechloromonas	1.50	denitrifiers	(Gentile et al., 2006)
Rhodobacter	1.50	nitrite-reducing bacteria	(Tosques et al., 1997)
Flavobacterium	1.39	heterotrophs	(Benedict and Carlson, 1971)
Alicycliphilus	1.32	denitrifiers	(Ntougias et al., 2015)
Rhizobium-Allorhizobium-Neorhizobium-Pararhizobium (R-A-N-P)	1.05	nitrogen-fixing bacteria	(de Lajudie et al., 1998)
Azospira	1.02	denitrifiers	(Rossi et al., 2014)
Bdellovibrio	1.00	predator	(Rendulic et al., 2004)
Azonexus	1.00	denitrifiers	(Quan et al., 2006)

Thauera	0.89	denitrifiers	(Han et al., 2015)
Hydrogenophaga	0.84	denitrifiers	(Visvanathan et al., 2008)
Haliangium	0.78	nitrite-reducing bacteria	(McIlroy et al., 2016)
Cloacibacterium	0.72	heterotrophs	(Allen et al., 2006)
Rivicola	0.67	heterotrophs	(Sheu et al., 2014)
Terrimonas	0.46	heterotrophs	(Shi et al., 2019)
Aquimonas	0.40	heterotrophs	(Rodriguez-Sanchez et al., 2016)
Luteimonas	0.33	nitrite-reducing bacteria	(Qian et al., 2017)
Paludibacter	0.32	anaerobic digestion bacteria	(Felföldi et al., 2015)
Chlorobium	0.32	sulfate-reducing bacteria	(Kirchhoff and Truper, 1974)
Specific genus			
Nitrospira	0.20	NOB	(Cébron and Garnier, 2005)
Nitrosomonas	0.18	AOB	(Stein et al., 2007)

Table A3. Top 25 genera of aerobic effluent biomass (Sample H3)

Genus	Relative Abundance	Function	References
Arcobacter	26.28	nitrogen-fixing bacteria	(Collado and Figueras, 2011)
NA	24.12		
Zoogloea	7.44	denitrifiers	(Strand et al., 1988)
Paludibacter	5.97	anaerobic digestion bacteria	(Felföldi et al., 2015)
Thiothrix	4.93	denitrifiers	(Peng et al., 2014)
Rhodoferax	2.05	nitrite-reducing bacteria	(McIlroy et al., 2016)
Haliangium	2.00	nitrite-reducing bacteria	(McIlroy et al., 2016)
A7P-90m	1.85		
WCHB1-32	1.76	heterotrophs	(Engel et al., 2010)
Proteocatella	1.22	fermenters	(Sun et al., 2014)
Dechloromonas	1.13	denitrifiers	(Gentile et al., 2006)
Clostridium_sensu_stricto_13	1.12	denitrifiers	(Kostrytsia et al., 2018)
Luteolibacter	0.92	PAOs	(García et al., 2017)
Phreatobacter	0.90	heterotrophs	(Toth et al., 2014)
Acidibacter	0.90	heterotrophs	(Gao et al., 2019)
Flavobacterium	0.87	heterotrophs	(Benedict and Carlson, 1971)

Sulfurospirillum	0.82	denitrifiers	(Hubert and Voordouw, 2007)
Ferruginibacter	0.75	heterotrophs	(Liu et al., 2017)
Pseudomonas	0.75	denitrifiers	(van Rijn et al., 1996)
Acinetobacter	0.72	PAOs	(Cloete and Steyn, 1988)
Azonexus	0.69	denitrifiers	(Quan et al., 2006)
Rivicola	0.61	heterotrophs	(Sheu et al., 2014)
Rhodobacter	0.61	nitrite-reducing bacteria	(Tosques et al., 1997)
Hydrogenophaga	0.53	denitrifiers	(Visvanathan et al., 2008)
Bdellovibrio	0.50	predator	(Rendulic et al., 2004)
Dechlorobacter	0.47	denitrifiers	(Han et al., 2018)
Specific genus			
Nitrosomonas	0.39	AOB	(Stein et al., 2007)
Nitrospira	0.30	NOB	(Cébron and Garnier, 2005)
Chlorobium	0.01	Sulfate reducing bacteria	(Kirchhoff and Truper, 1974)

References

Allen, T.D., Lawson, P.A., Collins, M.D., Falsen, E., Tanner, R.S., 2006. Cloacibacterium normanense gen. nov., sp. nov., a novel bacterium in the family Flavobacteriaceae isolated from municipal wastewater. Int. J. Syst. Evol. Microbiol. 56, 1311–1316.

Benedict, R.G., Carlson, D.A., 1971. Aerobic heterotrophic bacteria in activated sludge. Water Res. 5, 1023–1030.

Cébron, A., Garnier, J., 2005. Nitrobacter and Nitrospira genera as representatives of nitrite-oxidizing bacteria: Detection, quantification and growth along the lower Seine River (France). Water Res. 39, 4979–4992.

Cloete, T.E., Steyn, P.L., 1988. The role of Acinetobacter as a phosphorus removing agent in activated sludge. Water Res. 22, 971–976.

Collado, L., Figueras, M.J., 2011. Taxonomy, epidemiology, and clinical relevance of the genus Arcobacter. Clin. Microbiol. Rev. 24, 174–92. https://doi.org/10.1128/CMR.00034-10

de Lajudie, P., Laurent-Fulele, E., Willems, A., Torek, U., Coopman, R., Collins, M.D., Kersters, K., Dreyfus, B., GILLIS, M., 1998. Allorhizobium undicola gen. nov., sp. nov., nitrogen-fixing bacteria that efficiently nodulate Neptunia natans in Senegal. Int. J. Syst. Bacteriol. 48, 1277–1290.

Engel, A.S., Porter, M.L., Kinkle, B.K., Kane, T.C., 2010. Geomicrobiology Journal Ecological Assessment and Geological Significance of Microbial Communities from Cesspool Cave, Virginia. Communities from Cesspool Cave 18, 259–274.

Felföldi, T., Jurecska, L., Vajna, B., Barkács, K., Makk, J., Cebe, G., Szabó, A., Záray, G., Márialigeti, K., 2015. Texture and type of polymer fiber carrier determine bacterial colonization and biofilm properties in wastewater treatment. Chem. Eng. J. 264, 824–834.

Gao, P., Sun, X., Xiao, E., Xu, Z., Li, B., Sun, W., 2019. Characterization of iron-metabolizing communities in soils contaminated by acid mine drainage from an abandoned coal mine in Southwest China. Environ. Sci. Pollut. Res. 26, 9585–9598.

García, D., Alcántara, C., Blanco, S., Pérez, R., Bolado, S., Muñoz, R., 2017. Enhanced carbon, nitrogen and phosphorus removal from domestic wastewater in a novel anoxic-aerobic photobioreactor coupled with biogas upgrading. Chem. Eng. J. 313, 424–434.

Gentile, M., Yan, T., Tiquia, S.M., Fields, M.W., Nyman, J., Zhou, J., Criddle, C.S., 2006. Stability in a Denitrifying Fluidized Bed Reactor. Microb. Ecol. 52, 311–321.

Geueke, B., Busse, H.-J., Fleischmann, T., Kampfer, P., Kohler, H.-P.E., 2007. Description of Sphingosinicella xenopeptidilytica sp. nov., a beta-peptide-degrading species, and emended descriptions of the genus Sphingosinicella and the species Sphingosinicella microcystinivorans. Int. J. Syst. Evol. Microbiol. 57, 107–113.

Grenier, D., Mayrand, D., 1987. Selected characteristics of pathogenic and nonpathogenic strains of Bacteroides gingivalis. J. Clin. Microbiol. 25, 738–40.

Han, F., Ye, W., Wei, D., Xu, W., Du, B., Wei, Q., 2018. Simultaneous nitrification-denitrification and membrane fouling alleviation in a submerged biofilm membrane bioreactor with coupling of sponge and biodegradable PBS carrier. Bioresour. Technol. 270, 156–165.

Han, X., Wang, Z., Ma, J., Zhu, C., Li, Y., Wu, Z., 2015. Membrane bioreactors fed with different COD/N ratio wastewater: impacts on microbial community, microbial products, and membrane fouling. Environ. Sci. Pollut. Res. 22, 11436–11445.

Horsnell, G.E., Young, M., Pagel, J.E., Desjardins, R.M., Seyfried, P.L., 1991. Characterization of aerobic heterotrophic bacteria isolated from marshes. Environ. Toxicol. Water Qual. 6, 329–340.

Hubert, C., Voordouw, G., 2007. Oil field souring control by nitrate-reducing Sulfurospirillum spp. that outcompete sulfate-reducing bacteria for organic electron donors. Appl. Environ. Microbiol. 73, 2644–52.

Johnson, D.B., Ghauri, M.A., Said, M.F., 1992. Isolation and characterization of an acidophilic, heterotrophic bacterium capable of oxidizing ferrous iron. Appl. Environ. Microbiol. 58, 1423–1428.

Kirchhoff, J., Truper, H.G., 1974. Adenylylsulfate reductase of Chlorobium limicola. Arch. Microbiol. 100, 115–120. 1

Kostrytsia, A., Papirio, S., Morrison, L., Ijaz, U.Z., Collins, G., Lens, P.N.L., Esposito, G., 2018. Biokinetics of microbial consortia using biogenic sulfur as a novel electron donor for sustainable denitrification. Bioresour. Technol. 270, 359–367.

Layton, A.C., Karanth, P.N., Lajoie, C.A., Meyers, A.J., Gregory, I.R., Stapleton, R.D., Taylor, D.E., Sayler, G.S., 2000. Quantification of Hyphomicrobium populations in activated sludge from an industrial wastewater treatment system as determined by 16S rRNA analysis. Appl. Environ. Microbiol. 66, 1167–74.

Liu, T., Mao, Y., Shi, Y., Quan, X., 2017. Start-up and bacterial community compositions of partial nitrification in moving bed biofilm reactor. Appl. Microbiol. Biotechnol. 101, 2563–2574.

McIlroy, S.J., Starnawska, A., Starnawski, P., Saunders, A.M., Nierychlo, M., Nielsen, P.H., Nielsen, J.L., 2016. Identification of active denitrifiers in full-scale nutrient removal wastewater treatment systems. Environ. Microbiol. 18, 50–64.

Ntougias, S., Melidis, P., Navrozidou, E., Tzegkas, F., 2015. Diversity and efficiency of anthracene-degrading bacteria isolated from a denitrifying activated sludge system treating municipal wastewater. Int. Biodeterior. Biodegradation 97, 151–158.

Peng, X., Guo, F., Ju, F., Zhang, T., 2014. Shifts in the microbial community, nitrifiers and denitrifiers in the biofilm in a full-scale rotating biological contactor. Environ. Sci. Technol. 48, 8044–8052.

Qian, G., Li, L., Hu, X., Yu, X., Ye, L., 2017. Enhancement of the biodegradability of activated sludge by the electric-coagulation multistage A/O membrane bioreactor treating low C/N industrial wastewater. Int. Biodeterior. Biodegradation 125, 1–12.

Quan, Z.-X., Im, W.-T., Lee, S.-T., 2006. Azonexus caeni sp. nov., a denitrifying bacterium isolated from sludge of a wastewater treatment plant. Int. J. Syst. Evol. Microbiol. 56, 1043–1046.

Rendulic, S., Jagtap, P., Rosinus, A., Eppinger, M., Baar, C., Lanz, C., Keller, H., Lambert, C., Evans, K.J., Goesmann, A., Meyer, F., Sockett, R.E., Schuster, S.C., 2004. A predator unmasked: life cycle of Bdellovibrio bacteriovorus from a genomic perspective. Science 303, 689–92.

Rodriguez-Sanchez, A., Munoz-Palazon, B., Maza-Marquez, P., Gonzalez-Lopez, J., Vahala, R., Gonzalez-Martinez, A., 2016. Process performance and bacterial community dynamics of partial-nitritation biofilters subjected to different concentrations of cysteine amino acid. Biotechnol. Prog. 32, 1254–1263.

Rossi, F., Motta, O., Matrella, S., Proto, A., Vigliotta, G., Rossi, F., Motta, O., Matrella, S., Proto, A., Vigliotta, G., 2014. Nitrate removal from wastewater through biological denitrification with OGA 24 in a batch reactor. Water 7, 51–62.

Sheu, S.-Y., Chen, J.-C., Young, C.-C., Chen, W.-M., 2014. Rivicola pingtungensis gen. nov., sp. nov., a new member of the family Neisseriaceae isolated from a freshwater river. Int. J. Syst. Evol. Microbiol. 64, 2009–2016.

Shi, J., Xu, C., Han, Y., Han, H., 2019. Enhanced anaerobic biodegradation efficiency and mechanism of quinoline, pyridine, and indole in coal gasification wastewater. Chem. Eng. J. 361, 1019–1029.

Stein, L.Y., Arp, D.J., Berube, P.M., Chain, P.S.G., Hauser, L., Jetten, M.S.M., Klotz, M.G., Larimer, F.W., Norton, J.M., Op den Camp, H.J.M., Shin, M., Wei, X., 2007. Whole-genome analysis of the ammonia-oxidizing bacterium, Nitrosomonas eutropha C91: implications for niche adaptation. Environ. Microbiol. 9, 2993–3007.

Strand, S.E., McDonnell, A.J., Unz, R.F., 1988. Oxygen and nitrate reduction kinetics of a nonflocculating strain of Zoogloea ramigera. Antonie Van Leeuwenhoek 54, 245–255.

Sun, R., Xing, D., Jia, J., Liu, Q., Zhou, A., Bai, S., Ren, N., 2014. Optimization of high-solid waste activated sludge concentration for hydrogen production in microbial electrolysis cells and microbial community diversity analysis. Int. J. Hydrogen Energy 39, 19912–19920.

Tosques, I.E., Kwiatkowski, A. V, Shi, J., Shapleigh, J.P., 1997. Characterization and regulation of the gene encoding nitrite reductase in Rhodobacter sphaeroides 2.4.3. J. Bacteriol. 179, 1090–1095.

Toth, E.M., Vengring, A., Homonnay, Z.G., Keki, Z., Sproer, C., Borsodi, A.K., Marialigeti, K., Schumann, P., 2014. Phreatobacter oligotrophus gen. nov., sp. nov., an alphaproteobacterium isolated from ultrapure water of the water purification system of a power plant. Int. J. Syst. Evol. Microbiol. 64, 839–845.

van Rijn, J., Tal, Y., Barak, Y., 1996. Influence of Volatile Fatty Acids on Nitrite Accumulation by a Pseudomonas stutzeri Strain Isolated from a Denitrifying Fluidized Bed Reactor. Appl. Environ. Microbiol. 62, 2615–20.

Visvanathan, C., Hung, N.Q., Jegatheesan, V., 2008. Hydrogenotrophic denitrification of synthetic aquaculture wastewater using membrane bioreactor. Process Biochem. 43, 673–682.
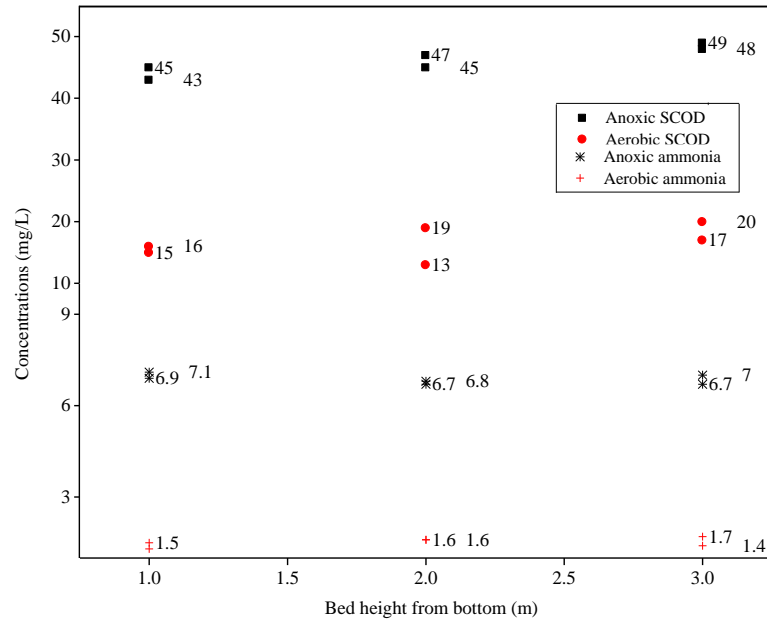
Appendix B. Biowin simulation data (Chapter 4)

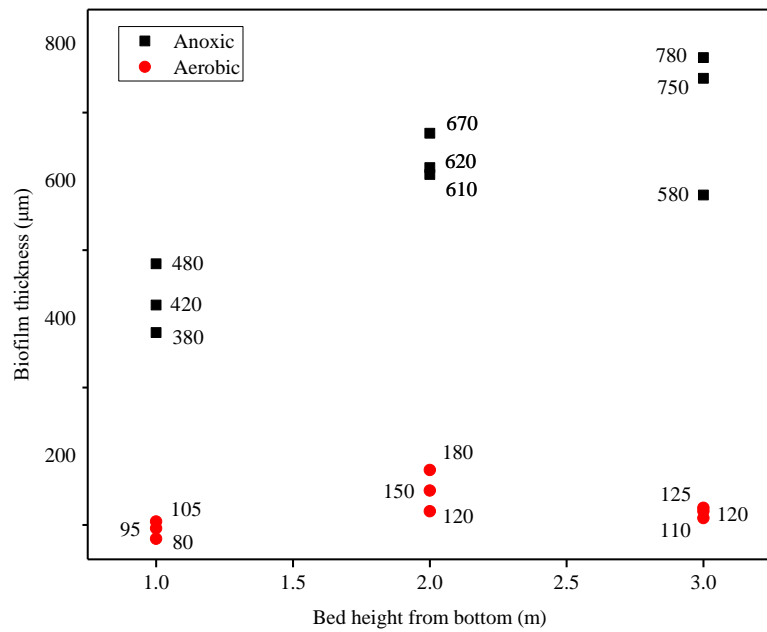**Figure B1.** SCOD and ammonia concentrations along the column.

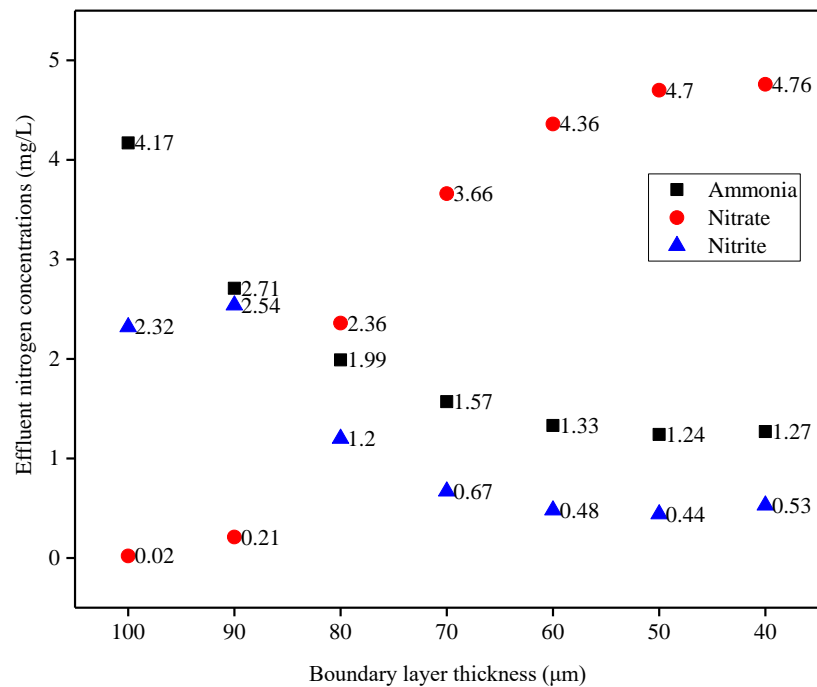**Figure B2.** Biofilm thickness at different height.

Figure B3. The effect of boundary layer thickness on effluent nitrogen concentrations.
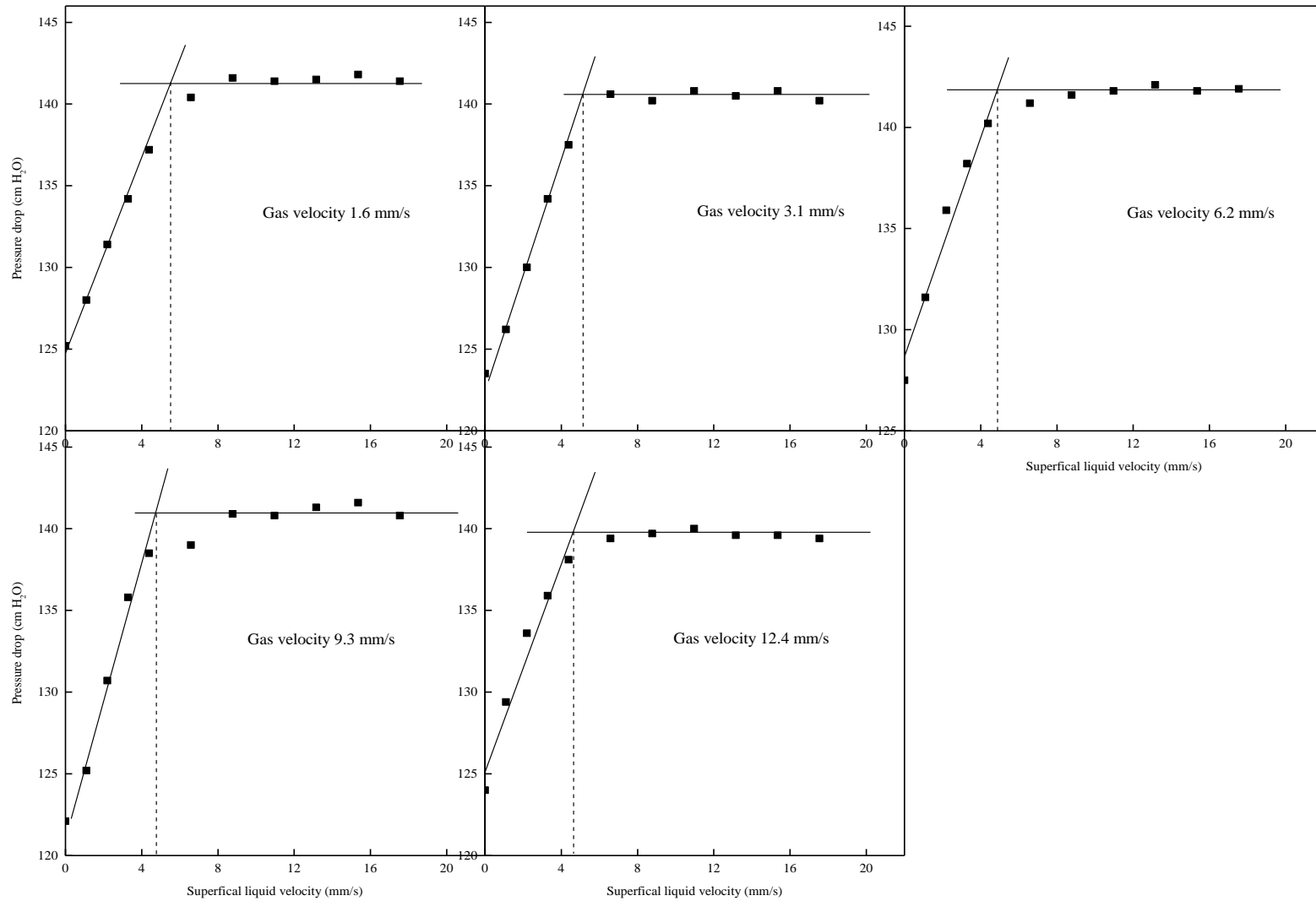
Appendix C. Minimum fluidization velocity (Chapter 5)

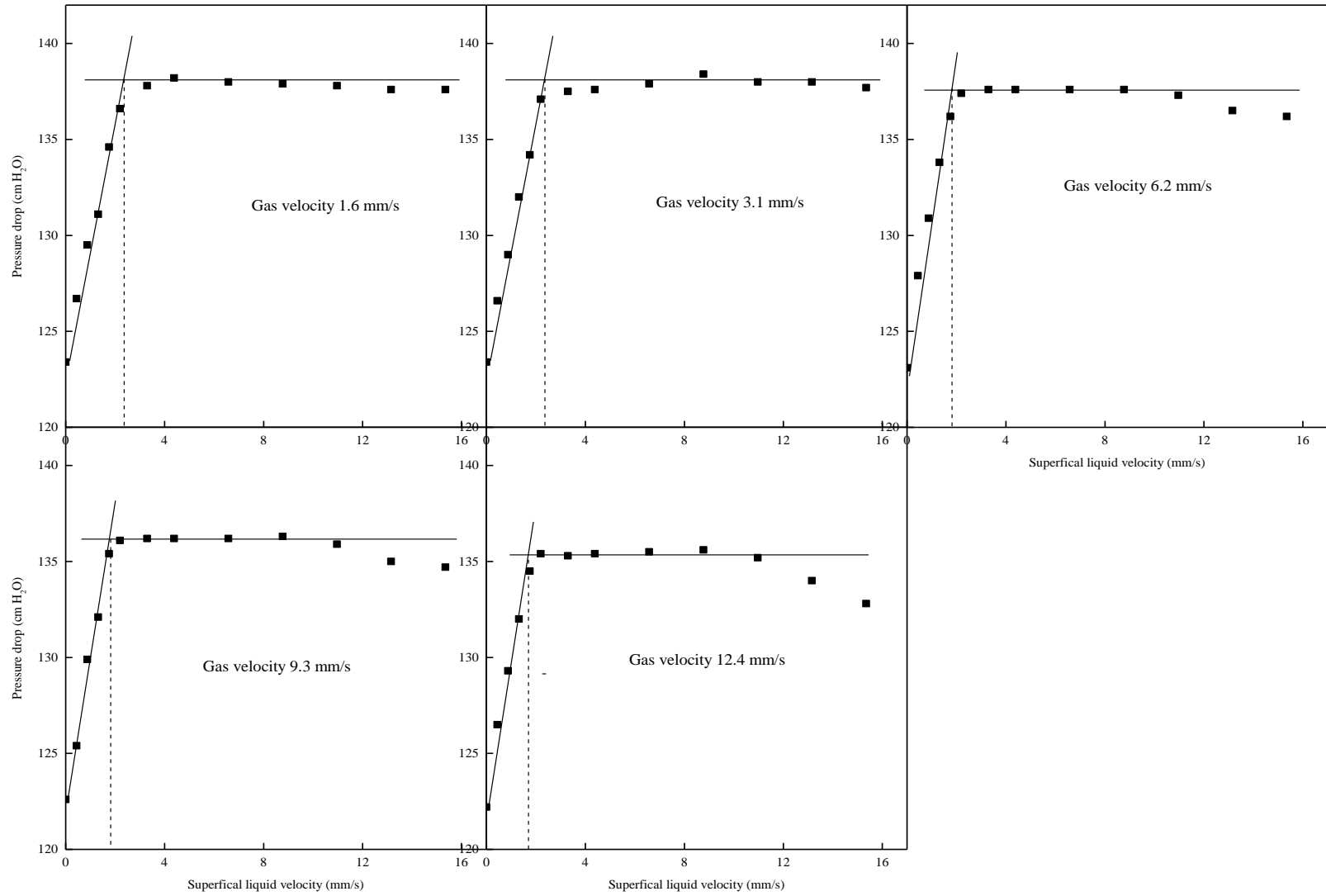**Figure C1**. Minimum fluidization velocity of carrier particles L-HDPE at different superficial gas velocities

Figure C2. Minimum fluidization velocity of carrier particles S-HDPE at different superficial gas velocities
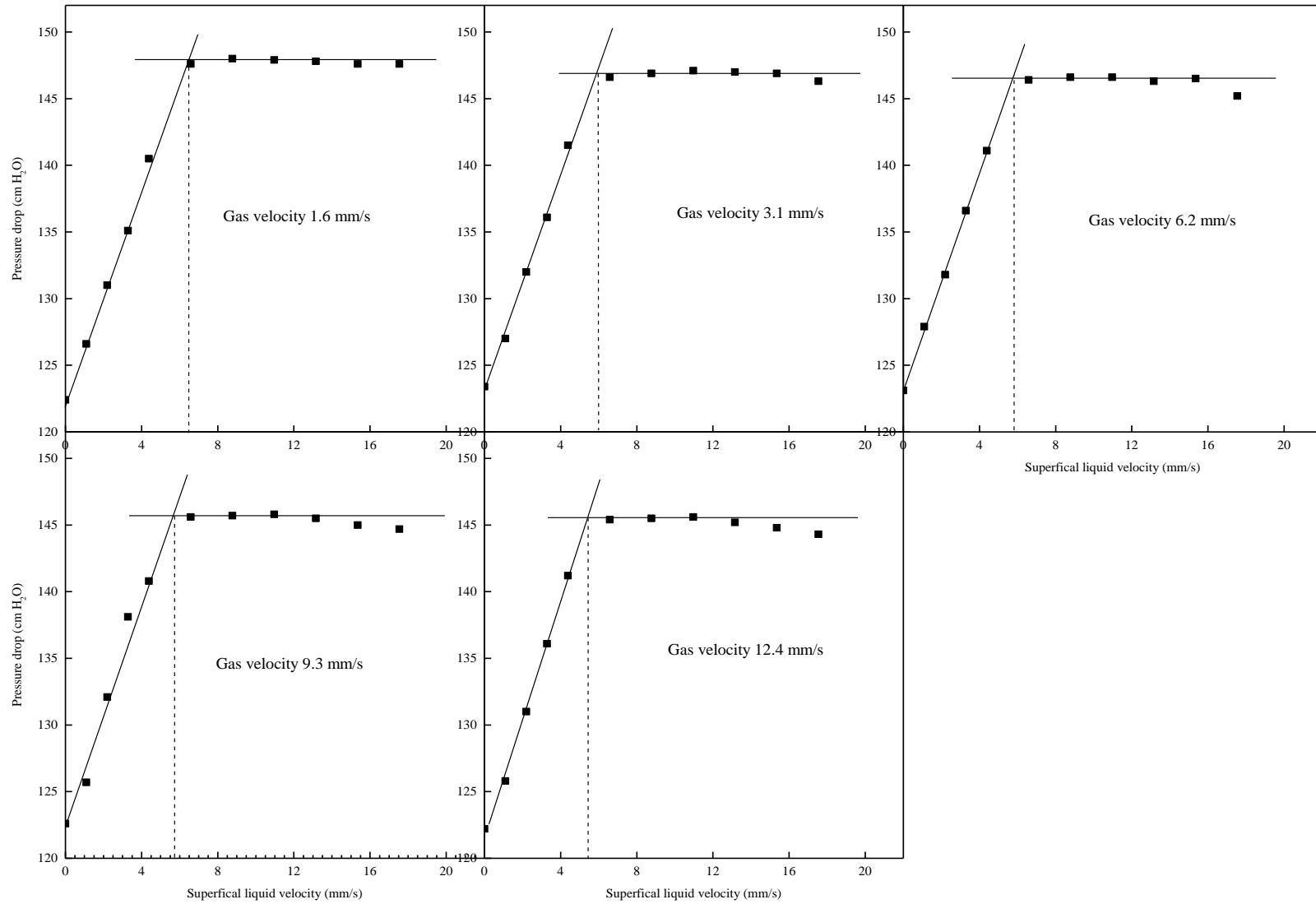
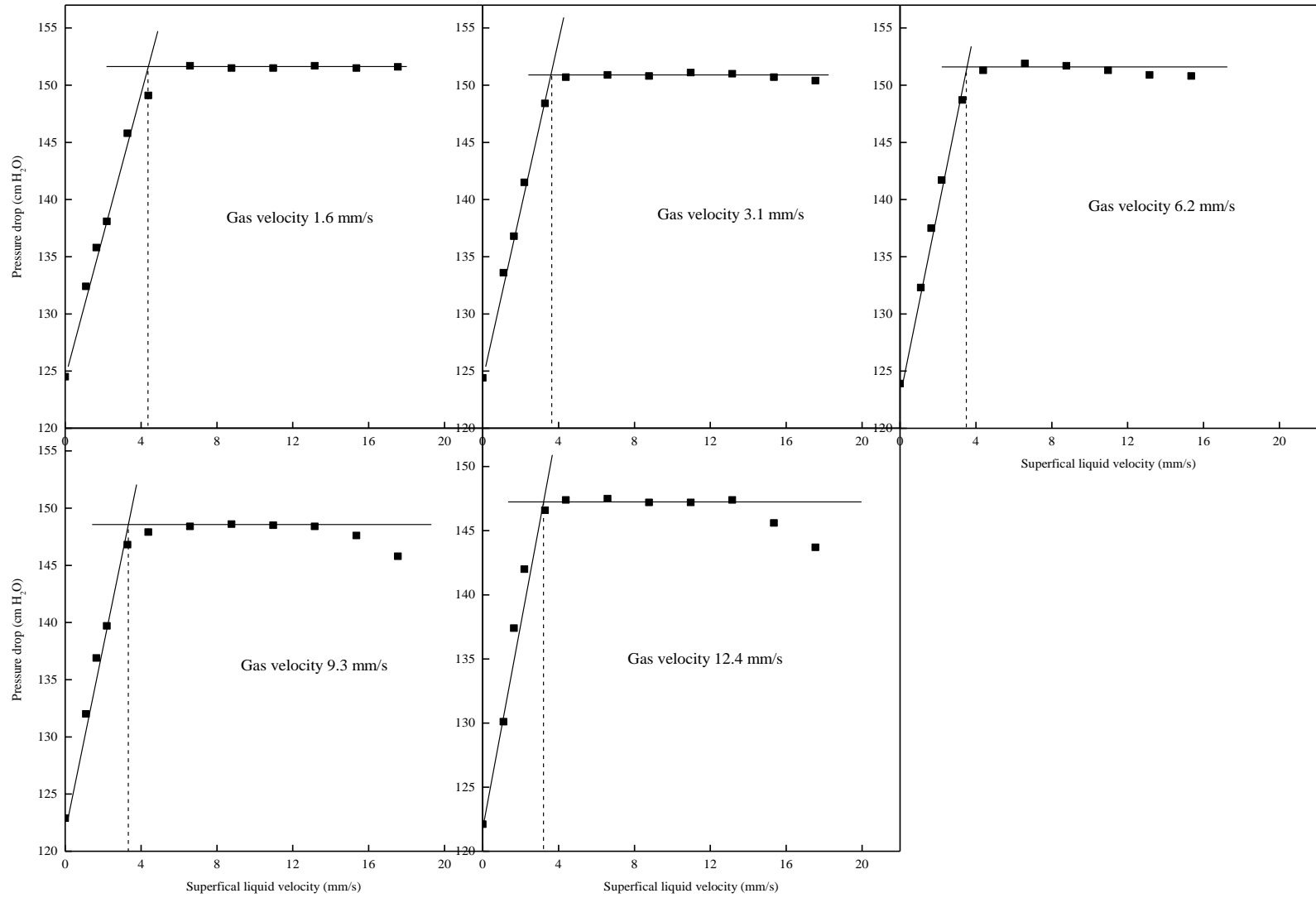**Figure C3**. Minimum fluidization velocity of carrier particles Pottery at different superficial gas velocities

Figure C4. Minimum fluidization velocity of carrier particles Zeolite at different superficial gas velocities

Curriculum Vitae

Name:	Haolong Wang

Post-secondary Education and Degrees:

Beijing University of Chemical Technology
Beijing, China
2010-2014 B.A.

Tianjin University
Tianjin, China
2014-2017 M.A.

The University of Western Ontario
London, Ontario, Canada
2015-2019 Ph.D.

Honours and Awards:

Chinese Graduate Research Scholarship
2015-2019

Related Work Experience

Teaching Assistant
The University of Western Ontario
2016-2018

Volunteer
The 10th Global Chinese Chemical Engineers Symposium
2018.08

Conference:

53rd CENTRAL Canadian Symposium on Water Quality Research
Toronto, ON, Canada 2018.02

4th IWA Specialized International Conference on ecoSTP
London, ON, Canada 2018.06

54th CENTRAL Canadian Symposium on Water Quality Research
Toronto, ON, Canada 2019.02

Publications:

Wang, H., Kim, M., Li, K., Shao, Y., Zhu, J., Nakhla, G., 2019. Effective partial nitrification of ammonia in a fluidized bed bioreactor, Environ. Technol. 40, 94–101.